University of Nottingham



School of Mathematical Sciences

Asymptotic and Stability Analysis of a Tumour Growth Model

Andrea Genovese de Oliveira, MMath

A thesis submitted to the
University of Nottingham
for the degree of
Doctor of Philosophy

February 14, 2017

I dedicate this thesis to
my supervisors,
my lecturers,
my teachers,
my friends,
my brothers,
my parents,
and my husband.

Abstract

We investigate avascular tumour growth as a two-phase process consisting of cells and liquid. Initially, we simulate a continuum moving-boundary model formulated by (*Byrne, King, McElwain, Preziosi, Applied Mathematics Letters, 2003, 16, 567-573*) in one dimension and analyse the dependence of the tumour growth on the natural nutrient and cell concentration levels outside of the tumour along with its ability to model known biological dynamics of tumour growth. We investigate linear stability of time-dependent solution profiles in the moving-boundary formulation of a limit case (with negligible nutrient consumption and cell drag) and compare analytical predictions of their saturation, growth and exponential decay against numerical simulations of the full one dimensional model formulated in the article cited above. With this limit case and its time-dependent solution, we analytically obtained a critical nutrient concentration that determines whether a tumour will grow or decay.

Then, we formulated the analogous model and boundary conditions for tumour growth in two dimensions. By considering the same limit case and its time-dependent solutions in two dimensions, we obtain an asymptotic limit of the two-dimensional perturbations for large time in the case where the tumour is growing by using the method of matched asymptotic approximations. Having characterised an asymptotic limit of the perturbations, we compare it to its numerical counterpart and to the time-dependent solution profiles in order to analytically obtain a condition for instability.

Acknowledgements

This work was produced with the support of CAPES, *Coordenação de Aperfeiçoamento de Pessoal de Nível Superior* - Brazil and the University of Nottingham, via the *PhD Scholarship for Research Excellence from Brazil*.

First, I would like to thank my supervisors for all their time and consideration. I am certain this would not have been possible without you.

I would also like to thank CAPES/*Coordenação de Aperfeiçoamento de Pessoal de Nível Superior* - Brazil for funding this research. This research would not have been possible without these funds.

Additionally, I would like to thank the University of Nottingham and the School of Mathematical Sciences for the support I have received, including the fee waiver and conference travel grants that made this work possible.

Thank you to all the teachers, lecturers, and previous supervisors who believed in me and inspired me to continue researching.

Thank you to all my friends and colleagues, with their never-ending supply of moral support, coffee and, most importantly, chocolate.

Thank you to my brothers, who taught me to dream to be like them.

I also owe a huge thank you to my husband. You've been my strength from day one to the end. I will never be able to thank you enough. You've left everything behind to allow me to follow my dream. Yet, your talent was so great that you managed to fulfil one of yours too in the meantime. You make me very proud. I quite simply could not have done this without you.

Finally, I owe everything I have achieved to my parents. You have sacrificed for my education more than I can even imagine. I cannot begin to express my gratitude for all you have done for me. You've been a light and a guide. May you enjoy the pride of having three sons and daughters that are now all doctors. You are an example of courage, unity, and success.

CONTENTS

1 INTRODUCTION AND LITERARY REVIEW 1

1.1 Biological Overview of Tumour Growth 1

1.2 Motivation and Importance of Tumour Growth Models . . 2

1.3 Motivation of Mathematical and Modelling Approaches . 3

1.3.1 Exploring Avascular Tumours 3

1.3.2 Studying Stability 3

1.3.3 Using a Multiphase Model 4

1.4 Literary Review 4

1.4.1 The Early Biological and Mathematical Discoveries 4

1.4.2 The Birth of Mathematical Models of Tumour Growth 8

1.4.3 The Modern Mathematical Models of Tumour Growth 9

2 FORMULATION OF A TWO-PHASE MODEL OF AVASCULAR TUMOUR GROWTH 16

2.1 General Model Formulation 16

2.1.1 Introduction and Motivation 16

2.1.2 Mass Balances 17

2.1.3 Momentum Balances 17

2.1.4 Constitutive Assumptions 18

2.1.5 Nutrient Diffusion 19

2.1.6 Important Functions 20

2.1.7 Conclusion 23

2.2 One Dimensional Model Formulation 24

2.2.1 Equations and their Domain 24

2.2.2 Boundary Conditions 25

2.2.3 Solving for v_w and p 25
2.2.4 Simplified One Dimensional Model - Conclusion . 26
2.2.5 Global Mass Equation 27
2.3 Asymptotic Limits of the One Dimensional Model 27
2.3.1 Negligible Cell Viscosity ($\hat{\mu}_c \to 0$) 28
2.3.2 Negligible Cell Viscosity and Drag $\left(\hat{\mu}_c, \frac{k(\alpha)}{(\alpha\Sigma_c(\alpha))'} \to 0\right)$ 29
2.4 Conclusion 31

3 NUMERICAL SIMULATIONS IN ONE DIMENSION 32
3.1 Full One Dimensional Model 32
3.1.1 Formulation 32
3.1.2 Finite Difference Scheme 34
3.1.3 Four Cases 40
3.2 One Dimensional Model with Negligible Cell Viscosity . . 51
3.2.1 Formulation 52
3.2.2 Finite Difference Scheme 53
3.2.3 Four Cases with $\nu_2(\alpha) > 0$ 56
3.2.4 Two Cases with $\nu_2(\alpha) < 0$ 65
3.2.5 Limitations of the Negligible Viscosity Limit Model 75
3.3 Conclusion 79

4 NEGLIGIBLE NUTRIENT UPTAKE & CELL DRAG LIMIT AND THE STABILITY OF A TIME-DEPENDENT SOLUTION IN ONE DIMENSION 81
4.1 Introduction and Motivation 81
4.2 Full One Dimensional System 83
4.2.1 Homogeneous Steady State Solution 83
4.2.2 A Non-Homogeneous Solution 84
4.3 Limit with Negligible Nutrient Uptake & Cell Drag 84
4.3.1 Formulation 84
4.3.2 Homogeneous Steady State Solutions 85

4.3.3 A Time-Dependent Non-homogeneous Solution . . 87
4.3.4 Linearisation about the Travelling Solution 89
4.3.5 Summary 92
4.4 Critical Nutrient Concentration 93
4.4.1 Motivation and Definition 93
4.4.2 Simulations with Negligible Nutrient Uptake & Cell Drag 94
4.4.3 Simulations of System with Small Nutrient Uptake & Cell Drag 98

5 TRAVELLING SOLUTIONS: INSTABILITY IN ONE DIMENSION AND $\Sigma_c(\alpha)$ 102
5.1 Introduction and Motivation 102
5.2 Changing the Parameters of $\Sigma_c(\alpha)$ in Search of Instability 104
5.2.1 Formulation 104
5.2.2 Simulations 105
5.2.3 Conclusion 117
5.3 Changing $\Sigma_c(\alpha)$ in Search of a Growing Unstable Solution 118
5.3.1 Objective and Motivation 118
5.3.2 Defining New $\Sigma_c(\alpha)$ 119
5.3.3 Simulations 121
5.3.4 Conclusion 138
5.4 Considerations about New $\Sigma_c(\alpha)$ 138

6 LINEAR STABILITY ANALYSIS IN ONE DIMENSION 140
6.1 General One Dimensional System 141
6.1.1 Motivation 141
6.1.2 Linearisation about Non-homogeneous Solution . . 142
6.2 Negligible Nutrient Consumption and Cell Drag 144

7 LINEAR STABILITY ANALYSIS IN TWO DIMENSIONS 146
7.1 General Two Dimensional System 147

7.1.1 Definition and Notation 147
7.1.2 Linearisation about One Dimensional Solution . . . 149
7.1.3 Fixing the Domain 151
7.1.4 Separation of Variables 152
7.2 Negligible Nutrient Consumption and Cell Drag 154
7.2.1 Definition 154
7.2.2 Linearisation about One Dimensional Travelling Solution 155

8 ASYMPTOTIC ANALYSIS OF NEGLIGIBLE NUTRIENT CONSUMPTION AND CELL DRAG LIMIT IN TWO DIMENSIONS 159
8.1 Set Up and Motivation 159
8.2 Outer Solution 160
8.2.1 Analytical Characterisation of Outer Solution . . . 160
8.2.2 Comparison of Analytical vs. Numerical Outer Solution 167
8.3 Inner Solution near Outer Boundary 175
8.3.1 Analytical Characterisation of Inner Solution near Outer Boundary $\xi = 1$ 175
8.3.2 Comparison of Analytical vs. Numerical Outer Boundary Inner Solution 191
8.4 Inner Solution near Inner Boundary 196
8.4.1 Analytical Characterisation of Inner Solution near Inner Boundary $\xi = 0$ 196
8.4.2 Comparison of Analytical vs. Numerical Inner Boundary Inner Solution 203
8.5 Numerical Limitations 206
8.5.1 Discussion and Definition of Mock Model 206
8.5.2 Attempting to Apply Lessons from Mock Model onto Original Model 209
8.6 Conclusion - Linear Stability 210

9 CONCLUSION 213
9.1 Summary . . . 213
9.2 Conclusion . . . 216
9.3 Literature Context . . . 217
9.4 Biological Relevance . . . 217
9.5 Future Work . . . 219

A SIMULATIONS OF 1-D MODEL: TESTING C_{crit} 220

B SIMULATIONS OF ONE DIMENSIONAL MODEL WITH DIFFERENT $\Sigma_c(\alpha)$ 233

C DETAILS OF CHAPTER 8 249
C.1 Discarding Trivial Asymptotic Balances . . . 249

D VALIDATION OF NUMERICAL RESULTS OF CHAPTER 8 253
D.1 Checking Numerical Definition of Equation's RHS . . . 253
D.2 Checking Outer Solution . . . 257
D.2.1 Checking Outer Solution Asymptotic Balance . . . 257
D.2.2 Considering a Different Asymptotic Balance . . . 259
D.2.3 Numerical Checks with Larger Times . . . 260
D.2.4 Taking a Hint from Numerics . . . 261
D.2.5 Comparing Magnitudes . . . 264

E ASYMPTOTIC ANALYSIS SUMMARY 267

1

INTRODUCTION AND LITERARY REVIEW

1.1 BIOLOGICAL OVERVIEW OF TUMOUR GROWTH

The process by which tumours develop has two main stages: *avascular* and *vascular*. Initially, healthy cells undergo a mutation which allows them to bypass the strong controls present in normal cell growth. It is not quite understood why this happens, but it is generally accepted that it is due to a mixture of both hereditary and environmental factors. This way, these cells start proliferating faster than normal healthy cells, creating a clump of cells with an unnaturally high proliferation rate, namely a *tumour*.

During this phase, the tumour does not have blood vessels, i.e., is *avascular*, and therefore relies mostly on diffusion of nutrients from nearby sources. Due to this dependence, as the tumour grows, less nutrients are provided to the tumour's innermost cells. At this point, cells in its center start dying, creating a *necrotic core*.

One of the largest discoveries regarding this phase is that tumour growth is limited while avascular, thus reaching a *diffusion-limited steady state*, [28, 38, 29, 30, 67, 11]. With this discovery, came the hypothesis that in order for a tumour to actually become malignant it must grow beyond the avascular phase, undergoing *angiogenesis*, the process of developing its own blood supply.

Of course, with this hypothesis, many researchers searched for a cure for cancer by understanding in depth the process of angiogenesis, including

what triggers it along with substances that inhibit it. In fact, some clinical trials testing antiangiogenic medication therapies, using Bevacizumab (Avastin), for example, have produced encouraging results [32].

Although the angiogenesis process is intricate, it is safe to say that the main components in this process are substances secreted by the oxygen-deprived tumour cells that catalyse blood vessel formation and chemotactically attract fully-formed blood vessels towards the tumour. These substances are called *tumour angiogenenic factors (TAFs)*. Once this process has taken place, the tumour is able to grow radically as it now has an appropriate nutrient supply.

Eventually, tumour cells break off and spread through the circulatory system, a process called *metastasis*. Surgically, it is usually feasible to remove a solid primary tumour and treat any residues with chemotherapy and radiotherapy. However, if the primary tumour has undergone metastasis, it is physically impossible to remove all the secondary tumours. Therefore, angiogenesis and metastasis are in fact what make a tumour malignant.

More information regarding this section can be found in [41, 42, 44, 2].

1.2 MOTIVATION AND IMPORTANCE OF TUMOUR GROWTH MODELS

Having understood the basic stages of tumour growth, it is visible that experiments in the vascular stage are the most important ones from a clinical point of view. Indeed, angiogenesis, vascular growth and metastasis are what make patients actually die. However, any experiments within the vascular stage must be performed *in vivo*, making these costly, time consuming, and extremely hard to control. In some cases, the technology available may be even insufficient to allow for proper experimentation. Additionally the use of animal testing in laboratory experiments has been increasingly criticised while tighter regulations have been put into place in many countries.

Thus, modelling can help experimentalists check hypotheses and design experiments in order to test their theories, while also reducing the amount of animal testing performed. Therefore, advances in mathematical modelling, such as formulating and solving a relevant mathematical model, may shorten the route to discovery of better treatment possibilities or even a cure.

1.3 MOTIVATION OF MATHEMATICAL AND MODELLING APPROACHES

1.3.1 *Exploring Avascular Tumours*

Most of the models that attempt to characterise vascular tumour growth are actually based on avascular tumour growth models. Not only are these simpler, but there is data regarding *in vitro* experiments in literature in order to validate them, which makes them ideal for a first approach. On the other hand, there are clear parallels between avascular and vascular growth, especially at the beginning of the process of vascularisation, which makes avascular growth ultimately relevant.

1.3.2 *Studying Stability*

The study of stability is important in tumour growth models. Stability can represent a non-malignant dormant tumour that stabilises at a certain size and can potentially be moved by redirecting its nutrient supply. On the other hand, instability may represent a malignant tumour that grows uncontrollably, disintegrates or even breaks into pieces. In the study of avascular tumours, particularly, the distinction between dormant and malignant tumours is a central point of research and this motivates the use of linear stability and perturbation methods to study the model proposed in the next chapter.

1.3.3 *Using a Multiphase Model*

In this thesis, we will study a two phase model of avascular tumour growth. Multiphase models consider the simultaneous movement of materials in different states (liquids, gases and solids) or with different chemical properties, such as viscosity and heterogeneity. In tumour modelling, these phases can be, among others, healthy and cancer cells, extra-cellular material, and blood vessels, which will clearly have different properties. Additionally, these phases may not be all included simultaneously in every model, depending on the complexity needed.

Indeed, this makes multiphase formulations conveniently constructive. For example, it is not hard to find a four phase model of vascular tumour growth based upon the two phase model of avascular tumour growth which we will consider here (see [19] [43]). Thus, the chosen model will be a strong foundation for working with multiphase models of vascular tumour growth in the future.

1.4 LITERARY REVIEW

1.4.1 *The Early Biological and Mathematical Discoveries*

The understanding of tumour growth is based on three main discoveries to date:

1. An avascular tumour depends on the diffusion of nutrients through its outer surface. Therefore, as it grows larger, its innermost cells gradually receive less nutrients, which triggers the creation of a necrotic core and leads to a stable diffusion-limited steady state.

2. A tumour needs to vascularise to grow past the diffusion-limited steady state.

3. In order to become truly harmful and incurable, a tumour must metastasise.

Although a complete review of the literature available about tumour growth would require much more space than available, here we shall explore some of the first experiments and models representing each of the discoveries above and present a seminal model before delving into more modern models of avascular tumour growth in the next sections.

For other information on the research done in tumour growth models, we refer to the following reviews: [3, 65, 20, 34, 14, 15], and the references therein.

The avascular tumour and the diffusion-limited steady state

The earliest tumour models focused solely on growth dynamics of avascular tumours. It was expected initially that the entire volume of the tumour would proliferate and that the tumour would grow exponentially. However, as Maneord set out to compare the natural growth of tumours to that of tumours under the effect of X-radiations, he unexpectedly discovered that these tumours grew linearly after some time, as opposed to exponentially [52]. He also noticed that opened tumours proved the existence of a necrotic core. This, in turn, hinted that only the outermost cells reproduce, accounting therefore for a more moderate growth than expected.

While radiation continued to be explored, interest shifted towards understanding the effect of radiation on cells provided with different levels of oxygen. In this regard, it was discovered that anoxic cells are less effected by irradiation than well oxygenated cells ([22, 55, 56, 37]). This prompted clinicians to start coupling radiotherapy treatment with increased oxygen pressures [24, 54].

Continuing to delve into the relationship between oxygen and growth, Thomlinson and Gray [69] calculated an estimate of the radius of a tumour cord at the time in which oxygen stops reaching the center and the average size of the tumour at the onset of necrosis and noticed that the latter is

slightly larger than the former. Although this seems to suggest that the supply of oxygen is a strong factor for determining the onset of necrosis, the authors warned that "this numerical agreement is not advanced as evidence that cells at the center in fact die, through lack of oxygen" [69].

Then, in 1964, analyzing tumour growth on a larger time scale, Laird noticed that the time it takes the tumour cell population to double increases faster than it would if the population were growing at an exponential rate. Having noticed this, she successfully applied the Gompertzian equation to the growth of mouse, rat, and rabbit tumours over larger time scales [45].

The Gompertzian equation originated from an actuarial model [36] and can be written as

$$\frac{R(t)}{R(0)} = e^{\frac{A}{\alpha}(1-e^{-\alpha t})},$$

where R is here the tumour size and A, α are positive constants. Notice that this implies, particularly, that

$$\lim_{t\to\infty} \frac{R(t)}{R(0)} = e^{A/\alpha}$$

and, if we express $e^{-\alpha t}$ as a power series of αt, for small values of αt we have that

$$\frac{R(t)}{R(0)} \approx e^{At}.$$

Therefore, this approximation accounts for both the diffusion limited steady state and the initial exponential growth and agrees very well with the data of several types of tumours grown *in vivo*.

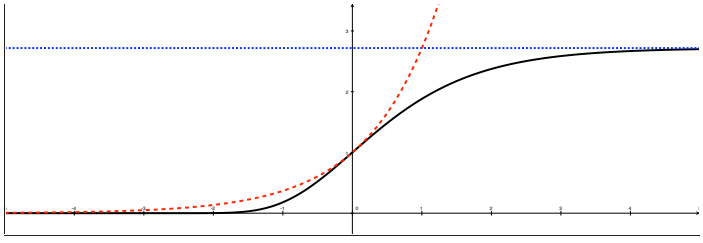


Figure 1.: The Gompertzian with Corresponding Exponential and Asymptote

To explain this exponential retardation, Burton proposed a diffusion model that studied not only the oxygen levels but also its effect on the relationship between the necrotic core radius and the tumour radius [12]. With this, he proposed that, with the formation of the necrotic core, proliferation continued on an outer ring with a constant mitotic rate. Through this mechanistic model, he was able to improve on the Gompertzian approximation by predicting also the intermediate linear growth that was seen in previous experiments.

The Importance of Vascularisation

One of the crucial results in angiogenesis research was Folkman's discovery of dormant avascular tumour nodules in vivo [28]. Folkman also developed the technique of isolated organ perfusion, while searching for a way to view solid tumours growing in a more detached way from its host than a purely in vivo approach [29]. Through this technique, he observed that neovascularisation of in vitro tumours was crucial to providing significant growth.

The Origin of Metastases

Although the metastatic process was not always understood, the importance of secondary tumours in the prognosis of a patient had already been clinically recognised in the sixteenth century [75]. The relation between invasion and the primary tumour started to be explored with the work of Cruveilier and Lomer, in the nineteenth century, who suggested a link between the circulation of tumour cells and the development of metastases [23, 51]. A stronger result came from Liotta et al [49], who observed that just after the formation of a vascular network, tumour cells appeared in the surrounding liquid, which was subjected to perfusion. Later, the same researchers added that larger primary tumours produced more secondary

tumours, which therefore reinforced the idea that in fact these secondary tumours originated from the primary tumours and spread through the circulatory system [50].

1.4.2 *The Birth of Mathematical Models of Tumour Growth*

One of the most seminal models of avascular tumour growth was an influential model set up by Greenspan [39, 40] to extend the models of Burton [12] and Thomlinson and Gray [69]. This model worked with a compartmental view of the tumour, which was taken to be spherical with three distinct areas: a necrotic core, a thin proliferating external ring and an intermediate quiescent region which was eventually disregarded.

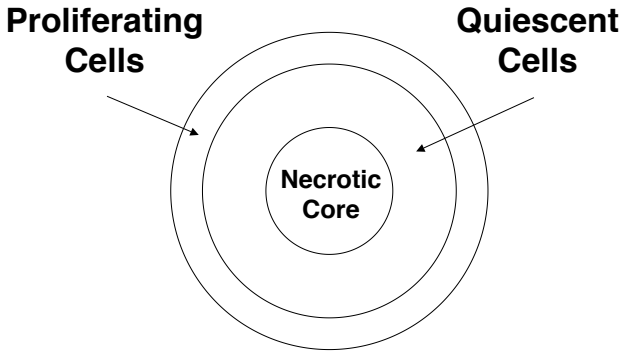


Figure 2.: The tumour according to Greenspan

Greenspan assumed the existence of both a nutrient and a chemical mitosis inhibitor which together drive the dynamics of the tumour. Critical nutrient and inhibitor concentrations define the position of each of the compartments within the tumour. He also assumed that the debris generated by dying cells is eventually broken down into simpler chemical compounds which are then diffused out of the tumour into its surroundings. When this happens, forces of adhesion and surface tension pull the cells inwardly.

Equations were written and solved in each of the regions, inspiring many other subsequent compartmental models, e.g [53],[16]. On the other hand, the assumptions involved in this model carried onto most of the following models of avascular tumour growth (compartmental or not).

1.4.3 *The Modern Mathematical Models of Tumour Growth*

It is impossible to consider all the mathematical models of tumour growth here, so we will consider the beginnings of multiphase models and their applications to tumour growth. More models of tumour growth can be found in the following reviews: [3, 65].

From the very definition of the multiphase model, it is possible to see that it is a versatile approach in modelling many dynamic processes including weather changes, avalanches, mud slides, glacier melting, sediment transport, debris flows, oil and gas recovery, among many others. Although the theory was developed from the 1960s [71, 70, 6, 4, 5, 7, 26, 60, 64], and applied in many problems in industrial mathematics [27, 25, 31], it has only recently been applied to tumour growth, with papers starting mostly in the mid 1990s.

The main difference of these new multiphase models is that they consider the stresses, forces and mechanical interactions in the system and how they dictate the evolution of the tumour. Previous models would simply assume that a necrotic core would form at a critical nutrient/oxygen concentration. In the mid 1990s, there was not much modelling done to explore how this necrotic region actually appeared. Multiphase models incorporate the dependence on the nutrient concentration into the rate of proliferation and decay of cells and thus the model can bring about the existence of a necrotic core naturally rather than as an initial supposition. The use of such a technique was driven by experimental evidence which suggested

that a more complex set of processes are involved in the development of the necrotic core, such as apoptosis, or programmed cell death [57].

One of the first models to use this approach was one proposed by Ward and King in [72], which was later expanded in [73]. In the first article, they considered a tumour as a mixture of two species: live cells and dead cells, in which the live cells proliferate and die in rates that depend on the local nutrient concentration. In this manner, cell death is actually a continuous process and not imposed by a nutrient concentration threshold set *a priori*. Indeed, these changes in volume generate a velocity field for the cells which drives the growth dynamics of the tumour. However, the authors recognised that this model did not include the mechanisms that allow for a diffusion limited steady state, and these were added in the second article ([73]), which we will describe here in more detail.

Indeed, in [73], the tumour was modelled as a mixture of two species: living cells and cellular material, with concentrations n and p, respectively. As cells die, they become cellular material which then is either consumed by living cells in order to drive cell mitosis or is leaked out of the tumour. These two mechanisms of depletion of cellular material were added onto the previous formulation in [72] in order to allow for a diffusion limited steady state. This yields the equations

$$\begin{cases} \dfrac{\partial n}{\partial t} = [k_m(c,p) - k_d(c)]n - \nabla \cdot (\mathbf{v}n), \\ 0 = D\nabla^2 c - k(c,p)n, \\ \dfrac{\partial p}{\partial t} = D_p \nabla^2 p + \mu k_d(c)n - \lambda k_m(c,p)n - \nabla \cdot (\mathbf{v}p), \\ \nabla \cdot \mathbf{v} = (V_L - \lambda V_p)k_m(c,p)n - (V_L - V_D)k_d(c)n + V_p D_p \nabla^2 p, \end{cases}$$

where c is the nutrient concentration and $\mathbf{v}$ is the velocity field, and the following rates are given by Michaelis–Menten type expressions:

$$k_m(c,p) = A\Big(\frac{c^{m_1}}{c_c^{m_1}+c^{m_1}}\Big)\Big(\frac{p^{m_3}}{p_c^{m_3}+p^{m_3}}\Big), \qquad \text{(cell birth rate)},$$

$$k_d(c) = B\Big(1-\sigma\frac{c^{m_2}}{c_d^{m_2}+c^{m_2}}\Big), \qquad \text{(cell death rate)},$$

$$k(c,p) = A\Big(\frac{c^{m_1}}{c_c^{m_1}+c^{m_1}}\Big)\Big[\beta_1+\beta_2 A\Big(\frac{p^{m_3}}{p_c^{m_3}+p^{m_3}}\Big)\Big], \quad \text{(nutrient uptake rate)}.$$

Here, the authors also used V_D as the volume of a dead cell, V_p as the volume of a molecule of basic cellular material, and V_L as the average volume of a living cell, where $V_L - \lambda V_p$ is the volume change during mitosis and $V_L - V_D$ the volume change during death and these satisfy

$$V_D = \mu V_p, \qquad 1 = V_L n + V_p p \text{ (no void)}.$$

All other details can be found in [74] and [72].

Because the same velocity was assigned to both species, this is not quite a multiphase model. However, it was one of the first to move away from the supposition of a nutrient threshold driving cell death towards one in which the cell net proliferation rate depends on the local nutrient concentration and thus drives the tumour dynamics. No assumptions were made about the heterogeneity of the tumour, and this is a great step away from the Greenspan model described in the last section. Another interesting legacy of this model was the choice of Michaelis-Menten type expressions for the cell birth, death and nutrient uptake rates described above, which are more realistic than the simplistic expressions used in other models.

Soon after, one of the first multiphase models of tumour growth was proposed by Please *et al.* [61], who considered a one dimensional model of a tumour composed of two phases: extracellular water and tumour cells, which were treated as inviscid fluids with different velocities U_l and U_c, respectively, which were assumed to be related by $U_l = -U_c$. However, the authors made an assumption on the pressure of the cells and water that was never biologically proven and it was soon modified

in future formulations. Indeed, this model supposed that cells ripped apart and ruptured if the local cell pressure became smaller than the local water pressure. Nevertheless, applying this model to a tumour grown in a test tube, the authors were able to observe initial exponential growth, the onset of cell death, and consequent linear growth with an outer rim of proliferating cells exhibiting a fixed thickness. However, this model did not include surface tension, which is crucial in maintaining the compactness of the tumour. Consequently, this was included in [62], which then considered cell movement as being a slow viscous flow in a spherical geometry.

One simplification these last two models adopted was the neglect of interphase drag forces in the force balance equation, which were then inserted in [46], where a smoother assumption was also made on the relationship between the cell and water pressures. Indeed, they assumed that if the cell pressure became smaller than the water pressure, then the cell in such a region would die and the cell material would continue to fill the space, characterising the necrotic region. With this set-up, these authors concentrated their analysis on the effects of surface tension in the development of a necrotic region and the possibility of the tumour reaching a diffusion-limited steady state. They concluded that smaller surface tension made the spheroid grow linearly in time and develop a large necrotic region, while larger surface tension permitted a steady state with a necrotic region.

Building on these previous works, the model with which we will work in this thesis was posed in [19]. The authors proposed a two phase model of tumour growth where the tumour was composed of cells and water, which were treated as viscous and inviscid incompressible fluids, respectively. To each of these phases, the authors assigned a velocity, a pressure, and a volume-fraction-average stress tensor. By applying mass and momentum balances to each phase, they obtained a model, which was fully formulated in one dimension.

Here, for the first time, the relationship between the cell and water pressures (p_c, p_w) was defined as

$$p_c = p_w + \Sigma_c(\alpha), \qquad \Sigma_c(\alpha) = \frac{\hat{\Sigma}_c |\alpha - \alpha^*|^{r-1}}{(1-\alpha)^q}(\alpha - \alpha^*)H(\alpha - \alpha_{min}),$$

where H is the Heaviside function and q, r, and $\hat{\Sigma}_c$ are positive constants. Additionally, $0 < \alpha_{min} < \alpha^* < 1$ with α^* being the natural cell packing density. Here, the cell pressure p_c represents the isotropic stresses associated with cell-cell interactions and the fluid pressure p_w is the hydrodynamic pressure in the water. In summary, the equation above states that the difference in pressure between the two phases may depend on the cell concentration. Choosing $\Sigma_c(\cdot)$ wisely, this allows the authors to model cell-cell interaction and membrane stress. For this, they devised the definition above.

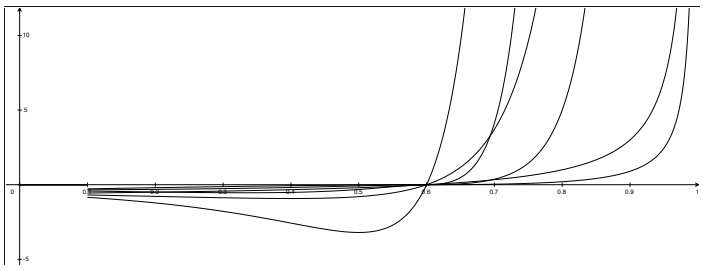


Figure 3.: Examples of the function $\Sigma_c(\alpha)$ for several values of r and q, and $\alpha_{min} = 0.1$, $\alpha^* = 0.6$, $\hat{\Sigma}_c = 1$.

It implies that, if the cells are packed closely together, i.e. $\alpha > \alpha^*$, then cells tend to move apart. If they are far apart, i.e. $\alpha < \alpha^*$, the cell's filopodia may come into contact and stimulate cell aggregation. However, if they are too far apart, i.e. $\alpha < \alpha_{min}$, cell and water pressure will be the same, and cells will not be repelled or attracted to other cells. Since the correct behaviour in multiphase models depends strongly on the interaction between the phases, it is invaluable to have such a detailed description of the difference between the pressure of the water and the cells.

The definition of $\Sigma_c(\alpha)$ and its effect on the dynamics of the tumour will be considered in this thesis. The formulation of this model according to the article [19] will be discussed in more detail in the next chapter.

A slightly simpler model based on this two-phase model was considered in [9], in which the authors hypothesised a relationship between cell viscosity and the degree of differentiation of tumour cells, and therefore of the tumour's invasiveness. They discovered that poorly differentiated tumours (i.e. the most aggressive ones) are characterised by less inter-cellular cohesion and thus may be hypothesised to have a smaller cell viscosity than their well-differentiated counterparts. Indeed, through simulations it was seen that lower cell viscosity implied faster tumour growth than higher cell viscosity. They also investigated the relationship between drag and tension and tumour growth, concluding that an increase in the drag parameter decelerates growth while an increase in the tension coefficient (akin to $\hat{\Sigma}_c$ in the definition of $\Sigma_c(\alpha)$ above) accelerates growth.

The two previous two-phase models have inspired later multiphase models, notably, the models of vascular tumour growth of three and four phases seen in [10, 43]. In the former, the authors model vascular tumour growth by adding a third phase to represent the blood vessels. By considering the three phases as inviscid fluids and tracking the pressure inside the tumour, the authors were able to model the collapse of vessels due to high pressure. The authors assumed that this collapse causes the death of surrounding cells and the consequent decrease of pressure which may allow the vessel to decompress.

In [43], the authors model and simulate vascular tumour growth by considering four phases: normal cells, tumour cells, blood vessels, and extracellular material. In this case, each phase is taken to behave as a viscous fluid. A hybrid finite volume and finite element algorithm is described to accompany the simulations performed of this model, where the tumour boundary is not tracked explicitly, but as a slightly diffuse moving front.

Extensions of these multiphase models have also been used to model tissue engineering. In these applications, extracellular fluids and cells flow through a fixed, solid phase which is added to represent a porous scaffold used by experimentalists to allow cell attachment and migration and ultimately guide tissue growth. See, for example, [48, 47, 58, 59].

2

FORMULATION OF A TWO-PHASE MODEL OF AVASCULAR TUMOUR GROWTH

2.1 GENERAL MODEL FORMULATION

2.1.1 *Introduction and Motivation*

We turn now to exploring the two-phase model of avascular tumour growth that will permeate the entire thesis and was proposed by Byrne, King, McElwain and Preziosi in 2003 [19]. As we have mentioned in the previous chapter, this is one of the seminal multiphase models of tumour growth. By considering two limit cases of this model, the authors were able to draw parallels to previous models of tumour growth such as [35], [66], [39], and [1]. On the other hand, it has been extended to three and four phase models of vascular tumour growth in [10] and [43], respectively, using similar arguments as the ones used in this chapter.

In this two-phase model, the authors assume that the tumour is composed only of cells and water, whose volume fractions we denote by α and β, respectively. This way, they satisfy the no void relation, i.e.

$$\alpha + \beta = 1, \qquad 0 < \alpha, \beta < 1.$$

For each phase, consider the quantities $(\mathbf{v}_c, p_c, \boldsymbol{\sigma}_c)$ and $(\mathbf{v}_w, p_w, \boldsymbol{\sigma}_w)$, the velocity, pressure, and volume-fraction-averaged stress tensor for the cell and the water phases, respectively. The equations that define the dynamics

of the tumour were derived from the application of mass and momentum balances to each phase, along with the definition of constitutive equations based on the assumptions on the viscosity of each phase.

2.1.2 *Mass Balances*

Indeed, considering both phases as incompressible fluids, mass balance equations may be expressed as

$$\frac{\partial \alpha}{\partial t} + \nabla \cdot (\mathbf{v}_c \alpha) = S_c \qquad \frac{\partial \beta}{\partial t} + \nabla \cdot (\mathbf{v}_w \beta) = S_w = -S_c$$

where S_c and S_w are the net cell proliferation and water conversion rates, respectively. The authors also assume that the volume conversion rate is $S_w = -S_c$ and thus that cells are mostly made up of water. In other words, cells use water to undergo mitosis and proliferate and later become water when they die. This guarantees the conservation of total volume, since volume lost from one phase is balanced by an equal volume increase in the other phase.

Adding the equations above and using the no-void condition, one can represent the mass balance equations as

$$\frac{\partial \alpha}{\partial t} + \nabla \cdot (\mathbf{v}_c \alpha) = S_c \qquad \nabla \cdot (\alpha \mathbf{v}_c + (1-\alpha)\mathbf{v}_w) = 0. \tag{1}$$

2.1.3 *Momentum Balances*

The authors assumed that the Reynolds number of the flow was low enough to neglect inertial effects, that the momentum due to phase change is negligible, and that there are no external forces acting on the system. Therefore, momentum laws became merely a question of force balances.

Indeed, if $\mathbf{F}_{cw}$ is the force exerted on the cells by the water and $\mathbf{F}_{wc}$ is defined analogously, then $\mathbf{F}_{cw} = -\mathbf{F}_{wc}$ and the momentum balance equations for the cell, liquid, and mixture may be written as

$$0 = \nabla \cdot (\alpha \boldsymbol{\sigma}_c) + \mathbf{F}_{cw} \tag{2}$$

$$0 = \nabla \cdot [(1-\alpha)\boldsymbol{\sigma}_w] + \mathbf{F}_{wc} \tag{3}$$

$$0 = \nabla \cdot (\alpha \boldsymbol{\sigma}_c + (1-\alpha)\boldsymbol{\sigma}_w), \tag{4}$$

since $\beta = 1 - \alpha$.

2.1.4 *Constitutive Assumptions*

Now, using properties of avascular tumours inferred from the literature, the authors determined the constitutive equations for σ_c, σ_w, $\mathbf{F}_{wc}$, and S_c that will close the system.

For example, by treating cells as a viscous incompressible fluid and water as an inviscid incompressible fluid, we see that

$$\boldsymbol{\sigma}_c = -p_c\mathbf{I} + \mu_c(\nabla \mathbf{v}_c + \nabla \mathbf{v}_c^T) + \lambda_c(\nabla \cdot \mathbf{v}_c)\mathbf{I} \qquad \boldsymbol{\sigma}_w = -p_w\mathbf{I}, \tag{5}$$

where μ_c and λ_c are shear and bulk viscosity coefficients of the cell phase, and $\mathbf{I}$ the identity tensor.

The authors also assumed that the pressure difference between the cell and water phases is a function of α, i.e:

$$p_c = p + \Sigma_c(\alpha), \qquad p := p_w. \tag{6}$$

In other words, the difference in pressure between the two phases may depend on the cell concentration. Choosing $\Sigma_c(\cdot)$ wisely, this allows the authors to model cell-cell interaction and membrane stress.

Finally, the authors assume that the forces applied on the water by the cells consists of contributions due to pressure and drag, such that

$$\mathbf{F}_{wc} = p\nabla(1-\alpha) - k(\alpha)(\mathbf{v}_w - \mathbf{v}_c), \tag{7}$$

where $k(\alpha)$ is the drag coefficient.

The two equations extracted from the constitutive assumptions will be obtained through some algebra. Indeed, by inserting (5) and (6) into (4), we see that

$$\begin{aligned}
0 &= \nabla \cdot (\alpha \boldsymbol{\sigma}_c + (1-\alpha)\boldsymbol{\sigma}_w) \\
&= \nabla \cdot (-\alpha p_c \mathbf{I} + \mu_c \alpha (\nabla \mathbf{v}_c + \nabla \mathbf{v}_c^T) + \lambda_c \alpha (\nabla \cdot \mathbf{v}_c)\mathbf{I} - (1-\alpha)p_w \mathbf{I}) \\
&= \nabla \cdot (-\alpha (p + \Sigma_c(\alpha))\mathbf{I} + \mu_c \alpha (\nabla \mathbf{v}_c + \nabla \mathbf{v}_c^T) + \lambda_c \alpha (\nabla \cdot \mathbf{v}_c)\mathbf{I} - (1-\alpha)p\mathbf{I}) \\
&= \nabla \cdot (-p\mathbf{I} - \alpha \Sigma_c(\alpha)\mathbf{I} + \mu_c \alpha (\nabla \mathbf{v}_c + \nabla \mathbf{v}_c^T) + \lambda_c \alpha (\nabla \cdot \mathbf{v}_c)\mathbf{I}). \qquad (8)
\end{aligned}$$

Similarly, inserting (3), (5), and (6) into (7), we have that

$$\begin{aligned}
p\nabla(1-\alpha) - k(\alpha)(\mathbf{v}_w - \mathbf{v}_c) = \mathbf{F}_{wc} &= -\nabla \cdot ((1-\alpha)\boldsymbol{\sigma}_w) \\
&= -\nabla \cdot ((1-\alpha)(-p_w \mathbf{I})) = \nabla \cdot ((1-\alpha)p\mathbf{I}) \\
&= \nabla((1-\alpha)p) = p\nabla(1-\alpha) + (1-\alpha)\nabla p \qquad \text{(Product Rule)}
\end{aligned}$$

and therefore

$$0 = (1-\alpha)\nabla p + k(\alpha)(\mathbf{v}_w - \mathbf{v}_c). \qquad (9)$$

2.1.5 *Nutrient Diffusion*

Finally, as in the Greenspan model, the authors assume that the growth rate of the tumour cells is regulated by only one nutrient which is distributed homogeneously and abundantly in the material surrounding the tumour. As it is consumed, it diffuses through the tumour. In this manner, by assuming a pseudo-steady state approximation, the nutrient concentration C is taken to satisfy

$$0 = \nabla^2 C - Q_c(\alpha, C), \qquad (10)$$

where $Q_c \geq 0$ is the rate at which the tumour cells consume nutrients.

This type of pseudo steady state approximation for the nutrient is quite common in tumour modelling ([61, 9, 8, 74, 73, 72, 39]), and we will consider

briefly why this is indeed reasonable. Notice that, accounting for advection and diffusion, our equation would be the following:

$$\frac{\partial C}{\partial t} + \nabla \cdot (\mathbf{v}_w C) = D\nabla^2 C - Q_c(\alpha, C).$$

Moreover, as seen for example in [11], [72], [39], an appropriate nondimensionalisation of the equation above would lead to an equation of the type

$$\epsilon \left[\frac{\partial \tilde{C}}{\partial \tau} + \nabla \cdot (\tilde{\mathbf{v}}_w \tilde{C}) \right] = \nabla^2 \tilde{C} - \tilde{Q}_c(\tilde{\alpha}, \tilde{C}),$$

where

$$\epsilon = \frac{\text{nutrient diffusion timescale}}{\text{tumour doubling timescale}}.$$

Therefore, since the nutrient diffusion timescale (hours) is much smaller than the tumour proliferation timescale (months), it is expected that ϵ will be in fact small, justifying then the approximation in equation (10). In other words, nutrient distribution adapts quickly to changes in the size of a tumour [1], [18].

2.1.6 *Important Functions*

All that remains to be done is to define the functions $S_c(\alpha, C)$, $\Sigma_c(\alpha)$, $k(\alpha)$, and $Q_c(\alpha, C)$, which we will consider separately. Equations obtained above for this multiphase model come mainly from first principles of continuum mechanics and the assumptions on incompressibility and viscosity of phases. However, the definitions of the following functions are derived from assumptions on the local interaction between the phases and ultimately drive the dynamics within the tumour. Thus, they will be studied separately in detail.

$S_c(\alpha, C)$

Consider the following definition for the net cell proliferation term S_c:

$$S_c(\alpha, C) = \Big(\frac{s_0 C}{1 + s_1 C}\Big)\alpha(1-\alpha) - \Big(\frac{s_2 + s_3 C}{1 + s_4 C}\Big)\alpha,$$

where $s_i > 0$ for all $i = 0 \dots 4$. The first term in S_c is the cell proliferation rate, while the second is the cell death rate.

In fact, it claims that cells reproduce at a rate proportional to the cell and water density with coefficient $\dfrac{s_0 C}{1 + s_1 C}$, an increasing function of C, thus accounting for importance of nutrients, water and cells in the process of mitosis. Indeed, these components are not only important but also necessary for cell proliferation, as the limits of the first term above when $C \to 0$, $\alpha \to 0$ and $\beta = 1 - \alpha \to 0$ are all null.

On the other hand, in the second term, the rate of cell death is proportional to the cell density, with coefficient $\dfrac{s_2 + s_3 C}{1 + s_4 C}$, which is

$$\begin{cases} \text{an increasing function of } C, & \text{if } s_3 - s_2 s_4 > 0 \\ \text{a decreasing function of } C, & \text{if } s_3 - s_2 s_4 < 0. \end{cases} \tag{11}$$

Since, cells tend to die less when there are more nutrients, the most important cases to consider are the ones with $s_3 - s_2 s_4 < 0$. (However, in numerical simulations we have also considered cases with $s_3 - s_2 s_4 > 0$ for completion, as one could, for example, choose to see C as a drug rather than a nutrient concentration.)

Notice that here the authors do not differentiate between different cell loss mechanisms such as necrosis and apoptosis, or programmed cell death. For this, see [17], [53].

Notice also that

$$\lim_{\alpha \to 0} S_c = 0, \qquad \lim_{\alpha \to 1} S_c = \lim_{\beta \to 0} S_c = -\frac{s_2 + s_3 C}{1 + s_4 C} < 0, \qquad \lim_{C \to 0} S_c = -s_2 \alpha < 0.$$

These are all expected, since cells are (obviously) necessary for cell proliferation or death, and cells tend to die when deprived of water or nutrients.

$\Sigma_c(\alpha)$

Recall that the function $\Sigma_c(\alpha)$ is defined as the difference between the pressures of the two phases. As stated in the last chapter, the authors chose this function to be

$$\Sigma_c(\alpha) = p_c - p_w = \frac{\hat{\Sigma}_c|\alpha - \alpha^*|^{r-1}}{(1-\alpha)^q}(\alpha - \alpha^*)H(\alpha - \alpha_{min})$$

where H is the Heaviside function and q, r, and $\hat{\Sigma}_c$ are positive constants. Additionally, $0 < \alpha_{min} < \alpha^* < 1$ with α^* being the natural cell density. The Σ_c function will become especially important in the study of linear stability in Chapters 4 and 5. (A detailed biological explanation of Σ_c can also be found in the previous chapter.)

$k(\alpha)$

Consider the following definition for the drag coefficient:

$$k(\alpha) = k_0\alpha(1-\alpha), \qquad k_0 > 0.$$

It is easy to see that $k(\alpha)$ is a quadratic with zeros at $\alpha = \{0, 1\}$ and maximum at $\alpha = 1/2$ where $k(\alpha) = k_0/4$. In other words, the inter-phase drag tends to disappear as water or cells become scarce and is maximum when both water and cell density are maximum (and equal).

$Q_c(\alpha, C)$

Finally, consider the following definition for the nutrient uptake:

$$Q_c(\alpha, C) = \frac{Q_0 C\alpha}{1 + Q_1 C}, \qquad Q_0, Q_1 > 0.$$

This definition of Q_c implies that the cells consume nutrients at a rate proportional to the cell concentration, with coefficient $\dfrac{Q_0 C}{1 + Q_1 C}$, an increasing function of C. This demonstrates the importance (and indeed, the necessity) of cell and nutrients in the process of nutrient uptake, (as the limit of Q_c when either C or α tend to zero is null).

Moreover, it is easy to see that

$$\sup_{0<\alpha<1} Q_c = \lim_{\alpha\to 1} Q_c = \frac{Q_0 C}{1+Q_1 C}, \qquad \sup_{C>0} Q_c(\alpha, C) = \lim_{C\to\infty} Q_c = \frac{Q_0\alpha}{Q_1}.$$

The former is obvious, as the greater nutrient consumption must take place with higher cell concentration. The latter, signifies that no matter how much nutrient is available, cells can only consume so much, and this quantity is proportional to the density of the cell population.

2.1.7 *Conclusion*

Therefore, from equations (1), (8), (9) and (10), the authors have developed the following system:

$$\begin{cases} \dfrac{\partial \alpha}{\partial t} &= S_c(\alpha, C) - \nabla\cdot(\mathbf{v}_c\alpha), \\ 0 &= \nabla\cdot(\alpha\mathbf{v}_c + (1-\alpha)\mathbf{v}_w), \\ 0 &= \nabla\cdot(-p\mathbf{I} - \alpha\Sigma_c(\alpha)\mathbf{I} + \mu_c\alpha(\nabla\mathbf{v}_c + \nabla\mathbf{v}_c^T) + \lambda_c\alpha(\nabla\cdot\mathbf{v}_c)\mathbf{I}), \\ 0 &= (1-\alpha)\nabla p + k(\alpha)(\mathbf{v}_w - \mathbf{v}_c), \\ 0 &= \nabla^2 C - Q_c(\alpha, C). \end{cases} \tag{12}$$

Additionally, the following choices were made for $S_c(\alpha, C)$, $Q_c(\alpha, C)$, $k(\alpha)$, and $\Sigma_c(\alpha)$:

$$S_c(\alpha, C) = \Big(\frac{s_0 C}{1+s_1 C}\Big)\alpha(1-\alpha) - \Big(\frac{s_2 + s_3 C}{1+s_4 C}\Big)\alpha \tag{13}$$

$$Q_c(\alpha, C) = \frac{Q_0 C\alpha}{1+Q_1 C} \tag{14}$$

$$k(\alpha) = k_0\alpha(1-\alpha) \tag{15}$$

$$\Sigma_c(\alpha) = \frac{\hat{\Sigma}_c|\alpha-\alpha^*|^{r-1}}{(1-\alpha)^q}(\alpha-\alpha^*)H(\alpha-\alpha_{min}), \tag{16}$$

where s_i $(i = 0\ldots 4)$, Q_0, Q_1, k_0, q, r, $0 < \alpha_{min} < \alpha^* < 1$ and $\hat{\Sigma}_c$ are all positive constants, and α^* is the natural cell density.

As in the paper in question, we will consider next the one dimensional formulation along with its boundary conditions and postpone the definition of the boundary conditions for the two dimensional system until Chapter 7.

2.2 ONE DIMENSIONAL MODEL FORMULATION

In order to define a complete one dimensional model from the equations above, the authors were left with the task of defining a domain along with boundary and initial conditions, which we will explore in this section.

2.2.1 *Equations and their Domain*

Consider a symmetric tumour that grows in one direction, parallel to the x-axis such that $(x, y) \in \mathbb{R}^2$ within the tumour at time t satisfies $-R(t) \leq x \leq R(t)$. With these assumptions, the equations of the system defined in the previous section become

$$\begin{cases} \dfrac{\partial \alpha}{\partial t} = S_c - \dfrac{\partial}{\partial x}(v_c \alpha) & (17) \\ 0 = \dfrac{\partial}{\partial x}(\alpha v_c + (1-\alpha) v_w) & (18) \\ 0 = \dfrac{\partial}{\partial x}\Big(- p - \alpha \Sigma_c(\alpha) + \hat{\mu}_c \alpha \dfrac{\partial v_c}{\partial x}\Big) & (19) \\ 0 = (1-\alpha)\dfrac{\partial p}{\partial x} + k(\alpha)(v_w - v_c) & (20) \\ 0 = \dfrac{\partial^2 C}{\partial x^2} - Q_c(\alpha, C), & (21) \end{cases}$$

where $\hat{\mu}_c = 2\mu_c + \lambda_c$.

In this formulation, the tumour boundary $R(t)$ will grow or shrink depending on the velocity of the cells at the boundary, and thus can be modelled by the following moving boundary condition:

$$\frac{dR}{dt}(t) = v_c(R(t), t).$$

2.2.2 *Boundary Conditions*

For the other unknowns, the authors considered the following boundary conditions

$$\begin{cases} v_c = v_w = \dfrac{\partial C}{\partial x} = 0, & \text{at } x = 0, \\ C = C_\infty, \quad p = 0, \quad \hat{\mu}_c \dfrac{\partial v_c}{\partial x} - \Sigma_c(\alpha) = 0, & \text{on } x = R(t). \end{cases} \tag{22}$$

Here, the first three conditions account for symmetry of the velocities and the nutrient concentration about $x = 0$. The subsequent condition guarantees the continuity of the nutrient concentration, where C_∞ represents the concentration of nutrients outside of the tumour, kept constant by an abundant source.

The last two conditions on the moving boundary require a bit more care. These stem from assuming that the pressure is normalised such that $p = 0$ represents the ambient water pressure outside of the tumour and that the tumour boundary is taken to be stress free, thus guaranteeing the continuity of the normal component of the cell and water stress tensors. In other words, using the definitions of the stress tensors posed in two dimensions in the previous section, the last two boundary conditions can be extracted from

$$0 = \boldsymbol{\sigma}_c \cdot \mathbf{n} = (-p - \Sigma_c(\alpha) + \hat{\mu}_c \frac{\partial v_c}{\partial x})\mathbf{n}, \qquad 0 = \boldsymbol{\sigma}_w \cdot \mathbf{n} = -p\mathbf{n}$$

when growth is one dimensional and therefore $\mathbf{n} = (1, 0)$.

2.2.3 *Solving for v_w and p*

By integrating and using the boundary conditions described above, the authors could obtain expressions for v_w and p in terms of the other unknowns and thus reduce the system to one on only four unknowns, namely

$$(\alpha(x,t), v_c(x,t), C(x,t), R(t)).$$

Indeed, by integrating (18) from 0 to $x < R(t)$ and using the boundary condition $v_c = v_w = 0$ at $x = 0$, we see that

$$0 = \int_0^x \frac{\partial}{\partial s}(\alpha v_c + (1-\alpha)v_w)\mathrm{d}s = \alpha v_c + (1-\alpha)v_w,$$

i.e., the following equation defines v_w within the tumour:

$$v_w = -\frac{\alpha}{1-\alpha}v_c. \tag{23}$$

Similarly, integrating (19) from $x < R(t)$ to $R(t)$ and using the boundary conditions $p = 0$, and $\hat{\mu}_c \frac{\partial v_c}{\partial x} - \Sigma_c(\alpha) = 0$ at $x = R(t)$, we have that

$$0 = \int_x^{R(t)} \frac{\partial}{\partial s}\Big(- p - \alpha\Sigma_c(\alpha) + \hat{\mu}_c \alpha \frac{\partial v_c}{\partial s}\Big)\mathrm{d}s = p + \alpha\Sigma_c(\alpha) - \hat{\mu}_c\alpha\frac{\partial v_c}{\partial x},$$

i.e., the following equation defines p within the tumour:

$$p = \hat{\mu}_c \alpha \frac{\partial v_c}{\partial x} - \alpha\Sigma_c(\alpha). \tag{24}$$

2.2.4 *Simplified One Dimensional Model - Conclusion*

Therefore, by simple substitution of (23) and (24) into (20), we have that the one dimensional model can be simplified to be

$$\begin{cases} \dfrac{\partial \alpha}{\partial t} = S_c(\alpha, C) - \dfrac{\partial}{\partial x}(\alpha v_c) & (25) \\ 0 = \dfrac{\partial}{\partial x}\Big(\hat{\mu}_c \alpha \dfrac{\partial v_c}{\partial x} - \alpha\Sigma_c(\alpha)\Big) - \dfrac{k(\alpha)}{(1-\alpha)^2}v_c & (26) \\ 0 = \dfrac{\partial^2 C}{\partial x^2} - Q_c(\alpha, C), & (27) \end{cases}$$

subject to the moving boundary condition

$$\frac{dR}{dt}(t) = v_c(R(t), t),$$

and the boundary and initial conditions

$$\begin{cases} v_c = \dfrac{\partial C}{\partial x} = 0, & \text{at } x = 0, \\ C = C_\infty, \quad \hat{\mu}_c \dfrac{\partial v_c}{\partial x} - \Sigma_c(\alpha) = 0, & \text{on } x = R(t), \\ \alpha = \alpha_0, \quad R = R_0, \quad v_c = v_0, \quad C = C_0, & \text{at } t = 0. \end{cases} \tag{28}$$

Additionally, once the system above is determined, v_w, p and p_c can therefore be characterised by the expressions

$$v_w = -\frac{\alpha}{1-\alpha}v_c \qquad p = \hat{\mu}_c \alpha \frac{\partial v_c}{\partial x} - \alpha \Sigma_c(\alpha) \qquad p_c = p + \Sigma_c(\alpha).$$

2.2.5 *Global Mass Equation*

Furthermore, notice that, by applying Leibniz integral rule and using the moving boundary equation, one can obtain

$$\begin{aligned} \frac{d}{dt}\int_0^{R(t)} \alpha \mathrm{d}x &= \int_0^{R(t)} \frac{\partial \alpha}{\partial t}\mathrm{d}x + \alpha(R(t),t)\frac{dR}{dt} \\ &= \int_0^{R(t)} \frac{\partial \alpha}{\partial t}\mathrm{d}x + \alpha(R(t),t)v_c(R(t),t). \end{aligned} \tag{29}$$

On the other hand, using (25), it is possible to see that

$$\begin{aligned} \int_0^{R(t)} S_c \mathrm{d}x &= \int_0^{R(t)} \left(\frac{\partial \alpha}{\partial t} + \frac{\partial}{\partial x}(\alpha v_c)\right)\mathrm{d}x \\ &= \int_0^{R(t)} \frac{\partial \alpha}{\partial t}\mathrm{d}x + \alpha(R(t),t)v_c(R(t),t) - \alpha(0,t)v_c(0,t) \\ &= \int_0^{R(t)} \frac{\partial \alpha}{\partial t}\mathrm{d}x + \alpha(R(t),t)v_c(R(t),t), \end{aligned} \tag{30}$$

since $v_c(0,t) = 0$. Therefore, comparing the last two equalities, the authors obtain the following global mass equation, which will be used later:

$$\frac{d}{dt}\int_0^{R(t)} \alpha \mathrm{d}x = \int_0^{R(t)} S_c \mathrm{d}x. \tag{31}$$

2.3 ASYMPTOTIC LIMITS OF THE ONE DIMENSIONAL MODEL

Additionally, the authors considered two limit cases of the formulation described in Subsection 2.2.4. In the first of these, cell viscosity is considered to be negligible. The second limit case is then obtained from the first one by assuming that cell drag is also negligible. With these simplifications, each of these formulations resemble simpler models of tumour growth found in the literature.

2.3.1 *Negligible Cell Viscosity* ($\hat{\mu}_c \to 0$)

First, consider the case where cell viscosity is negligible, i.e. when $\hat{\mu}_c \to 0$. In this limit, (26) implies that

$$v_c = -\frac{(1-\alpha)^2}{k(\alpha)}\frac{\partial}{\partial x}(\alpha\Sigma_c(\alpha)). \tag{32}$$

Substituting this expression into (25), one obtains

$$\frac{\partial \alpha}{\partial t} = -\frac{\partial}{\partial x}(\alpha v_c) + S_c(\alpha, C) = \frac{\partial}{\partial x}\left[\frac{\alpha(1-\alpha)^2}{k(\alpha)}\frac{\partial}{\partial x}(\alpha\Sigma_c(\alpha))\right] + S_c(\alpha, C).$$

Directly from (32), it is possible to extract a moving boundary equation for $R(t)$, namely

$$\frac{dR}{dt}(t) = v_c(R(t), t) = -\left[\frac{(1-\alpha)^2}{k(\alpha)}\frac{\partial}{\partial x}(\alpha\Sigma_c(\alpha))\right]_{x=R(t)}.$$

Therefore, the equations in this limit case can be reduced to

$$\begin{cases} \dfrac{\partial \alpha}{\partial t} &= \dfrac{\partial}{\partial x}\left[\dfrac{\alpha(1-\alpha)^2}{k(\alpha)}\dfrac{\partial}{\partial x}(\alpha\Sigma_c(\alpha))\right] + S_c(\alpha, C), \\ 0 &= \dfrac{\partial^2 C}{\partial x^2} - Q_c(\alpha, C), \end{cases} \tag{33}$$

with moving boundary equation

$$\frac{dR}{dt}(t) = -\left[\frac{(1-\alpha)^2}{k(\alpha)}\frac{\partial}{\partial x}(\alpha\Sigma_c(\alpha))\right]_{x=R(t)}.$$

Consider the following boundary conditions:

$$\begin{cases} \dfrac{\partial C}{\partial x} = \dfrac{\partial \alpha}{\partial x} = 0, & \text{at } x = 0, \\ C = C_\infty, \quad \alpha = \alpha^*, & \text{on } x = R(t), \\ \alpha = \alpha_0, \quad R = R_0, \quad C = C_0, & \text{at } t = 0. \end{cases} \tag{34}$$

Notice that the conditions on C and R were kept as before. However, one must impose the two boundary conditions previously assigned to v_c via the boundary conditions on α. First, notice that $\alpha = \alpha^*$ on the outer boundary implies that $\Sigma_c(\alpha^*) = 0$ and therefore $\hat{\mu}_c\dfrac{\partial v_c}{\partial x} - \Sigma_c(\alpha) \to 0$, when $x = R(t)$ and $\hat{\mu}_c \to 0$. On the other hand, by expanding (32), it is possible to see that

$$v_c = -\frac{(1-\alpha)^2}{k(\alpha)}\frac{\partial}{\partial x}(\alpha\Sigma_c(\alpha)) = -\frac{(1-\alpha)^2}{k(\alpha)}(\alpha\Sigma_c(\alpha))'\frac{\partial \alpha}{\partial x}$$

and therefore $\frac{\partial \alpha}{\partial x}(0,t) = 0$ implies that $v_c(0,t) = 0$ and consequently $v_w(0,t) = 0$, from (23). In other words, the conditions in (34) define one possible (non-unique) set of boundary conditions that guarantee that the original boundary conditions in (22) are satisfied when $\hat{\mu}_c \to 0$.

Additionally, one can also pull together equations (24), (32), and (23) to find relationships between the pressure and velocity of each phase. Indeed, from (24), we see that, if viscosity is neglected,

$$p_w = p = -\alpha \Sigma_c(\alpha) \tag{35}$$

$$p_c = p_w + \Sigma_c(\alpha) = -\alpha \Sigma_c(\alpha) + \Sigma_c(\alpha) = (1-\alpha)\Sigma_c(\alpha). \tag{36}$$

Therefore, by (35), (32), (23), and (15), we see that

$$\begin{aligned} \frac{\partial p_w}{\partial x} &= -\frac{\partial}{\partial x}(\alpha \Sigma_c(\alpha)) = \frac{k(\alpha)}{(1-\alpha)^2} v_c = -\frac{k(\alpha)}{(1-\alpha)^2} \cdot \frac{(1-\alpha)}{\alpha} v_w \\ &= -\frac{k(\alpha)}{\alpha(1-\alpha)} v_w = -\frac{k_0 \alpha (1-\alpha)}{\alpha(1-\alpha)} v_w = -k_0 v_w. \end{aligned} \tag{37}$$

Similarly, from (36) and (32) we see that

$$\frac{\partial}{\partial x}\left(\alpha \frac{p_c}{1-\alpha}\right) = \frac{\partial}{\partial x}(\alpha \Sigma_c(\alpha)) = -\frac{k(\alpha)}{(1-\alpha)^2} v_c = -\frac{k_0 \alpha}{(1-\alpha)} v_c. \tag{38}$$

Therefore, this limit case is made up of a reaction diffusion equation for α and a quasi-steady reaction diffusion equation for C, where the velocities are given by darcy-type laws. This is similar to reaction-difusion models of tumour growth, e.g. [35] and [66], except for the fact that this model tracks the tumour as a moving boundary problem and that the cell-cell interaction defines the cell diffusion term, rather than random motion.

2.3.2 *Negligible Cell Viscosity and Drag* $\left(\hat{\mu}_c, \frac{k(\alpha)}{(\alpha \Sigma_c(\alpha))'} \to 0\right)$

From (37), we see that

$$v_w = \frac{1}{k_0} \frac{\partial}{\partial x}(\alpha \Sigma_c(\alpha)) = \frac{(\alpha \Sigma_c(\alpha))'}{k_0} \frac{\partial \alpha}{\partial x} = \frac{1}{k_0 / (\alpha \Sigma_c(\alpha))'} \frac{\partial \alpha}{\partial x}$$

which we may insert into (23) to conclude that

$$v_c = -\frac{1-\alpha}{\alpha} v_w = -\frac{1-\alpha}{k_0 \alpha / (\alpha \Sigma_c(\alpha))'} \frac{\partial \alpha}{\partial x}$$
$$= -\frac{(1-\alpha)^2}{k_0 \alpha (1-\alpha) / (\alpha \Sigma_c(\alpha))'} \frac{\partial \alpha}{\partial x} = -\frac{(1-\alpha)^2}{k(\alpha) / (\alpha \Sigma_c(\alpha))'} \frac{\partial \alpha}{\partial x}.$$

With this, consider the effects of a negligible drag, i.e.

$$\frac{k(\alpha)}{(\alpha \Sigma_c(\alpha))'} \to 0.$$

Assuming $\alpha \geq \alpha_{min}$ and $\dfrac{(\alpha \Sigma_c(\alpha))'}{k(\alpha)} \dfrac{\partial \alpha}{\partial x} > 0$ in this limit, then

$$-(1-\alpha)^2 \geq -(1-\alpha_{min})^2$$

and

$$v_c = -\frac{(1-\alpha)^2}{k(\alpha) / (\alpha \Sigma_c(\alpha))'} \frac{\partial \alpha}{\partial x} \geq -\frac{(1-\alpha_{min})^2}{k(\alpha) / (\alpha \Sigma_c(\alpha))'} \frac{\partial \alpha}{\partial x}.$$

Therefore, if $v_c < \infty$, then we must have

$$\frac{\partial \alpha}{\partial x} \to 0 \qquad \text{as} \qquad \frac{k(\alpha)}{(\alpha \Sigma_c(\alpha))'} \to 0.$$

Thus, with negligible viscosity and drag, while increasing the distance from the axis of symmetry, the cell concentration adjusts rapidly to a constant in x, which in fact is constant in t and equal to α^* due to the outside boundary condition in (34).

In this case, the global mass balance equation (31) becomes

$$\int_0^{R(t)} S_c(\alpha^*, C) \mathrm{d}x = \frac{d}{dt} \int_0^{R(t)} \alpha \mathrm{d}x = \frac{d}{dt} \int_0^{R(t)} \alpha^* \mathrm{d}x = \alpha^* \frac{d}{dt} \int_0^{R(t)} \mathrm{d}x = \alpha^* \frac{dR}{dt},$$

and therefore our model reduces to

$$\begin{cases} \dfrac{dR}{dt} = \dfrac{1}{\alpha^*} \displaystyle\int_0^{R(t)} S_c(\alpha^*, C) \mathrm{d}x \\ \\ 0 = \dfrac{\partial^2 C}{\partial x^2} - Q_c(\alpha^*, C) \end{cases}$$

with boundary and initial conditions

$$\frac{\partial C}{\partial x}(0,t) = 0, \qquad C(R(t),t) = C_\infty, \qquad R(0) = R_0.$$

This model is based on the diffusion of the nutrient and its effect on the cell proliferation rate and tumour growth as were the earliest models of avascular tumour growth, for example [39], [1].

2.4 CONCLUSION

In this chapter, we described the formulation of the two phase model of avascular tumour growth found in [19]. Following the authors, we considered the multidimensional definitions for the model equations, the full one dimensional model, and two limit cases. Numerical simulations of the full one dimensional model and the negligible viscosity limit case will be presented in the next chapter.

3

NUMERICAL SIMULATIONS IN ONE DIMENSION

In this chapter, we use a finite difference method to perform numerical simulations of both the full one dimensional model and its negligible viscosity limit case. These two formulations can be found in Subsections 2.2.4 and 2.3.1, which may serve as helpful references in Subsections 3.1.1 and 3.2.1, respectively.

The aim is to observe the biological dynamics of tumour growth in the numerical solutions. By exploring several parameter sets, we discuss the dependence of the tumour growth and decay on the natural cell packing density α^*. Finally we compare the results of the full one dimensional model and its negligible viscosity limit case and consider the numerical limitations of the latter model.

3.1 FULL ONE DIMENSIONAL MODEL

3.1.1 *Formulation*

Consider again the one dimensional model described in Subsection 2.2.4. For simplicity, we choose $r = q = 1$ and $\alpha_{min} = 0$ in the definition of $\Sigma_c(\alpha)$, i.e,

$$\Sigma_c(\alpha) = \frac{\hat{\Sigma}_c|\alpha - \alpha^*|^{r-1}}{(1-\alpha)^q}(\alpha - \alpha^*)H(\alpha - \alpha_{min}) = \hat{\Sigma}_c\frac{\alpha - \alpha^*}{1-\alpha}. \tag{39}$$

Since most of the cases we simulate remain in regions of high cell density, we expect that the choice $\alpha_{min} = 0$ will not significantly effect our simulations. However, some effects will be discussed at the end of this chapter.

With this definition, through the chain and quotient rule, we may obtain

$$\frac{\partial}{\partial x}\big(\alpha\Sigma_c(\alpha)\big) = \hat{\Sigma}_c\frac{\partial}{\partial x}\left[\frac{\alpha(\alpha-\alpha^*)}{1-\alpha}\right] = -\hat{\Sigma}_c\left[\frac{\alpha^2-2\alpha+\alpha^*}{(1-\alpha)^2}\right]\frac{\partial\alpha}{\partial x}. \tag{40}$$

So, in reality, by using the expression above and the definition of $k(\alpha)$, the second equation in the full one dimensional model in Subsection 2.2.4 becomes

$$\begin{aligned} 0 &= \frac{\partial}{\partial x}\Big(\hat{\mu}_c\alpha\frac{\partial v_c}{\partial x} - \alpha\Sigma_c(\alpha)\Big) - \frac{k(\alpha)}{(1-\alpha)^2}v_c \\ &= \hat{\mu}_c\frac{\partial}{\partial x}\Big(\alpha\frac{\partial v_c}{\partial x}\Big) + \hat{\Sigma}_c\left[\frac{\alpha^2-2\alpha+\alpha^*}{(1-\alpha)^2}\right]\frac{\partial\alpha}{\partial x} - \frac{k_0\alpha v_c}{1-\alpha}. \end{aligned} \tag{41}$$

Therefore, through simple algebra, the one dimensional model in Subsection 2.2.4 can be recast as

$$\begin{cases} \dfrac{\partial\alpha}{\partial t} &= S_c(\alpha, C) - \dfrac{\partial}{\partial x}(\alpha v_c) \\ 0 &= \eta\dfrac{\partial}{\partial x}\Big(\alpha\dfrac{\partial v_c}{\partial x}\Big) + \nu_1(\alpha)\dfrac{\partial\alpha}{\partial x} - \kappa(\alpha, v_c) \\ 0 &= \dfrac{\partial^2 C}{\partial x^2} - Q_c(\alpha, C), \end{cases} \tag{42}$$

with moving boundary condition

$$\frac{dR}{dt}(t) = v_c(R(t), t),$$

subject to the boundary and initial conditions

$$\begin{cases} v_c = \dfrac{\partial C}{\partial x} = 0, & \text{at } x = 0, \\ C = C_\infty, \quad \eta\dfrac{\partial v_c}{\partial x} - \gamma\Big(\dfrac{\alpha-\alpha^*}{1-\alpha}\Big) = 0, & \text{at } x = R(t), \\ R = R_0, \quad \alpha = \alpha_0, \quad v_c = v_0, \quad C = C_0, & \text{at } t = 0, \end{cases} \tag{43}$$

where

$$\kappa(\alpha, v_c) = \frac{\alpha v_c}{1-\alpha}, \quad \nu_1(\alpha) = \gamma\left[\frac{\alpha^2-2\alpha+\alpha^*}{(1-\alpha)^2}\right], \quad \gamma = \frac{\hat{\Sigma}_c}{k_0}, \quad \eta = \frac{\hat{\mu}_c}{k_0}.$$

3.1.2 *Finite Difference Scheme*

Change of Variable - Fixing the Domain

Before applying a finite difference method, we will define our problem in a fixed domain. Since the current domain is

$$\{(x,t) \in (0,R(t)) \times (0,\infty)\},$$

we will consider the following change of variable:

$$x = x(t) = \xi R(t), \qquad \xi \in [0,1], \quad t \in (0,\infty).$$

Notice that, with this rescaling, the domain of interest becomes a fixed domain, namely:

$$\{(\xi,t) \in (0,1) \times (0,\infty)\},$$

where $\xi = 0$ and $\xi = 1$ are the inner and outer boundaries, respectively. When applying this rescaling, we obtain

$$\begin{aligned}
\frac{\partial}{\partial x} &\longrightarrow \frac{1}{R(t)}\frac{\partial}{\partial \xi} \\
\frac{\partial^2}{\partial x^2} &\longrightarrow \frac{1}{R(t)^2}\frac{\partial^2}{\partial \xi^2} \\
\frac{\partial}{\partial t} &\longrightarrow \frac{\partial}{\partial t} - \frac{\xi}{R(t)}\frac{dR}{dt}\frac{\partial}{\partial \xi}
\end{aligned}$$

by using the chain rule.

Finally, inserting this variable change into the system obtained in the previous section, it is possible to see that

$$\begin{cases}
\dfrac{\partial \alpha}{\partial t} = \dfrac{\xi}{R(t)}\dfrac{dR}{dt}\dfrac{\partial \alpha}{\partial \xi} - \dfrac{1}{R(t)}\dfrac{\partial}{\partial \xi}(\alpha v_c) + S_c(\alpha, C), & (44) \\
0 = \dfrac{\eta}{R(t)^2}\dfrac{\partial}{\partial \xi}\left(\alpha \dfrac{\partial v_c}{\partial \xi}\right) + \dfrac{\nu_1(\alpha)}{R(t)}\dfrac{\partial \alpha}{\partial \xi} - \kappa(\alpha, v_c), & (45) \\
0 = \dfrac{1}{R(t)^2}\dfrac{\partial^2 C}{\partial \xi^2} - Q_c(\alpha, C), & (46)
\end{cases}$$

with moving boundary condition

$$\frac{dR}{dt}(t) = v_c(1,t),$$

subject to the boundary and initial conditions:

$$\begin{cases} v_c = \dfrac{\partial C}{\partial \xi} = 0, & \text{at } \xi = 0, \\ C = C_\infty, \quad \dfrac{\eta}{R(t)} \dfrac{\partial v_c}{\partial \xi} - \gamma\Big(\dfrac{\alpha - \alpha^*}{1-\alpha}\Big) = 0, & \text{at } \xi = 1, \\ R = R_0, \quad \alpha = \alpha_0(\xi R_0), \quad v_c = v_0(\xi R_0), \quad C = C_0(\xi R_0), & \text{at } t = 0. \end{cases}$$

Notice that, inserting the moving boundary condition into (44) yields

$$\frac{\partial \alpha}{\partial t} = \frac{\xi}{R(t)} v_c(1,t) \frac{\partial \alpha}{\partial \xi} - \frac{1}{R(t)} \frac{\partial}{\partial \xi}(\alpha v_c) + S_c(\alpha, C), \tag{47}$$

which will be used in lieu of equation (44) in the next sections.

Now, we turn to defining a notation and formulating a finite difference scheme that will be used to numerically simulate solutions of the system above.

Notation

In what follows, functions taken on vectors are calculated entry by entry and the symbol "$\circ$" will denote the Hadamard Product, i.e.

$$\psi(\mathbf{x}) = \psi((x_1, x_2, \cdots, x_n)) = (\psi(x_1), \psi(x_2), \cdots, \psi(x_n))$$
$$\mathbf{x} \circ \mathbf{y} = (x_1, x_2, \cdots, x_n) \circ (y_1, y_2, \cdots, y_n) = (x_1 y_1, x_2 y_2, \cdots, x_n y_n),$$

for any function ψ and vectors $\mathbf{x}$ and $\mathbf{y}$. We will also occasionally employ the notation $P_i^j(\mathbf{x})$ to represent the vector formed by the entries i through j of the original vector $\mathbf{x}$, i.e.

$$P_i^j(\mathbf{x}) = (x_i, x_{i+1}, \ldots, x_{j-1}, x_j).$$

Defining a Partition

Consider a partition of $(0,1)$ with N evenly spaced nodes. Put differently, let

$$\boldsymbol{\xi} = (\xi_i)_1^N, \qquad \xi_i = \frac{i-1}{N-1}, \qquad i = 1, \ldots N.$$

Notice, particularly, that this implies that the first and last nodes correspond to the boundaries $\xi = \xi_1 = 0$ and $\xi = \xi_N = 1$. Accordingly, define

$$U_i(t) = \alpha(\xi_i, t), \qquad V_i(t) = C(\xi_i, t), \qquad W_i(t) = v_c(\xi_i, t),$$

and therefore the column vectors

$$\mathbf{U}(t) = (U_i(t))_1^N, \qquad \mathbf{V}(t) = (V_i(t))_1^N, \qquad \mathbf{W}(t) = (W_i(t))_1^N.$$

Applying the boundary conditions, with this notation, it is possible to obtain

$$\begin{cases} V_N(t) & = C(\xi_N, t) = C(1, t) = C_\infty, \\ W_1(t) & = v_c(\xi_1, t) = v_c(0, t) = 0. \end{cases}$$

Similarly, the boundary condition

$$\frac{\partial v_c}{\partial \xi} = \frac{\gamma R(t)}{\eta}\Big(\frac{\alpha - \alpha^*}{1 - \alpha}\Big), \quad \text{at } \xi = 1$$

allows us to approximate $W_N(t)$ by a function of $W_{N-1}(t)$, $W_{N-2}(t)$, $U_N(t)$, and $R(t)$. Indeed, using the backward second order finite difference approximation of the derivative in the equation above, we see that the boundary condition may be approximated by

$$\frac{W_{N-2}(t) - 4W_{N-1}(t) + 3W_N(t)}{2\Delta\xi} = \frac{\gamma R(t)}{\eta}\left(\frac{U_N(t) - \alpha^*}{1 - U_N(t)}\right),$$

and therefore, rearranging, we may set

$$W_N(t) = \frac{2(\Delta\xi)\gamma R(t)}{3\eta}\left(\frac{U_N(t) - \alpha^*}{1 - U_N(t)}\right) - \frac{1}{3}W_{N-2}(t) + \frac{4}{3}W_{N-1}(t). \tag{48}$$

Therefore, since V_N, W_1, and W_N are accounted in terms of the value of the unknown functions on the other nodes and $R(t)$, these motivate the following definitions:

$$\mathbf{v}(t) = P_1^{N-1}(\mathbf{V}(t)), \qquad \mathbf{w}(t) = P_2^{N-1}(\mathbf{W}(t)).$$

With this set-up, we conclude that our system may be approximated through a standard finite difference methods by a system on

$$\begin{aligned} \mathbf{Z}(t) &= (\mathbf{U}(t); \mathbf{v}(t); \mathbf{w}(t); R(t)) \\ &= (U_1(t), \cdots, U_N(t), V_1(t), \cdots, V_{N-1}(t), W_2(t), \cdots, W_{N-1}(t), R(t))^T \end{aligned}$$

of the form

$$M\frac{d\mathbf{Z}}{dt} = F(\mathbf{Z}),$$

where M is a square mass matrix of order $3N-2$ and $F(\mathbf{Z})$ is a column vector of length $3N-2$. Once solved, this approximation allows us to calculate W_N via equation (48) and thus piece together the vectors $(\mathbf{U};\mathbf{V};\mathbf{W};R)$ that approximate (α, C, v_c, R) for each time step.

All simulations in this Chapter were performed using MATLAB® ordinary differential equation solver "*ode23t*."

Defining $F(\mathbf{Z})$

With this notation, we may turn back to our equations to define F from the right hand side of our system. For that, we used standard second order finite difference approximations of the derivatives and applied the boundary conditions described above. The results of this process are stated below.

Equation on α:

According to the equation on α, the first N terms of $F(\mathbf{Z})$ are given by the right hand side of the column vector equation

$$\frac{d\mathbf{U}}{dt} = \frac{W_N}{R}(\boldsymbol{\xi} \circ D_x\mathbf{U}) - \frac{1}{R}(\mathbf{W} \circ D_x\mathbf{U}) - \frac{1}{R}(\mathbf{U} \circ D_x\mathbf{W}) + S_c(\mathbf{U},\mathbf{V}),$$

with $D_x\mathbf{U} = \dfrac{1}{2\Delta\boldsymbol{\xi}}(\underline{D_{x,u}}\mathbf{U})$, where

$$\underline{D_{x,u}} = \begin{pmatrix} -3 & 4 & -1 & & & \\ -1 & 0 & 1 & & & \\ & -1 & 0 & 1 & & \\ & & \ddots & \ddots & \ddots & \\ & & & -1 & 0 & 1 \\ & & & 1 & -4 & 3 \end{pmatrix}_{N\times N}$$

and $D_x\mathbf{W} = \frac{1}{2\Delta\xi}(\underline{D_{x,w}}\mathbf{w} + \mathbf{b})$, where

$$\underline{D_{x,w}} = \begin{pmatrix} 4 & -1 & & & & & \\ 0 & 1 & & & & & \\ -1 & 0 & 1 & & & & \\ & -1 & 0 & 1 & & & \\ & & \ddots & \ddots & \ddots & & \\ & & & -1 & 0 & 1 & \\ & & & & -1 & 0 & \\ & & & & 1 & -4 & \end{pmatrix}_{N\times(N-2)}$$

and

$$\mathbf{b} = W_N(0,\ldots,0,1,3)^T, \qquad b \in \mathbb{M}(N,1).$$

Equation on C:

Similarly, the next $N-1$ elements of $F(\mathbf{Z})$ are given by the right hand side of the column vector equation

$$0 = \frac{1}{R^2}D_{xx}\mathbf{V} - Q_c(\mathbf{u},\mathbf{v}),$$

where $D_{xx}\mathbf{V} = \frac{1}{(\Delta\xi)^2}(\underline{D_{xx,v}}\mathbf{v} + \mathbf{c})$, with

$$\underline{D_{xx,v}} = \begin{pmatrix} -2 & 2 & & & & & \\ 1 & -2 & 1 & & & & \\ & 1 & -2 & 1 & & & \\ & & \ddots & \ddots & \ddots & & \\ & & & 1 & -2 & 1 & \\ & & & & 1 & -2 & \end{pmatrix}_{(N-1)\times(N-1)}$$

and

$$\mathbf{c} = C_\infty(0,\ldots,0,1)^T, \qquad \mathbf{c} \in \mathbb{M}(N-1,1). \tag{49}$$

Equation on $\mathbf{v_c}$:

Again, by the same process, the next $N-2$ elements of $F(\mathbf{Z})$ may be written as the right hand side of the column vector equation

$$0 = P_2^{N-1}\left[\frac{\eta}{R^2}(D_x\mathbf{U}\circ D_x\mathbf{W}) + \frac{\eta}{R^2}(\mathbf{U}\circ D_{xx}\mathbf{W}) + \frac{1}{R}(\nu_1(\mathbf{U})\circ D_x\mathbf{U}) - \kappa(\mathbf{U},\mathbf{W})\right],$$

where $D_{xx}\mathbf{W} = \dfrac{1}{(\Delta\xi)^2}(\underline{D_{xx,w}}\mathbf{w} + \mathbf{d})$,

$$\underline{D_{xx,w}} = \begin{pmatrix} -5 & 4 & -1 & & & \\ -2 & 1 & & & & \\ 1 & -2 & 1 & & & \\ & 1 & -2 & 1 & & \\ & & \ddots & \ddots & \ddots & \\ & & & 1 & -2 & 1 \\ & & & & 1 & -2 \\ & & & -1 & 4 & -5 \end{pmatrix}_{N\times(N-2)}$$

and

$$\mathbf{d} = W_N(0,\ldots 0,1,2)^T, \qquad d \in \mathbb{M}(N,1).$$

Equation on R:

Finally, the moving boundary equation may be approximated by

$$\frac{dR}{dt}(t) = (F(\mathbf{Z}))_{3N-2,1} = v_c(1,t) = W_N(t)$$

and equation (48).

Defining M

To complete this formulation, we must define the mass matrix M to represent the left hand side of the system in question. Since a pseudo-steady

state approximation is assumed on the diffusion equation for C and $\frac{\partial v_c}{\partial t}$ does not appear in the equations, we must have

$$M = \begin{pmatrix} I_N & 0 & 0 & 0 \\ 0 & 0_{N-1} & 0 & 0 \\ 0 & 0 & 0_{N-2} & 0 \\ 0 & 0 & 0 & 1, \end{pmatrix},$$

where I and 0 are the identity and zero matrices of the designated orders.

Conclusion

Defining $\mathbf{Z}$, $F(\mathbf{Z})$ and M in the manner described above, we posses all the components necessary to approximate the system in question via a numerical approximation of the following problem:

$$\begin{cases} M\dfrac{d\mathbf{Z}}{dt} & = F(\mathbf{Z}) \\ \\ \mathbf{Z}(0) & = \begin{pmatrix} \alpha_0(\xi R_0) \\ P_1^{N-1}[C_0(\xi R_0)] \\ P_2^{N-1}[v_0(\xi R_0)] \\ R_0 \end{pmatrix}. \end{cases}$$

Indeed, once we obtain numerical results for $\mathbf{Z} = (\mathbf{U}; \mathbf{v}; \mathbf{w}; R)$, it is possible to retrieve an approximation $\tilde{\mathbf{Z}} = (\mathbf{U}; \mathbf{V}; \mathbf{W}; R)$ of the system in Subsection 3.1.2 by using the boundary conditions $V_N = C_\infty$, $W_1 = 0$ and the equation (48) to calculate W_N.

3.1.3 *Four Cases*

In this section, we simulate four cases of a one dimensional tumour evolving according to different parameter sets of the system above. The first two cases are ones in which the tumour grows while the last two cases are ones in which the tumour shrinks. We also consider higher values for the natural

cell packing density α^* in Cases 1 & 3 than in Cases 2 & 4 in order to hypothesise on the effect of the natural cell packing density on the tumour's development.

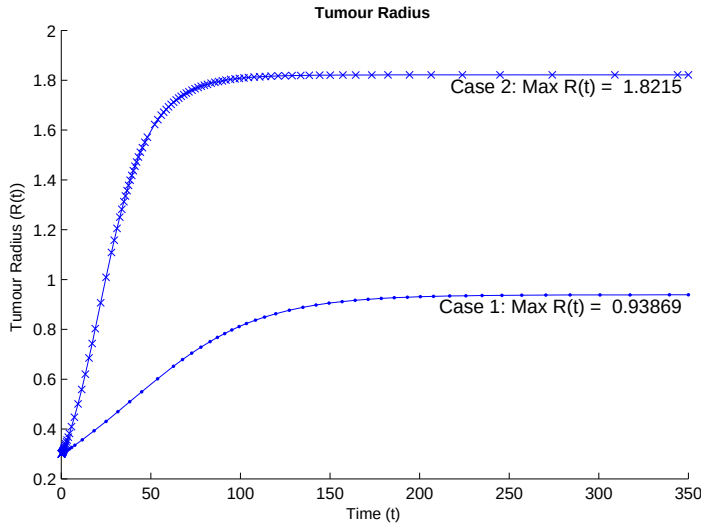


Figure 4.: Evolution of tumour radius in Cases 1 and 2 in the full one dimensional formulation. The only difference between these cases is the natural cell packing density α^*, which is 0.6 and 0.55, respectively. Therefore, here we see that the case with the lowest natural cell packing density grows faster and larger.

CASE 1: Here, we consider a tumour with high reproduction and low death rates, and therefore with a positive net cell proliferation rate. The nutrient outside the tumour is abundant and the speed of nutrient uptake is high. The natural cell packing density is 0.6.

CASE 2: Case 2 consists of a situation identical to Case 1, except that the natural cell packing density is taken to be 0.55.

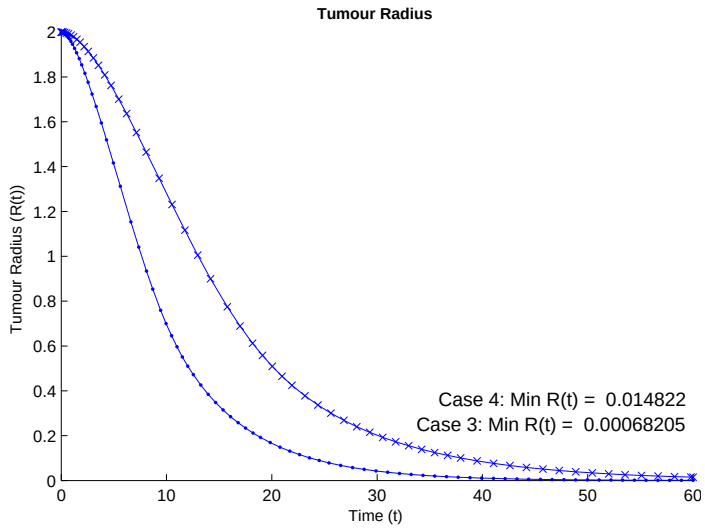


Figure 5.: Evolution of tumour radius in Cases 3 and 4 in the full one dimensional formulation. The only difference between these cases is the natural cell packing density α^*, which is 0.6 and 0.3, respectively. Therefore, here we see that the case with the highest natural cell packing density decays faster.

CASE 3: The third case considers a tumour with a negative net proliferation rate where cell decay is faster than cell mitosis. Nutrients are taken to be scarce, and consequently, the cells' nutrient uptake is taken to be slow. The natural cell packing density is 0.6.

CASE 4: The fourth case mirrors the third case, now with a natural cell packing density of 0.3.

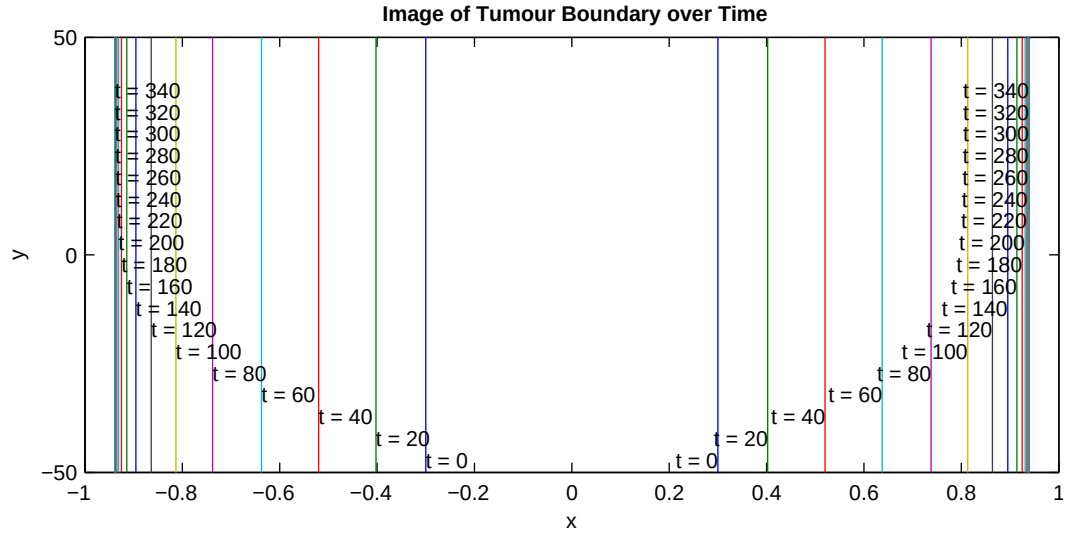


Figure 6.: Evolution of a tumour in Case 1 in the full one dimensional formulation.

From the graphs above, we may see that in fact the first two cases are ones in which the tumour radius $R(t)$ grows until it stabilises. From the literature, this is an expected behaviour. Indeed, as the tumour grows, diffusion becomes an increasingly ineffective way of supplying nutrients to the cells and thus causing cell death. Consequently, this decreases proliferation rates and diminishes the initially fast radius growth.

Now, notice that, the tumour in Case 2 grows faster and larger than the one in Case 1 and that the tumour in Case 4 recedes slower than the one in Case 3. Since the difference within these two pairs of cases is a variation in the value of α^*, we may hypothesize that lower natural packing densities make tumours grow faster and larger and recede slower than higher packing densities. This prediction does seem plausible biologically, as healthy cells naturally tend to reproduce more when there is sufficient space [65].

Below are the graphs of the cell concentration, nutrient concentration, and cell velocity that resulted from simulations of Cases 1 and 2:

Case 1 Graphs

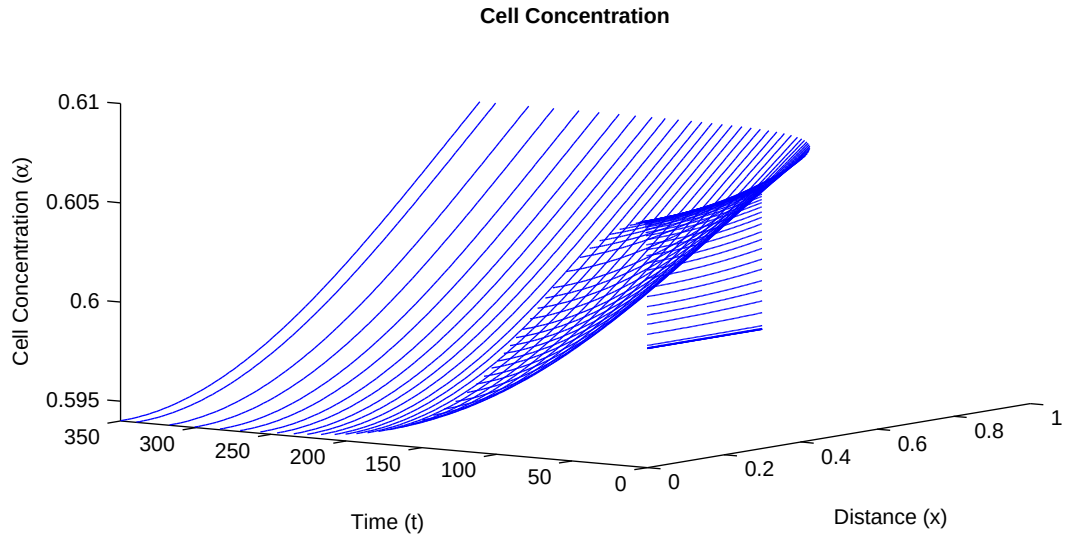


Figure 7.: Evolution of the cell concentration in Case 1 in the full one dimensional formulation.

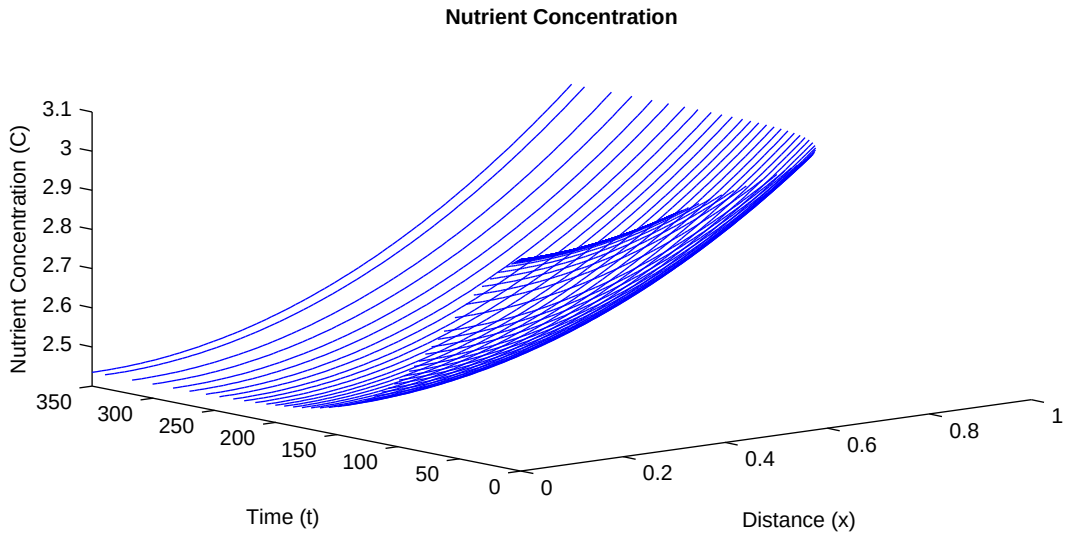


Figure 8.: Evolution of the nutrient concentration in Case 1 in the full one dimensional formulation.

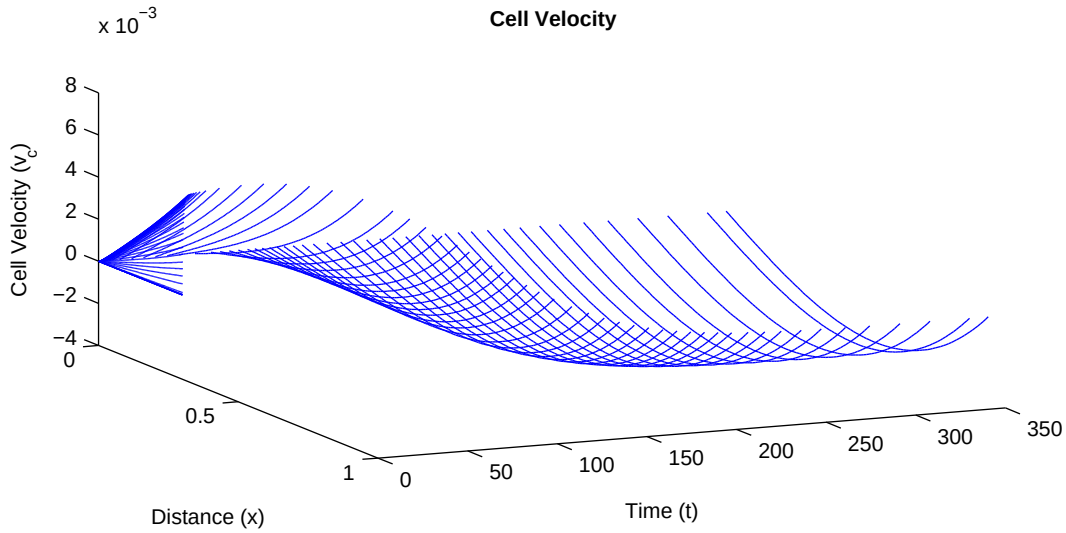


Figure 9.: Evolution of the cell velocity in Case 1 in the full one dimensional formulation.

Case 2 Graphs

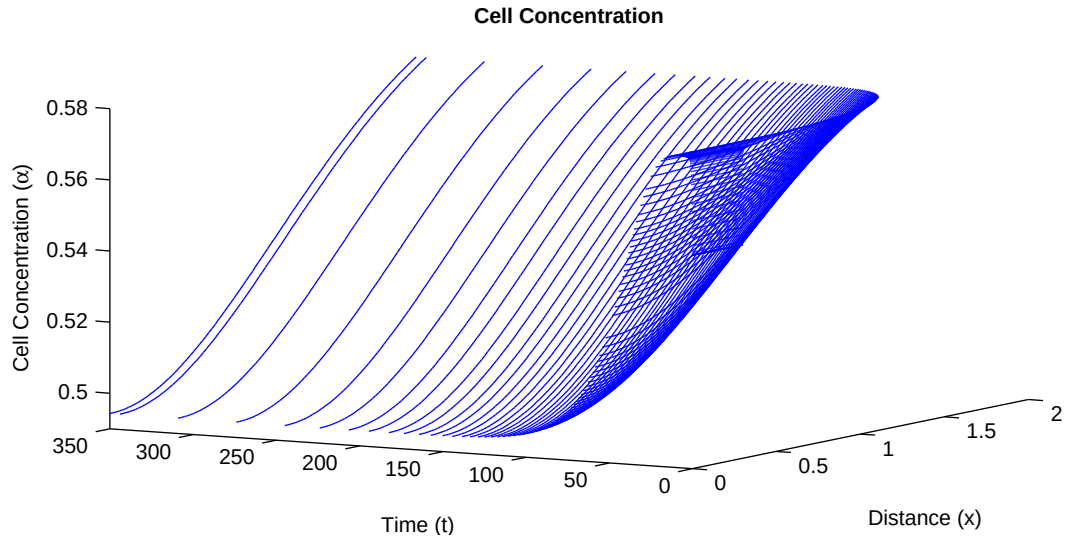


Figure 10.: Evolution of the cell concentration in Case 2 in the full one dimensional formulation.

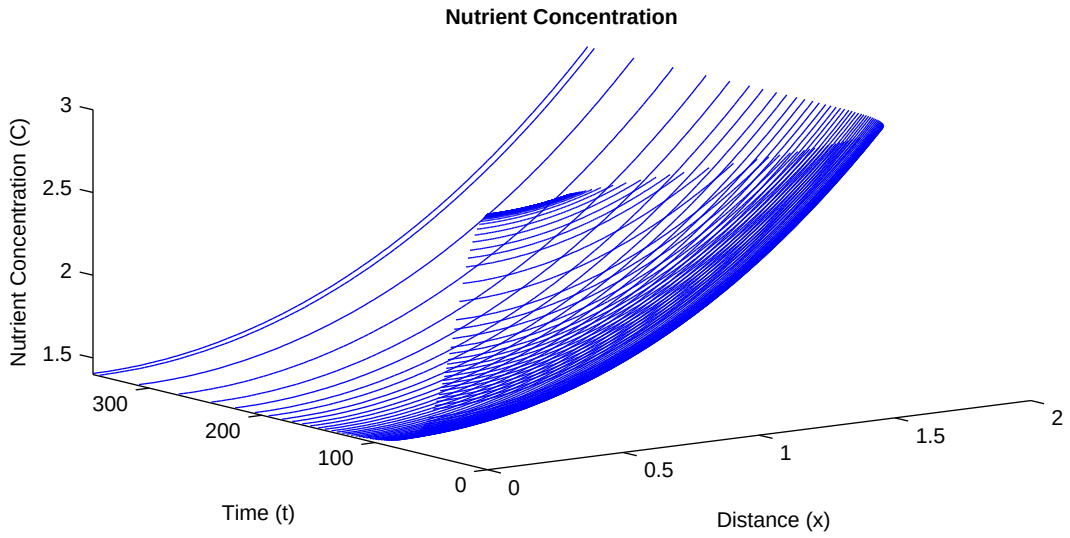


Figure 11.: Evolution of the nutrient concentration in Case 2 in the full one dimensional formulation.

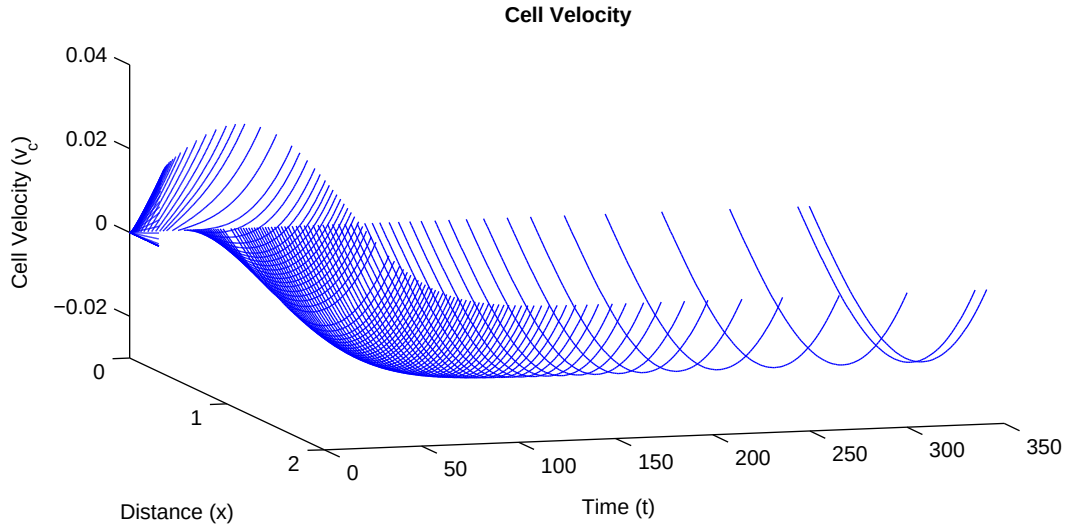


Figure 12.: Evolution of the cell velocity in Case 2 in the full one dimensional formulation.

Consider now the graphs above regarding the first two cases. Recall that the only difference between these two cases is the natural cell packing concentration, α^*, which is 0.6 in Case 1 and 0.55 in Case 2. Nevertheless, both cases present similar dynamics. Indeed, as the tumour grows, after a small increase in the cell concentration, the cells become more sparse in the

core and packed together near the border. The different α^* values account for the higher cell concentration in the boundary and also suggest the higher nutrient levels in the core in Case 1 as compared to the Case 2.

Biologically, this is all expected behaviour. Indeed, as it begins, the tumour is small with tumour cells at a natural state with high nutrient availability. Therefore, as expected, the tumour grows quickly. In fact, the tumour becomes crowded with a large amount of cells, which rapidly consume nutrients, thus decreasing the nutrient levels, especially in the core where the supply is deficient. This, in turn, will spur cell death, diminishing drastically the cell concentration in the core, leading to a smaller and ultimately negligible tumour growth.

From the velocity graphs, we may see that, initially, the cells exhibit rapidly increasing positive velocities, justifying the fast initial growth. However, as the innermost cells start dying, the velocity diminishes and becomes mostly negative within the tumour. Indeed, as the cells near the center die and turn into water, the core of the tumour attracts either reproducing cells in search of water or cramped cells in search of space. In any case, this movement is represented in the velocity graphs above by the negative valley-like shape formed after the initial period of exponential growth. Eventually, the velocity at the boundary becomes almost null, accounting therefore for the plateaus in Figure 4 that represent the diffusion limited steady state.

Consider below the graphs of the nutrient concentration, cell concentration, and cell velocity of the two decaying Cases (3 & 4).

Case 3 Graphs

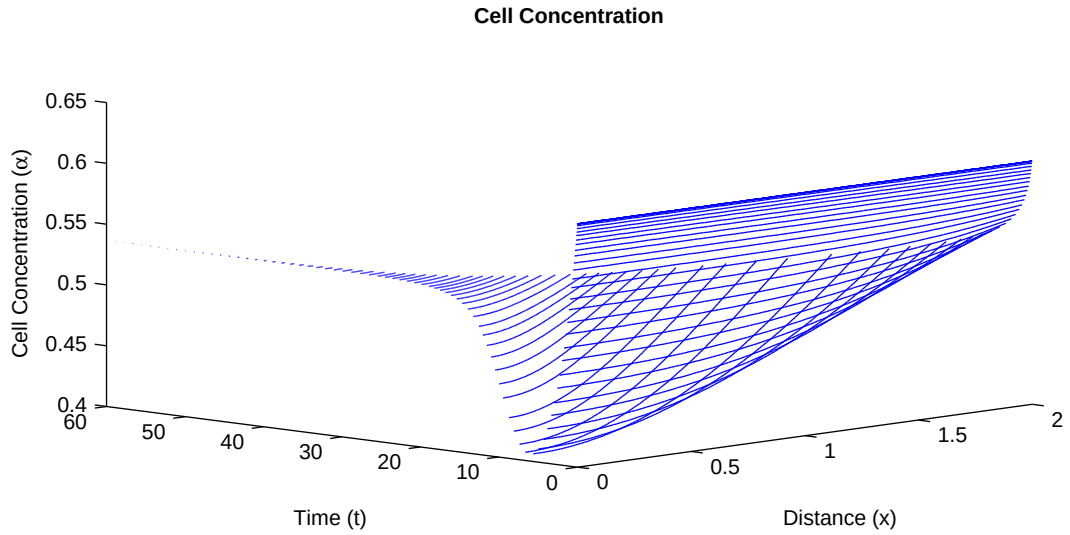


Figure 13.: Evolution of the cell concentration in Case 3 in the full one dimensional formulation.

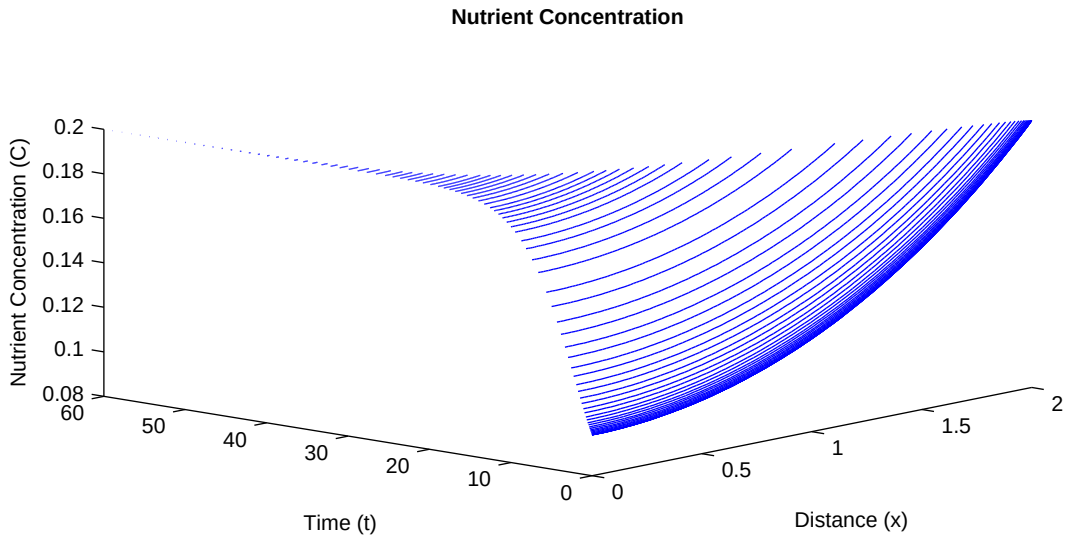


Figure 14.: Evolution of the nutrient concentration in Case 3 in the full one dimensional formulation.

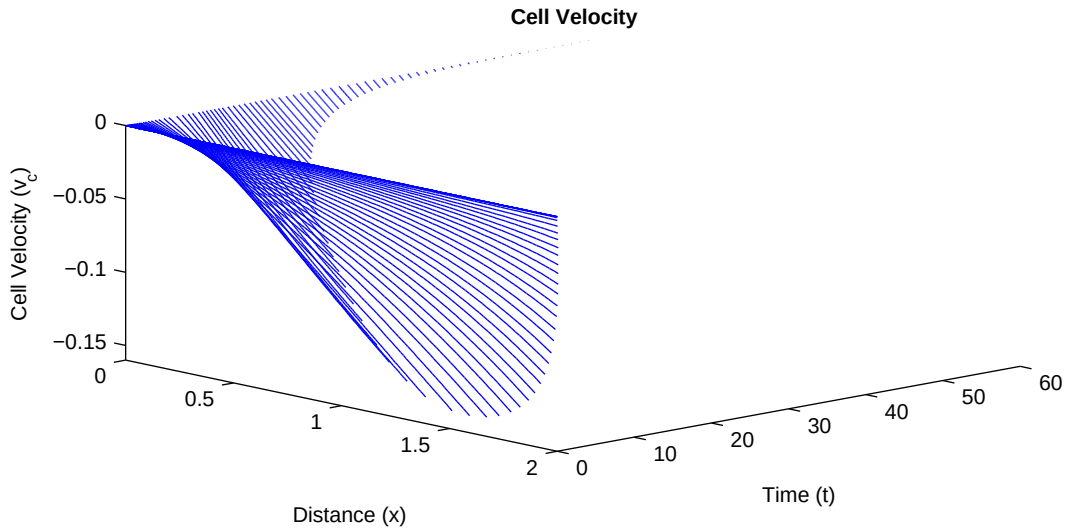


Figure 15.: Evolution of the cell velocity in Case 3 in the full one dimensional formulation.

Case 4 Graphs

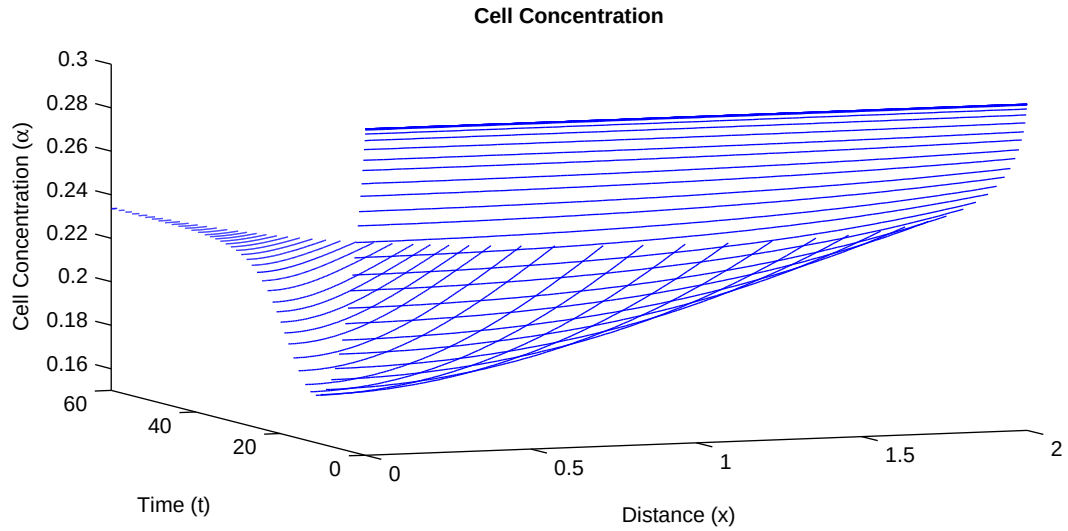


Figure 16.: Evolution of the cell concentration in Case 4 in the full one dimensional formulation.

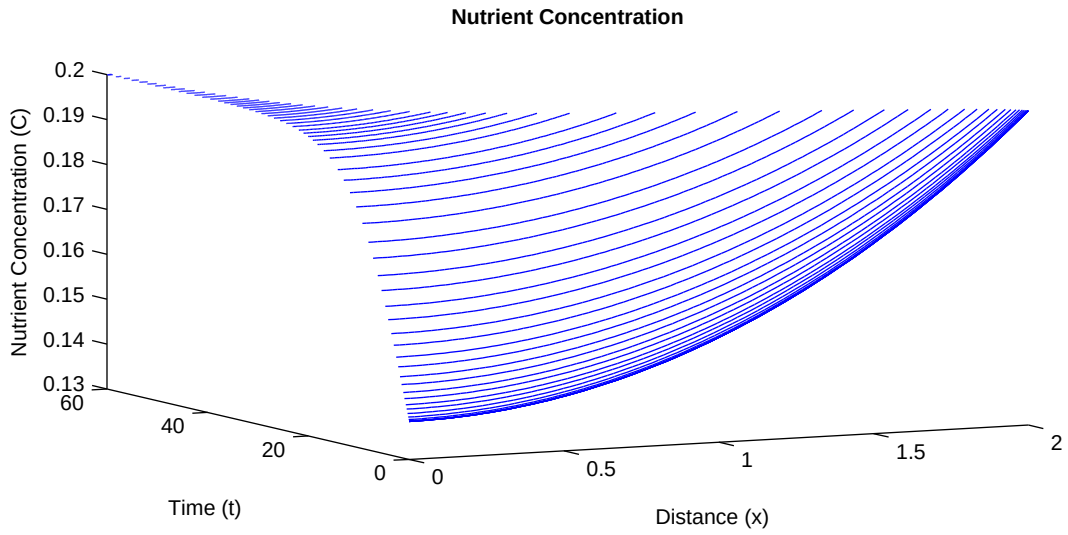


Figure 17.: Evolution of the nutrient concentration in Case 4 in the full one dimensional formulation.

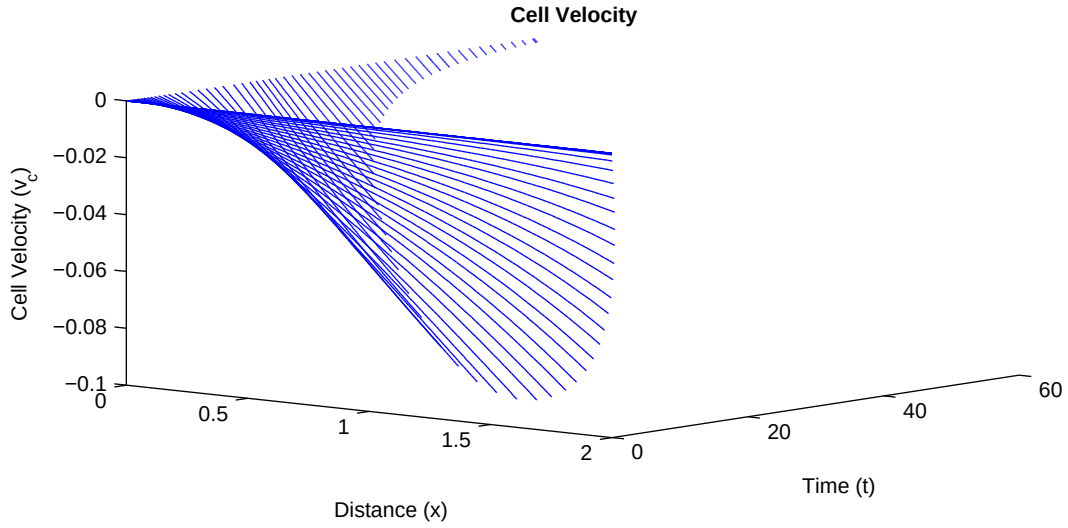


Figure 18.: Evolution of the cell velocity in Case 4 in the full one dimensional formulation.

As before, considering the graphs representative of Cases 3 and 4, we see that although α^* was changed between the cases, the overall behaviour was similar in all. As the tumour shrinks, the inner core cell concentration dips due to cell hypoxia and then rises towards a value close to α^* while the concentration near the boundary remains apparently constant, close to α^*.

Similarly, the nutrient starts with low values at the tumour core and stabilises towards C_∞, as the tumour shrinks and disappears. This is expected, since a small tumour has no difficulty spreading nutrients to its innermost cells. However, since the nutrient levels outside of the tumour are low, the tumour continues to shrink.

On the other hand, the cell velocity starts out null and quickly becomes negative as the tumour shrinks rapidly. Then, the velocity approaches a null velocity as the tumour tends to gradually disappear.

Final Remarks Regarding Simulations

For the sake of completeness, we specify the parameters used in each case:

Table 1.: Parameter Values of Cases 1 through 4

Case	α^*	C_∞	s_0	s_1	s_2	s_3	s_4	Q_0	Q_1	R_0	γ	η
1	0.60	3.0	2	1	1.0	1	2	3	1	0.3	1	1
2	0.55	3.0	2	1	1.0	1	2	3	1	0.3	1	1
3	0.60	0.2	1	1	0.1	1	2	1	3	2.0	1	1
4	0.30	0.2	1	1	0.1	1	2	1	3	2.0	1	1

Notice that the constants s_1, s_3, s_4, γ and η are taken to be the same in all cases. In particular, this means that the effects of changes in $\gamma = \widehat{\Sigma}_c/k_0$ and $\eta = \hat{\mu}_c/k_0$ were not analysed. Additionally, notice that the external nutrient concentration C_∞ was large and the initial tumour size R_0 was small in Cases 1 & 2 to promote growth and vice versa in Cases 3 & 4. Furthermore, all the initial conditions where constant:

$$\alpha = \alpha^*, \qquad C = C_\infty, \qquad v_c = 0, \qquad R = R_0.$$

3.2 ONE DIMENSIONAL MODEL WITH NEGLIGIBLE CELL VISCOSITY

In this section, we will perform numerical simulations on the one dimensional model which assumes negligible cell viscosity and was

described in Subsection 2.3.1. Much of the numerical scheme described here is analogous to the one used in the previous section.

3.2.1 *Formulation*

We will again consider the specific case where $\Sigma_c(\alpha)$ is defined by the equation (39). Therefore, by substituting (40) into system (33), we obtain the model with which we will work in this section, namely:

$$\begin{cases} \dfrac{\partial \alpha}{\partial t} &= \dfrac{\partial}{\partial x}\Big(\nu_2(\alpha)\dfrac{\partial \alpha}{\partial x}\Big) + S_c(\alpha, C) \\ 0 &= \dfrac{\partial^2 C}{\partial x^2} - Q_c(\alpha, C), \end{cases} \tag{50}$$

with moving boundary condition

$$\frac{dR}{dt}(t) = -\gamma \frac{\partial \alpha}{\partial x}(R(t), t)$$

subject to the boundary and initial conditions

$$\begin{cases} \dfrac{\partial \alpha}{\partial x} = \dfrac{\partial C}{\partial x} = 0, & \text{at } x = 0 \\ \alpha = \alpha^*, \quad C = C_\infty, & \text{at } x = R(t) \\ \alpha = \alpha_0, \quad C = C_0, \quad R = R_0, & \text{at } t = 0, \end{cases}$$

where

$$\nu_2(\alpha) = \gamma\left(\frac{-\alpha^2 + 2\alpha - \alpha^*}{1 - \alpha}\right), \qquad \gamma = \frac{\hat{\Sigma}_c}{k_0}.$$

Notice that, by the quadratic equation, the diffusivity coefficient ν_2 satisfies

$$\begin{cases} \nu_2(\alpha) > 0, & \text{if } \alpha > \alpha_d, \\ \nu_2(\alpha) < 0, & \text{if } \alpha < \alpha_d. \end{cases} \tag{51}$$

where

$$\alpha_d = 1 - \sqrt{1 - \alpha^*}.$$

Therefore, when $\alpha > \alpha_d$ and thus the cells are sufficiently packed together, we may apply numerical methods to visualise a solution since, in this case,

the problem is well-posed when initial and boundary conditions are chosen accordingly. On the other hand, if cells become spread out such that $\alpha < \alpha_d$, then the numerical scheme will indeed fail. We will see examples of both of these cases.

3.2.2 *Finite Difference Scheme*

Fixing the Domain

In order to apply a finite difference scheme to approximate a solution to this system, we first apply the same change of variable described in Subsection 3.1.2 to fix the moving boundary. By doing so, we may obtain a (ξ, t) formulation that is equivalent to the (x, t) formulation above, i.e.:

$$\begin{cases} \dfrac{\partial \alpha}{\partial t} &= \dfrac{\xi}{R(t)}\dfrac{dR}{dt}\dfrac{\partial \alpha}{\partial \xi} + \dfrac{1}{R(t)^2}\dfrac{\partial}{\partial \xi}\left(\nu_2(\alpha)\dfrac{\partial \alpha}{\partial \xi}\right) + S_c(\alpha, C) \\ 0 &= \dfrac{1}{R(t)^2}\dfrac{\partial^2 C}{\partial \xi^2} - Q_c(\alpha, C) \end{cases}$$

with moving boundary equation

$$\frac{dR}{dt}(t) = -\frac{\gamma}{R(t)}\frac{\partial \alpha}{\partial \xi}(1, t)$$

and boundary and initial conditions

$$\begin{cases} \dfrac{\partial \alpha}{\partial x} = \dfrac{\partial C}{\partial x} = 0, & \text{at } \xi = 0 \\ \alpha = \alpha^*, \quad C = C_\infty, & \text{at } \xi = 1 \\ R = R_0, \quad \alpha = \alpha_0(\xi R_0), \quad C = C_0(\xi R_0), & \text{at } t = 0, \end{cases}$$

As before, inserting the moving boundary equation into the first equation of the system above, we have

$$\frac{\partial \alpha}{\partial t} = -\frac{\gamma \xi}{R(t)^2}\frac{\partial \alpha}{\partial \xi}(1, t)\frac{\partial \alpha}{\partial \xi} + \frac{1}{R(t)^2}\frac{\partial}{\partial \xi}\left(\nu_2(\alpha)\frac{\partial \alpha}{\partial \xi}\right) + S_c(\alpha, C), \tag{52}$$

which will be used in lieu of the first equation of the system.

Defining a Partition

Consider the same partition used in Section 3.1.1, i.e. let

$$U_i(t) = \alpha(\xi_i, t), \qquad V_i(t) = C(\xi_i, t), \qquad \xi_i = \frac{i-1}{N-1}, \qquad i = 1, \dots N \in \mathbb{N}$$

and

$$\mathbf{U}(t) = (U_i(t))_1^N, \qquad \mathbf{V}(t) = (V_i(t))_1^N, \qquad \boldsymbol{\xi} = (\xi_i)_1^N.$$

With this notation, the boundary conditions at $\xi = 1$ imply that $U_N(t) = \alpha^*$ and $V_N(t) = C_\infty$. Consequently, these inspire the following definitions:

$$\mathbf{u}(t) = P_1^{N-1}(\mathbf{U}(t)), \qquad \mathbf{v}(t) = P_1^{N-1}(\mathbf{V}(t))$$

Then, as a variation of what was done in section 3.2.2, our system may be approximated by one on

$$\begin{aligned}\mathbf{Z}(t) &= (\mathbf{u}(t); \mathbf{v}(t); R(t)) \\ &= (U_1(t), \cdots U_{N-1}(t), V_1(t), \cdots V_{N-1}(t), R(t))^T\end{aligned}$$

of the form

$$M\frac{d\mathbf{Z}}{dt} = F(\mathbf{Z}),$$

where M is a squared mass matrix of order $2N-1$ and $F(\mathbf{Z})$ is a column vector of size $2N-1$.

Defining $F(\mathbf{Z})$

Equation for α

With this notation, according to (52), the first $N-1$ terms of $F(\mathbf{Z})$ are given by the right hand side of the column vector equation

$$\begin{aligned}\frac{d\mathbf{u}}{dt} = \frac{1}{R^2}\Bigg[\gamma\left(\frac{4U_{N-1} - U_{N-2} - 3\alpha^*}{2\Delta\boldsymbol{\xi}}\right)(P_1^{N-1}(\boldsymbol{\xi}) \circ D_x\mathbf{U}) \\ + \frac{\partial \nu_2}{\partial \alpha}(\mathbf{u}) \circ D_x\mathbf{U} \circ D_x\mathbf{U} + \nu_2(\mathbf{u}) \circ D_{xx}\mathbf{U}\Bigg] + S_c(\mathbf{u}, \mathbf{v})\end{aligned}$$

with $D_x\mathbf{U} = \frac{1}{2(\Delta\xi)}(\underline{D_x}\mathbf{u} + \mathbf{a})$ and $D_{xx}\mathbf{U} = \frac{1}{(\Delta\xi)^2}(\underline{D_{xx}}\mathbf{u} + \mathbf{a})$, where

$$\underline{D_x} = \begin{pmatrix} 0 & 0 & & & & \\ -1 & 0 & 1 & & & \\ & -1 & 0 & 1 & & \\ & & \ddots & \ddots & \ddots & \\ & & & -1 & 0 & 1 \\ & & & & -1 & 0 \end{pmatrix}_{(N-1)\times(N-1)},$$

$$\mathbf{a} = (0, \ldots 0, \alpha^*)^T, \qquad a \in \mathbb{M}(N-1, 1)$$

and

$$\underline{D_{xx}} = \begin{pmatrix} -2 & 2 & & & & \\ 1 & -2 & 1 & & & \\ & 1 & -2 & 1 & & \\ & & \ddots & \ddots & \ddots & \\ & & & 1 & -2 & 1 \\ & & & & 1 & -2 \end{pmatrix}_{(N-1)\times(N-1)}.$$

Equation for C

Similarly, the next $N-1$ elements of $F(\mathbf{Z})$ are given by the right hand side of the column vector equation

$$0 = \frac{1}{R^2}D_{xx}\mathbf{V} - Q_c(\mathbf{u}, \mathbf{v}),$$

where $D_{xx}\mathbf{V} = \frac{1}{(\Delta\xi)^2}(\underline{D_{xx}}\mathbf{v} + \mathbf{c})$, with $\underline{D_{xx}}$ defined above and $\mathbf{c}$ as in Equation (49).

Equation on R

Finally, the moving boundary equation may be approximated by

$$\frac{dR}{dt}(t) = (F(\mathbf{Z}))_{(2N-1,1)} = \frac{\gamma}{R(t)}\left(\frac{4U_{N-1}(t) - U_{N-2}(t) - 3\alpha^*}{2\Delta\xi}\right).$$

Defining M

Now, we must define the mass matrix M. In fact, since a pseudo-steady state approximation is made on the diffusion equation for C, then

$$M = \begin{pmatrix} I_{N-1} & 0 & 0 \\ 0 & 0_{N-1} & 0 \\ 0 & 0 & 1 \end{pmatrix},$$

where I_{N-1} and 0_{N-1} are the squared identity and zero matrices of order $(N-1)$, respectively.

Conclusion

Defining $F(\mathbf{Z})$ in the manner done above, we see that our system may be indeed approximated by

$$\begin{cases} M\dfrac{d\mathbf{Z}}{dt} & = F(\mathbf{Z}) \\ \\ \mathbf{Z}(0) & = \begin{pmatrix} P_1^{N-1}(\alpha_0(\xi R_0)) \\ P_1^{N-1}(C_0(\xi R_0)) \\ R_0 \end{pmatrix}. \end{cases}$$

3.2.3 *Four Cases with $v_2(\alpha) > 0$*

By our own design, the four cases analysed in Section 3.1.3 are cases in which $v_2(\alpha) > 0$ for the time period analysed. Running simulations of these cases according to the setup made above, with negligible viscosity, it is possible to observe roughly the same dynamics as seen in Section 3.1.3. For comparison with the full one dimensional formulation simulated in previous section, we also calculate v_c from numerical approximations of α by using the equation (32) and present these graphs here for each one of the four cases in question.

See resulting graphs below:

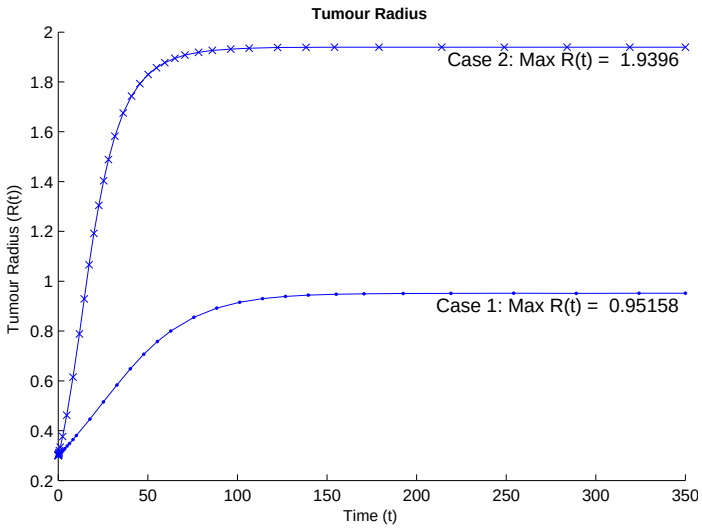


Figure 19.: Evolution of tumour radius in Cases 1 and 2 in the negligible cell viscosity limit.

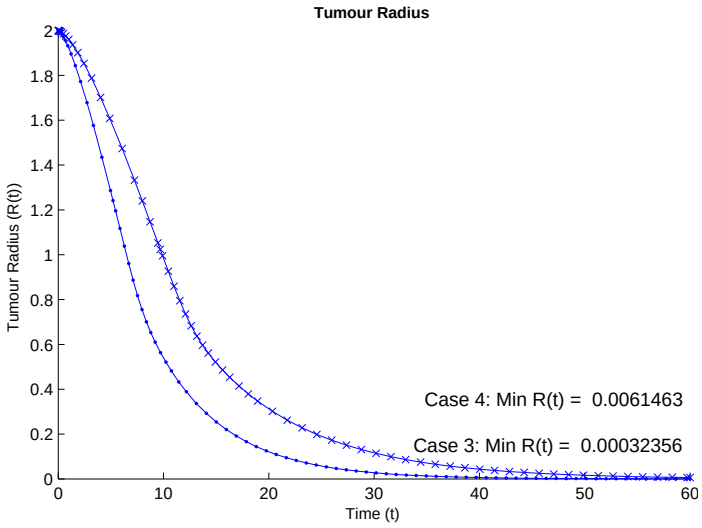


Figure 20.: Evolution of tumour radius in Cases 3 and 4 in the negligible cell viscosity limit.

Case 1 Graphs

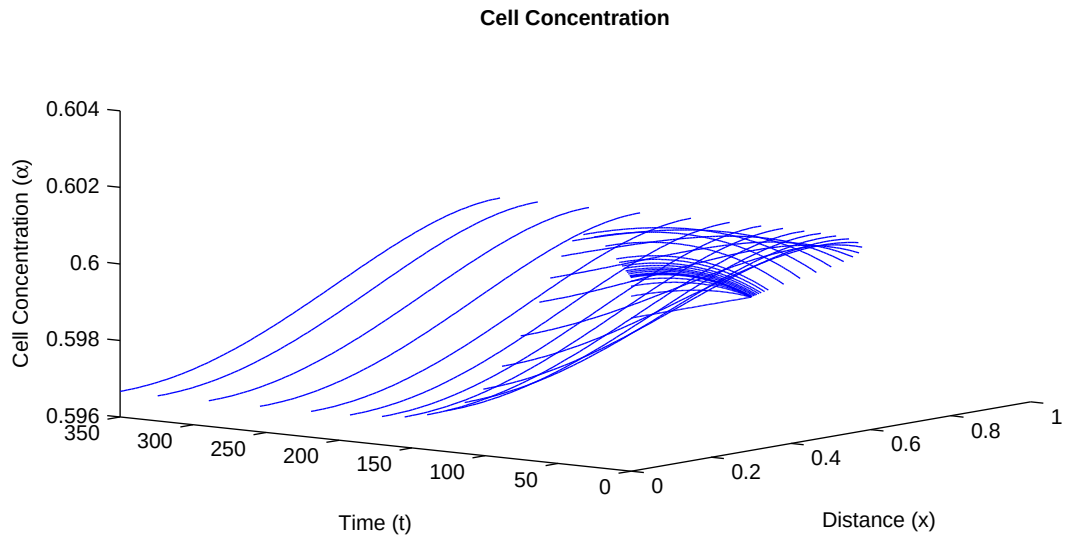


Figure 21.: Evolution of the cell concentration in Case 1 in the negligible cell viscosity limit.

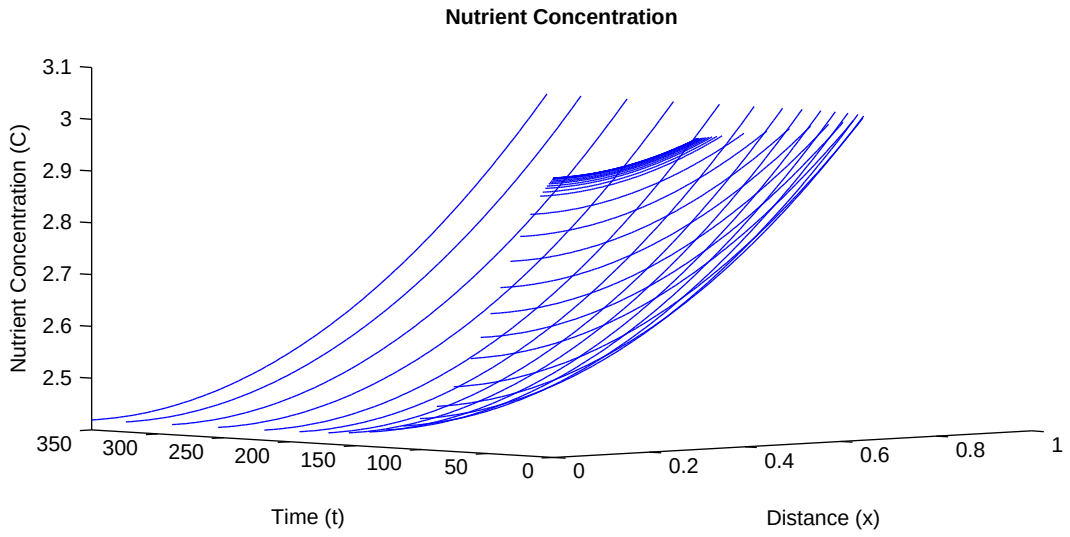


Figure 22.: Evolution of the nutrient concentration in Case 1 in the negligible cell viscosity limit.

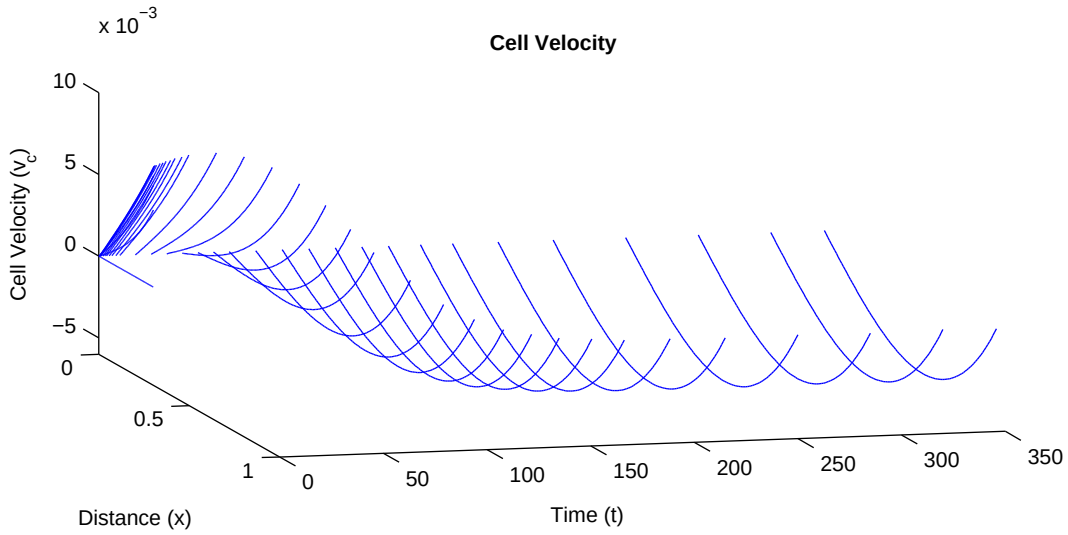


Figure 23.: Evolution of the cell velocity in Case 1 in the negligible cell viscosity limit.

Case 2 Graphs

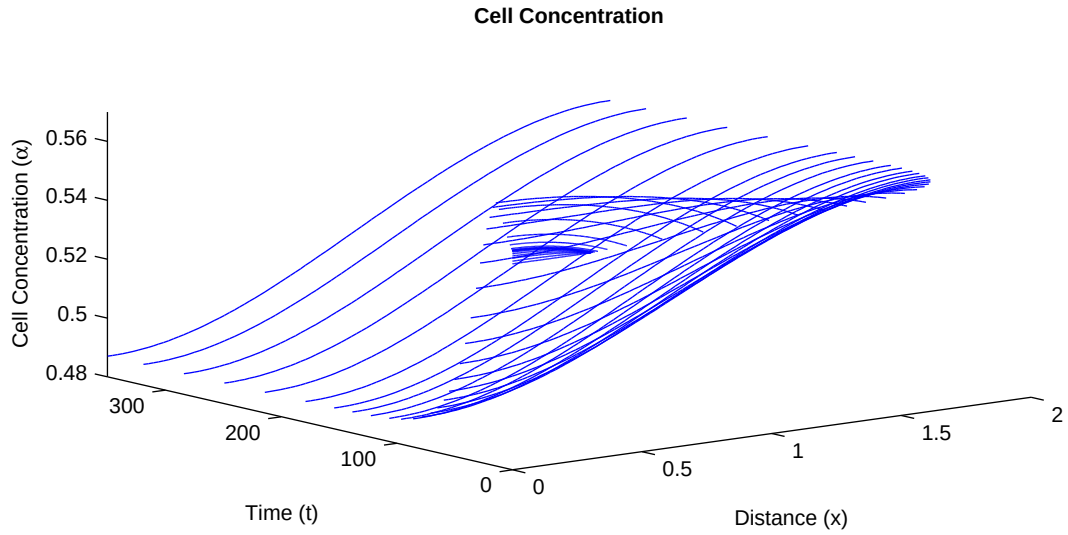


Figure 24.: Evolution of the cell concentration in Case 2 in the negligible cell viscosity limit.

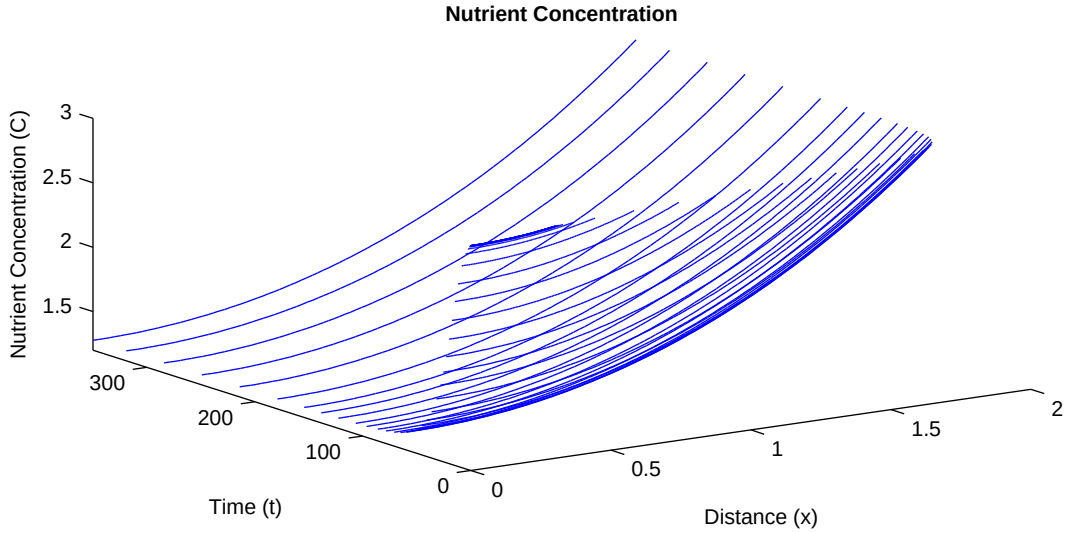


Figure 25.: Evolution of the nutrient concentration in Case 2 in the negligible cell viscosity limit.

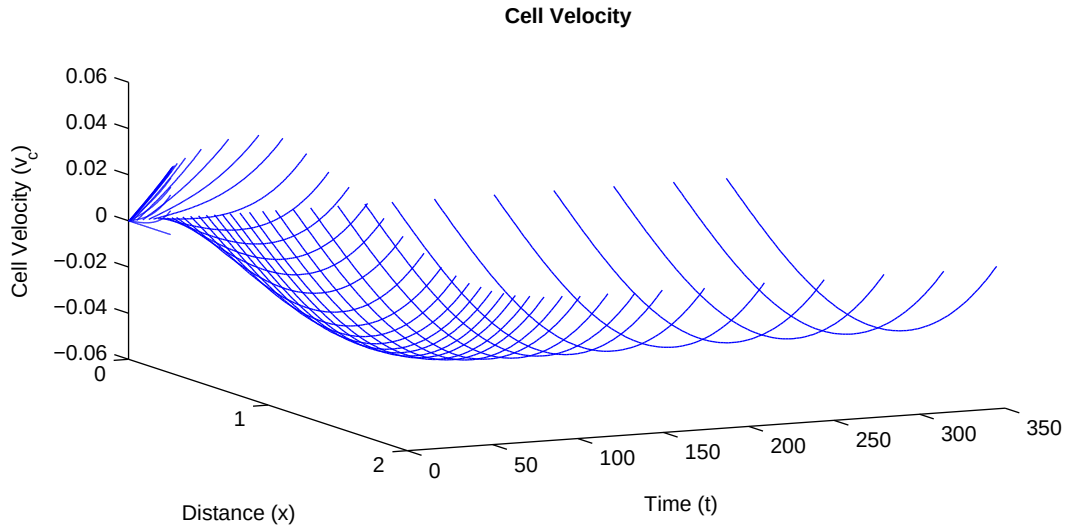


Figure 26.: Evolution of the cell velocity in Case 2 in the negligible cell viscosity limit.

Case 3 Graphs

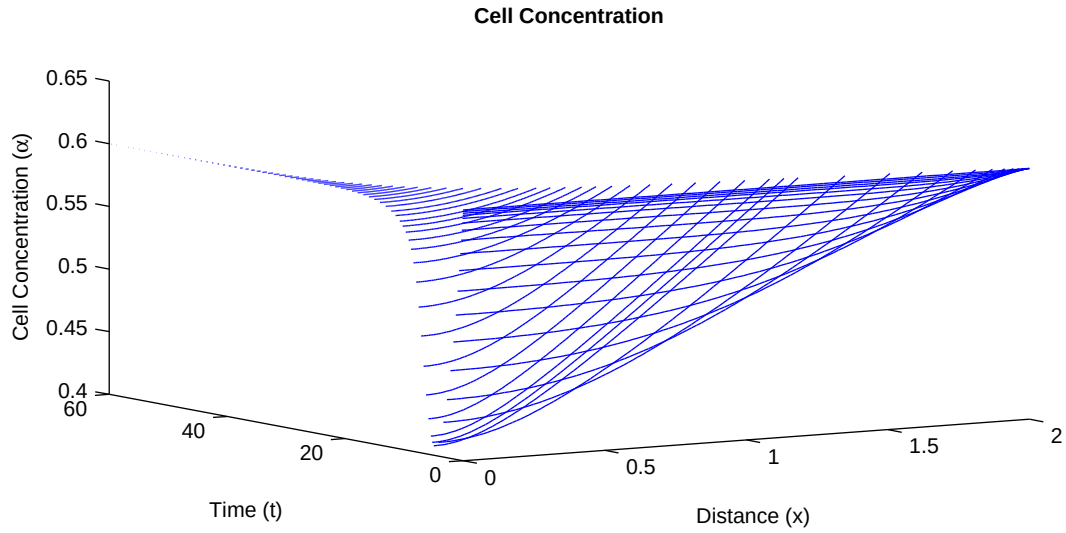


Figure 27.: Evolution of the cell concentration in Case 3 in the negligible cell viscosity limit.

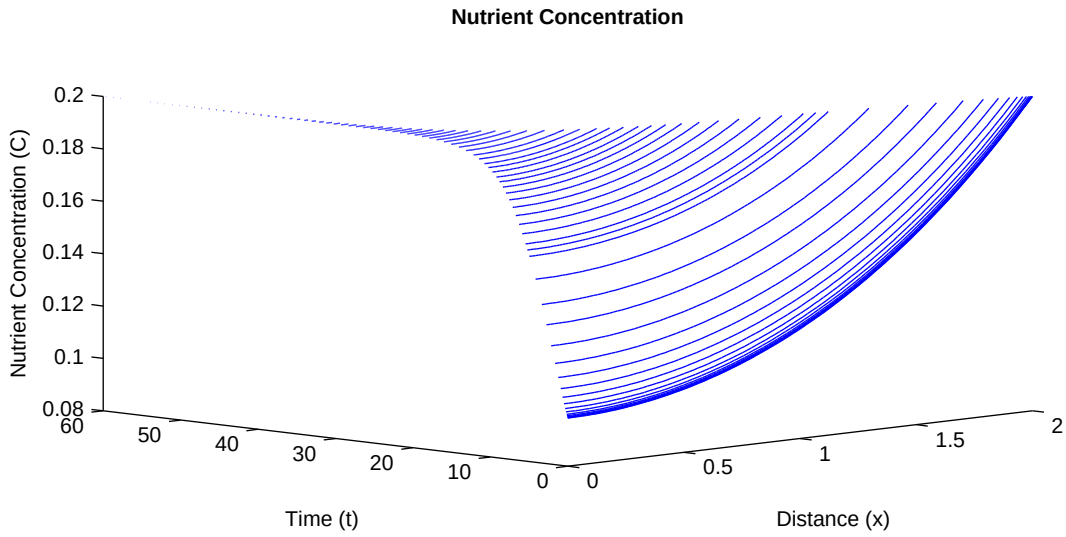


Figure 28.: Evolution of the nutrient concentration in Case 3 in the negligible cell viscosity limit.

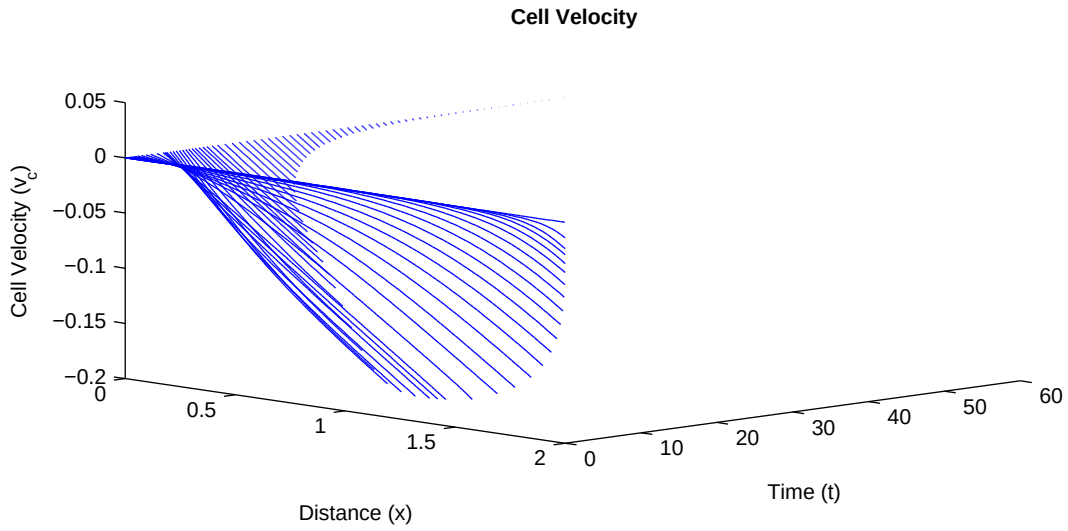


Figure 29.: Evolution of the cell velocity in Case 3 in the negligible cell viscosity limit.

Case 4 Graphs

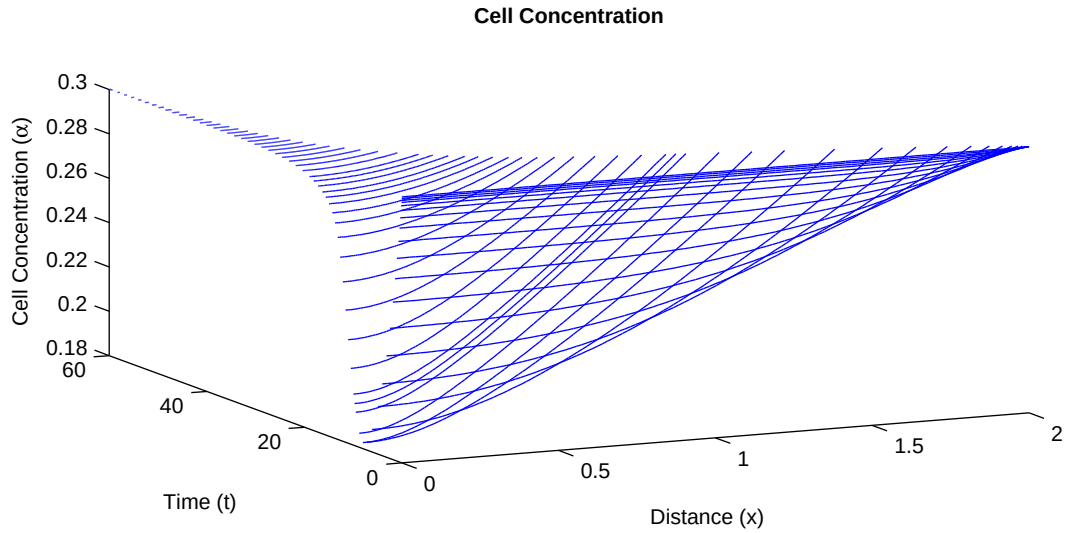


Figure 30.: Evolution of the cell concentration in Case 4 in the negligible cell viscosity limit.

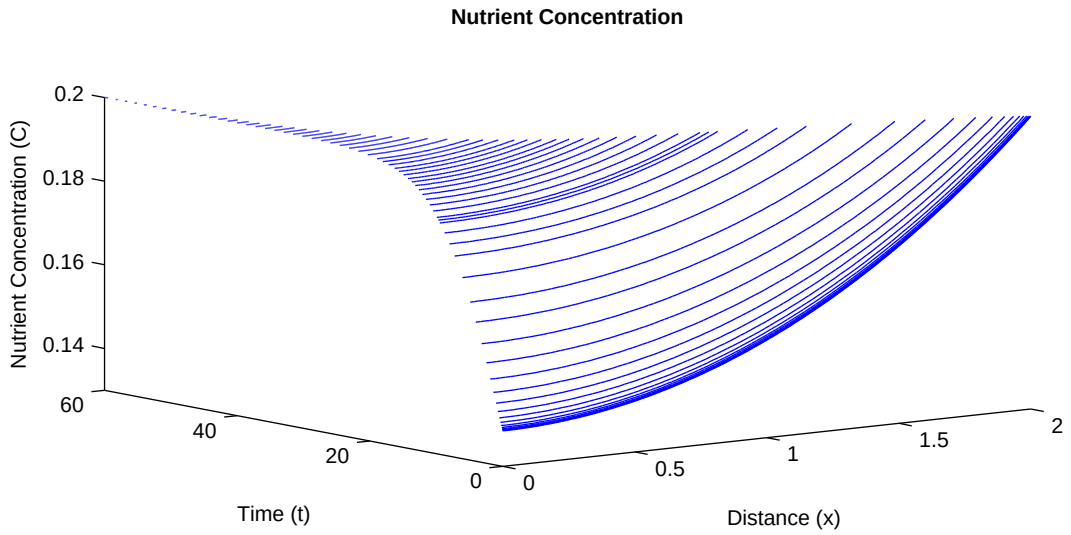


Figure 31.: Evolution of the nutrient concentration in Case 4 in the negligible cell viscosity limit.

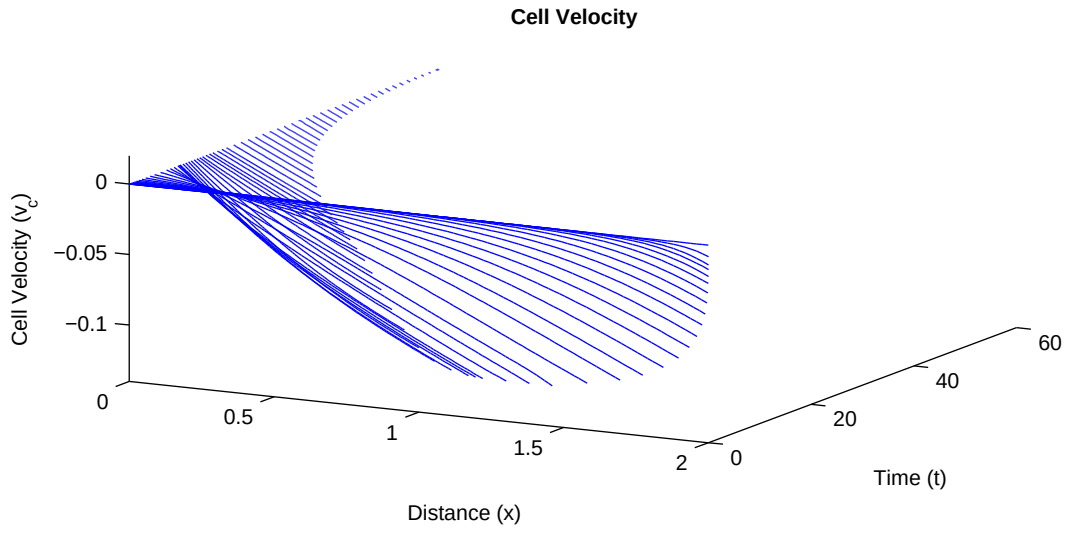


Figure 32.: Evolution of the cell velocity in Case 4 in the negligible cell viscosity limit.

Observations

The general dynamics of solutions in both the full one dimensional formulation and its negligible viscosity limit case are comparable. However, a noticeable difference between the behaviour in the general and in the limit case is generated by the boundary condition $\alpha = \alpha^*$ on $R(t)$, which exists

only in the latter formulation. Indeed, as the tumour decays in Cases 3 and 4, the cell concentration tends to α^* in the negligible viscosity limit case, but tends to a value strictly smaller than α^* in the general formulation. Similarly, as the tumour grows in Cases 1 and 2, the cell concentration on the boundary is always α^* in the negligible viscosity limit case, but tends to a value strictly larger than α^* in the general formulation.

Additionally, in Cases 1 and 2, it is possible to note that, for fixed large t, the slope at which $\alpha(\cdot, t)$ approaches $x = R(t)$ is quite different in the general and the negligible viscosity limit case. Compare, for example, Figures 7 and 21. Indeed, in the limit case where viscosity is considered negligible, $\alpha(\cdot, t)$ seems to plateau onto α^* while $\alpha(\cdot, t)$ in the full one dimensional formulation has a positive slope when approaching $x = R(t)$. This comes from the fact that, in the negligible viscosity limit case, the moving boundary condition and the diffusion limited steady state imply that

$$-\gamma \frac{\partial \alpha}{\partial x}(R(t), t) = \frac{dR}{dt}(t) \to 0$$

and therefore

$$\frac{\partial \alpha}{\partial x}(R(t), t) \to 0$$

as $t \to \infty$.

Additionally, in possession of the simulations above, we would like to revisit the choice $\alpha_{min} = 0$. In the beginning of this chapter, we claimed that this simplification would not be an issue for most of our simulations. Indeed, in the graphs of the cell concentration obtained for Cases 1 through 4 (Figures 7,10,13,16,21,24,27,30), one can see that $\alpha(x, t) > 0.15$ is always satisfied. Thus, if we were to chose $\alpha_{min} = 0.15$, *a priori*, none of the simulations above would change since $\Sigma_c(\alpha)$ would remain the same in the range of values of the cell concentration. Although we keep $\alpha_{min} = 0$, the choice of $\alpha_{min} \neq 0$ may be deemed beneficial to improve the well-posedness of the negligible viscosity limit case and this will be discussed at the end of this chapter.

3.2.4 *Two Cases with $\nu_2(\alpha) < 0$*

In the four cases delineated above, we particularly searched for parameter sets for which the diffusivity coefficient $\nu_2(\alpha)$ was positive at any point in the time frame of interest. This implies that these cases were numerically tractable in this time frame and thus allowed us to visualise and compare the predicted dynamics of the tumour growth to known biological behaviour.

Now, we turn to analysing two cases where $\nu_2(\alpha) < 0$ after a short period of time. From (51), recall that $\nu_2(\alpha) < 0$ if $\alpha < \alpha_d$, with $\alpha_d = 1 - \sqrt{1 - \alpha^*}$. Since our initial cell concentration is equal to α^*, we consider two cases in which α_d and α^* are sufficiently close, namely:

CASE 5: Parameter set of Case 1, except for $\alpha^* = 0.1$.

CASE 6: Parameter set of Case 3 except for $\alpha^* = 0.1$.

In other words, consider both cases with very low natural cell concentration. Notice then that

$$\alpha_d = 1 - \sqrt{1 - 0.1} = 1 - \sqrt{0.9} = 0.0513$$

for both set-ups. Therefore, we expect simulations of the negligible viscosity limit case to break down as α approaches $\alpha_d = 0.0513$ while the simulations of the full formulation will carry on.

Indeed, this can be seen from the graphs below, which represent the simulations of both Cases 5 and 6 with and without the supposition of negligible viscosity.

Case 5 Graphs

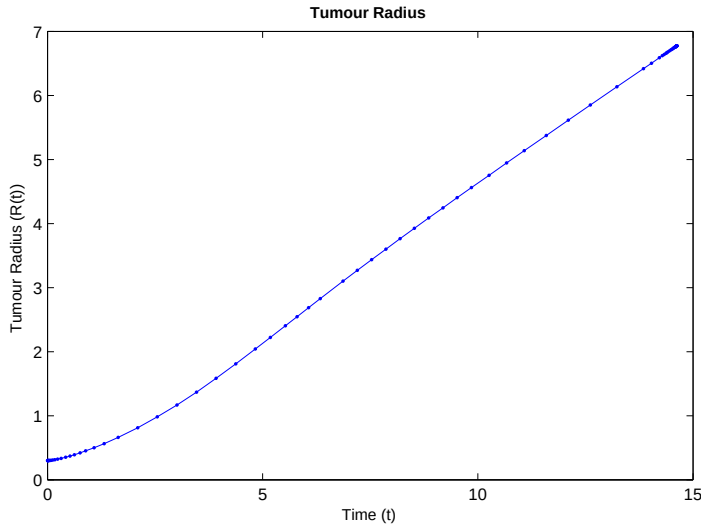


Figure 33.: Evolution of the radius in Case 5 in the negligible cell viscosity limit.

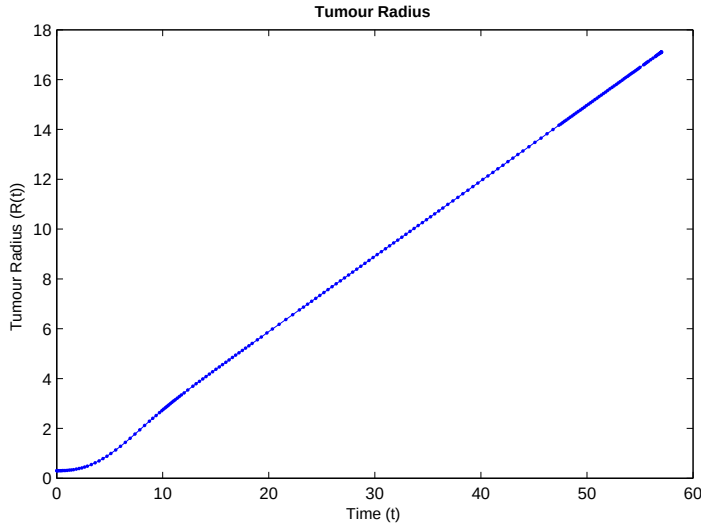


Figure 34.: Evolution of the radius in Case 5 in the full one dimensional formulation, with viscosity.

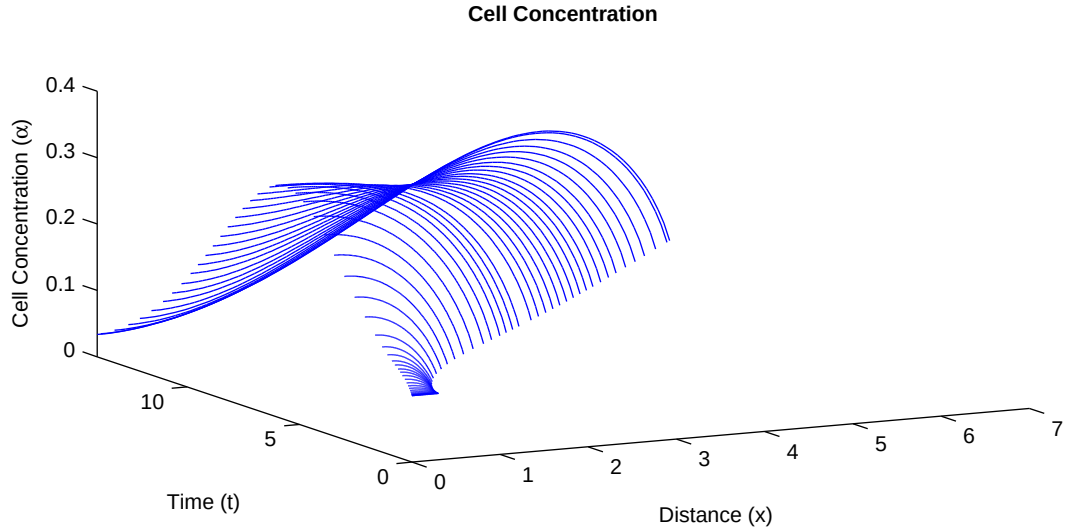


Figure 35.: Evolution of the cell concentration in Case 5 in the negligible cell viscosity limit. Notice that this simulation breaks down when α approaches $\alpha_d = 0.0513$.

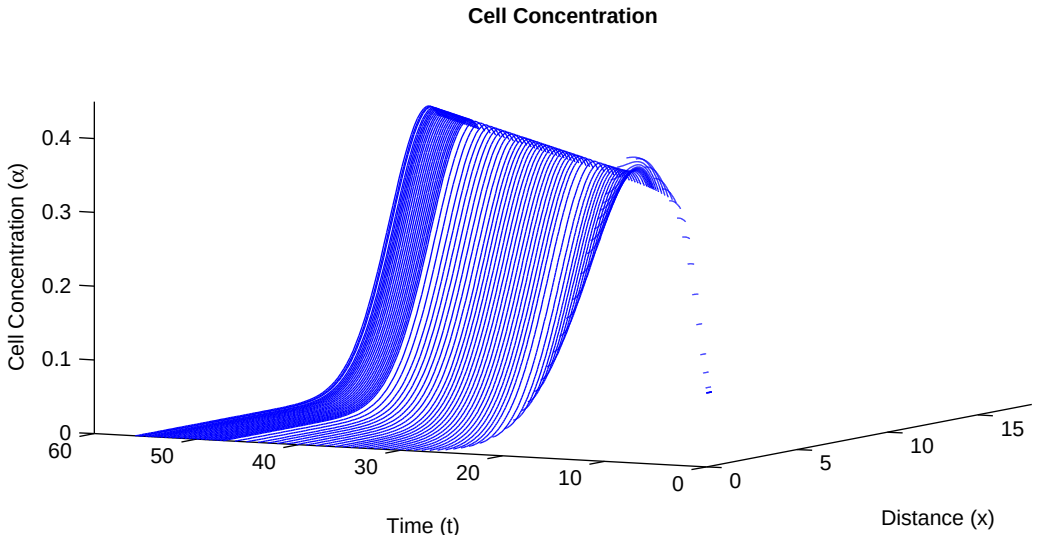


Figure 36.: Evolution of the cell concentration in Case 5 in the full one dimensional formulation, with viscosity. Notice the existence of a necrotic core and a thin proliferating rim of fixed thickness near the moving boundary.

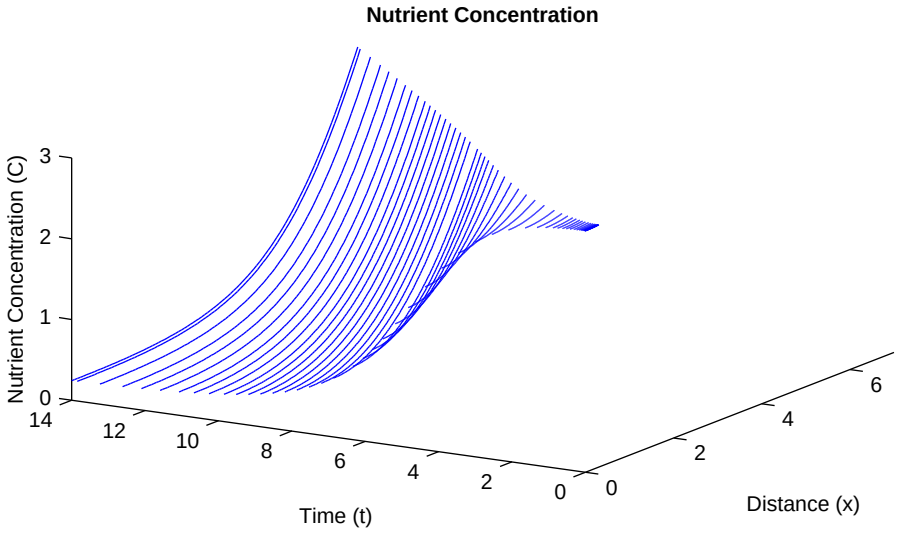


Figure 37.: Evolution of the nutrient concentration in Case 5 in the negligible cell viscosity limit.

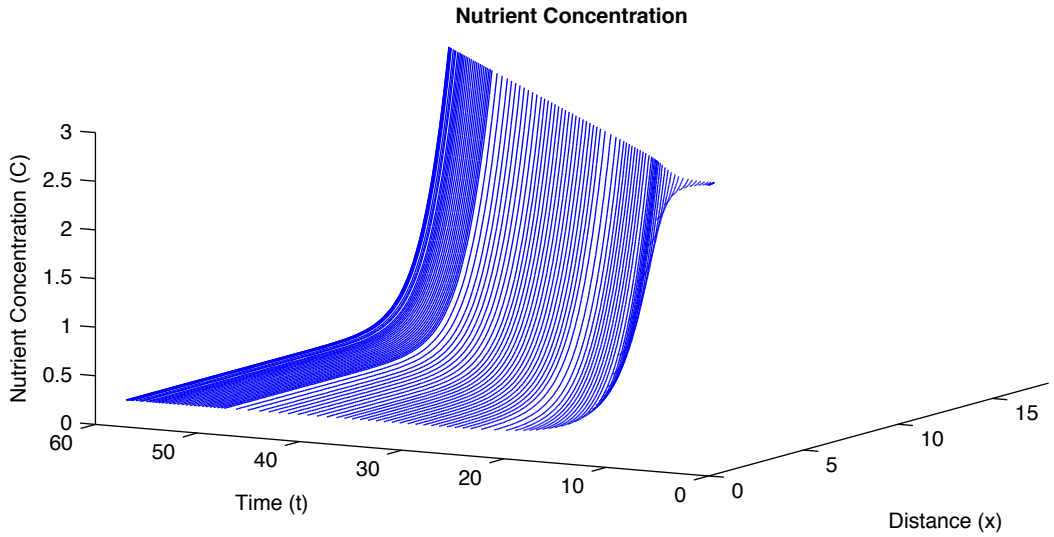


Figure 38.: Evolution of the nutrient concentration in Case 5 in the full one dimensional formulation, with viscosity.

For comparison purposes, we calculate the cell velocity in the negligible viscosity case by using equation (32) and compare it to the solution obtained numerically for the cell velocity using the full one dimensional model.

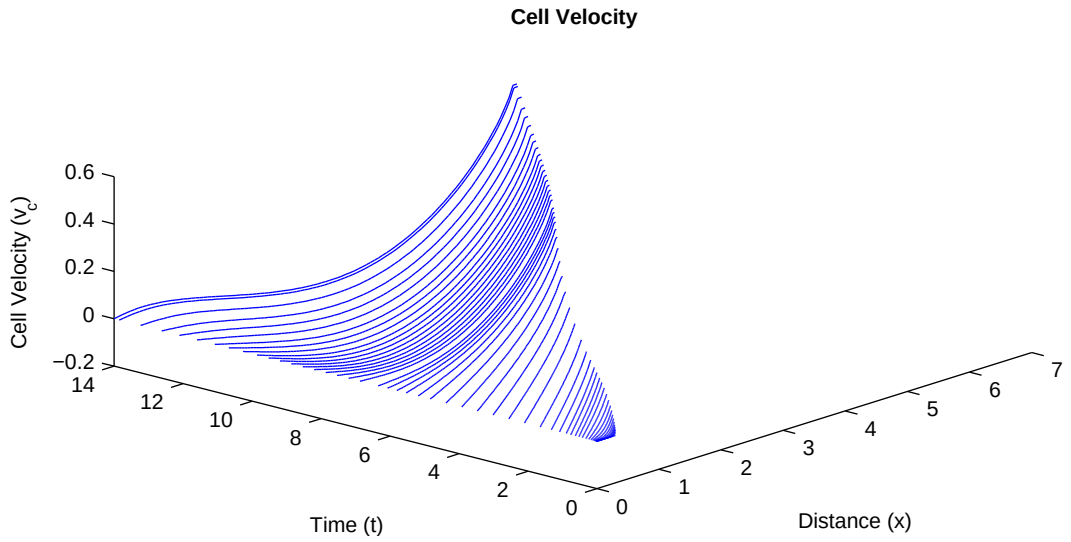


Figure 39.: Evolution of the cell velocity in Case 5 in the negligible cell viscosity limit.

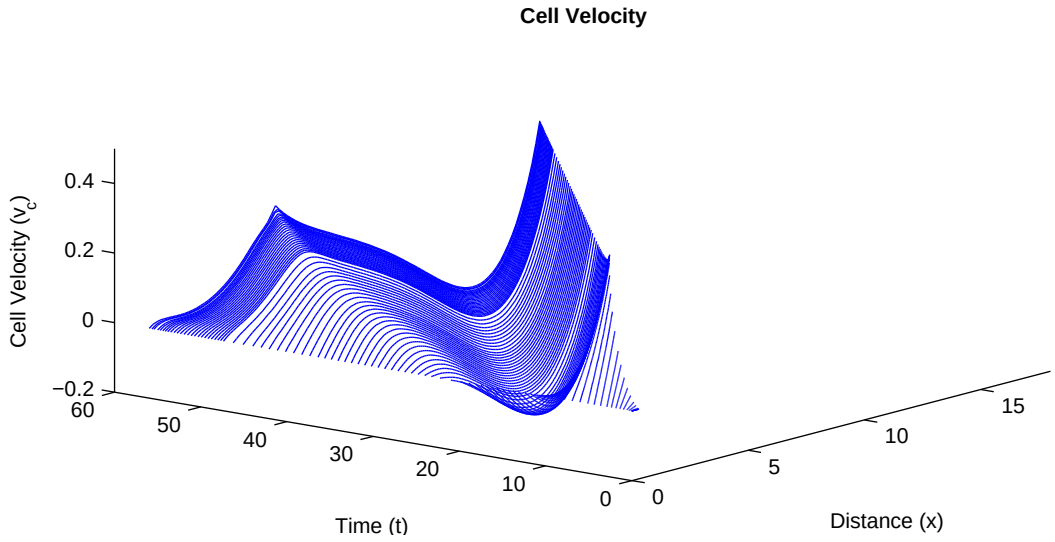


Figure 40.: Evolution of the cell velocity in Case 5 in the full one dimensional formulation, with viscosity.

Observation

It is worth to mention an interesting behaviour apparent in the viscous formulation of Case 5 that was not observed in any of the previous cases. Indeed, notice that the graph of the cell concentration (Figure 36) presents a highly packed clump of cells close to the boundary of the tumour that moves outwards as the tumour grows. Additionally, this strip of cells appears to be of a fixed thickness. Similarly, the shape of the velocity graph (Figure 40) at about $t = 25$ suggests the beginning of the formation of such a clump.

This shows that the full viscous model is capable of predicting the thin proliferating rim of fixed thickness that develops with the creation of the necrotic core. Indeed, in this case, from Figure 36, we see that the innermost cell concentration is almost null, which represents the existence of a fully formed necrotic core and not simply a region with relatively low cell concentration, as we had seen in previous cases.

In the limit case, though, it is impossible to see such behaviour. As discussed before, the limit case is not well posed for $\alpha < \alpha_d = 0.0513$. Therefore, the numerical scheme described here will break down when the cell concentration in the core becomes sufficiently small, thus preventing this limit case from predicting the formation of a necrotic core and a thin proliferating rim. This limitation can be seen more readily when comparing Figures 36 and 35.

Consider now the numerical results obtained for Case 6. Once again, we present first the simulations of the limit case followed by the ones of the full formulation, for easy comparison.

Case 6 Graphs

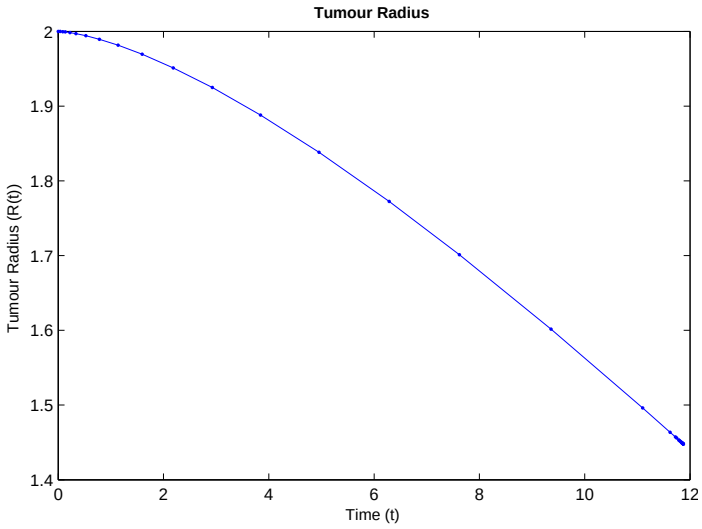


Figure 41.: Evolution of the radius in Case 6 in the negligible cell viscosity limit.

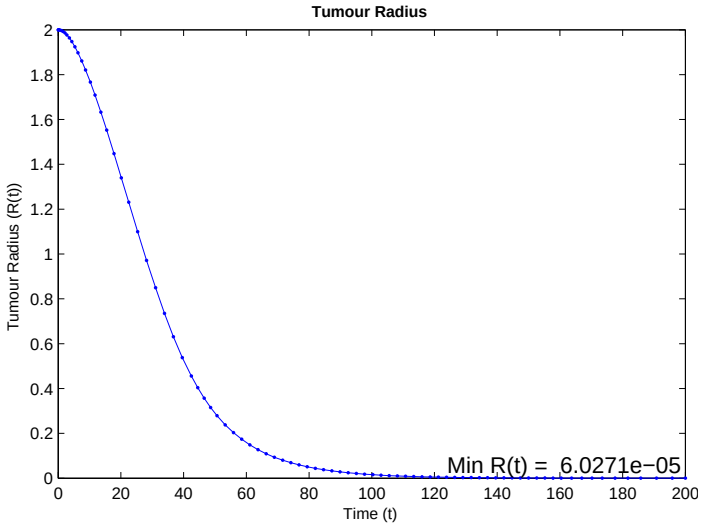


Figure 42.: Evolution of the radius in Case 6 in the full one dimensional formulation, with cell viscosity.

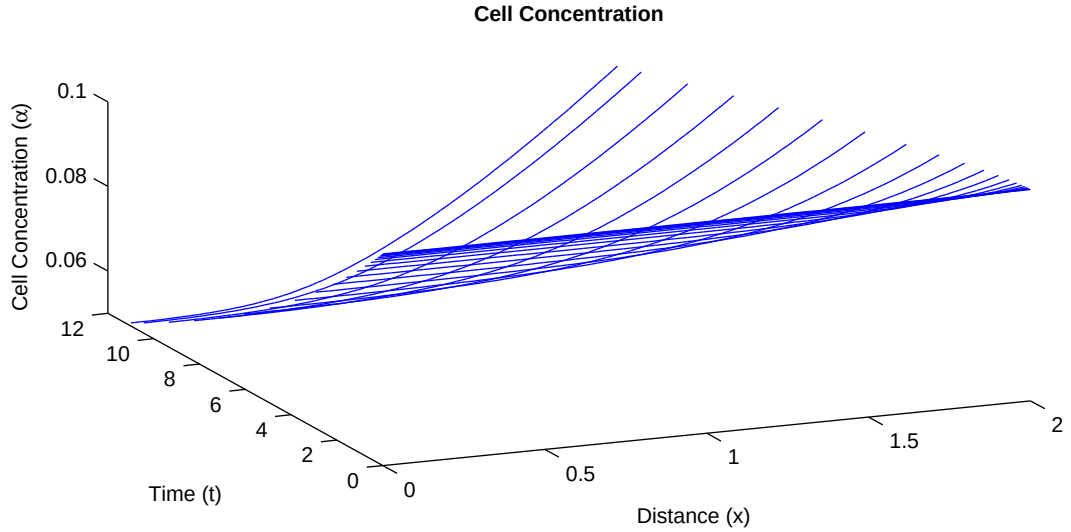


Figure 43.: Evolution of the cell concentration in Case 6 in the negligible cell viscosity limit. Notice that this simulation breaks down when α approaches $\alpha_d = 0.0513$.

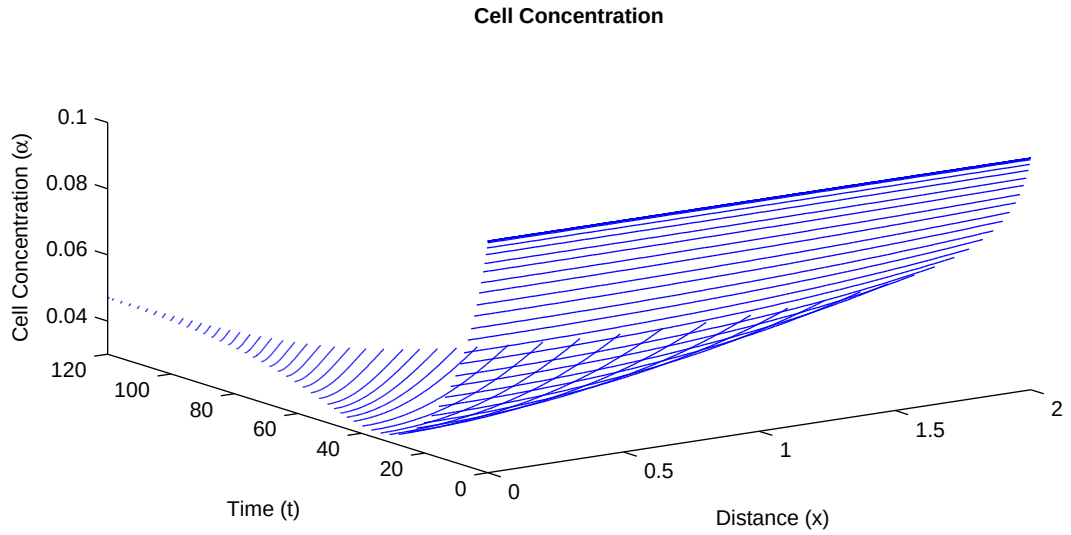


Figure 44.: Evolution of the cell concentration in Case 6 in the full one dimensional formulation, with cell viscosity.

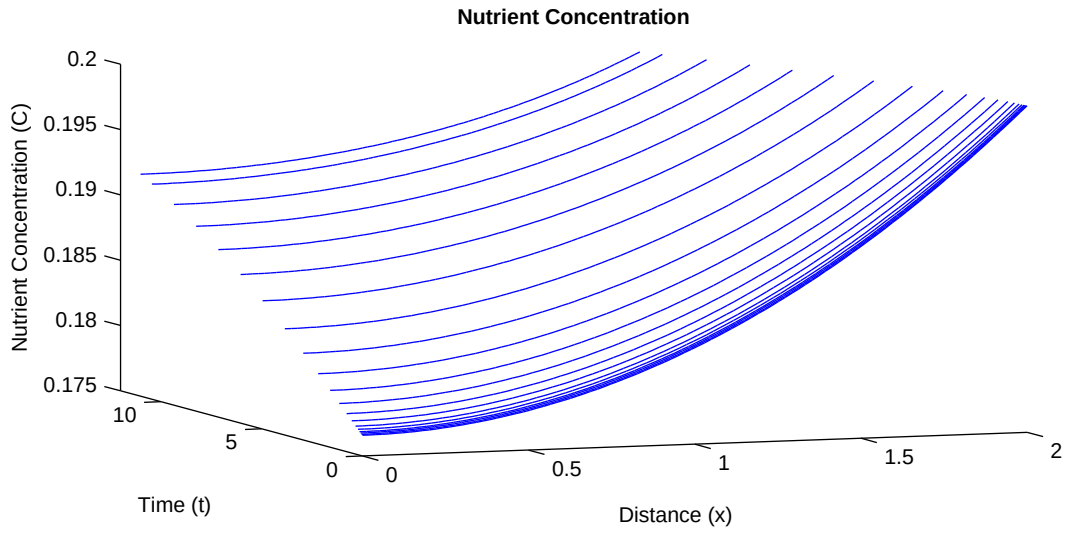


Figure 45.: Evolution of the nutrient concentration in Case 6 in the negligible cell viscosity limit.

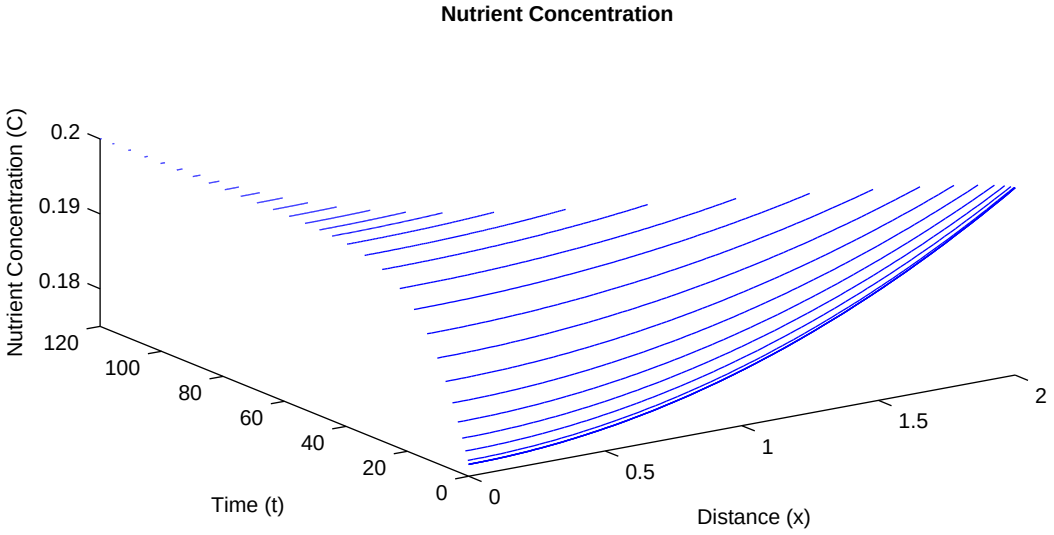


Figure 46.: Evolution of the nutrient concentration in Case 6 in the full one dimensional formulation, with cell viscosity.

As before, consider the velocity obtained from (32) in the limit case compared to the one obtained simulating the full one dimensional model.

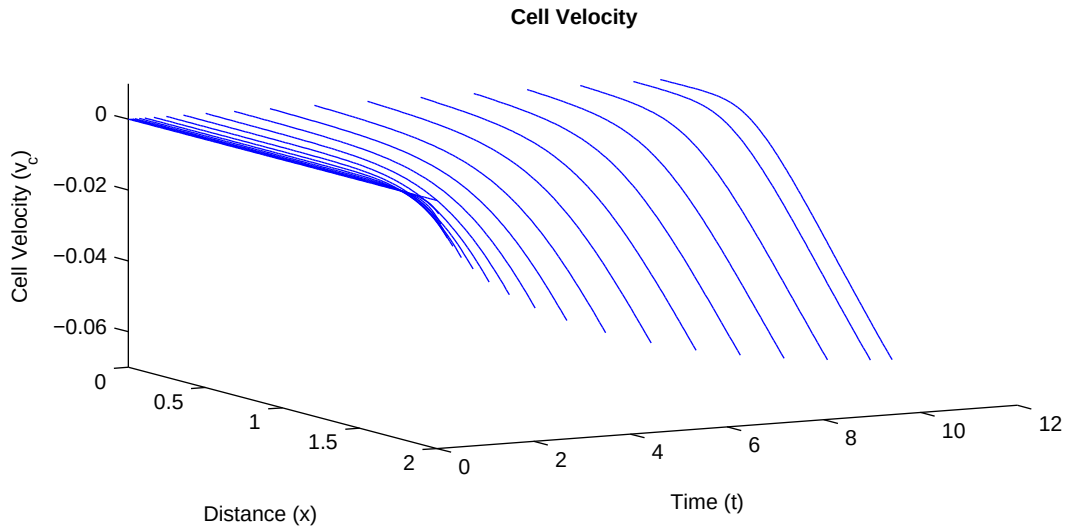


Figure 47.: Evolution of the cell velocity in Case 6 in the negligible cell viscosity limit.

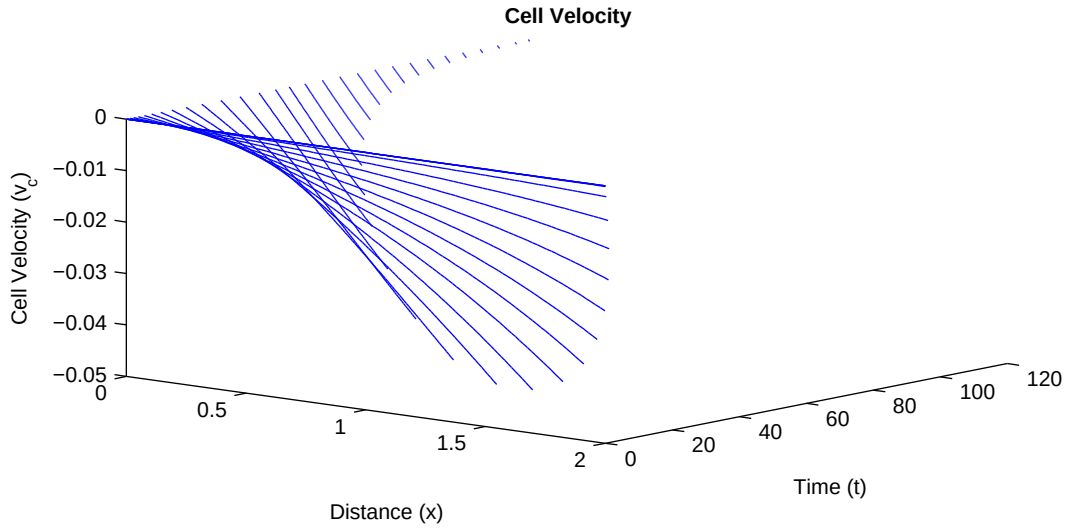


Figure 48.: Evolution of the cell velocity in Case 6 in the full one dimensional formulation, with viscosity.

For the sake of completion, we state the parameters used in the two cases considered above:

Table 2.: Parameter Values of Cases 5 and 6

Case	α^*	C_∞	s_0	s_1	s_2	s_3	s_4	Q_0	Q_1	R_0	γ
5	0.1	3.0	2	1	1.0	1	2	3	1	0.3	1
6	0.1	0.2	1	1	0.1	1	2	1	3	2.0	1

3.2.5 *Limitations of the Negligible Viscosity Limit Model*

Notice the time range of graphs of Cases 5 and 6. Simulations in the negligible viscosity limit break down well before the simulations of the general formulation in both Cases 5 and 6. Thus, it is possible to see that the negligible viscosity limit case has more significant numerical limitations than the general formulation.

Indeed, the negligible viscosity formulation is only well posed when $\nu_2(\alpha) > 0$ and thus $\alpha > \alpha_d$. Ultimately, this means that the viscous case can model very small cell concentration values which the limit case cannot in the current formulation. Particularly, in the limit case, we would never be able to see the necrotic core completely formed, as it would require $0 < \alpha < \epsilon < \alpha_d$ and thus would break the condition $\nu_2(\alpha) > 0$.

A Solution: Tailoring α_{min} to Guarantee Well-posedness

We would like to revisit the parameter choice $\alpha_{min} = 0$. In the simulations in Case 6, notice that $\alpha(x,t) > 0.03$ (Figures 43 and 44). Therefore, as argued in Cases 1 through 4, we could still choose $\alpha_{min} = 0.03$ to obtain the same results in the time frames considered here. Since α^* is small, namely $\alpha^* = 0.1$, such a choice for α_{min} is mathematically acceptable. However, in Case 5, it is virtually impossible to find a reasonable $\alpha_{min} > 0$ such that the simulations above would be unchanged. This can be seen clearly from the low values of α near the tumour's core in Figure 36.

On the other hand, defining

$$\alpha_{min} = \alpha_d = 1 - \sqrt{1 - \alpha^*} < \alpha^*$$

in the definition of $\Sigma_c(\alpha)$ may indeed turn the non-viscous limit case into a well posed problem for all α since the equation on the cell concentration could therefore be rewritten as

$$\frac{\partial \alpha}{\partial t} = \frac{\partial}{\partial x}\left(\nu_2(\alpha)\frac{\partial \alpha}{\partial x}\right) H(\alpha - \alpha_d) + S_c(\alpha, C). \tag{53}$$

Put differently, the diffusivity coefficient $\nu_2(\alpha)$ would only be present in the equation above in regions of cell concentration where $\nu_2(\alpha) > 0$, making this a well posed equation.

To exemplify, we offer here the graphs of numerical simulations of Case 5 performed now with $\alpha_{min} = \alpha_d$. Notice that these graphs seem to be a continuation of simulations shown in Figures 33, 35, 37, and 39 and approximate roughly the solutions of the full formulation seen in Figures 34, 36, 38, and 40, except for the differences already explained in the previous subsection (for Cases 1 through 4) and the one described below.

Case 5 Graphs, with $\alpha_{min} = \alpha_d$

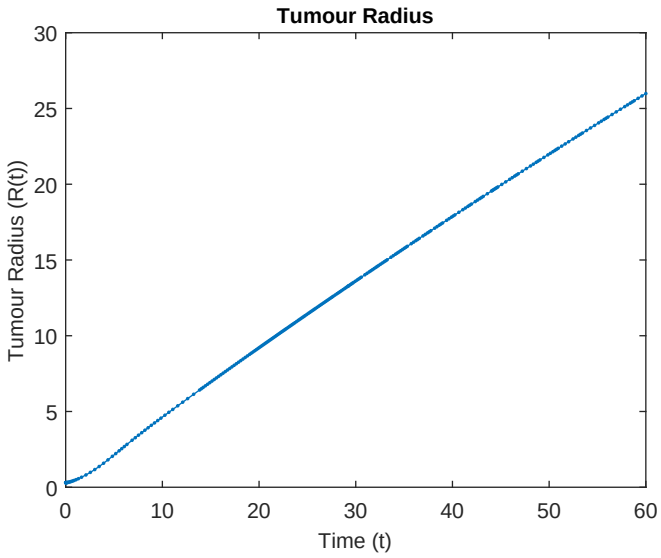


Figure 49.: Evolution of the tumour radius in Case 5 with $\alpha_{min} = \alpha_d$ in the negligible cell viscosity limit.

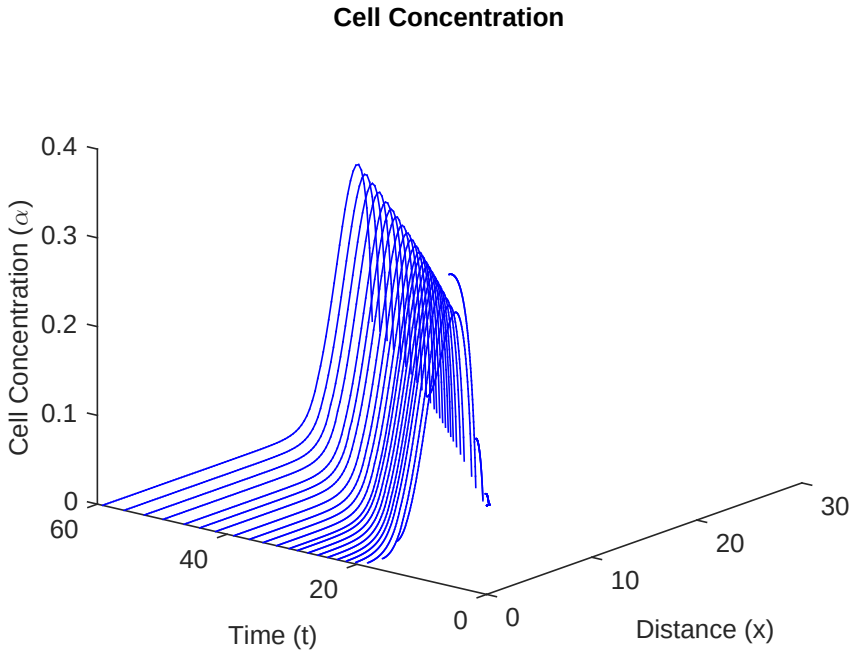


Figure 50.: Evolution of the cell concentration in Case 5 with $\alpha_{min} = \alpha_d$ in the negligible cell viscosity limit.

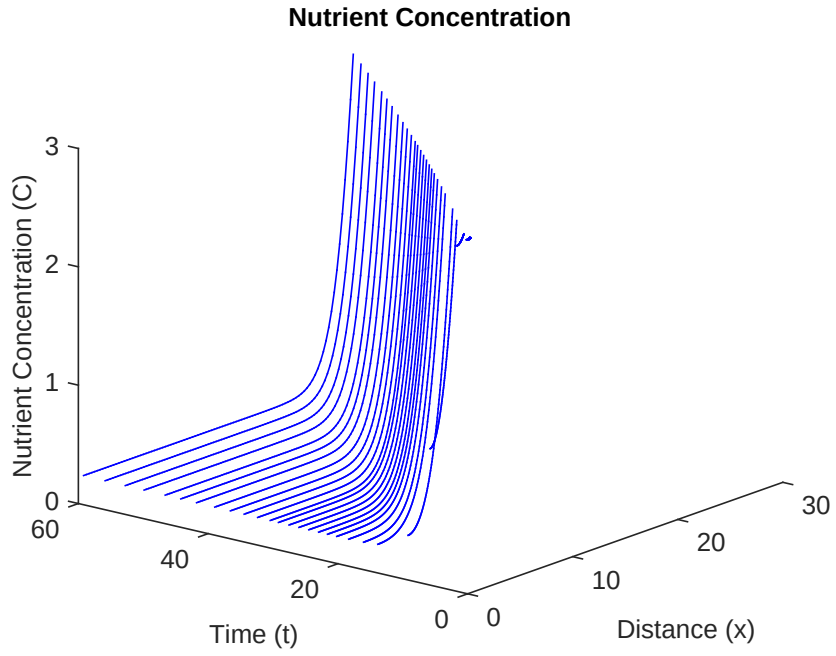


Figure 51.: Evolution of the nutrient concentration in Case 5 with $\alpha_{min} = \alpha_d$ in the negligible cell viscosity limit.

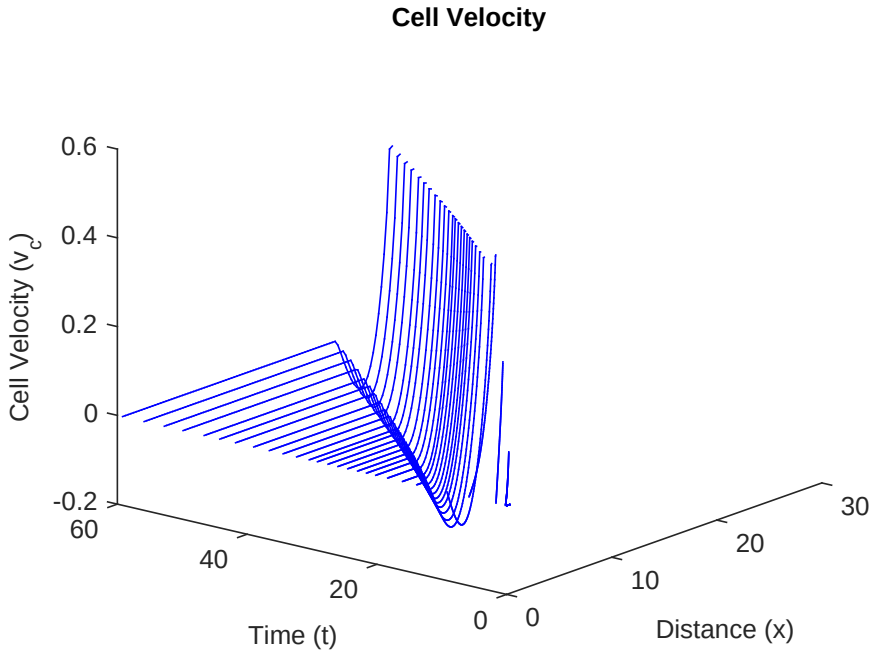


Figure 52.: Evolution of the cell velocity in Case 5 with $\alpha_{min} = \alpha_d$ in the negligible cell viscosity limit.

The main difference in the behaviour of these solutions and those of the full formulation stems from the choice $\alpha_{min} = \alpha_d$ instead of $\alpha_{min} = 0$ and can be seen by comparing Figures 40 and 52. Indeed, recall that, in the non-viscous limit case, v_c is calculated from

$$v_c = -\frac{(1-\alpha)^2}{k(\alpha)}\frac{\partial}{\partial x}(\alpha\Sigma_c(\alpha)) = -\hat{\Sigma}_c\frac{(1-\alpha)^2}{k(\alpha)}\frac{\partial}{\partial x}\left[\alpha\frac{\alpha-\alpha^*}{1-\alpha}\right]H(\alpha-\alpha_{min}).$$

Therefore, choosing $\alpha_{min} = \alpha_d$ makes $v_c = 0$ whenever $\alpha < \alpha_d$, which explains the zero cell velocity in the necrotic core present in Figure 52 but not in Figure 40.

Now, by the same reasoning employed above, since the diffusivity coefficient $\nu_2(\alpha)$ is a multiple of $\Sigma_c(\alpha)$, reinstating $\alpha_{min} \neq 0$ would modify the equation for α from the one in (50) into (53). Thus, one would expect $\alpha_{min} = \alpha_d$ to create a non-smooth graph for α (as seen for v_c) when $\alpha = \alpha_d$. However, notice that when $\alpha < \alpha_d$ in Figure 36, for example, the full viscous model presents an almost constant graph for α. Therefore, we expect that the diffusivity term in the non-viscous limit case in (53) will be negligible

when $\alpha < \alpha_d$ since $\dfrac{\partial \alpha}{\partial x}$ will be small. Ultimately, this is the reason why the graph of the cell concentration (Figure 50) looks fairly smooth.

However, with the change $\alpha_{min} = \alpha_d$, we are able to see the dynamics for longer period of time and thus notice another limitation of the non-viscous limit case that was not apparent in shorter time frames. Compare, for example, Figures 36 and 50. Because of the boundary condition $\alpha = \alpha^*$ at the moving boundary, the non viscous case is not able to predict high concentration near the boundary of a tumour with a thin proliferating rim as is the full viscous formulation.

Having said that, from now on, we focus on the full one dimensional formulation of the two phase model of tumour growth defined in Section 2.2.4.

3.3 CONCLUSION

Thus, in this chapter we have

1. Simulated the solutions in six different parameter regimes of the full one dimensional two phase model and its negligible viscosity limit case by using a finite difference scheme.

2. Confirmed the validity of the full two phase model by observing in these simulations known biological dynamics of tumour growth including nutrient depletion, cell death, cell movement, diffusion limited steady state, a necrotic core and a thin proliferating rim.

3. Explored the effects of the natural cell packing density on tumour growth and decay by observing that lower natural packing densities allow tumours to grow faster and larger and recede slower than higher packing densities.

4. Enumerated the differences between simulations of the negligible viscosity limit model and the full one dimensional formulation.

5. Studied numerical limitations of the negligible viscosity limit by exploring the well-posedness of its equations and its effects on simulations. In order to remedy this, we proposed and tested a parameter change that causes the limit model to become well-posed.

6. Observed from simulations that the non-viscous limit is not apt to model the thin proliferating rim as well as the full formulation because of the boundary condition of the cell concentration on the moving boundary.

Therefore, we return to the full two phase one dimensional model described in Subsection 2.2.4, which is generalised slightly in the next page.

4

NEGLIGIBLE NUTRIENT UPTAKE & CELL DRAG LIMIT AND THE STABILITY OF A TIME-DEPENDENT SOLUTION IN ONE DIMENSION

4.1 INTRODUCTION AND MOTIVATION

Consider again the full one dimensional model from Section 2.2.4

$$\begin{cases} \dfrac{\partial \alpha}{\partial t} &= S_c(\alpha, C) - \dfrac{\partial}{\partial x}(\alpha v_c), \\ 0 &= \dfrac{\partial^2 C}{\partial x^2} - Q_c(\alpha, C), \\ 0 &= \dfrac{\partial}{\partial x}\left(\hat{\mu}_c \alpha \dfrac{\partial v_c}{\partial x} - \alpha \Sigma_c(\alpha)\right) - \dfrac{k(\alpha)}{(1-\alpha)^2} v_c, \end{cases} \tag{54}$$

with moving boundary condition

$$\frac{dR}{dt}(t) = v_c(R(t), t)$$

subject to the boundary and initial conditions

$$\begin{cases} v_c = \dfrac{\partial C}{\partial x} = 0, & \text{at } x = 0, \\ \hat{\mu}_c \dfrac{\partial v_c}{\partial x} - \Sigma_c(\alpha) = 0, \quad C = C_\infty, & \text{on } x = R(t), \\ \alpha = \alpha_0, \quad R = R_0, \quad v_c = v_0, \quad C = C_0, & \text{at } t = 0, \end{cases}$$

where

$$S_c(\alpha, C) = \Big(\frac{s_0 C}{1+s_1 C}\Big)\alpha(1-\alpha) - \Big(\frac{s_2+s_3 C}{1+s_4 C}\Big)\alpha, \quad s_i > 0, (i = 0, \dots 4),$$
$$Q_c(\alpha, C) = \frac{Q_0 C \alpha}{1+Q_1 C}, \quad Q_0, Q_1 > 0,$$
$$k(\alpha) = k_0 \alpha(1-\alpha), \quad k_0 > 0.$$

In contrast to the previous formulation, in this Chapter we will allow $\Sigma_c(\alpha)$ to vary within a family of functions described subsequently.

Observations Regarding $\Sigma_c(\alpha)$

Consider now $\Sigma_c(\alpha)$ and recall that it was defined as the pressure difference between the cell and water phases, i.e.

$$\Sigma_c(\alpha) = p_c - p_w.$$

When formulating the model, we described the existence of two biologically meaningful parameters that are important in the definition of $\Sigma_c(\alpha)$, namely α_{min} and α^*. The first represents a minimal cell concentration necessary to generate a discrepancy between the cell and water pressure. In other words, $p_c = p_w$ whenever $0 \leq \alpha < \alpha_{min}$, as there are not enough cells to generate an instability between the cell and water pressure. We assume cells are sufficiently packed together such that α_{min} does not play an important role in our analysis. However, the second parameter, the natural cell density α^* is crucial in driving growth and will thus be central to the analysis that follows.

By definition, if $\alpha > \alpha^*$, cells are tightly packed and tend to move apart which implies that the pressure of the cells is stronger than the pressure of the water, i.e. $p_c > p_w$. Similarly, if $\alpha < \alpha^*$, cells are sparse and tend to aggregate and therefore $p_c < p_w$. With these in mind, we expect that, no

matter how general we may want to leave $\Sigma_c(\alpha)$, for a biologically significant definition it must satisfy the following conditions:

$$\Sigma_c(\alpha) = p_c - p_w \begin{cases} = 0, & \text{if } 0 \leq \alpha < \alpha_{min} \\ < 0, & \text{if } \alpha_{min} \leq \alpha < \alpha^*, \\ = 0, & \text{if } \alpha = \alpha^*, \\ > 0, & \text{if } \alpha^* < \alpha < 1. \end{cases} \tag{55}$$

Notice that the sign change at α^* implies necessarily that $\Sigma_c'(\alpha^*) > 0$.

With only these conditions on $\Sigma_c(\alpha)$, we will look at stability analysis of some steady state solutions of this model. However, these will turn out to be either trivial solutions or to generate absurd values for some of the parameters of the model, namely $Q_0 = 0 = k_0$. This contradiction will, in turn, steer our focus towards the limit case of this model found by assuming that nutrient uptake and cell drag are negligible, i.e. $Q_c(\alpha, C) \equiv 0 \equiv k(\alpha)$. Non-homogeneous time-dependent solutions to this limit case will give us insight on the solution of the original system above when Q_0 and k_0 are small and numerical simulations are performed to illustrate this.

4.2 FULL ONE DIMENSIONAL SYSTEM

4.2.1 *Homogeneous Steady State Solution*

Let $(\alpha_h, C_h, v_h, R_h)$ be a homogeneous steady state solution of the system above. Then, the boundary conditions imply that $v_h = 0$, $C_h = C_\infty$, $\Sigma_c(\alpha_h) = 0$, $R_h = R_0$ and equations in (54) imply that $S_c(\alpha_h, C_\infty) = 0$ and $Q_c(\alpha_h, C_\infty) = 0$. Particularly, from the S_c and Q_c chosen above and the fact that $\Sigma_c(0) = 0$, it becomes clear that the only homogeneous steady state for our system is the trivial solution

$$(\alpha_h, C_h, v_h, R_h) = (0, C_\infty, 0, R_0).$$

4.2.2 *A Non-Homogeneous Solution*

We now turn to find a non-trivial solution of the type:

$$(\alpha_h, C_h, v_s(x), R_*(t)), \qquad 0 < \alpha_h < 1, \qquad C_h > 0, \qquad v_s(x) \not\equiv 0.$$

From the equations in (54), we see that a solution of this type must satisfy $Q_c(\alpha_h, C_\infty) = 0$ and

$$S_c(\alpha_h, C_\infty) = \alpha_h \frac{\partial v_s}{\partial x} \tag{56}$$

$$\frac{k(\alpha_h) v_s}{(1-\alpha_h)^2} = \hat{\mu}_c \alpha_h \frac{\partial^2 v_s}{\partial x^2}. \tag{57}$$

However, differentiating equation (56) with respect to x we see that $0 \equiv \alpha_h \frac{\partial^2 v_s}{\partial x^2}$ and therefore equation (57) implies that $k(\alpha_h) v_s(x) \equiv 0$, i.e. $k(\alpha_h) = 0$. Particularly, from $Q_c(\alpha, C)$ and $k(\alpha)$ chosen above, it becomes clear that $Q_c(\alpha_h, C_\infty) = 0$ and $k(\alpha_h) = 0$ imply that $Q_0 = k_0 = 0$, which is absurd unless nutrient consumption and cell drag are null.

4.3 LIMIT WITH NEGLIGIBLE NUTRIENT UPTAKE & CELL DRAG

4.3.1 *Formulation*

Motivated now by the contradictions $Q_0 = k_0 = 0$, we choose to consider the limit case of our system where nutrient uptake and cell drag are taken to be negligible, i.e. $Q_c(\alpha, C) \equiv 0 \equiv k(\alpha)$. (Advantages of using this limit will be explored in Section 6.2). In this case, C is defined by

$$0 = \frac{\partial^2 C}{\partial x^2}(x,t), \qquad \frac{\partial C}{\partial x}(0,t) = 0, \qquad C(R(t),t) = C_\infty,$$

which imply that $C(x,t) \equiv C_\infty$ and therefore the system may be rewritten, as

$$\begin{cases} \dfrac{\partial \alpha}{\partial t} = S_c(\alpha, C_\infty) - \dfrac{\partial}{\partial x}(\alpha v_c), \\ 0 = \dfrac{\partial}{\partial x}\Big(\hat{\mu}_c \alpha \dfrac{\partial v_c}{\partial x} - \alpha \Sigma_c(\alpha)\Big), \end{cases}$$

with moving boundary equation

$$\frac{dR}{dt}(t) = v_c(R(t), t)$$

subject to boundary conditions

$$\begin{cases} 0 = v_c, & \text{at } x = 0, \\ 0 = \hat{\mu}_c \dfrac{\partial v_c}{\partial x} - \Sigma_c(\alpha) & \text{at } x = R(t). \end{cases}$$

Now, notice that, via integration, the second equation of the system and the last boundary condition above imply that

$$0 = \hat{\mu}_c \frac{\partial v_c}{\partial x} - \Sigma_c(\alpha) \qquad \forall (x,t) \in (0, R(t)] \times (0, \infty).$$

Therefore, this system may be recast as

$$\begin{cases} \dfrac{\partial \alpha}{\partial t} &= S_c(\alpha, C_\infty) - \dfrac{\partial}{\partial x}(\alpha v_c), \\ 0 &= \hat{\mu}_c \dfrac{\partial v_c}{\partial x} - \Sigma_c(\alpha), \end{cases} \tag{58}$$

with moving boundary equation

$$\frac{dR}{dt}(t) = v_c(R(t), t)$$

subject to the boundary condition $v_c(0,t) = 0$.

4.3.2 *Homogeneous Steady State Solutions*

Notice that any homogeneous steady state solutions of the system above would be of the form $(\alpha_h, 0, R_0)$, where α_h satisfies

$$S_c(\alpha_h, C_\infty) = 0 \qquad \text{and} \qquad \Sigma_c(\alpha_h) = 0.$$

Linearising about this steady state, we obtain the following system for perturbations $(\hat{\alpha}(x,t), \hat{v}_c(x,t), \hat{R}(t))$:

$$\begin{cases} \dfrac{\partial \hat{\alpha}}{\partial t} = \dfrac{\partial S_c}{\partial \alpha}(\alpha_h, C_\infty)\hat{\alpha} - \alpha_h \dfrac{\partial \hat{v}_c}{\partial x} \\ 0 = \hat{\mu}_c \dfrac{\partial \hat{v}_c}{\partial x} - \Sigma_c'(\alpha_h)\hat{\alpha} \\ \dfrac{d\hat{R}}{dt} = \hat{v}_c(R_0, t) \\ 0 = \hat{v}_c(0,t). \end{cases}$$

Using separation of variables, one can solve the system above to yield

$$\begin{cases} \hat{\alpha}(x,t) = \hat{\alpha}_0(x)e^{\lambda_0 t} \\ \hat{v}_c(x,t) = \dfrac{\Sigma_c'(\alpha_h)}{\hat{\mu}_c} e^{\lambda_0 t} \displaystyle\int_0^x \hat{\alpha}_0(s)\mathrm{d}s \\ \hat{R}(t) = \dfrac{\Sigma_c'(\alpha_h)}{\hat{\mu}_c} e^{\lambda_0 t} \displaystyle\int_0^{R_0} \hat{\alpha}_0(s)\mathrm{d}s. \end{cases}$$

with

$$\lambda_0 = \frac{\partial S_c}{\partial \alpha}(\alpha_h, C_\infty) - \alpha_h \frac{\Sigma_c'(\alpha_h)}{\hat{\mu}_c}.$$

Suppose that $\hat{\alpha}(x,0) = \hat{\alpha}_0(x)$ is continuous in $[0,R_0]$. Therefore, by the mean value theorem, for every $x \in [0,R_0]$ there is an $x_0 \in (0,R_0)$ such that

$$\left| \int_0^x \hat{\alpha}_0(s)\mathrm{d}s \right| = |\hat{\alpha}_0(x_0)x| \leq |\hat{\alpha}_0(x_0)|R_0 < \infty.$$

Consequently, one can see, from the expressions of $\hat{\alpha}$, $\hat{v}_c$ and $\hat{R}$ obtained above, that these perturbations tend to 0 or ∞ depending only on the sign of λ_0.

Thus, in order to characterise the stability of this solution, we must determine the sign of λ_0. For this, since $\Sigma_c(\alpha_h) = 0$, we must first use the properties assumed for $\Sigma_c(\cdot)$ in Subsection 4.1 and (55) to characterise α_h. Indeed, recall that

i. $\Sigma_c(\alpha_h) = 0$ if, and only if, $\alpha_h \in [0,\alpha_{min}) \cup \{\alpha^*\}$, and

ii. $\Sigma_c'(\alpha_h) \geq 0$ for all $\alpha_h \in [0,\alpha_{min}) \cup \{\alpha^*\}$.

Therefore we must search for the sign of λ_0 when $\alpha_h \in [0,\alpha_{min}) \cup \{\alpha^*\}$ using item $(ii.)$ and the fact that $S_c(\alpha_h, C_\infty) = 0$.

Suppose initially that $\alpha_h \neq 0$. Differentiating S_c with respect to α, we see that $S_c(\alpha_h, C_\infty) = 0$ implies that

$$\begin{aligned} \frac{\partial S_c}{\partial \alpha}(\alpha_h, C_\infty) &= \left(\frac{s_0 C_\infty}{1+s_1 C_\infty}\right)(1-2\alpha_h) - \frac{s_2 + s_3 C_\infty}{1+s_4 C_\infty} \\ &= \frac{S_c(\alpha_h, C_\infty)}{\alpha_h} - \frac{s_0 C_\infty \alpha_h}{1+s_1 C_\infty} = -\frac{s_0 C_\infty \alpha_h}{1+s_1 C_\infty}, \qquad \alpha_h \neq 0 \end{aligned}$$

and therefore

$$\lambda_0 = \frac{\partial S_c}{\partial \alpha}(\alpha_h, C_\infty) - \alpha_h \frac{\Sigma_c'(\alpha_h)}{\hat{\mu}_c} = -\alpha_h \left[\frac{s_0 C_\infty}{1 + s_1 C_\infty} + \frac{\Sigma_c'(\alpha_h)}{\hat{\mu}_c} \right], \qquad \alpha_h \neq 0.$$

From $(ii.)$ and the equation above, we see that $\lambda_0 < 0$ for all $\alpha_h \in (0, \alpha_{min}) \cup \{\alpha^*\}$.

Suppose now that $\alpha_h = 0$. Then,

$$\lambda_0 = \frac{\partial S_c}{\partial \alpha}(\alpha_h, C_\infty) - \alpha_h \frac{\Sigma_c'(\alpha_h)}{\hat{\mu}_c} = \frac{\partial S_c}{\partial \alpha}(0, C_\infty) = \frac{s_0 C_\infty}{1 + s_1 C_\infty} - \frac{s_2 + s_3 C_\infty}{1 + s_4 C_\infty}.$$

So, in summary, the steady state is unstable to homogeneous perturbations if, and only if, $\alpha_h = 0$ and

$$\frac{\partial S_c}{\partial \alpha}(0, C_\infty) = \frac{s_0 C_\infty}{1 + s_1 C_\infty} - \frac{s_2 + s_3 C_\infty}{1 + s_4 C_\infty} > 0.$$

Although this resolves the linear stability analysis of a constant steady state solution of the limit case where nutrient uptake and cell drag are negligible, we notice that this steady state is actually trivial. Indeed, both cell concentration and cell velocity are null and the tumour remains fixed at its initial size. Therefore, we will include some heterogeneity in the solution in order to find a more interesting base state solution.

4.3.3 *A Time-Dependent Non-homogeneous Solution*

We shall search now for a non-trivial solution of the limit case system (58) of the form

$$(\alpha_h, v_s(x), R_*(t)), \quad 0 < \alpha_h < 1, \quad v_s(x) \not\equiv 0, \quad R_*(t) > 0, \quad R_*(t) \not\equiv R_0,$$

From the second equation and the boundary condition $v_c(0,t) = 0$, we obtain that

$$v_s(x) = \lambda_2 x, \qquad \lambda_2 = \frac{\Sigma_c(\alpha_h)}{\hat{\mu}_c}.$$

Substituting v_s into the equation for $R(t)$, we see that

$$\frac{dR_*}{dt}(t) = v_s(R_*(t)) = \lambda_2 R_*(t) \quad \Longrightarrow \quad R_*(t) = R_0 e^{\lambda_2 t}.$$

On the other hand, substituting $\alpha = \alpha_h$ and v_s into the first equation of the system above, we see that

$$S_c(\alpha_h, C_\infty) = \alpha_h \frac{\partial v_s}{\partial x} = \alpha_h \lambda_2.$$

So, in summary, a non-trivial solution $(\alpha_h, C_h, v_s(x), R_*(t))$ of the limit case $Q_c(\alpha, C) \equiv 0 \equiv k(\alpha)$ of the system in question satisfies

$$(\alpha_h, C_h, v_s(x), R_*(t)) = (\alpha_h, C_\infty, \lambda_2 x, R_0 e^{\lambda_2 t}), \qquad \lambda_2 = \frac{\Sigma_c(\alpha_h)}{\hat{\mu}_c},$$

where α_h is defined as the solution to

$$\hat{\mu}_c S_c(\alpha_h, C_\infty) = \alpha_h \Sigma_c(\alpha_h).$$

Notice that, to guarantee that $v_s(x) \not\equiv 0$ and $R_*(t) \not\equiv R_0$, such solution must have $\Sigma_c(\alpha_h) \neq 0$. In particular, if we consider the sign profile of $\Sigma_c(\cdot)$ in (55), we must have $\alpha_{min} \leq \alpha_h < 1$ with $\alpha_h \neq \alpha^*$. Moreover,

$$v_s(x) = \begin{cases} \text{Positive and linearly increasing with } x, & \text{if } \alpha_h > \alpha^*, \\ \text{Negative and linearly decreasing with } x, & \text{if } \alpha_{min} \leq \alpha_h < \alpha^*, \end{cases}$$

and similarly

$$0 < R_*(t) = \begin{cases} \text{Increasing exponentially with } t, & \text{if } \alpha_h > \alpha^*, \\ \text{Decreasing exponentially with } t, & \text{if } \alpha_{min} \leq \alpha_h < \alpha^*. \end{cases}$$

In other words, if $(\alpha_h, v_s(x), R_*(t))$ is not trivial, then there are two possibilities for this non-homogeneous time-dependent solution, which depend on the sign of $\alpha_h - \alpha^*$, namely:

1. If $\alpha_h > \alpha^*$, then $\lambda_2 > 0$ and $(\alpha_h, v_s(x), R_*(t))$ is of the form

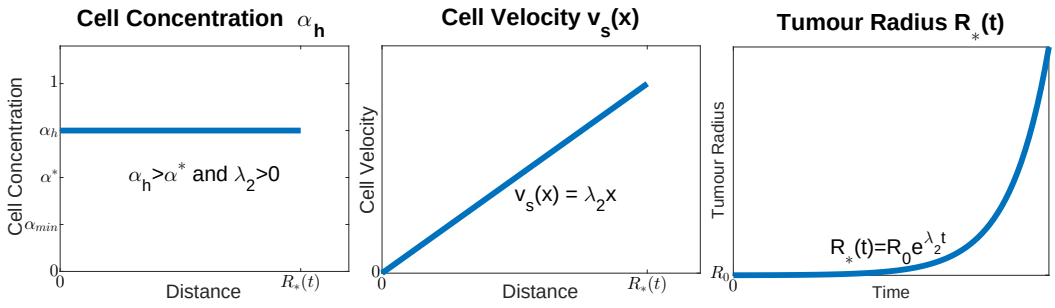


Figure 53.: Time-dependent non-homogeneous solutions of the negligible nutrient uptake and cell drag limit with growing tumour size.

2. If $\alpha_h < \alpha^*$, then $\lambda_2 < 0$ and $(\alpha_h, v_s(x), R_*(t))$ is of the form

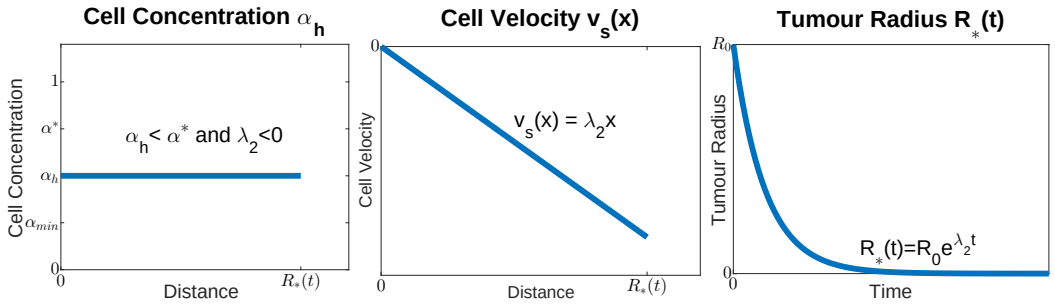


Figure 54.: Time-dependent non-homogeneous solutions of the negligible nutrient uptake and cell drag limit with decaying tumour size.

We will refer to these as the growing and decaying **travelling solutions**, respectively.

4.3.4 *Linearisation about the Travelling Solution*

Linearising the system (58) about the travelling solution:

$$(\alpha_h, v_s(x), R_*(t)) = \left(\alpha_h, \lambda_2 x, R_0 e^{\lambda_2 t}\right), \qquad \lambda_2 = \frac{\Sigma_c(\alpha_h)}{\hat{\mu}_c} = \frac{S_c(\alpha_h, C_\infty)}{\alpha_h},$$

we may see that the perturbations $(\hat{\alpha}(x,t), \hat{v}_c(x,t), \hat{R}(t))$ satisfy

$$\begin{cases} \dfrac{\partial \hat{\alpha}}{\partial t} = \left[\dfrac{\partial S_c}{\partial \alpha}(\alpha_h, C_\infty) - \lambda_2\right]\hat{\alpha} - \lambda_2 x \dfrac{\partial \hat{\alpha}}{\partial x} - \alpha_h \dfrac{\partial \hat{v}_c}{\partial x} \\ 0 = -\Sigma_c'(\alpha_h)\hat{\alpha} + \hat{\mu}_c \dfrac{\partial \hat{v}_c}{\partial x} \end{cases}$$

with moving boundary equation

$$\frac{d\hat{R}}{dt}(t) = \hat{v}_c(R_*(t), t) + \lambda_2 \hat{R}(t)$$

and boundary condition $\hat{v}_c(0,t) = 0$.

We will (once again) apply the change of variable

$$x = x(t) = \xi R_*(t)$$

to the system above. Consequently, we have

$$\frac{\partial}{\partial t} \longrightarrow \frac{\partial}{\partial t} - \frac{\xi}{R_*(t)}\frac{dR_*}{dt}\frac{\partial}{\partial \xi} = \frac{\partial}{\partial t} - \lambda_2 \xi \frac{\partial}{\partial \xi}$$
$$\frac{\partial}{\partial x} \longrightarrow \frac{1}{R_*(t)}\frac{\partial}{\partial \xi}$$

and thus the system may be recast as:

$$\begin{cases} \dfrac{\partial \hat{\alpha}}{\partial t} = \Big[\dfrac{\partial S_c}{\partial \alpha}(\alpha_h, C_\infty) - \lambda_2\Big]\hat{\alpha} - \dfrac{\alpha_h}{R_*(t)}\dfrac{\partial \hat{v}_c}{\partial \xi} & (59) \\ 0 = -\Sigma_c'(\alpha_h)\hat{\alpha} + \dfrac{\hat{\mu}_c}{R_*(t)}\dfrac{\partial \hat{v}_c}{\partial \xi} & (60) \end{cases}$$

in $\{\xi \in (0,1), t > 0\}$ and

$$\frac{d\hat{R}}{dt}(t) = \hat{v}_c(1,t) + \lambda_2 \hat{R}(t)$$

for $t > 0$, subject to the boundary condition $v_c(0,t) = 0$.

Notice that the last terms in each of the two equations of the system above are comparable. Thus, by substituting the second equation into the first, we obtain an equation for $\hat{\alpha}$, namely

$$\frac{\partial \hat{\alpha}}{\partial t} = \lambda_1 \hat{\alpha}, \qquad \text{where} \qquad \lambda_1 = \frac{\partial S_c}{\partial \alpha}(\alpha_h, C_\infty) - \frac{\alpha_h \Sigma_c'(\alpha_h)}{\hat{\mu}_c} - \lambda_2.$$

This can be solved for $\hat{\alpha}$, from which $\hat{v}_c$ and $\hat{R}$ follow. In this manner, returning to (x,t) variables, we obtained for $0 < x < R_*(t)$, and $t > 0$, that

$$\hat{\alpha}(x,t) = \hat{\alpha}\Big(\frac{x}{R_*(t)}, 0\Big)e^{\lambda_1 t} \tag{61}$$

$$\hat{v}_c(x,t) = \frac{\Sigma_c'(\alpha_h)}{\hat{\mu}_c} e^{\lambda_1 t} R_*(t) \int_0^{\frac{x}{R_*(t)}} \hat{\alpha}(z,0)\mathrm{d}z \tag{62}$$

$$\hat{R}(t) = \frac{\Sigma_c'(\alpha_h)}{\hat{\mu}_c \lambda_1} R_*(t) e^{\lambda_1 t} \int_0^1 \hat{\alpha}(z,0)\mathrm{d}z. \tag{63}$$

We shall say that a travelling solution $(\alpha_h, v_{cs}(x), R_*(t))$ is linearly unstable to small perturbations $(\hat{\alpha}(x,t), \hat{v}_c(x,t), \hat{R}(t))$ if one of the following is infinite:

$$\lim_{t\to\infty}\Big|\frac{\hat{\alpha}(x,t)}{\alpha_h}\Big|, \qquad \lim_{t\to\infty}\Big|\frac{\hat{v}_c(x,t)}{v_{cs}(x)}\Big|, \qquad \lim_{t\to\infty}\Big|\frac{\hat{R}(t)}{R_*(t)}\Big|$$

for any $x \in (0, R_*(t))$.

Since our base state solution is time-dependent, we use this definition because it is a natural extension of the definition of instability in fixed domains with steady state solutions but it also allows us to compare effectively the long time behaviour of solutions to that of this time-dependent base state.

From the equations above, it is possible to obtain

$$\begin{aligned}
\frac{\hat{\alpha}(x,t)}{\alpha_h} &= \frac{1}{\alpha_h}\hat{\alpha}\Big(\frac{x}{R_*(t)},0\Big)e^{\lambda_1 t} \\
\frac{\hat{v}_c(x,t)}{v_{cs}(x)} &= \frac{\Sigma_c'(\alpha_h)}{\hat{\mu}_c\lambda_2}e^{\lambda_1 t}\frac{R_*(t)}{x}\int_0^{\frac{x}{R_*(t)}}\hat{\alpha}(z,0)\mathrm{d}z \\
\frac{\hat{R}(t)}{R_*(t)} &= \frac{\Sigma_c'(\alpha_h)}{\hat{\mu}_c\gamma_1}e^{\lambda_1 t}\int_0^1\hat{\alpha}(z,0)\mathrm{d}z.
\end{aligned}$$

Now, using the mean value theorem, we see that if $\hat{\alpha}(\cdot,0)$ is continuous, then there exists a $z_0 \in \Big(0, \dfrac{x}{R_*(t)}\Big) \subset (0,1)$ such that

$$\Big|\frac{R_*(t)}{x}\int_0^{\frac{x}{R_*(t)}}\hat{\alpha}(z,0)dz\Big| = \Big|\frac{R_*(t)}{x}\hat{\alpha}(z_0,0)\frac{x}{R_*(t)}\Big| = |\hat{\alpha}(z_0,0)| < \infty.$$

Therefore, the travelling solution is unstable to small perturbations if, and only if,

$$\lambda_1 = \frac{\partial S_c}{\partial\alpha}(\alpha_h, C_\infty) - \frac{\alpha_h\Sigma_c'(\alpha_h)}{\hat{\mu}_c} - \lambda_2 > 0. \tag{64}$$

Particularly, this means that, when the travelling solution is stable, $\lambda_1 < 0$ and thus

$$\lim_{t\to\infty}\Big|\frac{\hat{R}(t)}{R_*(t)}\Big| = \lim_{t\to\infty}\Big|\frac{\Sigma_c'(\alpha_h)}{\hat{\mu}_c\gamma_1}e^{\lambda_1 t}\int_0^1\hat{\alpha}(z,0)\mathrm{d}z\Big| = 0.$$

Consequently, when the solution $R(t)$ is perturbed off of the base state $R_*(t)$, then

$$\lim_{t\to\infty}\left|\frac{R(t)}{R_*(t)}\right| = \lim_{t\to\infty}\left|\frac{R_*(t)+\epsilon\hat{R}(t)}{R_*(t)}\right| = \lim_{t\to\infty}\left|1+\epsilon\frac{\hat{R}(t)}{R_*(t)}\right| = 1, \tag{65}$$

which implies that $R(t)$ will grow or decay exponentially at the same rate as $R_*(t)$, when t is sufficiently large. This behaviour will be visible in subsequent simulations.

4.3.5 *Summary*

In summary, we have two possible travelling solutions, depending on the sign of $\alpha_h - \alpha^*$.

1. If $\alpha_h > \alpha^*$, then $\lambda_2 > 0$ and $(\alpha_h, v_s(x), R_*(t))$ is of the form

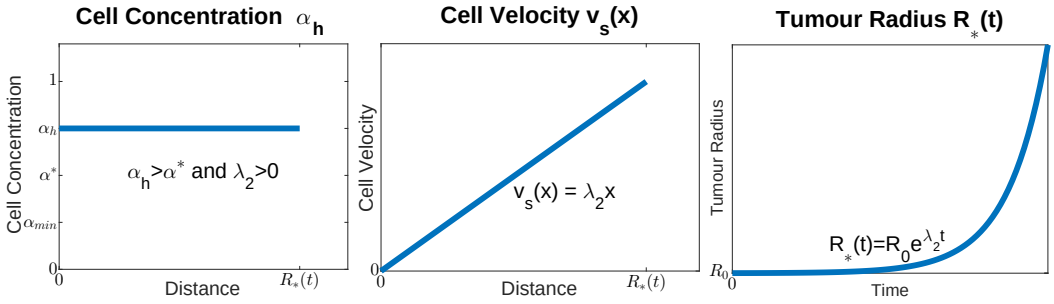


Figure 55.: Time-dependent non-homogeneous solutions of the negligible nutrient uptake and cell drag limit with growing tumour size, which we have called the **growing travelling solution**.

2. If $\alpha_h < \alpha^*$, then $\lambda_2 < 0$ and $(\alpha_h, v_s(x), R_*(t))$ is of the form

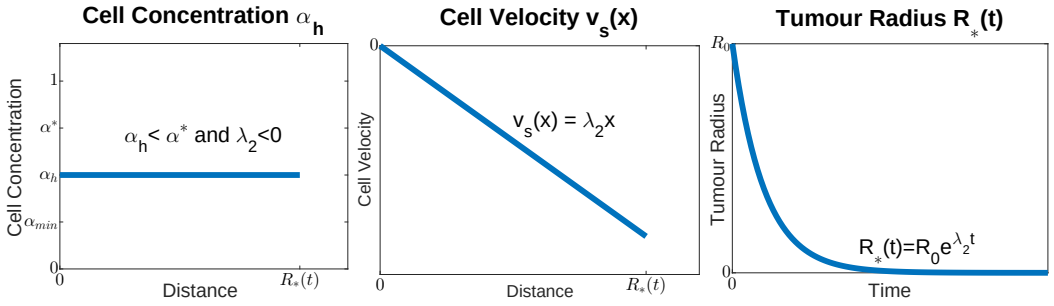


Figure 56.: Time-dependent non-homogeneous solutions of the negligible nutrient uptake and cell drag limit with decaying tumour size, which we have called the **decaying travelling solution**.

Additionally, these solutions are linearly unstable if, and only if,

$$\lambda_1 = \frac{\partial S_c}{\partial \alpha}(\alpha_h, C_\infty) - \frac{\alpha_h \Sigma_c'(\alpha_h)}{\hat{\mu}_c} - \lambda_2 > 0.$$

4.4 CRITICAL NUTRIENT CONCENTRATION

4.4.1 *Motivation and Definition*

We will now use this limit case and its travelling solutions to analyse the dependence of the original model (with small k_0 and Q_0) on the nutrient concentration outside of the tumour, namely C_∞. Notice from the graphs above that the profile of growth or saturation of $R_*(t)$ changes with the sign of $\alpha_h - \alpha^*$.

Therefore, we first find $C_{crit} > 0$ such that $\alpha_h = \alpha^*$ for $C_\infty = C_{crit}$. When such a critical value exists and $(\alpha_h, v_s(x), C_{crit}, R_*(t))$ is stable, it is reasonable to expect that the tumour will grow if $C_\infty > C_{crit}$ and shrink if $C_\infty < C_{crit}$.

To see this, we first search for this nutrient threshold C_{crit}. Indeed, if $\alpha_h = \alpha^*$ and $C_\infty = C_{crit}$, then by the definition of α_h and $\Sigma_c(\alpha^*) = 0$, we have that

$$\hat{\mu}_c S_c(\alpha^*, C_{crit}) = \hat{\mu}_c S_c(\alpha_h, C_\infty) = \alpha_h \Sigma_c(\alpha_h) = \alpha^* \Sigma_c(\alpha^*) = 0.$$

Therefore, C_{crit} is defined as the positive solution of

$$0 = S_c(\alpha^*, C) = \Big(\frac{s_0 C}{1 + s_1 C}\Big)\alpha^*(1 - \alpha^*) - \Big(\frac{s_2 + s_3 C}{1 + s_4 C}\Big)\alpha^*.$$

Thus, using the quadratic formula, we may find that

$$C_{crit} = \frac{-A_1 \pm \sqrt{A_1^2 - 4A_2A_0}}{2A_2}$$

such that $C_{crit} > 0$ and

$$A_0 = -s_2, \qquad A_1 = s_0(1 - \alpha^*) - s_3 - s_2 s_1, \qquad A_2 = s_0 s_4(1 - \alpha^*) - s_1 s_3.$$

It is worthwhile to mention that C_{crit} depends only on the parameters s_i of the net cell proliferation rate S_c and the natural cell packing density α^* such that $\Sigma_c(\alpha^*) = 0$. Therefore, it does not depend on the chosen $\Sigma_c(\alpha)$ function except through the value of α^*.

With this, we calculate λ_1 from (64) for each of the parameter cases simulated in the previous chapter using the definition of Σ_c found in (39) and choosing $\alpha_h = \alpha^*$ and C_∞ to be the positive value C_{crit} given by the equality above, if it exists. Indeed, the only case that does not possess a nutrient concentration threshold C_{crit} is Case 3, which thus presents a parameter set modelling a shrinking tumour, no matter how large C_∞ is taken to be.

Table 3.: Natural cell packing density, critical nutrient concentration & instability parameter for Cases 1, 2, 4, 5, 6.

Case	α^*	C_{crit}	λ_1
1	0.60	2.6330	-2.3697
2	0.55	2.0000	-1.9556
4	0.30	1.2071	-0.5927
5	0.10	0.6598	-0.1906
6	0.10	0.5000	-0.1444

Notice from the table above that $\lambda_1 < 0$ for all of these cases. Therefore, due to the continuity of S_c in $[0,1] \times [0,\infty)$ and Σ_c and λ_1 near α^*, a C_∞ sufficiently close to C_{crit} will imply that α_h is sufficiently close to α^*, which in turn will guarantee that λ_1 will remain negative. In other words, taking C_∞ sufficiently close to C_{crit} will preserve the stability of the travelling solution. Therefore, due to our stability analysis, in these cases we must see growth when $C_\infty = C_{crit} + \epsilon$ and decay when $C_\infty = C_{crit} - \epsilon$.

4.4.2 *Simulations with Negligible Nutrient Uptake & Cell Drag*

With these values of C_{crit} at our disposal, we simulated solutions for Cases 1, 2, 4, 5, and 6 with a modified $C_\infty = C_{crit} \pm \epsilon$, with $\epsilon = 0.1$, in order to observe and compare the simulated solution to the predicted solution

$$(\alpha_h, v_s(x), R_*(t)) = (\alpha_h, \lambda_2 x, R_0 e^{\lambda_2 t}) \qquad \hat{\mu}_c S_c(\alpha_h, C_\infty) = \alpha_h \Sigma_c(\alpha_h).$$

We shall call these Cases n^+ and n^-, respectively, to denote this change in C_∞. Since simulations of all of these cases show the same behaviour with regard to C_{crit}, we will present here only the values and simulations regarding Cases 1^+ and 1^- while Cases 2^+, 2^-, 4^+, 4^-, 5^+, 5^-, 6^+, and 6^- can be found in Appendix A. This way, for Cases 1^+ and 1^- we obtained the following values by choosing $C_\infty = C_{crit} \pm \epsilon$:

Table 4.: Important values for Cases 1^+ and 1^-

Case	C_{crit}	C_∞	α_h	α^*	λ_1	λ_2
Case 1^+	2.6330	2.7330	0.6021	0.60	-2.4028	0.0053
Case 1^-	2.6330	2.5330	0.5977	0.60	-2.3347	-0.0056

Notice that, from the discussion in the previous section, Case 1^+ represents a growing travelling solution ($\lambda_2 > 0$) while Case 1^- represents a decaying travelling solution ($\lambda_2 < 0$). Additionally, both of these cases are stable ($\lambda_1 < 0$).

Indeed, simulations of solutions of the system (58) of the negligible nutrient uptake and cell drag limit (i.e. the full formulation with $k_0 = Q_0 = 0$) will reinforce our definition of the critical nutrient threshold and our stability analysis. In each of the parameter sets simulated, it is possible to see that

$$\lim_{t\to\infty} \alpha(x,t) = \alpha_h, \qquad \lim_{t\to\infty} v_c(x,t) = \lambda_2 x$$

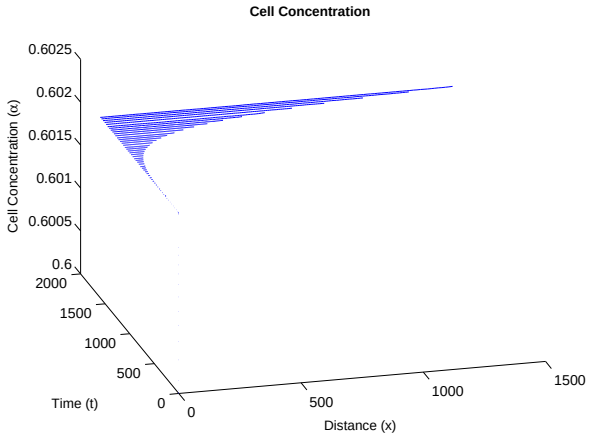
and that $R(t)$ tends to grow or decay as $R_*(t)$, when $t \to \infty$ and thus that the travelling solution is stable. Furthermore, we consider both cases in which $C_\infty = C_{crit} + \epsilon$ and $C_\infty = C_{crit} - \epsilon$ and thus $\lambda_2 > 0$ and $\lambda_2 < 0$, respectively. In comparing these graphs, we see that C_{crit} indeed acts as a nutrient threshold, making the first set of cases grow and the second decay.

We present below first the graphs of the solution of Case 1^+ where the nutrient concentration is chosen above the critical value C_{crit}, and then the graphs of Case 1^-, where the nutrient concentration is chosen below the critical value C_{crit}.

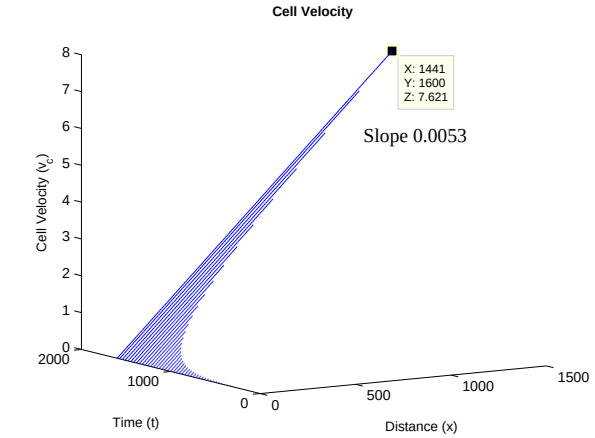
$$C_\infty = C_{crit} + \epsilon, \quad \alpha_h > \alpha^*, \quad \lambda_2 > 0, \quad k_0 = Q_0 = 0$$

Case 1^+: $\alpha_h = 0.6021$ and $\lambda_2 = 0.0053$

(a)



(b)



(c)

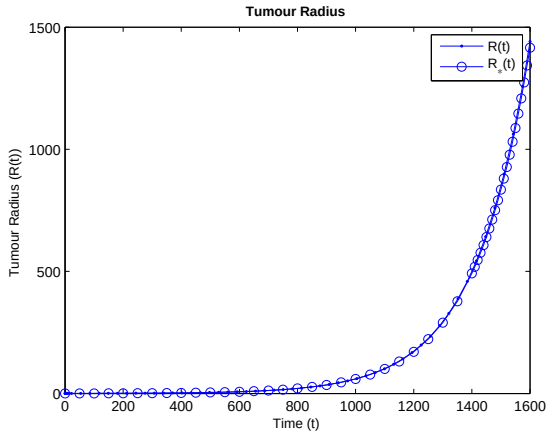
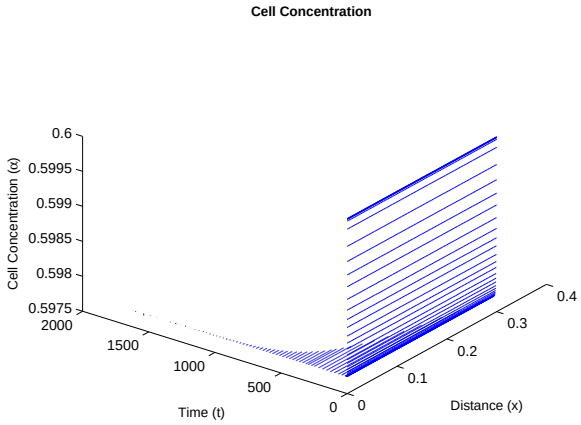


Figure 57.: Evolution of cell concentration (a), cell velocity (b), and tumour radius (c) in Case 1^+ in limit with negligible nutrient uptake and cell drag (i.e. $k_0 = Q_0 = 0$) and $C_\infty = C_{crit} + \epsilon$, $\alpha_h = 0.6021$, and $\lambda_2 = 0.0053$.

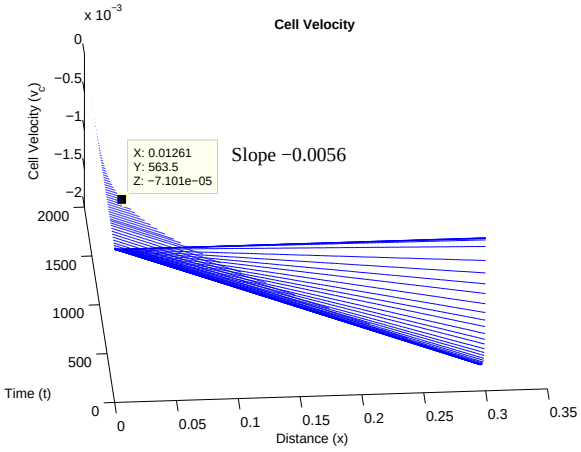
$$C_\infty = C_{crit} - \epsilon, \quad \alpha_h < \alpha^*, \quad \lambda_2 < 0, \quad k_0 = Q_0 = 0$$

Case 1$^-$: $\alpha_h = 0.5977$ and $\lambda_2 = -0.0056$

(a)



(b)



(c)

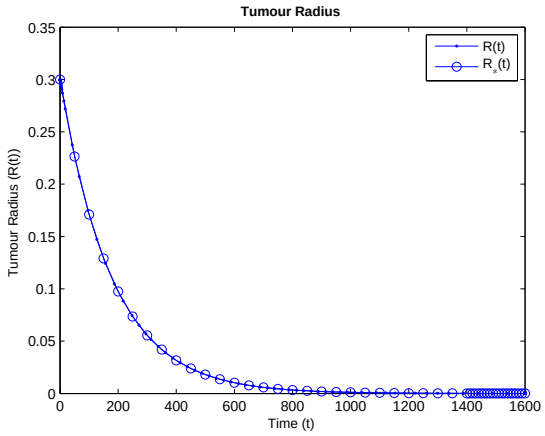


Figure 58.: Evolution of cell concentration (a), cell velocity (b), and tumour radius (c) in Case 1^- in limit with negligible nutrient uptake and cell drag (i.e. $k_0 = Q_0 = 0$) and $C_\infty = C_{crit} - \epsilon$, $\alpha_h = 0.5977$ and $\lambda_2 = -0.0056$.

Conclusion

All the cases considered are ones in which the travelling solution is growing when $C_\infty = C_{crit} + \epsilon$ and decaying when $C_\infty = C_{crit} - \epsilon$. Therefore, the C_{crit} defined analytically in this section is indeed the critical nutrient concentration that dictates if a tumour will grow or shrink, given all other conditions are kept the same. Notably, the value of C_{crit} only depends on the parameters s_i that define the net cell proliferation S_c and the natural packing cell density α^* and thus can be found analytically.

Additionally these travelling solutions are all stable to small perturbations in the limit case scenario where drag and nutrient uptake are taken to be negligible. Therefore,

$$\lim_{t\to\infty} \alpha(x,t) = \alpha_h, \qquad \lim_{t\to\infty} v_c(x,t) = \lambda_2 x$$

and $R(t)$ grows or decays exponentially at rates similar to those of $R_*(t)$.

4.4.3 *Simulations of System with Small Nutrient Uptake & Cell Drag*

Consider the simulations as above, yet now taking k_0 and Q_0 small, of the order 1e$-$4, rather than null:

Table 5.: Values for k_0 and Q_0.

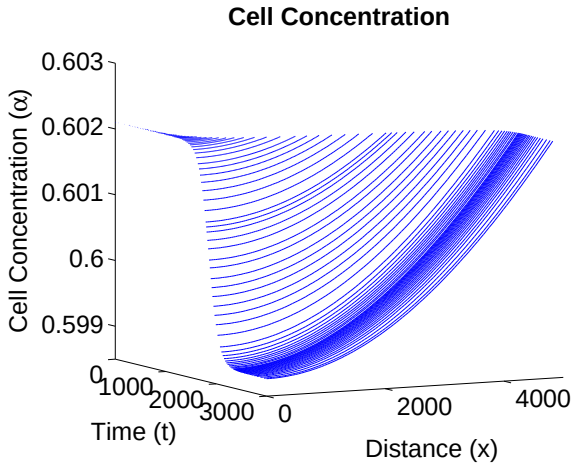
k_0	Q_0
1e$-$4	3e$-$4

In other words, we return to the general model and compare solutions of this system to the travelling solutions of the limit case model analysed above. By using the C_{crit} calculated with the help of the limit case system, we hope to see the tumour growing when $C_\infty > C_{crit}$ and shrinking otherwise, and indeed:

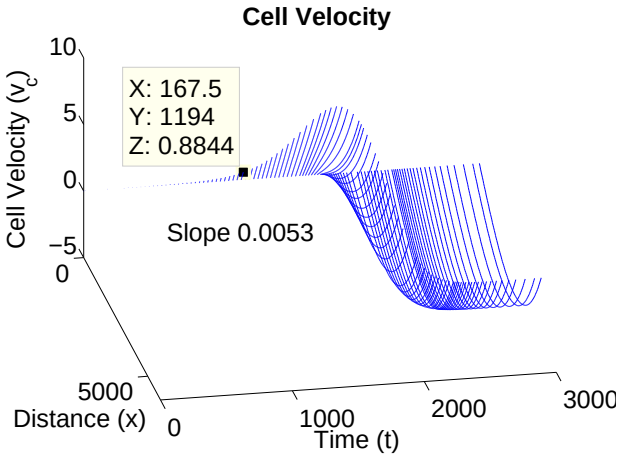
$$C_\infty = C_{crit} + \epsilon, \quad \alpha_h > \alpha^*, \quad \lambda_2 > 0, \quad k_0, Q_0 \text{ small}$$

Case 1$^+$: $\alpha_h = 0.6021$ and $\lambda_2 = 0.0053$

(a)



(b)



(c)

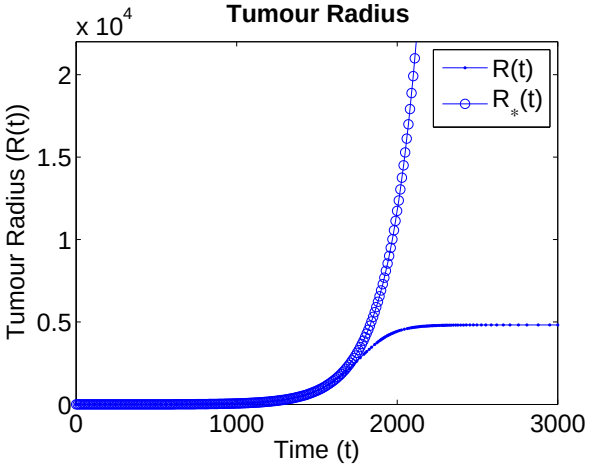
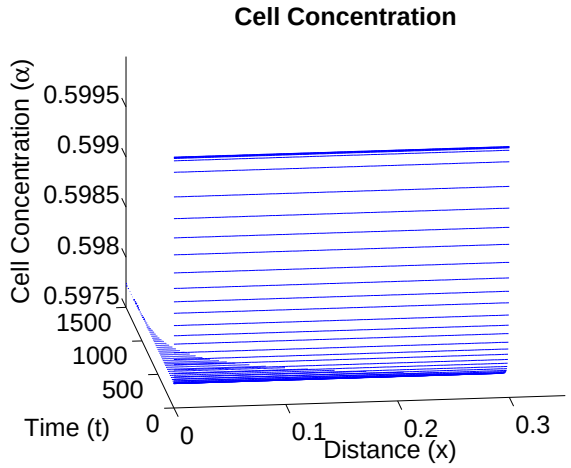


Figure 59.: Evolution of cell concentration (a), cell velocity (b), and tumour radius (c) in Case 1^+ with small nutrient uptake and cell drag (i.e. k_0, Q_0 small) and $C_\infty = C_{crit} + \epsilon$, $\alpha_h = 0.6021$, and $\lambda_2 = 0.0053$.

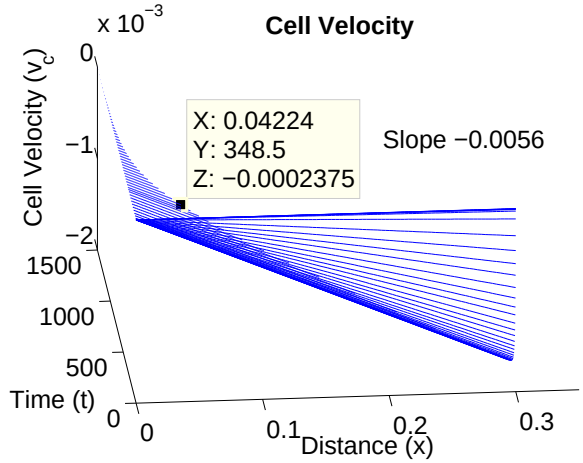
$$C_\infty = C_{crit} - \epsilon, \quad \alpha_h < \alpha^*, \quad \lambda_2 < 0, \quad k_0, Q_0 \text{ small}$$

Case 1$^-$: $\alpha_h = 0.5977$ and $\lambda_2 = -0.0056$

(a)



(b)



(c)

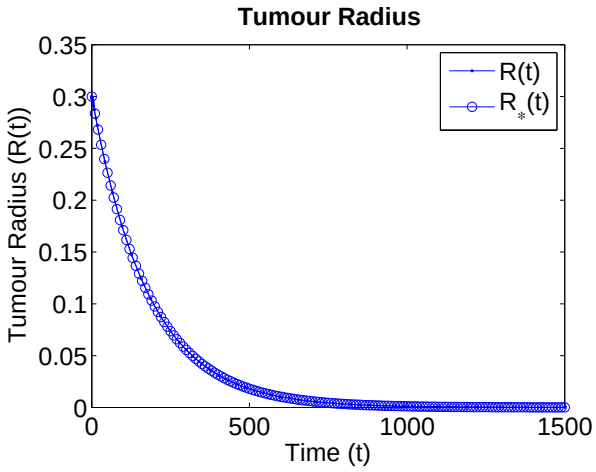


Figure 60.: Evolution of cell concentration (a), cell velocity (b), and tumour radius (c) in Case 1$^-$ with small nutrient uptake and cell drag (i.e. k_0, Q_0 small) and $C_\infty = C_{crit} - \epsilon$, $\alpha_h = 0.5977$, and $\lambda_2 = -0.0056$.

Conclusion

All the cases studied are ones in which the travelling solution is always stable to perturbations in the limit case scenario where drag and nutrient uptake are taken to be negligible. Moreover, C_{crit} as described above is the critical nutrient concentration that dictates if a tumour will grow or shrink, given all other conditions are kept the same. Indeed, if $C_\infty > C_{crit}$ then $\lambda_2 > 0$ and the tumour grows. Otherwise, $\lambda_2 < 0$ and the tumour shrinks.

When we take k_0 and Q_0 to be small, the tumour no longer grows exponentially, as the nutrient uptake eventually makes the growth plateau. However, the exponential growth still approximates the solution $R(t)$ fairly well for intermediate times. Most importantly, the C_{crit} calculated with the help of the limit case system (where drag and nutrient uptake were negligible) still acts as a reasonable approximation for the nutrient threshold that dictates whether the tumour will grow or shrink.

Thus, we have been able to draw information about the full two phase model from the stability of the travelling solutions of the simpler limit case where nutrient uptake and cell drag are negligible. Motivated by this, we continue to study the instability of these travelling solutions in the following chapter.

5

TRAVELLING SOLUTIONS: INSTABILITY IN ONE DIMENSION AND $\Sigma_c(\alpha)$

5.1 INTRODUCTION AND MOTIVATION

In the previous chapter, we formulated a limit case (with negligible nutrient uptake and cell drag) of the full one dimensional formulation of a two phase model of tumour growth. Additionally, we characterised non-homogeneous time-dependent solutions of this limit case and specified a condition for instability, namely $\lambda_1 > 0$. Exploring regions of stability, we were able to calculate a nutrient threshold that dictates whether the tumour will grow or decay both in the limit case and in the full one dimensional formulation.

In this chapter, on the other hand, we will explore the instability of the travelling solutions in one dimension. We will search for a formulation in which one of these solutions is linearly unstable. This will be studied numerically in order to validate the instability condition found in the previous chapter and to visualise its effect on the solutions of the full one dimensional formulation. For this, we must study the function $\Sigma_c(\alpha)$, as it plays a major role in the sign of λ_1.

Initially, we revisit the definition of λ_1 in order to guide our search of a case with an unstable solution, i.e. where $\lambda_1 > 0$. For that, notice that using the definition of S_c and λ_2, we have for $\alpha_h \neq 0$ that

$$\begin{aligned}\frac{\partial S_c}{\partial \alpha}(\alpha_h, C_\infty) &= \Big(\frac{s_0 C_\infty}{1+s_1 C_\infty}\Big)(1-2\alpha_h) - \Big(\frac{s_2+s_3 C_\infty}{1+s_4 C_\infty}\Big) \\ &= \frac{S_c(\alpha_h, C_\infty)}{\alpha_h} - \frac{s_0 C_\infty \alpha_h}{1+s_1 C_\infty} = \lambda_2 - \frac{s_0 C_\infty \alpha_h}{1+s_1 C_\infty},\end{aligned}$$

and therefore, by substitution,

$$\lambda_1 = \frac{\partial S_c}{\partial \alpha}(\alpha_h, C_\infty) - \lambda_2 - \alpha_h \frac{\Sigma_c'(\alpha_h)}{\hat{\mu}_c} = -\alpha_h\Big(\frac{s_0 C_\infty}{1+s_1 C_\infty} + \frac{\Sigma_c'(\alpha_h)}{\hat{\mu}_c}\Big). \tag{66}$$

Consider again the original definition of $\Sigma_c(\cdot)$ found in [19]:

$$\Sigma_c(\alpha) = \frac{\hat{\Sigma}_c |\alpha - \alpha^*|^{r-1}}{(1-\alpha)^q}(\alpha - \alpha^*) H(\alpha - \alpha_{min}), \tag{67}$$

for r, q, $\hat{\Sigma}_c$ positive and $0 \leq \alpha_{min} < \alpha^* < 1$. Notice initially that this particular $\Sigma_c(\alpha)$ satisfies all the conditions set in the beginning of the previous chapter. Also, by differentiation, we may calculate

$$\Sigma_c'(\alpha) = \frac{\hat{\Sigma}_c |\alpha - \alpha^*|^{r-1}}{(1-\alpha)^{q+1}}\Big(r(1-\alpha) + q(\alpha - \alpha^*)\Big) H(\alpha - \alpha_{min}). \tag{68}$$

Recall that, in all the parameter regimes considered so far, we chose $r = q(= 1)$, which in turn implies that

$$\Sigma_c'(\alpha) = \frac{\hat{\Sigma}_c r |\alpha - \alpha^*|^{r-1}}{(1-\alpha)^{r+1}}(1-\alpha^*) H(\alpha - \alpha_{min}) \geq 0.$$

Therefore, from (66), we may conclude that $\lambda_1 < 0$ whenever $r = q$. In other words, all travelling solutions are stable when $r = q$.

Similarly, suppose $\alpha_h > \alpha^*$ and therefore $\lambda_2 > 0$. Recall that, in this case, the travelling solution is one in which the tumour is growing exponentially with an increasing linear velocity in the x direction. Additionally, notice from (68) that $\Sigma_c'(\alpha_h) > 0$ whenever $\alpha_h > \alpha^*$ and therefore $\lambda_1 < 0$ from equation (66). Thus, any growing travelling solution is stable with the definition of $\Sigma_c(\cdot)$ obtained in the literature (67), for any r, q, $\hat{\Sigma}_c$ positive and $0 \leq \alpha_{min} \leq \alpha^* < 1$.

Therefore, in searching for an linearly unstable travelling solution, we will apply two procedures:

1. First, we will find values of r and q such that we have $\lambda_1 > 0$. From the reasoning above, this implies that $r \neq q$ and this will be necessarily a decaying travelling solution, i.e. $\lambda_2 < 0$ and $\alpha_h < \alpha^*$. Simulations will validate the stability analysis performed above.

2. In search of a growing (and thus more interesting) unstable travelling solution, we will modify the current definition of $\Sigma_c(\alpha)$ to obtain a case with three solutions displaying bi-stability. Once again, simulations will be used to validate this stability analysis.

In 1 and 2, numerical simulations will be performed in both of the cases $Q_c(\alpha, C) \equiv 0 \equiv k(\alpha)$ and with Q_0 and k_0 small. The objective is to observe the effectiveness of using such travelling solutions to predict the dynamics of the solutions of the original one dimensional system and thus motivate the use of these travelling solutions in the analysis of the two dimensional case in Chapter 7.

5.2 CHANGING THE PARAMETERS OF $\Sigma_c(\alpha)$ IN SEARCH OF INSTABILITY

5.2.1 *Formulation*

Motivated by the fact that $\lambda_1 < 0$ for all $r = q$, we consider a definition of $\Sigma_c(\cdot)$ that may render $\lambda_1 > 0$, namely,

$$\Sigma_c(\alpha) = \hat{\Sigma}_c \frac{\alpha - \alpha^*}{(1-\alpha)^q},$$

with $q > 1$. Notice that this is the original Σ_c with $\alpha_{min} = 0$, $r = 1$ and $q > 1$, instead of $q = 1$. This change will allow us to have $\lambda_1 > 0$ when q and C_∞ are picked such that α_h satisfies $\alpha_h \Sigma_c(\alpha_h) = \hat{\mu}_c S_c(\alpha_h, C_\infty)$ and

$$\Sigma_c'(\alpha_h) = \frac{\hat{\Sigma}_c\big(1 - \alpha_h + q(\alpha_h - \alpha^*)\big)}{(1-\alpha_h)^{q+1}} < -\hat{\mu}_c \cdot \frac{s_0 C_\infty}{1 + s_1 C_\infty}.$$

Since the right hand side of the inequality above is clearly negative, from the left hand side it is possible to see that we must consider cases where $\alpha_h < \alpha^*$ (and thus $\lambda_2 < 0$) and, particularly, $q > \dfrac{\alpha_h - 1}{\alpha_h - \alpha^*} > 1$. In the previous section, we learned that $\alpha_h < \alpha^*$ implies that $C_\infty < C_{crit}$. Therefore we may expect that sets of sufficiently small C_∞ and sufficiently large q will render a positive λ_1 and thus an unstable travelling solution that is decaying, i.e. $\lambda_1 > 0$, $\lambda_2 < 0$, and $\alpha_h < \alpha^*$.

It is worth mentioning here that C_{crit} was calculated with a general $\Sigma_c(\alpha)$ that satisfies some conditions on its sign and zeros, as specified in the beginning of the previous chapter. That is why, after choosing a different $\Sigma_c(\alpha)$, we may still consider C_{crit} relevant in choosing C_∞, given that this new $\Sigma_c(\alpha)$ still satisfies the aforementioned conditions.

5.2.2 *Simulations*

Consider particularly the set of parameters used in Case 1, except for $q = 3$ in the definition of $\Sigma_c(\alpha)$, and $C_\infty = 0.05$. We shall call this Case 1*.

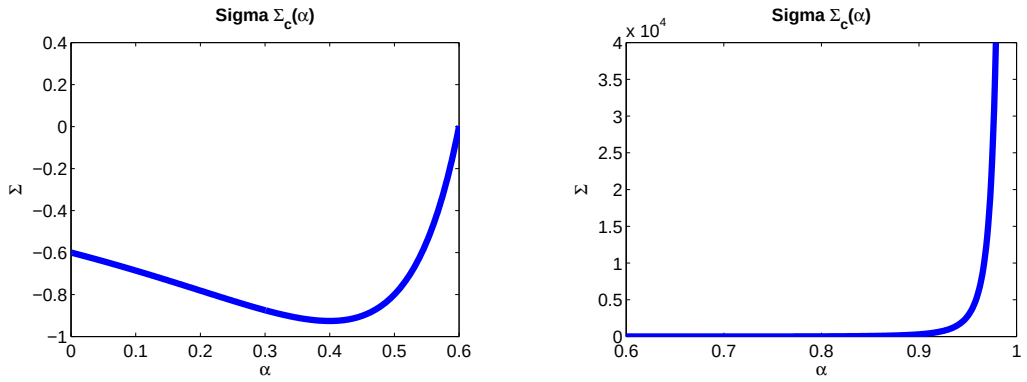


Figure 61.: $\Sigma_c(\alpha)$ function with $r = 1$, $q = 3$, $\hat{\Sigma}_c = 1$ and $\alpha^* = 0.6$

Here, we have two decaying solutions of the type

$$(\alpha_h, v_s(x), C_\infty, R_*(t)) = (\alpha_h, \lambda_2 x, C_\infty, R_0 e^{\lambda_2 t}), \qquad \lambda_2 = \frac{\Sigma_c(\alpha_h)}{\hat{\mu}_c} < 0,$$

generated by the two solutions $\alpha_h \in (0, \alpha^*)$ of the equation

$$\hat{\mu}_c S_c(\alpha_h, C_\infty) = \alpha_h \Sigma_c(\alpha_h).$$

First, these two values of α_h are found from the equation above via a root-finding algorithm (MATLAB® function *fsolve*). These values of α_h are then used to calculate λ_1 and λ_2 via equations

$$\lambda_1 = \frac{\partial S_c}{\partial \alpha}(\alpha_h, C_\infty) - \frac{\alpha_h \Sigma_c'(\alpha_h)}{\hat{\mu}_c} - \lambda_2, \qquad \lambda_2 = \frac{\Sigma_c(\alpha_h)}{\hat{\mu}_c}.$$

This process yields the following values:

Table 6.: Parameters of two decaying travelling solutions

Solution	α_h	λ_1	λ_2
Unstable Solution	0.3189	0.2092	-0.8897
Stable Solution	0.4495	-0.5341	-0.9021

Notice that, in both cases, $\lambda_1 + \lambda_2 < 0$ and $\lambda_2 < 0$. This implies, from equation (63) and the definition of $R_*(t)$, that

$$\lim_{t\to\infty} |\hat{R}(t)| = \lim_{t\to\infty} \left| \frac{\Sigma_c'(\alpha_h)}{\hat{\mu}_c \gamma_1} R_*(t) e^{\lambda_1 t} \int_0^1 \hat{\alpha}(z,0) \mathrm{d}z \right| = 0$$

$$\lim_{t\to\infty} R_*(t) = \lim_{t\to\infty} R_0 e^{\lambda_2 t} = 0.$$

Consequently, any perturbed solution $R(t) = R_*(t) + \epsilon \hat{R}(t)$ will also tend to zero when $t \to \infty$. Additionally, if $R_*(t)$ corresponds to a stable travelling solution, then any perturbed solution will eventually decay at the same rate as $R_*(t)$, as seen from equation (65).

Therefore, in all simulations, we should see $R(t)$ eventually decaying at the same rate as the $R_*(t)$ corresponding to the stable travelling solution. In this section, this means that the tumour radius should decay at the same rate as $R_*(t) = R_0 e^{\lambda_2 t}$, where $\lambda_2 = -0.9021$ (see table 6).

To observe this, we will present numerical simulations of the limit case system with negligible nutrient uptake and cell drag. Choosing initial conditions near the unstable solution, we can see the numerical solution

drift toward the predicted stable solution. Then, we consider simulations with initial conditions close to the stable solution in order to see it remain stable.

To aid the comparison, in addition to the solutions α, v_c and R, we have graphed the slope of the linear profiles of $v_c(\cdot, t)$ for each t. With this, one can observe that these linear profiles have a slope that tends to the λ_2 associated to the stable solution, i.e. -0.9021, as would be expected from the linear stability analysis. In the graphs of $R(t)$, we have also graphed the $R_*(t)$ corresponding to the stable solution, namely $R_*(t) = R_0 e^{\lambda_2 t}$ with $\lambda_2 = -0.9021$ for easy comparison.

Indeed, for the limit case, we have the following results:

Case 1^*, with $k_0 = 0 = Q_0$, $\alpha_h = 0.3189$, $\lambda_1 = 0.2092$, $\lambda_2 = -0.8897$

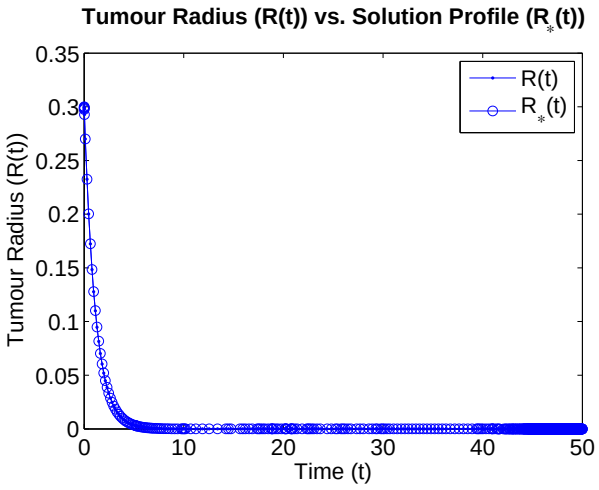


Figure 62.: Evolution of tumour radius in Case 1^* with negligible nutrient uptake and cell drag, i.e. $k_0 = 0 = Q_0$, initialised near the unstable travelling solution and graphed against the $R_*(t)$ corresponding to the stable travelling solution, namely $R_*(t) = R_0 e^{\lambda_2 t}$, where $\lambda_2 = -0.9021$.

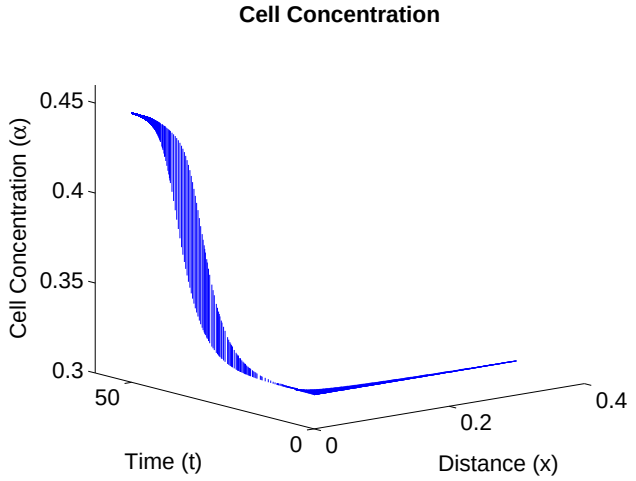


Figure 63.: Evolution of the cell concentration in Case 1*, with negligible nutrient uptake and cell drag, i.e. $k_0 = 0 = Q_0$, initialised near the unstable travelling solution (corresponding to $\alpha_h = 0.3189$) and stabilising near the stable travelling solution (corresponding to $\alpha_h = 0.4495$).

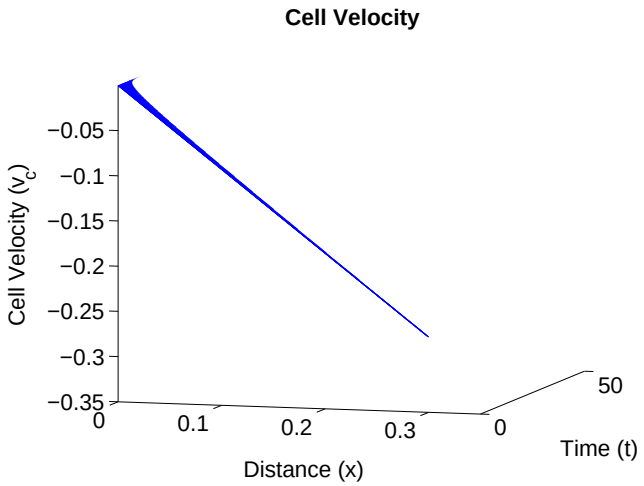


Figure 64.: Evolution of the cell velocity in Case 1*, with negligible nutrient uptake and cell drag, i.e. $k_0 = 0 = Q_0$, initialised near the unstable travelling solution (corresponding to $v_{cs}(x) = \lambda_2 x$ where $\lambda_2 = -0.8897$) and stabilising near the stable travelling solution (corresponding to $v_{cs}(x) = \lambda_2 x$ where $\lambda_2 = -0.9021$). See the following graph for more detail.

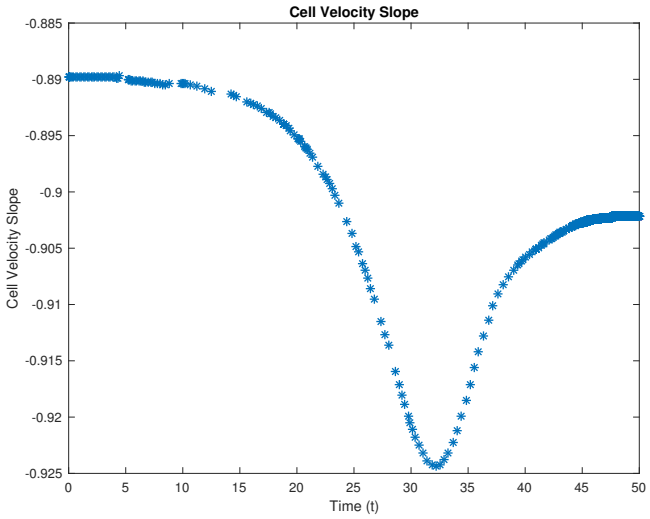


Figure 65.: Evolution of the slope of the cell velocity in the previous graph for each point in time in Case 1*, with negligible nutrient uptake and cell drag, i.e. $k_0 = 0 = Q_0$, initialised near the unstable travelling solution (corresponding to $v_{cs}(x) = \lambda_2 x$ where $\lambda_2 = -0.8897$) and stabilising near the stable travelling solution (corresponding to $v_{cs}(x) = \lambda_2 x$ where $\lambda_2 = -0.9021$). One might expect to see the dip seen in this graph represented in the previous one. However, the amplitude of the graph above is very small (about 0.035), thus explaining why this dip is not visible. This will be possible in the graphs seen in the next section. The outlier points are attributed to numerical limitations of dealing with small numbers as the tumour decays exponentially.

Case 1^*, with $k_0 = 0 = Q_0$, $\alpha_h = 0.4495$, $\lambda_1 = -0.5341$, $\lambda_2 = -0.9021$

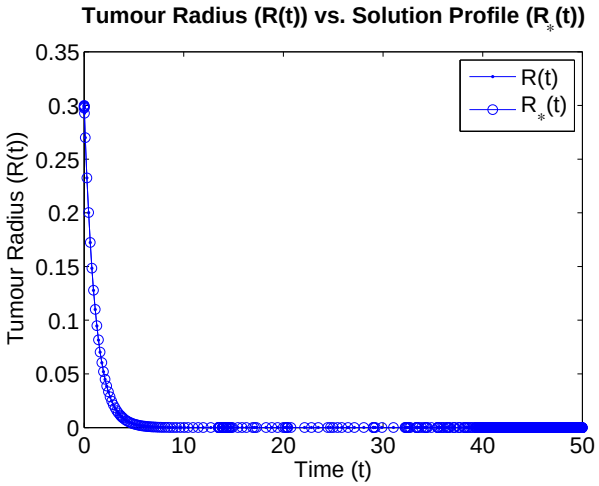


Figure 66.: Evolution of tumour radius in Case 1^* with negligible nutrient uptake and cell drag, i.e. $k_0 = 0 = Q_0$, initialised near the stable travelling solution and graphed against the $R_*(t)$ corresponding to the stable travelling solution, namely $R_*(t) = R_0 e^{\lambda_2 t}$, where $\lambda_2 = -0.9021$.

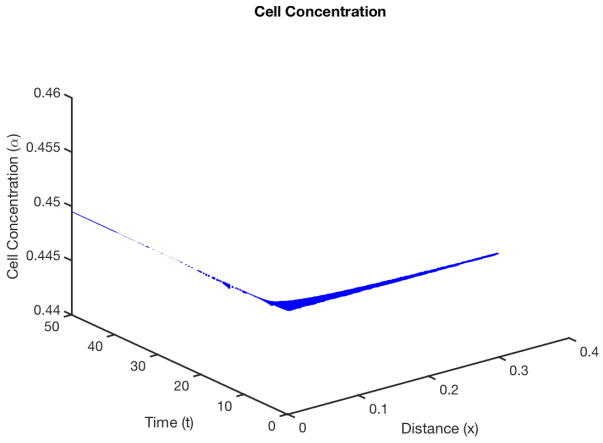


Figure 67.: Evolution of the cell concentration in Case 1^*, with negligible nutrient uptake and cell drag, i.e. $k_0 = 0 = Q_0$, initialised and stabilised near the stable travelling solution (corresponding to $\alpha_h = 0.4495$).

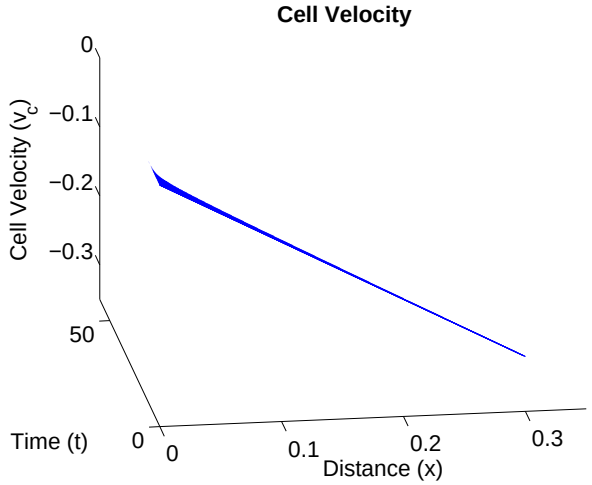


Figure 68.: Evolution of the cell velocity in Case 1*, with negligible nutrient uptake and cell drag, i.e. $k_0 = 0 = Q_0$, initialised and stabilised near the stable travelling solution (corresponding to $v_{cs}(x) = \lambda_2 x$ where $\lambda_2 = -0.9021$). See the following graph for more detail.

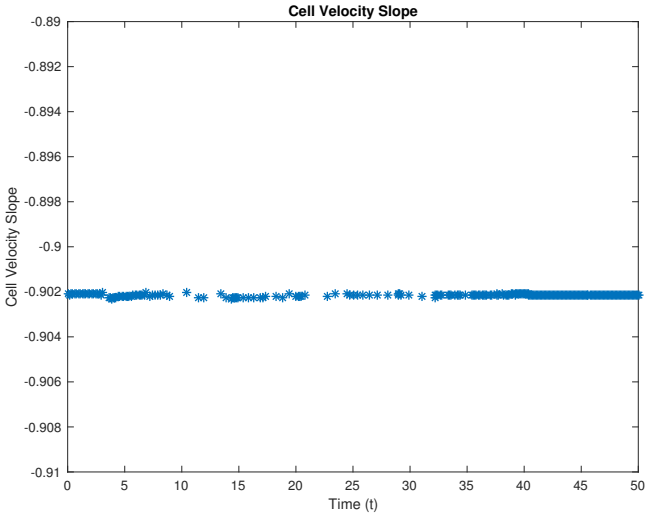


Figure 69.: Evolution of the slope of cell velocity in the previous graph for each point in time in Case 1*, with negligible nutrient uptake and cell drag, i.e. $k_0 = 0 = Q_0$, initialised and stabilised near the stable travelling solution (corresponding to $v_{cs}(x) = \lambda_2 x$ where $\lambda_2 = -0.9021$). The outlier points are attributed to numerical limitations of dealing with small numbers as the tumour decays exponentially.

Similarly, now consider the same simulations in the full case where nutrient uptake and cell drag are not negligible, but small, of order 1e−4:

Table 7.: Values for k_0 and Q_0.

k_0	Q_0
1e−4	3e−4

As before, we present first simulations with initial conditions close to the unstable solution and then to the stable solution.

Case 1^*, with k_0, Q_0 small, $\alpha_h = 0.3189$, $\lambda_1 = 0.2092$, $\lambda_2 = -0.8897$

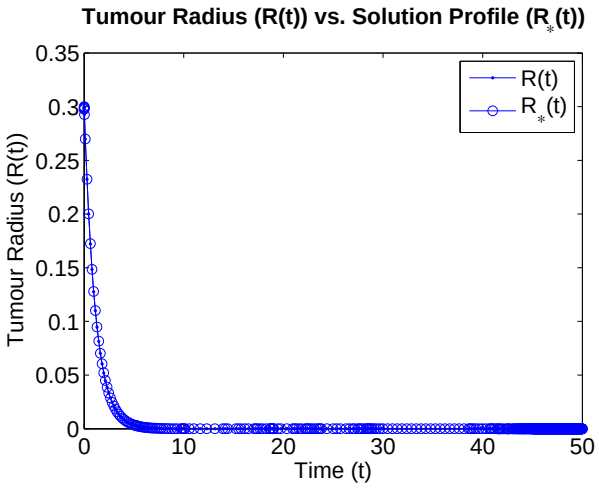


Figure 70.: Evolution of tumour radius in Case 1^* with small nutrient uptake and cell drag, i.e. k_0, Q_0 small, initialised near the unstable travelling solution and graphed against the $R_*(t)$ corresponding to the stable travelling solution, namely $R_*(t) = R_0 e^{\lambda_2 t}$, where $\lambda_2 = -0.9021$.

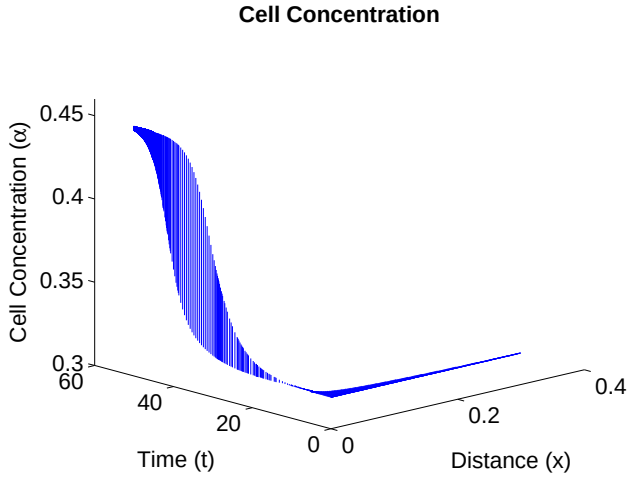


Figure 71.: Evolution of the cell concentration in Case 1^*, with small nutrient uptake and cell drag, i.e. k_0, Q_0 small, initialised near the unstable travelling solution (corresponding to $\alpha_h = 0.3189$) and stabilising near the stable travelling solution (corresponding to $\alpha_h = 0.4495$).

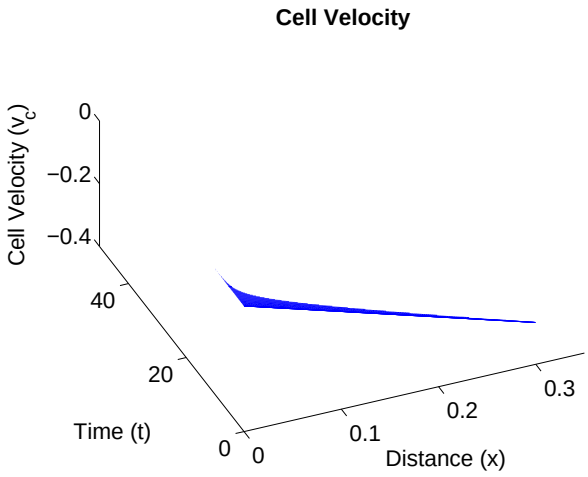


Figure 72.: Evolution of the cell velocity in Case 1^*, with small nutrient uptake and cell drag, i.e. k_0, Q_0 small, initialised near the unstable travelling solution (corresponding to $v_{cs}(x) = \lambda_2 x$ where $\lambda_2 = -0.8897$) and stabilising near the stable travelling solution (corresponding to $v_{cs}(x) = \lambda_2 x$ where $\lambda_2 = -0.9021$). See the following graph for more detail.

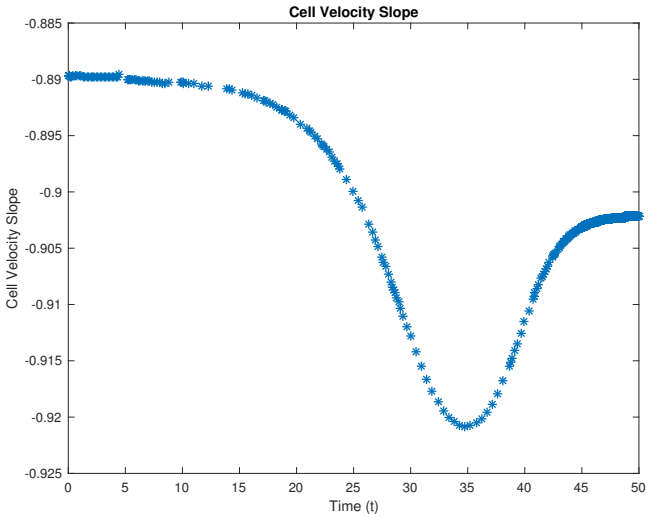


Figure 73.: Evolution of the slope of cell velocity in the previous graph for each point in time in Case 1*, with small nutrient uptake and cell drag, i.e. k_0, Q_0 small, initialised near the unstable travelling solution (corresponding to $v_{cs}(x) = \lambda_2 x$ where $\lambda_2 = -0.8897$) and stabilising near the stable travelling solution (corresponding to $v_{cs}(x) = \lambda_2 x$ where $\lambda_2 = -0.9021$). One might expect to see the dip seen in this graph represented in the previous one. However, the amplitude of the graph above is very small (about 0.03), thus explaining why this dip is not visible. This will be possible in the graphs seen in the next section. The outlier points are attributed to numerical limitations of dealing with small numbers as the tumour decays exponentially.

Case 1^*, with k_0, Q_0 small, $\alpha_h = 0.4495$, $\lambda_1 = -0.5341$, $\lambda_2 = -0.9021$

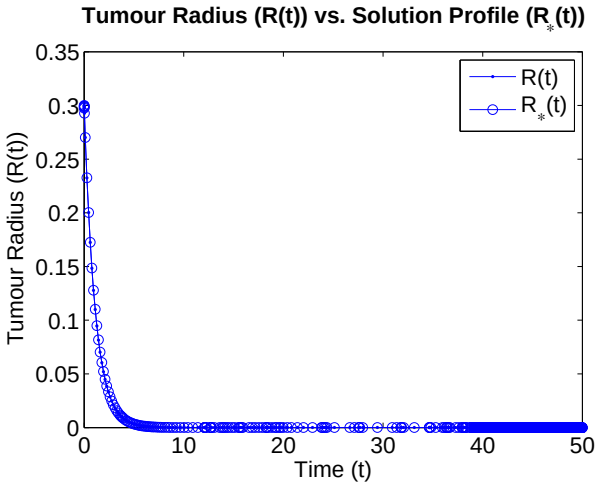


Figure 74.: Evolution of tumour radius in Case 1^* with small nutrient uptake and cell drag, i.e. k_0, Q_0 small, initialised near the stable travelling solution and graphed against the $R_*(t)$ corresponding to the stable travelling solution, namely $R_*(t) = R_0 e^{\lambda_2 t}$, where $\lambda_2 = -0.9021$.

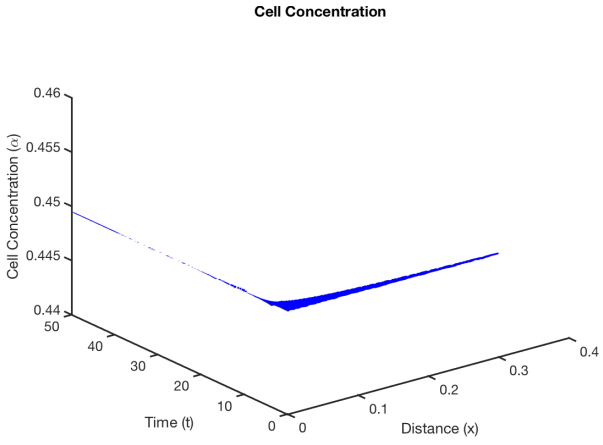


Figure 75.: Evolution of the cell concentration in Case 1^*, with small nutrient uptake and cell drag, i.e. k_0, Q_0 small, initialised and stabilised near the stable travelling solution (corresponding to $\alpha_h = 0.4495$).

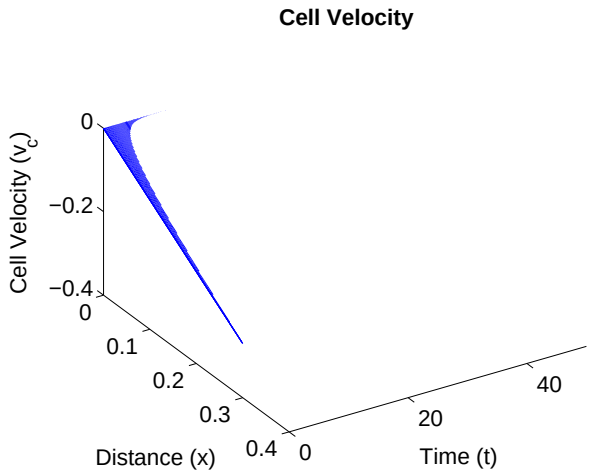


Figure 76.: Evolution of the cell velocity in Case 1*, with small nutrient uptake and cell drag, i.e. k_0, Q_0 small, initialised and stabilised near the stable travelling solution (corresponding to $v_{cs}(x) = \lambda_2 x$ where $\lambda_2 = -0.9021$). See the following graph for more detail.

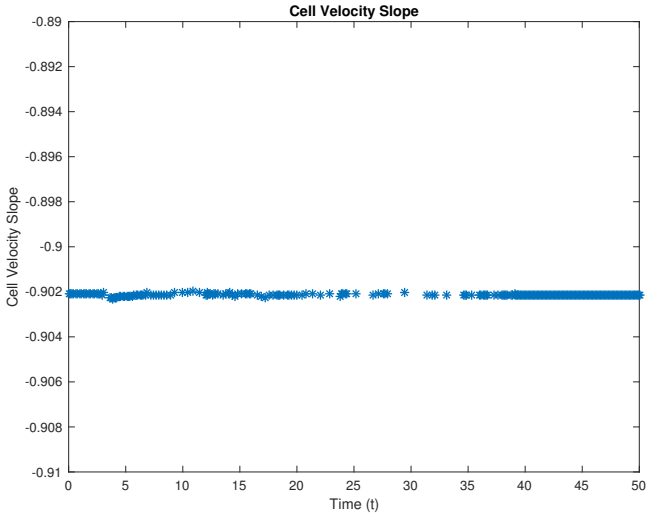


Figure 77.: Evolution of the slope of cell velocity in the previous graph for each point in time in Case 1*, with small nutrient uptake and cell drag, i.e. k_0, Q_0 small, initialised and stabilised near the stable travelling solution (corresponding to $v_{cs}(x) = \lambda_2 x$ where $\lambda_2 = -0.9021$). The outlier points are attributed to numerical limitations of dealing with small numbers as the tumour decays exponentially.

5.2.3 *Conclusion*

All the parameter regimes above are cases where the travelling solution of the limit case

$$(\alpha_h, v_s(x), C_\infty, R_*(t)) = (\alpha_h, \lambda_2 x, C_\infty, R_0 e^{\lambda_2 t})$$

is decaying, i.e. $\alpha_h < \alpha^*$ and $\lambda_2 < 0$. In this case we found that one such solution is unstable while the other is stable.

When we simulate the limit case near either solution, numerical results tend to a profile that imitates the stable solution, as we would expect from the analysis. However, this also holds when simulating the full one dimensional model, with small nutrient uptake and cell drag. This is interesting because the travelling solutions are solutions only of the limit case, and not of the full one dimensional formulation. Thus, it is not necessarily true that results in stability of the limit case must therefore imply anything about the full formulation, but they do appear to show strong compatibility in numerical results when we compare the limit case graphs (Figures displaying instability 62, 63, 64, 65, and Figures displaying stability 66, 67, 68, 69) with the full formulation graphs (Figures displaying instability 70, 71, 72, 73, and Figures displaying stability 74, 75, 76, 77).

Indeed, what we may observe from the graphs above is that as $t \to \infty$:

1. The cell concentration tends to the value of the cell concentration of the stable solution, namely $\alpha_h = 0.4495$.

2. The cell velocity becomes roughly linear with slope tending to the slope of the linear profile of the stable solution's cell velocity, namely $\lambda_2 = -0.9021$.

3. The radius profile decays exponentially at the same rate as the stable solution $R_*(t) = R_0 e^{\lambda_2 t}$, with $\lambda_2 = -0.9021$.

5.3 CHANGING $\Sigma_c(\alpha)$ IN SEARCH OF A GROWING UNSTABLE SOLUTION

5.3.1 *Objective and Motivation*

We continue in search for a $\Sigma_c(\alpha)$ that may render an unstable solution of the type

$$(\alpha_h, v_s(x), C_\infty, R_*(t)) = (\alpha_h, \lambda_2 x, C_\infty, R_0 e^{\lambda_2 t}),$$

except now we demand $\lambda_2 > 0$ (and thus $\alpha_h > \alpha^*$), as we would like to analyse a case where the solution $R_*(t)$ represents the radius of a growing tumour, rather than a decaying one, as seen in the last section.

Recall initially that the original Σ_c obtained in the literature will not be appropriate, no matter how we pick $\hat{\Sigma}_c$, r, q, α^*, and α_{min}, since

$$\Sigma_c'(\alpha_h) = \frac{\hat{\Sigma}_c |\alpha_h - \alpha^*|^{r-1}}{(1-\alpha_h)^{q+1}} \Big(r(1-\alpha_h) + q(\alpha_h - \alpha^*) \Big) > 0,$$

and therefore

$$\lambda_1 = -\alpha_h \Big(\frac{s_0 C_\infty}{1 + s_1 C_\infty} + \frac{\Sigma_c'(\alpha_h)}{\hat{\mu}_c} \Big) < 0,$$

whenever $\alpha^* < \alpha_h < 1$.

Therefore, we must consider an altogether different $\Sigma_c(\alpha)$. As stated in the beginning of the previous chapter, we will vary $\Sigma_c(\cdot)$ within a set of functions that satisfy the same sign profile as the the $\Sigma_c(\cdot)$ defined in the literature, as this has strong biological implications.

Recall now that α_h for any non-trivial travelling solution is defined by solving

$$\frac{\hat{\mu}_c S_c(\alpha; C_\infty)}{\alpha} = \Sigma_c(\alpha) \qquad\qquad \alpha \in (\alpha_{min}, \alpha^*) \cup (\alpha^*, 1).$$

Since $S_c(\cdot, C_\infty)$ is a quadratic in α with root at $\alpha = 0$, then the left hand side of the equation above is the equation of a line. Therefore, from the equation above, we must find a $\Sigma_c(\cdot)$ such that the aforementioned line intersects $\Sigma_c(\alpha)$ at $\alpha_h \in (\alpha^*, 1)$ such that $\Sigma_c'(\alpha_h) < 0$ and, more specifically,

$$\Sigma_c'(\alpha_h) < -\frac{s_0 C_\infty \hat{\mu}_c}{1 + s_1 C_\infty} < 0.$$

With the restriction above, we guarantee that $\lambda_1 > 0$ while $\alpha^* < \alpha_h < 1$ guarantees that $\lambda_2 > 0$. This way, we have set up a scheme to find a $\Sigma_c(\cdot)$ that allows for a growing unstable travelling solution.

We offer a diagram to explain how the original $\Sigma_c(\cdot)$ definition from literature (in blue) may be modified to allow the scheme above to be successful. In order to generate the negative slope for $\Sigma_c(\alpha)$, we introduced to the original $\Sigma_c(\alpha)$ a slight hill as can be seen in the red curve below.

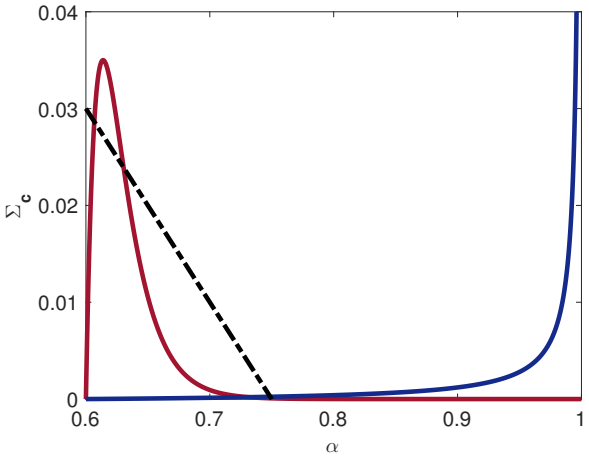


Figure 78.: Diagram to illustrate motivation for $\Sigma_c(\alpha)$ defined below

5.3.2 *Defining New* $\Sigma_c(\alpha)$

In light of the discussion above, we consider a $\Sigma_c(\alpha)$ of the type

$$\Sigma_c(\alpha) = F(\alpha) + \frac{\hat{\Sigma}_c(\alpha - \alpha^*)}{1 - \alpha},$$

where

$$F(\alpha) = M(e^{-a(\alpha-\alpha^*)} - e^{-b(\alpha-\alpha^*)}), \qquad M > 0, \quad 0 < a < b.$$

Notice that this $\Sigma_c(\alpha)$ satisfies all conditions set at the beginning of the previous chapter. Choosing M, a, and b wisely, we hope now to guarantee the existence of at least one unstable growing travelling solution. Indeed consider the following parameters:

Table 8.: Parameters defining new $\Sigma_c(\alpha)$

α^*	C_∞	s_0	s_1	s_2	s_3	s_4	Q_1	R_0	$\hat{\Sigma}_c$	$\hat{\mu}_c$	M	a	b
0.6	3	8/3	1	1	5/6	2	1	0.3	10^{-4}	1	2	50	100

Then, $\Sigma_c(\alpha)$ looks like this:

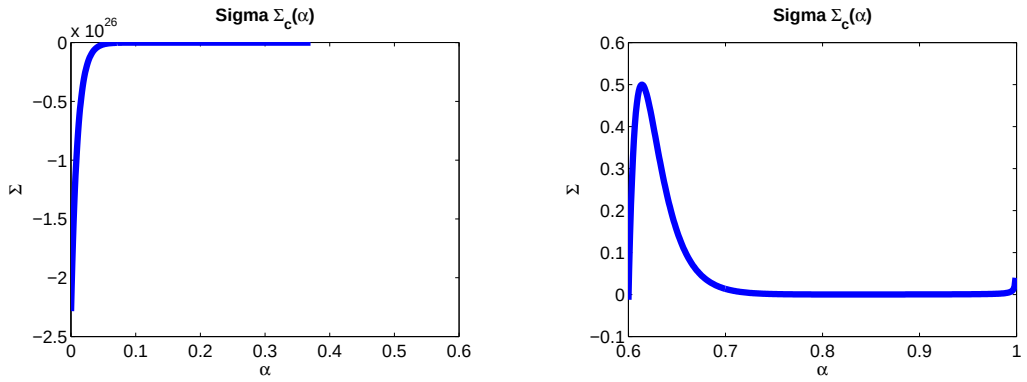


Figure 79.: Newly defined $\Sigma_c(\alpha)$

In this case, we obtain three solutions corresponding to cell concentrations α_{h_1}, α_{h_2} and α_{h_3} where $\alpha^* < \alpha_{h_1} < \alpha_{h_2} < \alpha_{h_3}$. In this section, we will call these solutions 1, 2, and 3, respectively. All of these solutions have $\lambda_2 > 0$ and are thus cases where $R_*(t)$ grows exponentially. On the other hand, we have

$$\lambda_1(\alpha_{h_1}) < 0 \qquad \lambda_1(\alpha_{h_2}) > 0 \qquad \lambda_1(\alpha_{h_3}) < 0,$$

which imply that the second solution is unstable while the other two are stable.

Values obtained can be seen in the following table:

Table 9.: Parameters of three growing travelling solutions

i	α_{h_i}	$\lambda_1(\alpha_{h_i})$	$\lambda_2(\alpha_{h_i})$
1	0.6039	−30.4960	0.2922
2	0.6419	4.5802	0.2163
3	0.7494	−1.4577	0.0012

5.3.3 *Simulations*

Now, if we simulate the limit case system with negligible nutrient uptake and cell drag with initial conditions near each one of these solutions, we expect to see solutions steering away from the unstable solution 2 towards the stable solutions 1 and 3. Once again, to facilitate comparison, we have inserted graphs of the slopes of the (roughly) linear cell velocity $v_c(\cdot, t)$ for each time t when they are deemed necessary. We have also graphed the $R_*(t)$ functions of the relevant unstable and stable solutions together with $R(t)$.

First, we present simulations of the limit case system where nutrient uptake and cell drag are considered negligible.

The first two cases (and thus the next eight graphs) pertain to perturbations of the unstable solution, first with

$$\alpha(x,0) = \alpha_h + \epsilon \qquad v_c(x,0) = \lambda_2(\alpha_h + \epsilon)x = \frac{\Sigma_c(\alpha_h + \epsilon)}{\hat{\mu}_c}x,$$

and then with

$$\alpha(x,0) = \alpha_h - \epsilon \qquad v_c(x,0) = \lambda_2(\alpha_h - \epsilon)x = \frac{\Sigma_c(\alpha_h - \epsilon)}{\hat{\mu}_c}x.$$

We will refer to these initial conditions as ones above and below the unstable solution, respectively. Because of the bistability predicted, the solutions with initial conditions above the unstable solution will display a tendency to steer towards Solution 3 while the solutions with initial conditions below the unstable solution will steer towards Solution 1.

Perturbation above Solution 2, with $k_0 = 0 = Q_0$

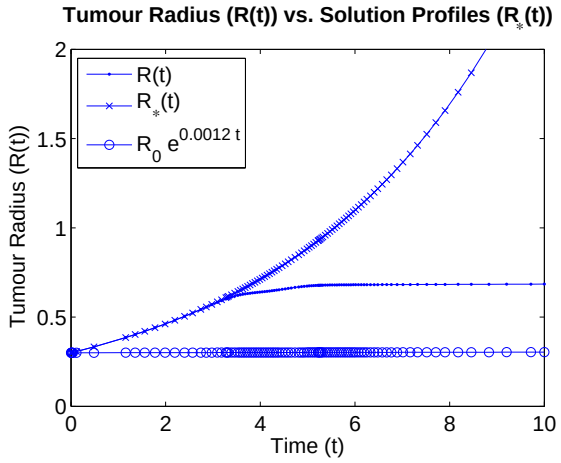


Figure 80.: Evolution of tumour radius with negligible nutrient uptake and cell drag, i.e. $k_0 = 0 = Q_0$, initialised above solution 2 and graphed against both $R_*(t)$ corresponding to solution 2 ($R_*(t) = R_0 e^{\lambda_2 t}$, where $\lambda_2 = 0.2163$) and $R_*(t)$ corresponding to solution 3 ($R_*(t) = R_0 e^{\lambda_2 t}$, where $\lambda_2 = 0.0012$). Notice that the solution initially grows at the rate of the unstable solution 2 and eventually at the rate of the stable solution 3.

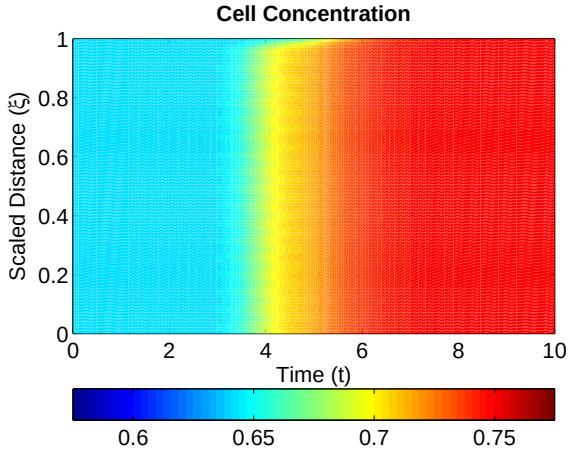


Figure 81.: Evolution of the cell concentration, with negligible nutrient uptake and cell drag, i.e. $k_0 = 0 = Q_0$, initialised above solution 2 (corresponding to $\alpha_h = 0.6419$) and stabilising near solution 3 (corresponding to $\alpha_h = 0.7494$).

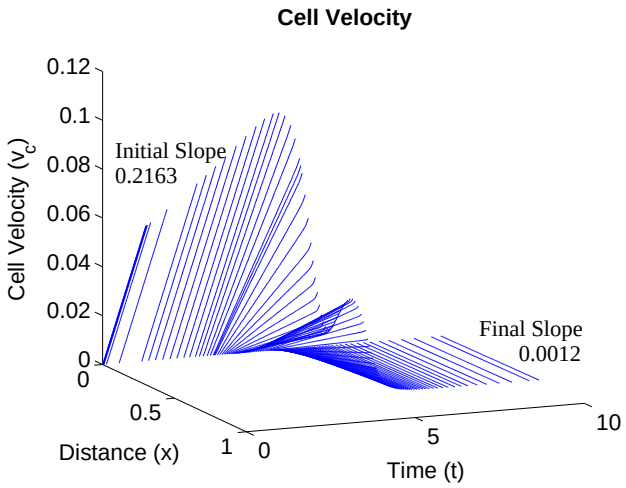


Figure 82.: Evolution of the cell velocity, with negligible nutrient uptake and cell drag, i.e. $k_0 = 0 = Q_0$, initialised above solution 2 (corresponding to $v_{cs} = \lambda_2 x$, with $\lambda_2 = 0.2163$) and stabilising near solution 3 (corresponding to $v_{cs} = \lambda_2 x$, with $\lambda_2 = 0.0012$). More details in the next graph.

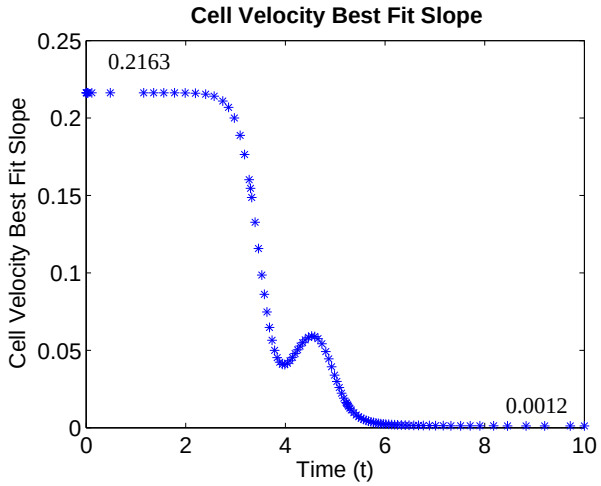


Figure 83.: Evolution of the slope of the cell velocity graph above at each point in time, with negligible nutrient uptake and cell drag, i.e. $k_0 = 0 = Q_0$, initialised above solution 2 (corresponding to $v_{cs} = \lambda_2 x$, with $\lambda_2 = 0.2163$) and stabilising near solution 3 (corresponding to $v_{cs} = \lambda_2 x$, with $\lambda_2 = 0.0012$). Notice that the same behaviour can be seen in the previous graph.

Perturbation below Solution 2, with $k_0 = 0 = Q_0$

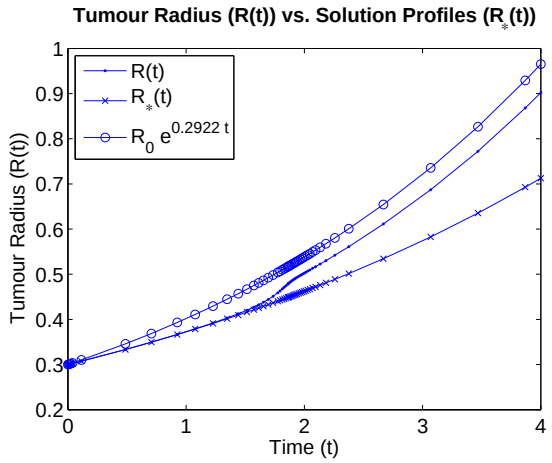


Figure 84.: Evolution of tumour radius with negligible nutrient uptake and cell drag, i.e. $k_0 = 0 = Q_0$, initialised below solution 2 and graphed against both $R_*(t)$ corresponding to solution 2 ($R_*(t) = R_0 e^{\lambda_2 t}$, where $\lambda_2 = 0.2163$) and $R_*(t)$ corresponding to solution 1 ($R_*(t) = R_0 e^{\lambda_2 t}$, where $\lambda_2 = 0.2922$). Notice that the solution initially grows at the rate of the unstable solution 2 and eventually at the rate of the stable solution 1.

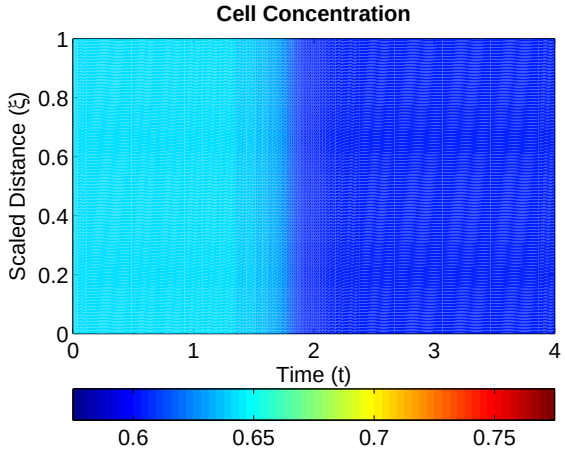


Figure 85.: Evolution of the cell concentration, with negligible nutrient uptake and cell drag, i.e. $k_0 = 0 = Q_0$, initialised below solution 2 (corresponding to $\alpha_h = 0.6419$) and stabilising near solution 1 (corresponding to $\alpha_h = 0.6039$).

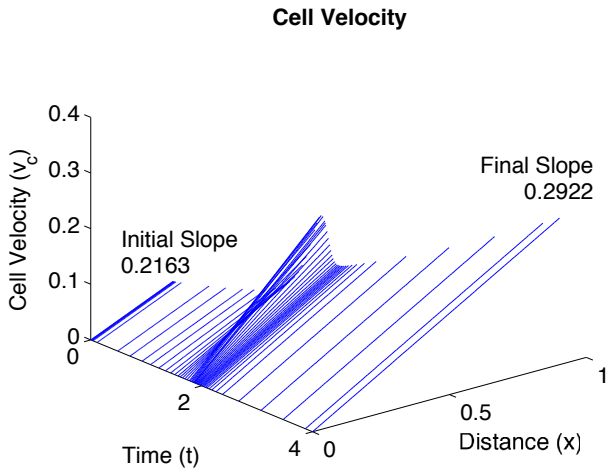


Figure 86.: Evolution of the cell velocity, with negligible nutrient uptake and cell drag, i.e. $k_0 = 0 = Q_0$, initialised below solution 2 (corresponding to $v_{cs} = \lambda_2 x$, with $\lambda_2 = 0.2163$) and stabilising near solution 1 (corresponding to $v_{cs} = \lambda_2 x$, with $\lambda_2 = 0.2922$). More details in the next graph.

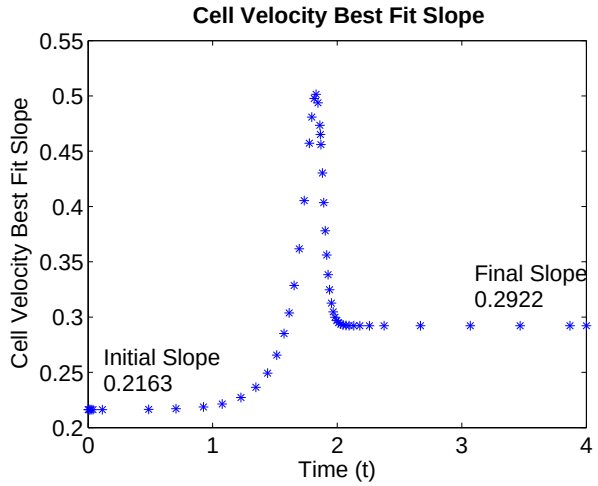


Figure 87.: Evolution of the slope of the cell velocity graph at each point in time, with negligible nutrient uptake and cell drag, i.e. $k_0 = 0 = Q_0$, initialised below solution 2 (corresponding to $v_{cs} = \lambda_2 x$, with $\lambda_2 = 0.2163$) and stabilising near solution 1 (corresponding to $v_{cs} = \lambda_2 x$, with $\lambda_2 = 0.2922$). Notice that the same behaviour can be seen in the previous graph.

The next two cases (and thus the next six graphs) pertain to perturbations of the stable solutions 1 and 3, with

$$\alpha(x,0) = \alpha_h + \epsilon \qquad v_c(x,0) = \lambda_2(\alpha_h + \epsilon)x = \frac{\Sigma_c(\alpha_h + \epsilon)}{\hat{\mu}_c}x.$$

Since this is a stable solution, small perturbations of any sort (even random ones) will render similar results with the solution remaining near Solutions 1 and 3, respectively, and thus confirming our linear stability analysis.

Perturbation of Solution 1, with $k_0 = 0 = Q_0$

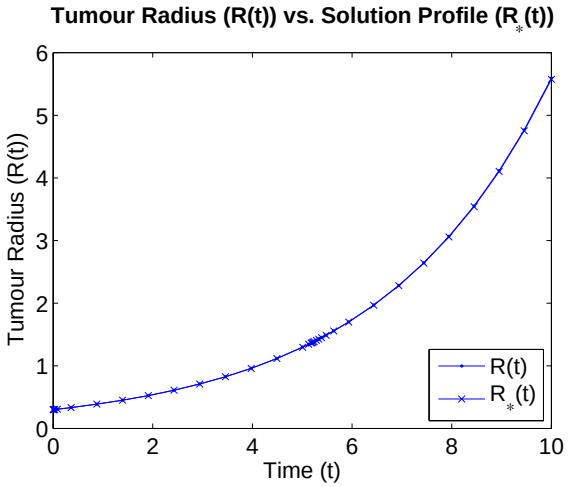


Figure 88.: Evolution of tumour radius with negligible nutrient uptake and cell drag, i.e. $k_0 = 0 = Q_0$, initialised and stabilised near solution 1 and graphed against $R_*(t)$ corresponding to solution 1 ($R_*(t) = R_0 e^{\lambda_2 t}$, where $\lambda_2 = 0.2922$).

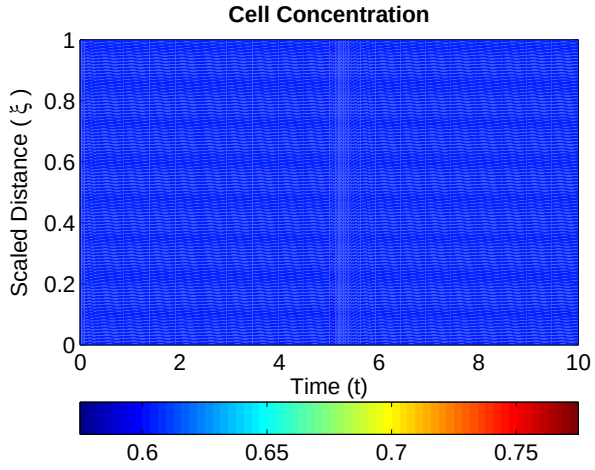


Figure 89.: Evolution of the cell concentration, with negligible nutrient uptake and cell drag, i.e. $k_0 = 0 = Q_0$, and initialised and stabilised near solution 1 (corresponding to $\alpha_h = 0.6039$).

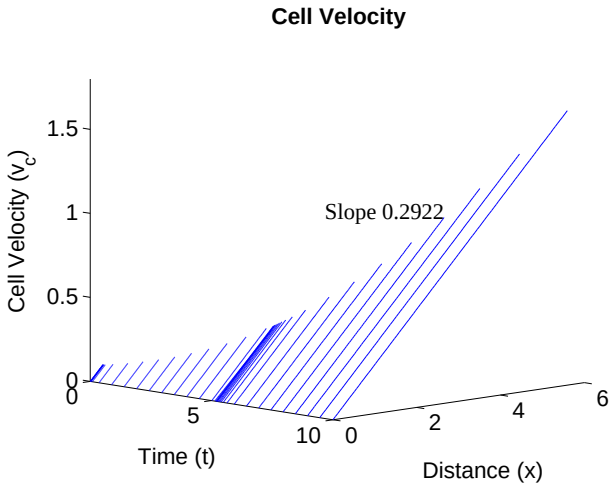


Figure 90.: Evolution of the cell velocity, with negligible nutrient uptake and cell drag, i.e. $k_0 = 0 = Q_0$, initialised and stabilised near solution 1 (corresponding to $v_{cs} = \lambda_2 x$, with $\lambda_2 = 0.2922$).

Perturbation of Solution 3, with $k_0 = 0 = Q_0$

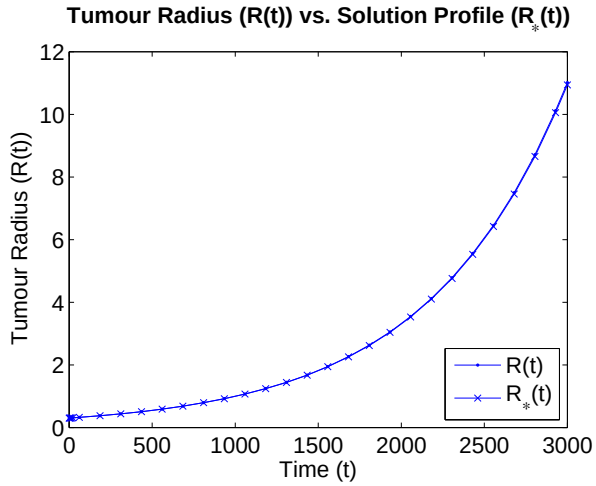


Figure 91.: Evolution of tumour radius with negligible nutrient uptake and cell drag, i.e. $k_0 = 0 = Q_0$, initialised and stabilised near solution 3 and graphed against $R_*(t)$ corresponding to solution 3 ($R_*(t) = R_0 e^{\lambda_2 t}$, where $\lambda_2 = 0.0012$).

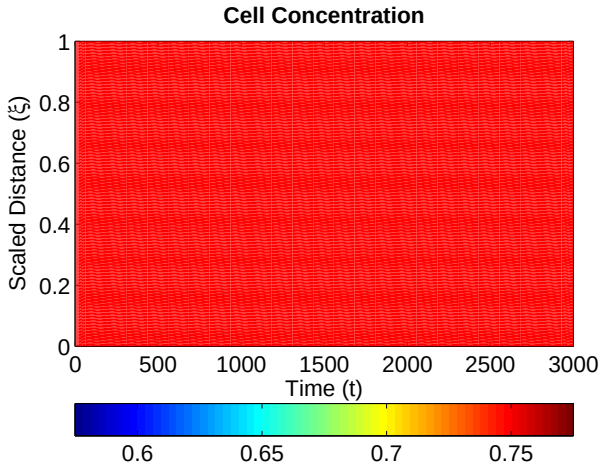


Figure 92.: Evolution of the cell concentration, with negligible nutrient uptake and cell drag, i.e. $k_0 = 0 = Q_0$, and initialised and stabilised near solution 3 (corresponding to $\alpha_h = 0.7494$).

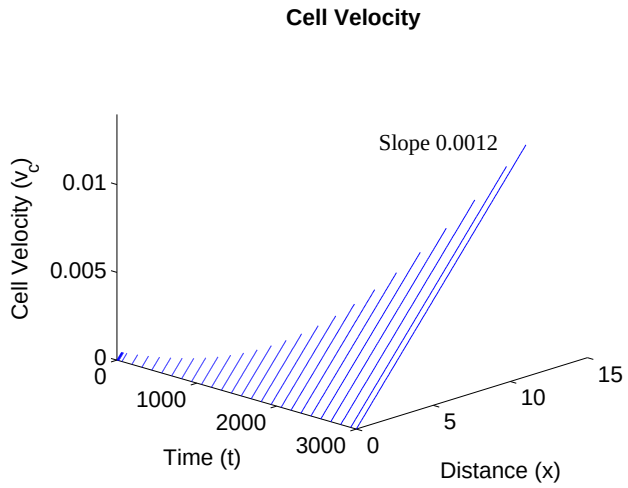


Figure 93.: Evolution of the cell velocity, with negligible nutrient uptake and cell drag, i.e. $k_0 = 0 = Q_0$, initialised and stabilised near solution 3 (corresponding to $v_{cs} = \lambda_2 x$, with $\lambda_2 = 0.0012$).

Consider now the results of the same simulations as the ones presented above, except now we work with the full one dimensional system with k_0, and Q_0 small, of the order 1e$-$4, rather than null:

Table 10.: Values for k_0 and Q_0.

k_0	Q_0
1e$-$4	3e$-$4

In this case, we see that simulations at initial conditions perturbed off the unstable solutions do not present much of a difference in the time frame analysed as compared to the limit case with $k_0 = 0 = Q_0$. We expect that differences arise when the nutrient uptake starts starving the innermost cells at a later time, as this can be seen in simulations where initial conditions perturbed off the stable solutions. Nevertheless, these graphs confirm that the travelling solutions and their stability analysis can provide information regarding the full formulation and, for this reason they have been included here.

Indeed, consider the graphs below:

Perturbation above Solution 2, with k_0, Q_0 small

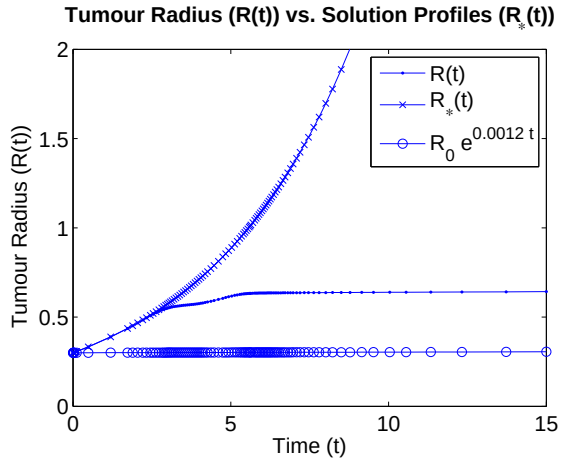


Figure 94.: Evolution of tumour radius with small nutrient uptake and cell drag, i.e. k_0, Q_0 small, initialised above solution 2 and graphed against both $R_*(t)$ corresponding to solution 2 ($R_*(t) = R_0 e^{\lambda_2 t}$, where $\lambda_2 = 0.2163$) and $R_*(t)$ corresponding to solution 3 ($R_*(t) = R_0 e^{\lambda_2 t}$, where $\lambda_2 = 0.0012$). Notice that the solution initially grows at the rate of the unstable solution 2 and eventually at the rate of the stable solution 3.

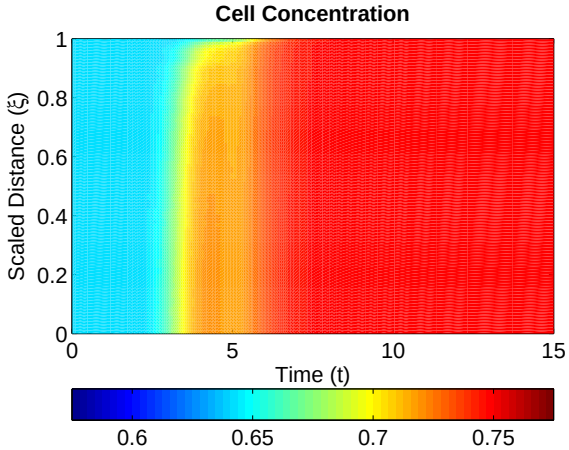


Figure 95.: Evolution of the cell concentration, with small nutrient uptake and cell drag, i.e. k_0, Q_0 small, initialised above solution 2 (corresponding to $\alpha_h = 0.6419$) and stabilising near solution 3 (corresponding to $\alpha_h = 0.7494$).

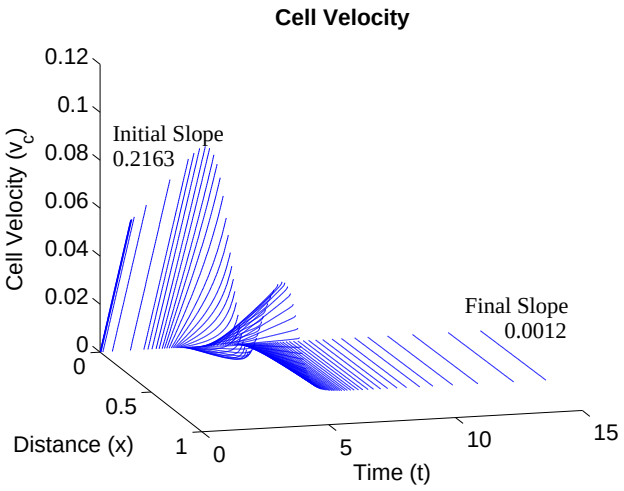


Figure 96.: Evolution of the cell velocity, with small nutrient uptake and cell drag, i.e. k_0, Q_0 small, initialised above solution 2 (corresponding to $v_{cs} = \lambda_2 x$, with $\lambda_2 = 0.2163$) and stabilising near solution 3 (corresponding to $v_{cs} = \lambda_2 x$, with $\lambda_2 = 0.0012$). More details in the next graph.

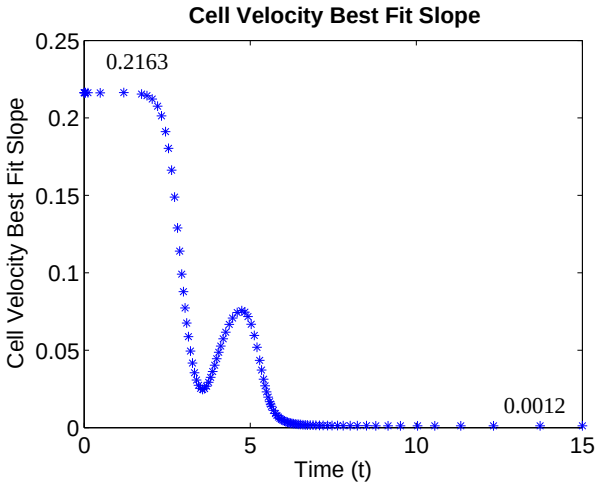


Figure 97.: Evolution of the slope of the cell velocity graph at each point in time, with small nutrient uptake and cell drag, i.e. k_0, Q_0 small, initialised above solution 2 (corresponding to $v_{cs} = \lambda_2 x$, with $\lambda_2 = 0.2163$) and stabilising near solution 3 (corresponding to $v_{cs} = \lambda_2 x$, with $\lambda_2 = 0.0012$). Notice that the same behaviour can be seen in the previous graph.

Perturbation below Solution 2, with k_0, Q_0 small

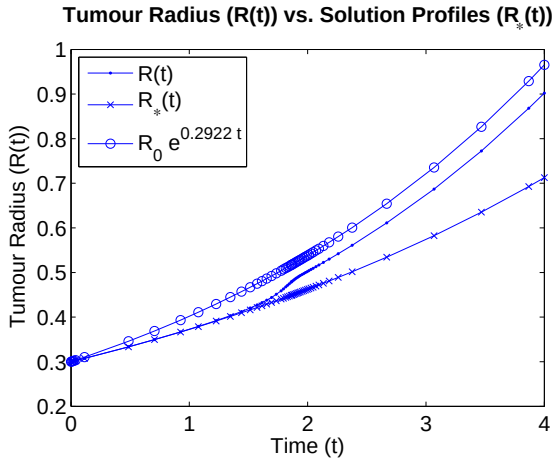


Figure 98.: Evolution of tumour radius with small nutrient uptake and cell drag, i.e. k_0, Q_0 small, initialised below solution 2 and graphed against both $R_*(t)$ corresponding to solution 2 ($R_*(t) = R_0 e^{\lambda_2 t}$, where $\lambda_2 = 0.2163$) and $R_*(t)$ corresponding to solution 1 ($R_*(t) = R_0 e^{\lambda_2 t}$, where $\lambda_2 = 0.2922$). Notice that the solution initially grows at the rate of the unstable solution 2 and eventually at the rate of the stable solution 1.

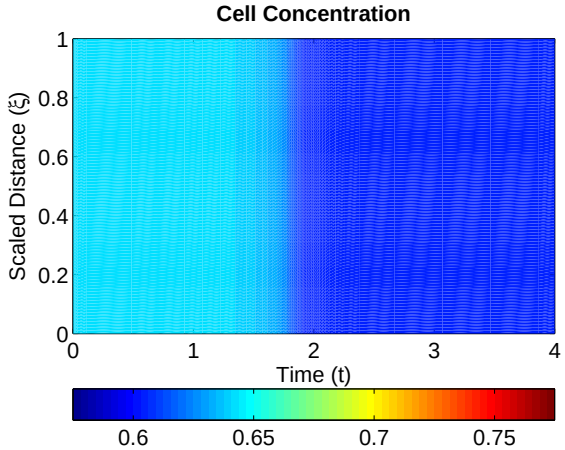


Figure 99.: Evolution of the cell concentration, with small nutrient uptake and cell drag, i.e. k_0, Q_0 small, initialised below solution 2 (corresponding to $\alpha_h = 0.6419$) and stabilising near solution 1 (corresponding to $\alpha_h = 0.6039$).

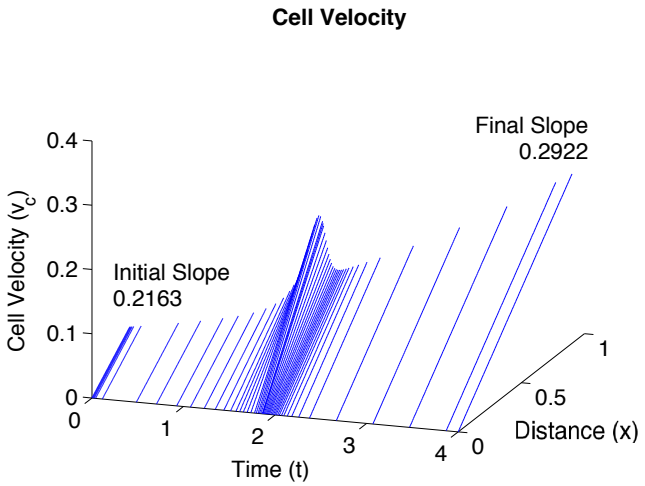


Figure 100.: Evolution of the cell velocity, with small nutrient uptake and cell drag, i.e. k_0, Q_0 small, initialised below solution 2 (corresponding to $v_{cs} = \lambda_2 x$, with $\lambda_2 = 0.2163$) and stabilising near solution 1 (corresponding to $v_{cs} = \lambda_2 x$, with $\lambda_2 = 0.2922$). More details in the next graph.

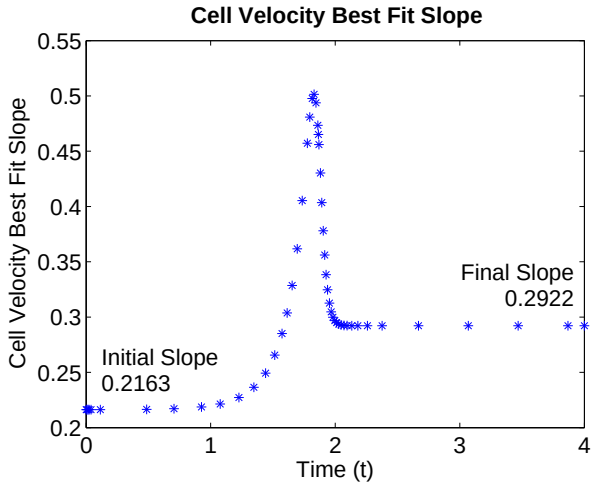


Figure 101.: Evolution of the slope of the cell velocity graph at each point in time, with small nutrient uptake and cell drag, i.e. k_0, Q_0 small, initialised below solution 2 (corresponding to $v_{cs} = \lambda_2 x$, with $\lambda_2 = 0.2163$) and stabilising near solution 1 (corresponding to $v_{cs} = \lambda_2 x$, with $\lambda_2 = 0.2922$). Notice that the same behaviour can be seen in the previous graph.

In the simulations where initial conditions were perturbed off the stable solutions 1 and 3, we see that the stable solution approximates the solutions well until either growth becomes linear and consequently starts to plateau (Figures 102, 103, and 104) or the numerics begins to break down (Figures 105, 106, and 107).

Perturbation of Solution 1, with k_0, Q_0 small

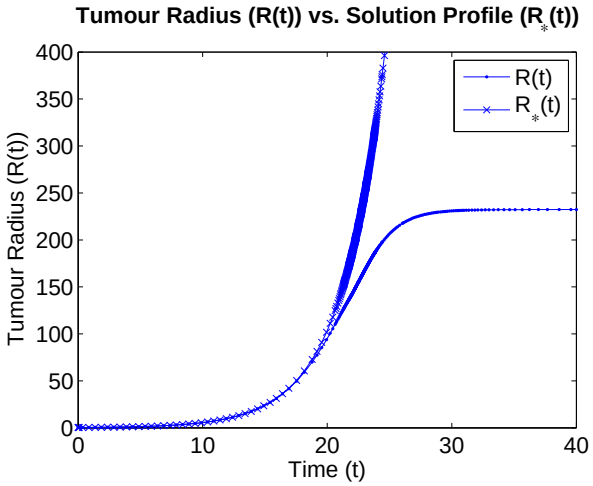


Figure 102.: Evolution of tumour radius with small nutrient uptake and cell drag, i.e. k_0, Q_0 small, initialised near solution 1 and graphed against $R_*(t)$ corresponding to solution 1 ($R_*(t) = R_0 e^{\lambda_2 t}$, where $\lambda_2 = 0.2922$). Although the stable solution of the limit case predicts the exponential growth of the solution of the full formulation for $t < 20$, it cannot predict the eventual growth plateau.

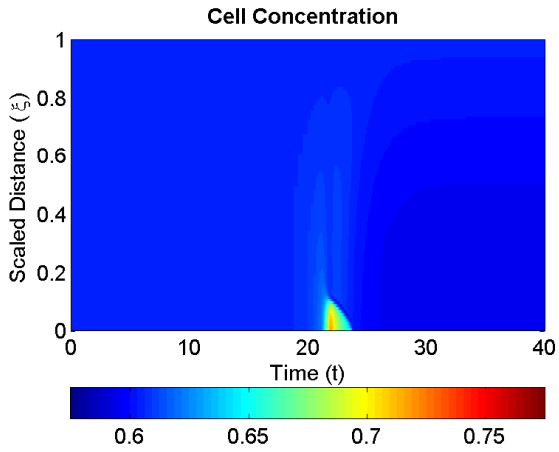


Figure 103.: Evolution of the cell concentration, with small nutrient uptake and cell drag, i.e. k_0, Q_0 small, and initialised near solution 1 (corresponding to $\alpha_h = 0.6039$). Notice that this solution remains constant until about $t = 20$. After this, the approximation of the full formulation by the limit case is no longer valid, as seen above.

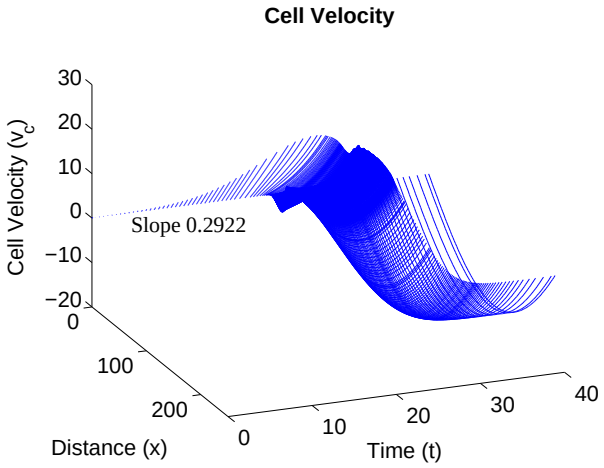


Figure 104.: Evolution of the cell velocity, with small nutrient uptake and cell drag, i.e. k_0, Q_0 small, initialised near solution 1 (corresponding to $v_{cs} = \lambda_2 x$, with $\lambda_2 = 0.2922$). Notice that this solution is approximated well by the stable solution until about $t = 20$. After this, the approximation of the full formulation by the limit case is no longer valid, as seen above.

Perturbation of Solution 3, with k_0, Q_0 small

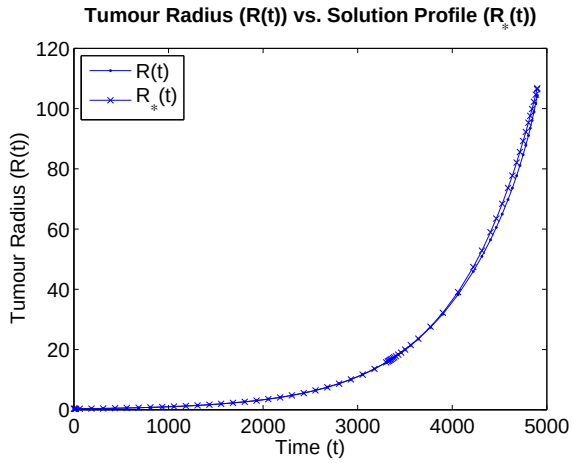


Figure 105.: Evolution of tumour radius with small nutrient uptake and cell drag, i.e. k_0, Q_0 small, initialised and stabilised near solution 3 and graphed against $R_*(t)$ corresponding to solution 3 ($R_*(t) = R_0 e^{\lambda_2 t}$, where $\lambda_2 = 0.0012$). Notice that this solution is approximated well by the stable solution until the code begins to break down at about $t = 4500$.

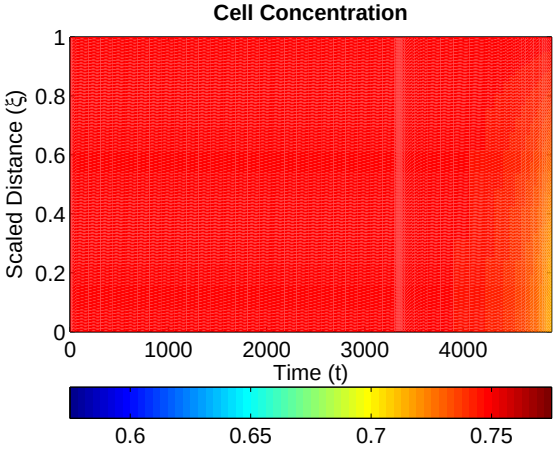


Figure 106.: Evolution of the cell concentration, with small nutrient uptake and cell drag, i.e. k_0, Q_0 small, and initialised near solution 3 (corresponding to $\alpha_h = 0.7494$). Notice that this solution remains constant until the code begins to break down at about $t = 4500$.

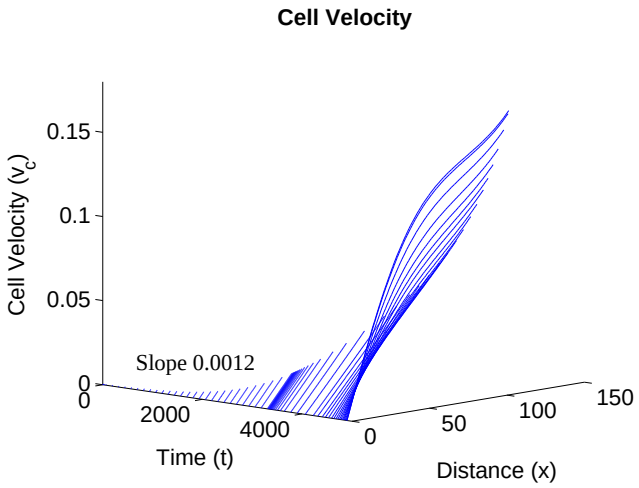


Figure 107.: Evolution of the cell velocity, with small nutrient uptake and cell drag, i.e. k_0, Q_0 small, initialised near solution 3 (corresponding to $v_{cs} = \lambda_2 x$, with $\lambda_2 = 0.0012$). Notice that this solution is approximated well by the stable solution until about $t = 4500$ when the code begins to break down.

If we consider the bistability presented here from a biological perspective, we see that the α_h corresponding to the unstable solution 2 effectively acts as a local cell concentration threshold. If the tumour is initially at a slightly higher cell concentration than the unstable solution 2, the tumour will tend to grow very slowly at the rate of solution 3 in intermediate times. On the other hand, if the tumour is initially at a slightly lower cell concentration than the unstable solution 2, the tumour will tend to grow very quickly at the rate of solution 1 in intermediate times, (see table 9 for precise values). Indeed, this is in line with the biology of tissue growth as normal cells tend to undergo mitosis more often if there is sufficient space to do so [65]. Furthermore, in the specific case of tumours, it is more difficult for cells to obtain nutrients in a tightly packed region due to high competition, thus hindering growth as compared to a sparse region.

5.3.4 *Conclusion*

Therefore, with this $\Sigma_c(\alpha)$, we have found three travelling solutions of the limit case where nutrient uptake and cell drag are negligible. These solutions all represent growing tumours and also display dynamics of bi-stability in both our analytical and numerical results.

Additionally, the behaviour observed in this limit case can also be seen in the full one dimensional system when t is sufficiently small. Compare for example, Figures 80, 81, 82, 83, 84, 85, 86, 87 in the limit case and Figures 94, 95, 96, 97, 98, 99, 100, 101 in the full one dimensional formulation. However, this parallel is limited since the solution steers away from our predictions as nutrient uptake and cell drag become more important (See for example Figures 102, 103, and 104). Thus, we will attempt to characterise stability for a general solution of the full one dimensional system in the following chapter.

5.4 CONSIDERATIONS ABOUT NEW $\Sigma_c(\alpha)$

One might argue that the high absolute value of $\Sigma_c(\alpha)$ for α small seen in the left hand side of Figure 79 is a limitation of this new Σ_c function. However, suppose that $\Sigma_c(\alpha)$ were defined differently for $\alpha < \alpha^*$. Since the three solutions obtained in the previous section were growing, i.e. $\lambda_2 > 0$ and thus $\alpha_h > \alpha^*$, we do not expect much of a difference in the behaviour of these solutions with the new $\Sigma_c(\alpha)$. Indeed, as we observed in the previous section, initial conditions chosen near any of the the solutions would tend to the stable solutions 1 or 3, i.e. $\alpha_{h_1} = 0.6039$ and $\alpha_{h_3} = 0.7494$. Particularly, the value of the cell concentration $\alpha(x,t)$ was limited by these stable solutions such that

$$\alpha^* = 0.6 < 0.6039 = \alpha_{h_1} \leq \alpha(x,t) \leq \alpha_{h_3} = 0.7494$$

in all of our simulations. This way, we could really choose any other function for $\Sigma_c(\alpha)$ when $\alpha < \alpha^*$. We could even choose $0 \neq \alpha_{min} < \alpha^*$ to our liking in order to avoid such large values and results would not be any different.

An example to illustrate this point can be seen in the Appendix B. There, we define yet another $\Sigma_c(\alpha)$ that mirrors the one in this section for $\alpha > \alpha^*$ and mirrors the original literature-based $\Sigma_c(\alpha)$ when $\alpha < \alpha^*$. Numerical results are comparable.

In any case, we do not argue that the $\Sigma_c(\alpha)$ defined in the previous section is the best definition of $\Sigma_c(\alpha)$ or indeed that it models the difference between the cell and water pressures any better than the $\Sigma_c(\alpha)$ proposed in the literature. However, respecting the biological arguments used to define the original $\Sigma_c(\alpha)$ as much as possible, we have been able to define a function that exemplifies the ability to use the linear stability of the travelling solutions in the limit case system as an approximation for the full one dimensional system. This was our main objective in this Chapter.

However, this parallel between the travelling solutions of the limit case and solutions of the full one dimensional formulation is limited. Indeed, when nutrient uptake begins to play an important role in causing cell death and restricting tumour growth, the growing travelling solution cannot approximate the tumour's diffusion limited steady state. See for example Figures 102, 103, and 104. For this reason, in the following Chapter, we will attempt to perform linear stability analysis on general solutions of the one dimensional formulation of the full two phase model presented in Chapter 2.

6

LINEAR STABILITY ANALYSIS IN ONE DIMENSION

Driven by the limitations discussed in the previous chapter regarding the negligible nutrient uptake and cell drag limit, we aim now to perform a linear stability analysis of a general non-homogeneous time-dependent solution of the full one dimensional model proposed in Chapter 2. However, due to the complexity of the equations obtained, we will eventually conclude that the full case is not tractable analytically. Consequently, we will pinpoint the reason that made it possible for us to fully characterise the perturbations of the limit case with negligible nutrient uptake and cell drag in Chapter 4 in order to motivate the study of this limit in a two dimensional formulation.

6.1 GENERAL ONE DIMENSIONAL SYSTEM

6.1.1 *Motivation*

In this section, we will consider the system obtained in Chapter 2:

$$\begin{cases} \dfrac{\partial \alpha}{\partial t} & = S_c(\alpha, C) - \dfrac{\partial}{\partial x}(\alpha v_c) \\ p & = -\alpha \Sigma_c(\alpha) + \hat{\mu}_c \alpha \dfrac{\partial v_c}{\partial x} \\ 0 & = (1-\alpha)\dfrac{\partial p}{\partial x} + k(\alpha)(v_w - v_c) \\ 0 & = \alpha v_c + (1-\alpha) v_w \\ \dfrac{\partial^2 C}{\partial x^2} & = Q_c(\alpha, C), \qquad (x,t) \in (0, R(t)) \times (0, \infty) \end{cases} \tag{69}$$

with moving boundary equation

$$\frac{dR}{dt}(t) = v_c(R(t), t), \qquad t \in (0, \infty)$$

subject to the following boundary conditions

$$\begin{cases} v_c = v_w = \dfrac{\partial C}{\partial x} = 0, & \text{at } x = 0, \\ \hat{\mu}_c \dfrac{\partial v_c}{\partial x} - \Sigma_c(\alpha) = 0, \quad p = 0, \quad C = C_\infty, & \text{at } x = R(t), \end{cases}$$

for all $t \in (0, \infty)$.

Although v_w and p may be eliminated to yield an equivalent yet simpler system for

$$\alpha(x,t), \qquad v_c(x,t), \qquad C(x,t), \qquad R(t),$$

we make a conscious choice to present it as stated above. It is possible to see from the equations in the next chapter that the elimination of v_w and p would unnecessarily complicate the (already) intricate statement of the two dimensional case. Therefore, we chose to state the one dimensional system as above, in order to facilitate comparisons between the one and two dimensional systems.

6.1.2 *Linearisation about Non-homogeneous Solution*

First, let

$$\alpha_s(x,t), \quad C_s(x,t), \quad v_{cs}(x,t), \quad v_{ws}(x,t), \quad p_s(x,t), \quad R_*(t),$$

be a non-homogeneous time-dependent solution of the one dimensional model (69). Linearising about it with respect to perturbations

$$\hat{\alpha}(x,t), \quad \hat{C}(x,t), \quad \hat{v}_c(x,t), \quad \hat{v}_w(x,t), \quad \hat{p}(x,t), \quad \hat{R}(t),$$

we may see that these perturbations satisfy:

$$\begin{cases} \dfrac{\partial \hat{\alpha}}{\partial t} & = \dfrac{\partial S_c}{\partial \alpha}(\alpha_s, C_s)\hat{\alpha} + \dfrac{\partial S_c}{\partial C}(\alpha_s, C_s)\hat{C} - \dfrac{\partial}{\partial x}(v_{cs}\hat{\alpha} + \alpha_s \hat{v}_c) \\ \hat{p} & = -\Big(\Sigma_c(\alpha_s) + \alpha_s \Sigma_c'(\alpha_s) - \hat{\mu}_c \dfrac{\partial v_{cs}}{\partial x}\Big)\hat{\alpha} + \hat{\mu}_c \alpha_s \dfrac{\partial \hat{v}_c}{\partial x} \\ 0 & = (1-\alpha_s)\dfrac{\partial \hat{p}}{\partial x} + k(\alpha_s)(\hat{v}_w - \hat{v}_c) + \Big(k'(\alpha_s)(v_{ws} - v_{cs}) - \dfrac{\partial p_s}{\partial x}\Big)\hat{\alpha} \\ 0 & = (v_{cs} - v_{ws})\hat{\alpha} + \alpha_s \hat{v}_c + (1-\alpha_s)\hat{v}_w \\ \dfrac{\partial^2 \hat{C}}{\partial x^2} & = \dfrac{\partial Q_c}{\partial C}(\alpha_s, C_s)\hat{C} + \dfrac{\partial Q_c}{\partial \alpha}(\alpha_s, C_s)\hat{\alpha}, \qquad (x,t) \in (0, R_*(t)) \times (0,\infty) \end{cases} \tag{70}$$

with

$$\frac{d\hat{R}}{dt}(t) = \frac{\partial v_{cs}}{\partial x}(R_*(t),t)\hat{R}(t) + \hat{v}_c(R_*(t),t), \quad t \in (0,\infty)$$

and boundary conditions

$$\begin{cases} \hat{v}_c = \hat{v}_w = \dfrac{\partial \hat{C}}{\partial x} = 0, & \text{on } x = 0, \\ \hat{p} = -\alpha_s \Sigma_c'(\alpha_s)\hat{\alpha} + \hat{\mu}_c \alpha_s \dfrac{\partial \hat{v}_c}{\partial x}, & \text{on } x = R_*(t), \\ 0 = \dfrac{\partial p_s}{\partial x}\hat{R} + \hat{p}, & \text{on } x = R_*(t), \\ 0 = \dfrac{\partial C_s}{\partial x}\hat{R} + \hat{C}, & \text{on } x = R_*(t) \end{cases}$$

for all $t \in (0,\infty)$.

To consider solutions of this system, we first fix the boundary. For this, we will apply the change of variable

$$x = x(t) = \xi R_*(t)$$

to the system above. This way, instead of working with equations valid in the moving domain $\{(x,t) \in (0,R_*(t)) \times (0,\infty)\}$, we will consider equations on a fixed domain, namely, $\{(\xi,t) \in (0,1) \times (0,\infty)\}$. Indeed, once we apply this change of variable, then

$$\begin{aligned}\frac{\partial}{\partial t} &\longrightarrow \frac{\partial}{\partial t} - \frac{\xi}{R_*(t)}\frac{dR_*}{dt}\frac{\partial}{\partial \xi}\\ \frac{\partial}{\partial x} &\longrightarrow \frac{1}{R_*(t)}\frac{\partial}{\partial \xi}\end{aligned}$$

and we obtain the following system:

$$\begin{cases}\dfrac{\partial \hat{\alpha}}{\partial t} &= \dfrac{1}{R_*}\Big[\xi\dfrac{dR_*}{dt} - v_{cs}\Big]\dfrac{\partial \hat{\alpha}}{\partial \xi} + \Big[\dfrac{\partial S_c}{\partial \alpha}(\alpha_s, C_s) - \dfrac{1}{R_*}\dfrac{\partial v_{cs}}{\partial \xi}\Big]\hat{\alpha}\\ &\quad + \dfrac{\partial S_c}{\partial C}(\alpha_s, C_s)\hat{C} - \dfrac{1}{R_*}\dfrac{\partial}{\partial \xi}(\alpha_s \hat{v}_c)\\ \hat{p} &= -\Big(\Sigma_c(\alpha_s) + \alpha_s\Sigma_c'(\alpha_s) - \dfrac{\hat{\mu}_c}{R_*}\dfrac{\partial v_{cs}}{\partial \xi}\Big)\hat{\alpha} + \dfrac{\hat{\mu}_c\alpha_s}{R_*}\dfrac{\partial \hat{v}_c}{\partial \xi}\\ 0 &= \dfrac{1-\alpha_s}{R_*}\dfrac{\partial \hat{p}}{\partial \xi} + k(\alpha_s)(\hat{v}_w - \hat{v}_c) + \Big(k'(\alpha_s)(v_{ws} - v_{cs}) - \dfrac{1}{R_*}\dfrac{\partial p_s}{\partial \xi}\Big)\hat{\alpha}\\ 0 &= (v_{cs} - v_{ws})\hat{\alpha} + \alpha_s\hat{v}_c + (1-\alpha_s)\hat{v}_w\\ \dfrac{\partial^2 \hat{C}}{\partial \xi^2} &= R_*^2\Big[\dfrac{\partial Q_c}{\partial C}(\alpha_s, C_s)\hat{C} + \dfrac{\partial Q_c}{\partial \alpha}(\alpha_s, C_s)\hat{\alpha}\Big], \quad (\xi,t) \in (0,1)\times(0,\infty)\end{cases} \tag{71}$$

and

$$\frac{d\hat{R}}{dt}(t) = \frac{1}{R_*(t)}\frac{\partial v_{cs}}{\partial \xi}(1,t)\hat{R}(t) + \hat{v}_c(1,t), \qquad t \in (0,\infty),$$

subject to the boundary conditions:

$$\begin{cases}\hat{v}_c = \hat{v}_w = \dfrac{\partial \hat{C}}{\partial \xi} = 0, & \text{on } \xi = 0,\\ \hat{p} = -\alpha_s\Sigma_c'(\alpha_s)\hat{\alpha} + \dfrac{\hat{\mu}_c\alpha_s}{R_*}\dfrac{\partial \hat{v}_c}{\partial \xi}, & \text{on } \xi = 1,\\ 0 = \dfrac{1}{R_*}\dfrac{\partial p_s}{\partial \xi}\hat{R} + \hat{p}, & \text{on } \xi = 1,\\ 0 = \dfrac{1}{R_*}\dfrac{\partial C_s}{\partial \xi}\hat{R} + \hat{C}, & \text{on } \xi = 1,\end{cases}$$

for all $t \in (0,\infty)$.

6.2 NEGLIGIBLE NUTRIENT CONSUMPTION AND CELL DRAG

We will consider briefly the limit case with negligible nutrient uptake and cell drag obtained in Chapter 4 by taking $Q_c(\alpha, C) \equiv 0 \equiv k(\alpha)$. There, we characterised the steady states and the stability of the travelling solutions of this limit case. However, in light of the equations above, we would like to comment on the advantage of using such a limit of the one dimensional system before we turn to the two dimensional model.

Indeed, it may have seemed arbitrary to look at the case with negligible cell drag and nutrient uptake in Chapter 4, so I propose a motivation. Recall that, from the full one dimensional system we obtained the following equation for $\hat{\alpha}$ in (71):

$$\begin{aligned}\frac{\partial \hat{\alpha}}{\partial t} = \frac{1}{R_*}\Big[\xi\frac{dR_*}{dt} - v_{cs}\Big]\frac{\partial \hat{\alpha}}{\partial \xi} + \Big[\frac{\partial S_c}{\partial \alpha}(\alpha_s, C_s) - \frac{1}{R_*}\frac{\partial v_{cs}}{\partial \xi}\Big]\hat{\alpha} \\ + \frac{\partial S_c}{\partial C}(\alpha_s, C_s)\hat{C} - \frac{1}{R_*}\frac{\partial}{\partial \xi}(\alpha_s \hat{v}_c). \qquad (72)\end{aligned}$$

However, in the limit case where cell drag and nutrient uptake were taken to be negligible, the equation above simplified to equation (59):

$$\frac{\partial \hat{\alpha}}{\partial t} = \Big[\frac{\partial S_c}{\partial \alpha}(\alpha_h, C_\infty) - \lambda_2\Big]\hat{\alpha} - \frac{\alpha_h}{R_*(t)}\frac{\partial \hat{v}_c}{\partial \xi}$$

due to the particularities of the solutions, such as $C_s = C_\infty$, $\hat{C} = 0$, $\alpha_s = \alpha_h$, and mainly the fact that

$$\xi\frac{dR_*}{dt} - v_{cs} = \xi\lambda_2 R_*(t) - \lambda_2 \xi R_*(t) = 0$$

because

$$R_*(t) = R_0 e^{\lambda_2 t}, \qquad v_{cs}(x) = \lambda_2 x, \qquad x = \xi R_*(t).$$

This simplification is precisely what makes this limit case more tractable. Notice that without this simplification, we cannot solve this system analytically as we did in the limit case. Particularly, the appearance of ξ and $R_*(t)$ in the coefficients of equation (72) implies that it is not possible to separate variables.

As we've seen in Chapters 4 and 5, this limit case is indeed a good approximation of the full one dimensional model for intermediate time, when nutrient uptake and cell drag are naturally smaller. Thus we will define the full two dimensional system in the next chapter, and eventually consider a two dimensional version of this limit case in section 7.2.

7

LINEAR STABILITY ANALYSIS IN TWO DIMENSIONS

In this chapter, we aim to perform a linear stability analysis on one dimensional, non-homogeneous time-dependent solutions of the two-dimensional two phase model of tumour growth obtained in Chapter 2. For this, we must define the domain of interest for the two dimensional model along with its boundary conditions. As in the previous chapter, we will see that the full two dimensional case is not tractable analytically. Consequently, this will motivate us to consider the limit case with negligible nutrient uptake and cell drag and the stability of its one dimensional travelling solutions with respect to two dimensional perturbations in the following chapter.

7.1 GENERAL TWO DIMENSIONAL SYSTEM

7.1.1 *Definition and Notation*

First, consider the two dimensional system obtained in Chapter 2:

$$\begin{cases} \dfrac{\partial \alpha}{\partial t} & = S_c - \nabla \cdot (\mathbf{v}_c \alpha), \\ 0 & = \nabla \cdot (-p\mathbf{I} + \alpha \mathbf{F}(\alpha, \mathbf{v}_c)), \\ 0 & = (1-\alpha)\nabla p + k(\alpha)(\mathbf{v}_w - \mathbf{v}_c), \\ 0 & = \nabla \cdot (\alpha \mathbf{v}_c + (1-\alpha)\mathbf{v}_w), \\ 0 & = \nabla^2 C - Q_c(\alpha, C), \end{cases} \tag{73}$$

with tensor

$$\mathbf{F}(\alpha, \mathbf{v}_c) = -\Sigma_c(\alpha)\mathbf{I} + \mu_c(\nabla \mathbf{v}_c + \nabla \mathbf{v}_c^T) + \lambda_c(\nabla \cdot \mathbf{v}_c)\mathbf{I}.$$

We define the outer boundary at time t by

$$\Gamma(t) :=: \{(x, y) \in \mathbb{R}^2 : x = R(y, t)\}$$

such that

$$\frac{\partial \mathbf{R}}{\partial t}(y, t) \cdot \mathbf{n}(y, t) = \mathbf{v}_c(\mathbf{R}(y, t), t) \cdot \mathbf{n}(y, t),$$

where $\mathbf{n}$ is the outward unit normal to the curve $\mathbf{R}(y, t) = (R(y, t), y)$, i.e.

$$\mathbf{n} = \Big(1, -\frac{\partial R}{\partial y}\Big) \Big/ \sqrt{1 + \Big(\frac{\partial R}{\partial y}\Big)^2}.$$

At the moving boundary $\Gamma(t)$ we define the following boundary conditions:

$$\mathbf{F} \cdot \mathbf{n} = \mathbf{0}, \qquad p = 0, \qquad (\mathbf{v}_w - \mathbf{v}_c) \cdot \boldsymbol{\tau} = 0, \qquad C = C_\infty,$$

where $\boldsymbol{\tau}$ is the unit tangent to the curve $\mathbf{R}(y, t) = (R(y, t), y)$, i.e.

$$\boldsymbol{\tau} = \Big(\frac{\partial R}{\partial y}, 1\Big) \Big/ \sqrt{1 + \Big(\frac{\partial R}{\partial y}\Big)^2}.$$

Additionally, at the inner boundary $x = 0$ we impose the following conditions:

$$\mathbf{v}_c = 0, \qquad v_w^1 := \mathbf{v}_w \cdot \mathbf{e}_1 = 0, \qquad \frac{\partial C}{\partial x} = 0,$$

where $\mathbf{e}_1$ is the unit vector in the x direction. This corresponds to assuming that $x = 0$ is a rigid impermeable boundary.

Notice that the boundary conditions imposed on the moving boundary can be reduced to the original conditions required in the one dimensional model in Chapter 2 by taking

$$\mathbf{R}(y,t) = (R(t), y), \qquad \text{and thus} \qquad \mathbf{n} = \mathbf{e}_1, \qquad \boldsymbol{\tau} = \mathbf{e}_2,$$

where $\mathbf{e}_2$ is the unit vector in the y direction. Additionally, recall that, in the one dimensional model, the outer boundary conditions on v_c and p were considered to be derived from 1-D versions of

$$\sigma_c \cdot \mathbf{n} = 0, \qquad \sigma_w \cdot \mathbf{n} = 0,$$

which are equivalent to the conditions $\mathbf{F} \cdot \mathbf{n} = 0$ and $p = 0$ required above on the two dimensional moving boundary.

On the other hand, the condition $(\mathbf{v}_w - \mathbf{v}_c) \cdot \boldsymbol{\tau} = 0$ represents the continuity of the water momentum equation on the moving boundary. Indeed, since $p = 0$ on the surface, the tangential derivative of the pressure $\nabla p \cdot \boldsymbol{\tau}$ is also zero on the boundary. Thus, the water momentum equation implies that

$$0 = (1-\alpha)\nabla p \cdot \boldsymbol{\tau} + k(\alpha)(\mathbf{v}_w - \mathbf{v}_c) \cdot \boldsymbol{\tau} = k(\alpha)(\mathbf{v}_w - \mathbf{v}_c) \cdot \boldsymbol{\tau}$$

and thus $(\mathbf{v}_w - \mathbf{v}_c) \cdot \boldsymbol{\tau} = 0$ on the moving boundary.

To complete the notation used in this chapter, let

$$\Omega(t) :=: \{(x,y) \in \mathbb{R}^2 : 0 < x < R(t,y)\}$$

denote our domain of interest for each $t > 0$.

7.1.2 *Linearisation about One Dimensional Solution*

For simplicity, consider now a one dimensional non-homogeneous time-dependent solution of (78), i.e:

$$\begin{gathered}\alpha_s(x,y,t)=\alpha_s(x,t), \qquad C_s(x,y,t)=C_s(x,t), \qquad p_s(x,y,t)=p_s(x,t)\\ \mathbf{v}_{cs}(x,y,t)=(v_{cs}(x,t),0), \qquad \mathbf{v}_{ws}(x,y,t)=(v_{ws}(x,t),0)\\ \mathbf{R}_*(y,t)=(R_*(t),y), \qquad \mathbf{n}_*(t,y)=(1,0), \quad \forall\, y\end{gathered}$$

that satisfies the system (78) in

$$\Omega_*(t)=\{(x,y)\in\mathbb{R}^2 : 0<x<R_*(t)\}$$

and its boundary equations in $x=0$ and

$$\Gamma_*(t)=\{(x,y)\in\mathbb{R}^2 : x=R_*(t)\}.$$

Particularly, by simple verification, we see that

$$\alpha_s(x,t), \quad C_s(x,t), \quad p_s(x,t), \quad v_{cs}(x,t), \quad v_{ws}(x,t), \quad R_*(t)$$

is a solution to the one dimensional system (69).

We shall consider two dimensional perturbations on this one dimensional solution. For this purpose, we linearise about this one dimensional solution and obtain the following system for the respective two-dimensional perturbations

$$\begin{gathered}\hat{\alpha}(x,y,t), \qquad \hat{C}(x,y,t), \qquad \hat{p}(x,y,t), \qquad \hat{\mathbf{R}}(y,t)=(\hat{R}(y,t),0)\\ \hat{\mathbf{v}}_c(x,y,t)=(\hat{v}_c^1(x,y,t),\hat{v}_c^2(x,y,t)), \quad \hat{\mathbf{v}}_w(x,y,t)=(\hat{v}_w^1(x,y,t),\hat{v}_w^2(x,y,t)) :\end{gathered}$$

$$
\begin{cases}
\dfrac{\partial \hat{\alpha}}{\partial t} & = \dfrac{\partial S_c}{\partial \alpha}(\alpha_s, C_s)\hat{\alpha} + \dfrac{\partial S_c}{\partial C}(\alpha_s, C_s)\hat{C} - \dfrac{\partial}{\partial x}(v_{cs}\hat{\alpha} + \alpha_s \hat{v}_c^1) - \alpha_s \dfrac{\partial \hat{v}_c^2}{\partial y} \\
\dfrac{\partial \hat{p}}{\partial x} & = \dfrac{\partial}{\partial x}\Big[\Big(-\Sigma_c(\alpha_s) - \alpha_s \Sigma_c'(\alpha_s) + \hat{\mu}_c \dfrac{\partial v_{cs}}{\partial x}\Big)\hat{\alpha} + \alpha_s\Big(\hat{\mu}_c \dfrac{\partial \hat{v}_c^1}{\partial x} + \lambda_c \dfrac{\partial \hat{v}_c^2}{\partial y}\Big)\Big] \\
& \quad + \mu_c \alpha_s \dfrac{\partial}{\partial y}\Big(\dfrac{\partial \hat{v}_c^2}{\partial x} + \dfrac{\partial \hat{v}_c^1}{\partial y}\Big) \\
\dfrac{\partial \hat{p}}{\partial y} & = \Big(-\Sigma_c(\alpha_s) - \alpha_s \Sigma_c'(\alpha_s) + \lambda_c \dfrac{\partial v_{cs}}{\partial x}\Big)\dfrac{\partial \hat{\alpha}}{\partial y} + \mu_c \dfrac{\partial}{\partial x}\Big[\alpha_s\Big(\dfrac{\partial \hat{v}_c^1}{\partial y} + \dfrac{\partial \hat{v}_c^2}{\partial x}\Big)\Big] \\
& \quad + \alpha_s \dfrac{\partial}{\partial y}\Big(\lambda_c \dfrac{\partial \hat{v}_c^1}{\partial x} + \hat{\mu}_c \dfrac{\partial \hat{v}_c^2}{\partial y}\Big) \\
0 & = (1-\alpha_s)\dfrac{d\hat{p}}{dx} + k(\alpha_s)(\hat{v}_w^1 - \hat{v}_c^1) + \Big(k'(\alpha_s)(v_{ws} - v_{cs}) - \dfrac{\partial p_s}{\partial x}\Big)\hat{\alpha} \\
0 & = (1-\alpha_s)\dfrac{\partial \hat{p}}{\partial y} + k(\alpha_s)(\hat{v}_w^2 - \hat{v}_c^2) \\
0 & = \dfrac{\partial}{\partial x}\Big((v_{cs} - v_{ws})\hat{\alpha} + \alpha_s \hat{v}_c^1 + (1-\alpha_s)\hat{v}_w^1\Big) + \alpha_s \dfrac{\partial \hat{v}_c^2}{\partial y} + (1-\alpha_s)\dfrac{\partial \hat{v}_w^2}{\partial y} \\
\nabla^2 \hat{C} & = \dfrac{\partial Q_c}{\partial C}(\alpha_s, C_s)\hat{C} + \dfrac{\partial Q_c}{\partial \alpha}(\alpha_s, C_s)\hat{\alpha} \qquad (x,y) \in \Omega_*(t), t \in (0,\infty).
\end{cases}
$$

Similarly, linearising the two dimensional moving boundary equation about the one dimensional solution implies that

$$
\frac{\partial \hat{R}}{\partial t}(y,t) = \frac{\partial v_{cs}}{\partial x}(R_*(t),t)\hat{R}(y,t) + \hat{v}_c^1(R_*(t),y,t), \qquad \forall t \in (0,\infty), y \in \mathbb{R}.
$$

Furthermore, applying the boundary conditions to the perturbed solutions, we obtain that

$$
\begin{cases}
\hat{v}_c^1 = \hat{v}_c^2 = \hat{v}_w^1 = \dfrac{\partial \hat{C}}{\partial x} = 0, & \text{at } x = 0, \\
\hat{p} = -\alpha_s \Sigma_c'(\alpha_s)\hat{\alpha} + \hat{\mu}_c \dfrac{\partial \hat{v}_c^1}{\partial x}\alpha_s + \lambda_c \alpha_s \dfrac{\partial \hat{v}_c^2}{\partial y}, & \text{at } x = R_*(t), \\
0 = \Big(\dfrac{\partial \hat{v}_c^1}{\partial y} + \dfrac{\partial \hat{v}_c^2}{\partial x}\Big) + 2\dfrac{\partial v_{cs}}{\partial x} \cdot \dfrac{\partial \hat{R}}{\partial y}, & \text{at } x = R_*(t), \\
0 = \dfrac{\partial p_s}{\partial x}\hat{R} + \hat{p}, & \text{at } x = R_*(t), \\
\hat{v}_w^2 = \dfrac{\partial \hat{R}}{\partial y}(v_{cs} - v_{ws}) + \hat{v}_c^2, & \text{at } x = R_*(t), \\
0 = \dfrac{\partial C_s}{\partial x}\hat{R} + \hat{C}, & \text{at } x = R_*(t),
\end{cases}
$$

for $t > 0$, $y \in \mathbb{R}$.

7.1.3 *Fixing the Domain*

To consider solutions of this, we first fix the boundary. For this, we make the following change of variable:

$$x = x(t) = \xi R_*(t)$$

and therefore

$$\begin{aligned}
\frac{\partial}{\partial t} &\longrightarrow \frac{\partial}{\partial t} - \frac{\xi}{R_*(t)}\frac{dR_*}{dt}\frac{\partial}{\partial \xi} \\
\frac{\partial}{\partial x} &\longrightarrow \frac{1}{R_*(t)}\frac{\partial}{\partial \xi} \\
\frac{\partial}{\partial y} &\longrightarrow \frac{\partial}{\partial y}
\end{aligned}$$

and we obtain the following system:

$$\begin{cases}
\dfrac{\partial \hat{\alpha}}{\partial t} & = \dfrac{1}{R_*}\Big[\xi\dfrac{dR_*}{dt} - v_{cs}\Big]\dfrac{\partial \hat{\alpha}}{\partial \xi} + \Big[\dfrac{\partial S_c}{\partial \alpha}(\alpha_s, C_s) - \dfrac{1}{R_*}\dfrac{\partial v_{cs}}{\partial \xi}\Big]\hat{\alpha} \\
& \quad + \dfrac{\partial S_c}{\partial C}(\alpha_s, C_s)\hat{C} - \dfrac{1}{R_*}\dfrac{\partial}{\partial \xi}(\alpha_s \hat{v}_c^1) - \alpha_s \dfrac{\partial \hat{v}_c^2}{\partial y} \\
\dfrac{\partial \hat{p}}{\partial \xi} & = \dfrac{\partial}{\partial \xi}\Big[\Big(-\Sigma_c(\alpha_s) - \alpha_s\Sigma_c'(\alpha_s) + \dfrac{\hat{\mu}_c}{R_*}\dfrac{\partial v_{cs}}{\partial \xi}\Big)\hat{\alpha} + \alpha_s\Big(\dfrac{\hat{\mu}_c}{R_*}\dfrac{\partial \hat{v}_c^1}{\partial \xi} + \lambda_c\dfrac{\partial \hat{v}_c^2}{\partial y}\Big)\Big] \\
& \quad + \mu_c\alpha_s\dfrac{\partial}{\partial y}\Big(\dfrac{\partial \hat{v}_c^2}{\partial \xi} + R_*\dfrac{\partial \hat{v}_c^1}{\partial y}\Big) \\
\dfrac{\partial \hat{p}}{\partial y} & = \Big(-\Sigma_c(\alpha_s) - \alpha_s\Sigma_c'(\alpha_s) + \dfrac{\lambda_c}{R_*}\dfrac{\partial v_{cs}}{\partial \xi}\Big)\dfrac{\partial \hat{\alpha}}{\partial y} \\
& \quad + \dfrac{\mu_c}{R_*}\dfrac{\partial}{\partial \xi}\Big[\alpha_s\Big(\dfrac{\partial \hat{v}_c^1}{\partial y} + \dfrac{1}{R_*}\dfrac{\partial \hat{v}_c^2}{\partial \xi}\Big)\Big] + \alpha_s\dfrac{\partial}{\partial y}\Big(\dfrac{\lambda_c}{R_*}\dfrac{\partial \hat{v}_c^1}{\partial \xi} + \hat{\mu}_c\dfrac{\partial \hat{v}_c^2}{\partial y}\Big) \\
0 & = \dfrac{1-\alpha_s}{R_*}\dfrac{\partial \hat{p}}{\partial \xi} + k(\alpha_s)(\hat{v}_w^1 - \hat{v}_c^1) + \Big(k'(\alpha_s)(v_{ws} - v_{cs}) - \dfrac{1}{R_*}\dfrac{\partial p_s}{\partial \xi}\Big)\hat{\alpha} \\
0 & = (1-\alpha_s)\dfrac{\partial \hat{p}}{\partial y} + k(\alpha_s)(\hat{v}_w^2 - \hat{v}_c^2) \\
0 & = \dfrac{1}{R_*}\dfrac{\partial}{\partial \xi}\Big[(v_{cs} - v_{ws})\hat{\alpha} + \alpha_s\hat{v}_c^1 + (1-\alpha_s)\hat{v}_w^1\Big] + \alpha_s\dfrac{\partial \hat{v}_c^2}{\partial y} + (1-\alpha_s)\dfrac{\partial \hat{v}_w^2}{\partial y} \\
\dfrac{\partial^2 \hat{C}}{\partial \xi^2} & = R_*^2\Big(\dfrac{\partial Q_c}{\partial C}(\alpha_s, C_s)\hat{C} + \dfrac{\partial Q_c}{\partial \alpha}(\alpha_s, C_s)\hat{\alpha} - \dfrac{\partial^2 \hat{C}}{\partial y^2}\Big),
\end{cases} \tag{74}$$

for $(\xi, y, t) \in (0,1) \times \mathbb{R} \times (0,\infty)$ and

$$\frac{\partial \hat{R}}{\partial t}(y,t) = \frac{1}{R_*(t)} \frac{\partial v_{cs}}{\partial \xi}(1,t)\hat{R}(y,t) + \hat{v}_c^1(1,y,t), \qquad \forall\, (y,t) \in \mathbb{R} \times (0,\infty),$$

subject to the boundary conditions:

$$\begin{cases} \hat{v}_c^1 &= \hat{v}_c^2 = \hat{v}_w^1 = \dfrac{\partial \hat{C}}{\partial \xi} = 0, & \text{at } \xi = 0, \\ \hat{p} &= -\alpha_s \Sigma_c'(\alpha_s)\hat{\alpha} + \dfrac{\hat{\mu}_c \alpha_s}{R_*} \dfrac{\partial \hat{v}_c^1}{\partial \xi} + \lambda_c \alpha_s \dfrac{\partial \hat{v}_c^2}{\partial y}, & \text{at } \xi = 1, \\ 0 &= \Big(\dfrac{\partial \hat{v}_c^1}{\partial y} + \dfrac{1}{R_*} \dfrac{\partial \hat{v}_c^2}{\partial \xi} \Big) + \dfrac{2}{R_*} \dfrac{\partial v_{cs}}{\partial \xi} \cdot \dfrac{\partial \hat{R}}{\partial y}, & \text{at } \xi = 1, \\ 0 &= \dfrac{1}{R_*} \dfrac{\partial p_s}{\partial \xi} \hat{R} + \hat{p}, & \text{at } \xi = 1, \\ \hat{v}_w^2 &= \dfrac{\partial \hat{R}}{\partial y}(v_{cs} - v_{ws}) + \hat{v}_c^2, & \text{at } \xi = 1, \\ 0 &= \dfrac{1}{R_*} \dfrac{\partial C_s}{\partial \xi} \hat{R} + \hat{C}, & \text{at } \xi = 1, \end{cases} \tag{75}$$

for all $(y,t) \in \mathbb{R} \times (0,\infty)$.

7.1.4 *Separation of Variables*

Notice from the equations above that it is not possible to separate variables in ξ or t as both ξ and t are present in the coefficients in ways that they cannot be extracted by simple exponentiation. However, it is possible to separate variables in y.

Indeed, consider now

$$\hat{\alpha}(\xi, y, t) = e^{i\kappa y}\tilde{\alpha}(\xi, t) + c.c.$$

$$\hat{C}(\xi, y, t) = e^{i\kappa y}\tilde{C}(\xi, t) + c.c. \qquad \hat{p}(\xi, y, t) = e^{i\kappa y}\tilde{p}(\xi, t) + c.c.,$$

$$\hat{\mathbf{v}}_c(\xi, y, t) = e^{i\kappa y}\tilde{\mathbf{v}}_c(\xi, t) + c.c. = e^{i\kappa y}(\tilde{v}_c^1(\xi, t), \tilde{v}_c^2(\xi, t)) + c.c.,$$

$$\hat{\mathbf{v}}_w(\xi, y, t) = e^{i\kappa y}\tilde{\mathbf{v}}_w(\xi, t) + c.c. = e^{i\kappa y}(\tilde{v}_w^1(\xi, t), \tilde{v}_w^2(\xi, t)) + c.c.$$

and

$$\hat{\mathbf{R}}(y,t) = (\hat{R}(y,t), 0) + c.c. = e^{i\kappa y}(\tilde{R}(t), 0) + c.c,$$

where *c.c.* stands for the complex conjugate of its preceding term and $\kappa \in \mathbb{R}$ is arbitrary corresponding to the wavelength of the perturbation in question.

Then, substituting these ansätze back into our system, we obtain

$$\begin{cases} \dfrac{\partial \tilde{\alpha}}{\partial t} & = \dfrac{1}{R_*}\Big[\xi \dfrac{dR_*}{dt} - v_{cs}\Big]\dfrac{\partial \tilde{\alpha}}{\partial \xi} + \Big[\dfrac{\partial S_c}{\partial \alpha}(\alpha_s, C_s) - \dfrac{1}{R_*}\dfrac{\partial v_{cs}}{\partial \xi}\Big]\tilde{\alpha} + \dfrac{\partial S_c}{\partial C}(\alpha_s, C_s)\tilde{C} \\ & \quad -\dfrac{1}{R_*}\dfrac{\partial}{\partial \xi}(\alpha_s \tilde{v}_c^1) - \alpha_s i\kappa \tilde{v}_c^2 \\ \dfrac{\partial \tilde{p}}{\partial \xi} & = \dfrac{\partial}{\partial \xi}\Big[\Big(-\Sigma_c(\alpha_s) - \alpha_s \Sigma_c'(\alpha_s) + \dfrac{\hat{\mu}_c}{R_*}\dfrac{\partial v_{cs}}{\partial \xi}\Big)\tilde{\alpha} + \alpha_s\Big(\dfrac{\hat{\mu}_c}{R_*}\dfrac{\partial \tilde{v}_c^1}{\partial \xi} + \lambda_c i\kappa \tilde{v}_c^2\Big)\Big] \\ & \quad +\mu_c \alpha_s i\kappa\Big(\dfrac{\partial \tilde{v}_c^2}{\partial \xi} + R_* i\kappa \tilde{v}_c^1\Big) \\ i\kappa \tilde{p} & = \Big(-\Sigma_c(\alpha_s) - \alpha_s \Sigma_c'(\alpha_s) + \dfrac{\lambda_c}{R_*}\dfrac{\partial v_{cs}}{\partial \xi}\Big) i\kappa \tilde{\alpha} \\ & \quad +\dfrac{\mu_c}{R_*}\dfrac{\partial}{\partial \xi}\Big[\alpha_s\Big(i\kappa \tilde{v}_c^1 + \dfrac{1}{R_*}\dfrac{\partial \tilde{v}_c^2}{\partial \xi}\Big)\Big] + \alpha_s i\kappa\Big(\dfrac{\lambda_c}{R_*}\dfrac{\partial \tilde{v}_c^1}{\partial \xi} + \hat{\mu}_c i\kappa \tilde{v}_c^2\Big) \\ 0 & = \dfrac{1-\alpha_s}{R_*}\dfrac{\partial \tilde{p}}{\partial \xi} + k(\alpha_s)(\tilde{v}_w^1 - \tilde{v}_c^1) + \Big(k'(\alpha_s)(v_{ws} - v_{cs}) - \dfrac{1}{R_*}\dfrac{\partial p_s}{\partial \xi}\Big)\tilde{\alpha} \\ 0 & = (1-\alpha_s) i\kappa \tilde{p} + k(\alpha_s)(\tilde{v}_w^2 - \tilde{v}_c^2) \\ 0 & = \dfrac{1}{R_*}\dfrac{\partial}{\partial \xi}\Big[(v_{cs} - v_{ws})\tilde{\alpha} + \alpha_s \tilde{v}_c^1 + (1-\alpha_s)\tilde{v}_w^1\Big] + \alpha_s i\kappa \tilde{v}_c^2 + (1-\alpha_s) i\kappa \tilde{v}_w^2 \\ \dfrac{\partial^2 \tilde{C}}{\partial \xi^2} & = R_*^2\Big[\Big(\dfrac{\partial Q_c}{\partial C}(\alpha_s, C_s) + \kappa^2\Big)\tilde{C} + \dfrac{\partial Q_c}{\partial \alpha}(\alpha_s, C_s)\tilde{\alpha}\Big] \end{cases} \tag{76}$$

for $(\xi, t) \in (0,1) \times (0, \infty)$ and

$$\frac{d\tilde{R}}{dt}(t) = \frac{1}{R_*(t)}\frac{\partial v_{cs}}{\partial \xi}(1,t)\tilde{R}(t) + \tilde{v}_c^1(1,t), \qquad \forall\, t \in (0,\infty),$$

subject to the boundary conditions:

$$\begin{cases} \tilde{v}_c^1 = \tilde{v}_c^2 = \tilde{v}_w^1 = \dfrac{\partial \tilde{C}}{\partial \xi} = 0, & \text{at } \xi = 0, \\ \tilde{p} = -\alpha_s \Sigma_c'(\alpha_s)\tilde{\alpha} + \dfrac{\hat{\mu}_c \alpha_s}{R_*}\dfrac{\partial \tilde{v}_c^1}{\partial \xi} + \lambda_c \alpha_s i\kappa \tilde{v}_c^2, & \text{at } \xi = 1, \\ 0 = i\kappa\left(\tilde{v}_c^1 + \dfrac{2}{R_*}\dfrac{\partial v_{cs}}{\partial \xi}\tilde{R}\right) + \dfrac{1}{R_*}\dfrac{\partial \tilde{v}_c^2}{\partial \xi}, & \text{at } \xi = 1, \\ 0 = \dfrac{1}{R_*}\dfrac{\partial p_s}{\partial \xi}\tilde{R} + \tilde{p}, & \text{at } \xi = 1, \\ \tilde{v}_w^2 = i\kappa\tilde{R}(v_{cs} - v_{ws}) + \tilde{v}_c^2, & \text{at } \xi = 1, \\ 0 = \dfrac{1}{R_*}\dfrac{\partial C_s}{\partial \xi} \tilde{+} \tilde{C}, & \text{at } \xi = 1, \end{cases} \tag{77}$$

for $t \in (0, \infty)$.

7.2 NEGLIGIBLE NUTRIENT CONSUMPTION AND CELL DRAG

7.2.1 *Definition*

Now, we will analyse a specific limit case of this system in which nutrient consumption and cell drag are taken to be negligible. With this simplification, we will obtain some analytical results in the following chapter.

Initially, recall that, this limit case was obtained from the one dimensional formulation by taking $Q_c(\alpha, C) \equiv 0 \equiv k(\alpha)$. However, in the two dimensional case, if $k(\alpha) \equiv 0$, then the conditions

$$\begin{cases} 0 = (1-\alpha)\nabla p + k(\alpha)(\mathbf{v}_w - \mathbf{v}_c), & (x,y) \in \Omega(t) \\ p = 0, & (x,y) \in \Gamma(t), \end{cases}$$

reduce to $p \equiv 0$. Since the first equation is a vector equation, we have thus retrieved only one equation from (essentially) two equations. To avoid this loss of information, we will consider instead the $k(\alpha)$ found in literature, namely, $k(\alpha) = k_0\alpha(1-\alpha)$ but with $k_0 > 0$ small. Then,

$$0 = (1-\alpha)\nabla p + k(\alpha)(\mathbf{v}_w - \mathbf{v}_c) = (1-\alpha)\nabla p + k_0\alpha(1-\alpha)(\mathbf{v}_w - \mathbf{v}_c)$$

and therefore

$$0 = \nabla p + k_0 \alpha (\mathbf{v}_w - \mathbf{v}_c).$$

Taking the curl of this equation yields

$$0 = \nabla \times [\alpha(\mathbf{v}_w - \mathbf{v}_c)], \qquad \forall\, k_0 > 0,$$

and thus we have obtained the second equation required.

Therefore, $p \equiv 0$ and $(\alpha, C, \mathbf{v}_c, \mathbf{v}_w, \mathbf{R})$ satisfy

$$\begin{cases} \dfrac{\partial \alpha}{\partial t} & = S_c(\alpha, C) - \nabla \cdot (\mathbf{v}_c \alpha), \\ 0 & = \nabla \cdot (\alpha \mathbf{F}(\alpha, \mathbf{v}_c)), \\ 0 & = \nabla \cdot (\alpha \mathbf{v}_c + (1-\alpha)\mathbf{v}_w), \\ 0 & = \nabla \times [\alpha(\mathbf{v}_w - \mathbf{v}_c)] \\ 0 & = \nabla^2 C, \qquad (x,y) \in \Omega(t), t \in (0,\infty), \end{cases} \tag{78}$$

with moving boundary equation

$$\frac{\partial \mathbf{R}}{\partial t}(y,t) \cdot \mathbf{n}(y,t) = \mathbf{v}_c(\mathbf{R}(y,t),t) \cdot \mathbf{n}(y,t), \quad (y,t) \in \mathbb{R} \times (0,\infty)$$

and boundary conditions

$$\begin{cases} v_c^1 = v_c^2 = v_w^1 = \dfrac{\partial C}{\partial x} = 0, & \text{on } x = 0 \\ \mathbf{F} \cdot \mathbf{n} = \mathbf{0}, \qquad (\mathbf{v}_w - \mathbf{v}_c) \cdot \boldsymbol{\tau} = 0, \qquad C = C_\infty, & \text{on } (x,y) \in \Gamma(t) \end{cases}$$

$\forall\, t \in (0,\infty)$.

7.2.2 *Linearisation about One Dimensional Travelling Solution*

It is possible to recast the travelling one dimensional solution of the limit case defined in Chapter 4 in such a way that these become a one dimensional solution to the two dimensional equations defined above. Indeed, let $\alpha_h \in (0,1)$ and λ_2 be defined by

$$\lambda_2 = \frac{\Sigma_c(\alpha_h)}{\hat{\mu}_c} = \frac{S_c(\alpha_h, C_\infty)}{\alpha_h}$$

and

$$C_s = C_\infty \qquad \mathbf{v}_{cs}(x) = \lambda_2 x \mathbf{e_1} \qquad \mathbf{v}_{ws}(x) = \frac{-\lambda_2 \alpha_h}{1-\alpha_h} x \mathbf{e_1}.$$

We can also define the two-dimensional moving boundary $\Gamma_*(t)$ and domain $\Omega_*(t)$, as in the beginning of the section, via the equation

$$\mathbf{R}_*(t,y) = (R_*(t), y) = (R_0 e^{\lambda_2 t}, y).$$

We would like to consider the stability of this solution. Recall that, in the general case above, we

1. Linearised about a general one dimensional solution.
2. Fixed the domain using the change of variable $x = x(t) = \xi R_*(t)$.
3. Separated variables in y.

We will employ the same method here in the limit case using the solution above. Although this can be done step by step, in essence this process would be a particular case of the previous one, with the following substitutions:

$$p_s \equiv 0, \qquad \hat{p} \equiv 0, \qquad \tilde{p} \equiv 0, \qquad k(\alpha) \equiv 0, \qquad Q_c(\alpha, C) \equiv 0$$

and the addition of the contributions of applying steps 1, 2, and 3 to the newly defined equation

$$0 = \nabla \times [\alpha(\mathbf{v}_w - \mathbf{v}_c)].$$

Linearising the equation above about the travelling solutions we see that perturbations satisfy

$$0 = \alpha_h \nabla \times [\hat{\mathbf{v}}_w - \hat{\mathbf{v}}_c] - (v_{ws} - v_{cs}) \frac{\partial \hat{\alpha}}{\partial y}.$$

Once we fix the domain, we obtain

$$0 = \alpha_h \Big[\frac{1}{R_*} \frac{\partial}{\partial \xi} (\hat{v}_w^2 - \hat{v}_c^2) - \frac{\partial}{\partial y} (\hat{v}_w^1 - \hat{v}_c^1) \Big] - (v_{ws} - v_{cs}) \frac{\partial \hat{\alpha}}{\partial y}.$$

Then, if we separate variables in y, we have

$$0 = \frac{\alpha_h}{R_*} \frac{\partial}{\partial \xi} (\tilde{v}_w^2 - \tilde{v}_c^2) - i\kappa \Big[\alpha_h (\tilde{v}_w^1 - \tilde{v}_c^1) + (v_{ws} - v_{cs}) \tilde{\alpha} \Big].$$

We also note that doing this process will lead to, among other equations, the following conditions on $\tilde{C}$:

$$\frac{\partial^2 \tilde{C}}{\partial \xi^2}(\xi,t) = \kappa^2 R_*(t)^2 \tilde{C}(\xi,t), \qquad \frac{\partial \tilde{C}}{\partial \xi}(0,t) = 0, \qquad \tilde{C}(1,t) = 0,$$

for all $t > 0$. Therefore, $\tilde{C} \equiv 0$ and the linearisation of the limit case system about the one dimensional travelling solution can be reduced to:

$$\begin{cases} \dfrac{\partial \tilde{\alpha}}{\partial t} &= \Big[\dfrac{\partial S_c}{\partial \alpha}(\alpha_h, C_\infty) - \lambda_2\Big]\tilde{\alpha} - \dfrac{\alpha_h}{R_*}\dfrac{\partial \tilde{v}_c^1}{\partial \xi} - \alpha_h i\kappa \tilde{v}_c^2 \\ 0 &= -\dfrac{\Sigma_c'(\alpha_h)}{R_*}\dfrac{\partial \tilde{\alpha}}{\partial \xi} + \dfrac{\hat{\mu}_c}{R_*^2}\dfrac{\partial^2 \tilde{v}_c^1}{\partial \xi^2} + \dfrac{(\lambda_c+\mu_c)}{R_*} i\kappa \dfrac{\partial \tilde{v}_c^2}{\partial \xi} - \mu_c \kappa^2 \tilde{v}_c^1 \\ 0 &= \Big(-\Sigma_c(\alpha_h) - \alpha_h \Sigma_c'(\alpha_h) + \lambda_c\lambda_2\Big) i\kappa\tilde{\alpha} + \dfrac{\mu_c \alpha_h}{R_*^2}\dfrac{\partial^2 \tilde{v}_c^2}{\partial \xi^2} \\ &\quad + (\mu_c + \lambda_c)\dfrac{\alpha_h i\kappa}{R_*}\dfrac{\partial \tilde{v}_c^1}{\partial \xi} - \alpha_h \kappa^2 \hat{\mu}_c \tilde{v}_c^2 \\ 0 &= \dfrac{\lambda_2}{1-\alpha_h}\Big(1 + \xi\dfrac{\partial}{\partial \xi}\Big)\tilde{\alpha} + \dfrac{\alpha_h}{R_*}\dfrac{\partial \tilde{v}_c^1}{\partial \xi} + \dfrac{1-\alpha_h}{R_*}\dfrac{\partial \tilde{v}_w^1}{\partial \xi} + \alpha_h i\kappa \tilde{v}_c^2 + (1-\alpha_h) i\kappa \tilde{v}_w^2 \\ 0 &= \dfrac{\alpha_h}{R_*^2}\dfrac{\partial}{\partial \xi}(\tilde{v}_w^2 - \tilde{v}_c^2) - \dfrac{i\kappa\alpha_h}{R_*}(\tilde{v}_w^1 - \tilde{v}_c^1) + \dfrac{i\kappa\lambda_2\xi}{1-\alpha_h}\tilde{\alpha} \end{cases} \tag{79}$$

for $(\xi, t) \in (0,1) \times (0,\infty)$, with

$$\frac{d\tilde{R}}{dt}(t) = \lambda_2 \tilde{R}(t) + \tilde{v}_c^1(1,t), \qquad t \in (0,\infty),$$

subject to the boundary conditions:

$$\begin{cases} \tilde{v}_c^1 &= \tilde{v}_c^2 = \tilde{v}_w^1 = 0, & \text{at } \xi = 0, \\ 0 &= -\Sigma_c'(\alpha_h)\tilde{\alpha} + \dfrac{\hat{\mu}_c}{R_*}\dfrac{\partial \tilde{v}_c^1}{\partial \xi} + \lambda_c i\kappa \tilde{v}_c^2, & \text{at } \xi = 1, \\ 0 &= i\kappa\Big(\tilde{v}_c^1 + 2\lambda_2 \tilde{R}\Big) + \dfrac{1}{R_*}\dfrac{\partial \tilde{v}_c^2}{\partial \xi}, & \text{at } \xi = 1, \\ \tilde{v}_w^2 &= \dfrac{i\kappa\lambda_2 R_*}{1-\alpha_h}\tilde{R} + \tilde{v}_c^2, & \text{at } \xi = 1, \end{cases} \tag{80}$$

for $t \in (0,\infty)$.

Observation

The limit case where nutrient uptake and cell drag were taken to be negligible certainly simplified the full two dimensional formulation

(compare (76) and (79), for example). In particular, notice that, we obtained in the full two dimensional case (76) the following equation for $\tilde{\alpha}$:

$$\frac{\partial \tilde{\alpha}}{\partial t} = \frac{1}{R_*}\Big[\xi \frac{dR_*}{dt} - v_{cs}\Big]\frac{\partial \tilde{\alpha}}{\partial \xi} + \Big[\frac{\partial S_c}{\partial \alpha}(\alpha_s, C_s) - \frac{1}{R_*}\frac{\partial v_{cs}}{\partial \xi}\Big]\tilde{\alpha} + \frac{\partial S_c}{\partial C}(\alpha_s, C_s)\tilde{C} - \frac{1}{R_*}\frac{\partial}{\partial \xi}(\alpha_s \tilde{v}_c^1) - \alpha_s i\kappa \tilde{v}_c^2. \tag{81}$$

On the other hand, in the limit case, we obtained in (79):

$$\frac{\partial \tilde{\alpha}}{\partial t} = \Big[\frac{\partial S_c}{\partial \alpha}(\alpha_h, C_s) - \lambda_2\Big]\tilde{\alpha} - \frac{\alpha_h}{R_*}\frac{\partial \tilde{v}_c^1}{\partial \xi} - \alpha_h i\kappa \tilde{v}_c^2. \tag{82}$$

However, we still cannot solve the limit case (79) analytically as we have done in the one dimensional formulation. Although equation (82) above seems to suggest that we may separate variables, the appearance of ξ and $R_*(t)$ in the coefficients of the other equations in (79) implies that we can't.

Nevertheless, in this chapter we have formulated the two dimensional problem by choosing the boundary conditions and the region of interest. With this, we also defined the negligible nutrient uptake and cell drag limit in two dimensions that will be explored in the next chapter. Additionally, we have devised a setup that could eventually be suitable for numerical treatment in the case of a general one dimensional solution (but is not implemented in this thesis).

Having seen the advantages of the negligible nutrient uptake and cell drag limit case, we will continue to work exclusively with the system (79). Particularly, in the next chapter, we obtain asymptotic expansions of the solutions of the system mentioned above. For that, we will restrict ourselves to the case where the travelling solution is one of a growing tumour, i.e. $\lambda_2 > 0$ and therefore

$$\epsilon = \epsilon(t) :=: \frac{1}{R_*(t)} = \frac{1}{R_0 e^{\lambda_2 t}} \longrightarrow 0, \qquad \text{when} \qquad t \to \infty.$$

Motivated by this limit, $\epsilon(t)$ will be used as a small parameter for t large in the asymptotic approximations that follow.

8

ASYMPTOTIC ANALYSIS OF NEGLIGIBLE NUTRIENT CONSUMPTION AND CELL DRAG LIMIT IN TWO DIMENSIONS

8.1 SET UP AND MOTIVATION

In the previous chapter, we investigated the possibility of performing linear stability analysis on one dimensional solutions of the full two dimensional model. However, we concluded that this was not a tractable case for an analytic approach and decided to focus on the simpler limit case obtained by assuming that nutrient uptake and cell drag are negligible.

Particularly, in this chapter, we will consider two dimensional perturbations on the travelling one dimensional solutions of the limit case. We have seen in the previous chapter that these perturbations satisfy the system of equations in (79) and its associated boundary conditions. Therefore, we will obtain approximations of the solution of this system when $t \to \infty$ using the method of matched asymptotic expansions and then compare predicted large time behaviour to numerical simulations. For this, we must restrict ourselves to the case where $\lambda_2 > 0$ and therefore $R_*(t) = R_0 e^{\lambda_2 t}$ represents a growing tumour.

Once we have characterised the asymptotic behaviour of the two dimensional perturbations, we will compare these to the travelling solution in order to, ultimately, reach a condition for instability of the growing

travelling solutions of the limit case with negligible nutrient uptake and cell drag.

8.2 OUTER SOLUTION

8.2.1 *Analytical Characterisation of Outer Solution*

In this subsection, we will characterise long time behaviour of the solution to the system (79) at a position $\xi \in [0,1]$ away from any possible boundary layers.

For that, we will consider first $\{\tilde{\alpha}, \tilde{v}_c^1, \tilde{v}_c^2\}$. Suppose that $\{a_0, a_1, a_2\}$ are decay rates of $\tilde{\alpha}$, $\tilde{v}_c^1$, and $\tilde{v}_c^2$, respectively, i.e.

$$\tilde{\alpha}(\xi,t) = e^{a_0 t}\overline{\alpha}(\xi), \qquad \tilde{v}_c^1(\xi,t) = e^{a_1 t}\overline{v}_c^1(\xi), \qquad \tilde{v}_c^2(\xi,t) = e^{a_2 t}\overline{v}_c^2(\xi),$$

with

$$\overline{\alpha}(\xi) = O(1), \qquad \overline{v}_c^1(\xi) = O(1), \qquad \overline{v}_c^2(\xi) = O(1), \qquad t \to 0,$$

for all relevant ξ (away from any possible boundary layers). Consider also the first three equations of (79):

$$\begin{cases} \dfrac{\partial \tilde{\alpha}}{\partial t} = \Big[\dfrac{\partial S_c}{\partial \alpha}(\alpha_h, C_\infty) - \lambda_2\Big]\tilde{\alpha} - \dfrac{\alpha_h}{R_*}\dfrac{\partial \tilde{v}_c^1}{\partial \xi} - \alpha_h i\kappa \tilde{v}_c^2 \\ 0 = -\dfrac{\Sigma_c'(\alpha_h)}{R_*}\dfrac{\partial \tilde{\alpha}}{\partial \xi} + \dfrac{\hat{\mu}_c}{R_*^2}\dfrac{\partial^2 \tilde{v}_c^1}{\partial \xi^2} + \dfrac{(\lambda_c+\mu_c)}{R_*} i\kappa \dfrac{\partial \tilde{v}_c^2}{\partial \xi} - \mu_c \kappa^2 \tilde{v}_c^1 \\ 0 = \Big(-\Sigma_c(\alpha_h) - \alpha_h \Sigma_c'(\alpha_h) + \lambda_c\lambda_2\Big) i\kappa\tilde{\alpha} + \dfrac{\mu_c \alpha_h}{R_*^2}\dfrac{\partial^2 \tilde{v}_c^2}{\partial \xi^2} \\ \qquad + (\mu_c + \lambda_c)\dfrac{\alpha_h i\kappa}{R_*}\dfrac{\partial \tilde{v}_c^1}{\partial \xi} - \alpha_h \kappa^2 \hat{\mu}_c \tilde{v}_c^2. \end{cases}$$

Notice that these only pertain to the three perturbations currently in question, $\{\tilde{\alpha}, \tilde{v}_c^1, \tilde{v}_c^2\}$. Thus, we may work with these first and then with $\{\tilde{v}_w^1, \tilde{v}_w^2\}$.

By substituting the new expressions for $\tilde{\alpha}$, $\tilde{v}_c^1$ and $\tilde{v}_c^2$ into the equations above, we may prove via case-by-case logic, that there is only one set of

values $\{a_0, a_1, a_2\}$ that balances these equations for large time and yields non-trivial solutions for $\{\overline{\alpha}, \overline{v}_c^1, \overline{v}_c^2\}$. Having found the values $\{a_0, a_1, a_2\}$, we may solve for expressions of $\{\overline{\alpha}, \overline{v}_c^1, \overline{v}_c^2\}$.

Indeed, substituting these rescalings into the equations above, we have that

$$\begin{cases} 0 = \Big[\dfrac{\partial S_c}{\partial \alpha}(\alpha_h, C_\infty) - \lambda_2 - a_0\Big]\overline{\alpha} - \dfrac{\alpha_h}{R_0 e^{(a_0-a_1+\lambda_2)t}}\dfrac{d\overline{v}_c^1}{d\xi} - \dfrac{\alpha_h i\kappa}{e^{(a_0-a_2)t}}\overline{v}_c^2 & (83) \\ 0 = -\Sigma_c'(\alpha_h)\dfrac{d\overline{\alpha}}{d\xi} + \dfrac{\hat{\mu}_c}{R_0 e^{(a_0-a_1+\lambda_2)t}}\dfrac{d^2\overline{v}_c^1}{d\xi^2} \\ \quad + \dfrac{(\lambda_c+\mu_c)i\kappa}{e^{(a_0-a_2)t}}\dfrac{d\overline{v}_c^2}{d\xi} - \dfrac{\mu_c\kappa^2 R_0}{e^{(a_0-a_1-\lambda_2)t}}\overline{v}_c^1 & (84) \\ 0 = \Big(-\Sigma_c(\alpha_h) - \alpha_h\Sigma_c'(\alpha_h) + \lambda_c\lambda_2\Big)i\kappa\overline{\alpha} + \dfrac{\mu_c\alpha_h}{R_0^2 e^{(a_0-a_2+2\lambda_2)t}}\dfrac{d^2\overline{v}_c^2}{d\xi^2} \\ \quad + \dfrac{(\mu_c+\lambda_c)\alpha_h i\kappa}{R_0 e^{(a_0-a_1+\lambda_2)t}}\dfrac{d\overline{v}_c^1}{d\xi} - \dfrac{\alpha_h\kappa^2\hat{\mu}_c}{e^{(a_0-a_2)t}}\overline{v}_c^2. & (85) \end{cases}$$

Initially, consider the first equation above, (83), as it has less terms than the other two and will thus be more tractable. From it, we see that there are four cases in which the balance of this equation is non-trivial for $t \to \infty$ and thus may yield non-trivial functions for $\{\overline{\alpha}, \overline{v}_c^1, \overline{v}_c^2\}$, namely:

Case 1: $a_0 - a_1 + \lambda_2 = a_0 - a_2 = 0$

Case 2: $a_0 - a_1 + \lambda_2 = 0$ and $a_0 - a_2 > 0$

Case 3: $a_0 - a_1 + \lambda_2 = a_0 - a_2 < 0$

Case 4: $a_0 - a_1 + \lambda_2 > 0$ and $a_0 - a_2 = 0$.

In Cases 1 and 2, $a_0 - a_1 + \lambda_2 = 0$ and therefore

$$a_0 - a_1 - \lambda_2 = (a_0 - a_1 + \lambda_2) - 2\lambda_2 = -2\lambda_2 < 0 \leq a_0 - a_2.$$

From this, we see that the $\overline{v}_c^1$ term dominates in equation (84) and that therefore $\overline{v}_c^1 \sim 0$ at first order. Similarly, in Case 3, we have that

$$a_0 - a_1 - \lambda_2 = (a_0 - a_1 + \lambda_2) - 2\lambda_2 < a_0 - a_1 + \lambda_2 = a_0 - a_2 < 0.$$

Therefore, equation (84) again implies that $\overline{v}_c^1 \sim 0$, through the same argument used above in Cases 1 and 2. Thus, although Cases 1-3 correspond to a non-trivial equation balance for equation (83), they imply a trivial balance for equation (84) such that $\overline{v}_c^1 \sim 0$ at first order.

Consider now Case 4, i.e. $a_0 - a_1 + \lambda_2 > 0$ and $a_0 - a_2 = 0$. Then, $a_0 - a_2 + 2\lambda_2 = 2\lambda_2 > 0$ and thus equations (83) and (85) become, at first order:

$$\begin{cases} 0 &= \Big[\dfrac{\partial S_c}{\partial \alpha}(\alpha_h, C_\infty) - \lambda_2 - a_0\Big]\overline{\alpha} - \alpha_h i\kappa \overline{v}_c^2 \\ 0 &= \dfrac{1}{\hat{\mu}_c}\Big(- \Sigma_c(\alpha_h) - \alpha_h \Sigma_c'(\alpha_h) + \lambda_c\lambda_2\Big)\overline{\alpha} + \alpha_h i\kappa \overline{v}_c^2. \end{cases} \tag{86}$$

Now, adding these two equations together we see that in order for this system to allow a non-trivial solution for $\{\overline{\alpha}, \overline{v}_c^2\}$, we must have that

$$\begin{aligned} 0 &= \Big[\frac{\partial S_c}{\partial \alpha}(\alpha_h, C_\infty) - \lambda_2 - a_0\Big] + \frac{1}{\hat{\mu}_c}\Big(- \Sigma_c(\alpha_h) - \alpha_h \Sigma_c'(\alpha_h) + \lambda_c\lambda_2\Big) \\ &= \frac{\partial S_c}{\partial \alpha}(\alpha_h, C_\infty) - \frac{\alpha_h \Sigma_c'(\alpha_h)}{\hat{\mu}_c} + \lambda_2\Big(\frac{\lambda_c}{\hat{\mu}_c} - 2\Big) - a_0 = \gamma_0 - \lambda_2 - a_0, \end{aligned}$$

where

$$\gamma_0 = \frac{\partial S_c}{\partial \alpha}(\alpha_h, C_\infty) - \frac{\alpha_h \Sigma_c'(\alpha_h)}{\hat{\mu}_c} + \lambda_2\Big(\frac{\lambda_c}{\hat{\mu}_c} - 1\Big),$$

and therefore,

$$a_0 = \gamma_0 - \lambda_2 \qquad \text{and} \qquad a_2 = \gamma_0 - \lambda_2.$$

With these, we also have that $a_0 - a_1 - \lambda_2 = \gamma_0 - 2\lambda_2 - a_1$ and thus Case 4 conditions imply that the equation (84) is, at first order,

$$0 = -\Sigma_c'(\alpha_h)\frac{d\overline{\alpha}}{d\xi} + (\lambda_c + \mu_c) i\kappa \frac{d\overline{v}_c^2}{d\xi} - \frac{\mu_c \kappa^2 R_0}{e^{(\gamma_0 - 2\lambda_2 - a_1)t}}\overline{v}_c^1.$$

Now, notice that the first order approximations of equations (83) and (85) seen in (86) no longer contain a single $\overline{v}_c^1$ term, as they were all deemed to be of order less than one. Therefore, $\overline{v}_c^1$ must be characterised by the equation above, which implies that $a_1 = \gamma_0 - 2\lambda_2$ and therefore, at first order,

$$0 = -\Sigma_c'(\alpha_h)\frac{d\overline{\alpha}}{d\xi} + (\lambda_c + \mu_c) i\kappa \frac{d\overline{v}_c^2}{d\xi} - \mu_c \kappa^2 R_0 \overline{v}_c^1. \tag{87}$$

With a_0, a_1 and a_2 determined, we can solve for $\overline{\alpha}$, $\overline{v}_c^1$ and $\overline{v}_c^2$ in equations (86) and (87), which in turn yield expressions for $\tilde{\alpha}$, $\tilde{v}_c^1$ and $\tilde{v}_c^2$:

$$\begin{aligned}
\tilde{\alpha}(\xi,t) &= R_0\frac{e^{\gamma_0 t}}{R_*(t)}\overline{\alpha}(\xi) = e^{(\gamma_0-\lambda_2)t}\overline{\alpha}(\xi)\\
\tilde{v}_c^1(\xi,t) &= R_0\gamma_1\frac{e^{\gamma_0 t}}{R_*(t)^2}\frac{d\overline{\alpha}}{d\xi}(\xi) = \frac{\gamma_1}{R_0}e^{(\gamma_0-2\lambda_2)t}\frac{d\overline{\alpha}}{d\xi}(\xi)\\
\tilde{v}_c^2(\xi,t) &= R_0\gamma_3\frac{e^{\gamma_0 t}}{R_*(t)}\overline{\alpha}(\xi) = \gamma_3 e^{(\gamma_0-\lambda_2)t}\overline{\alpha}(\xi),
\end{aligned}$$

where

$$\begin{aligned}
\gamma_1 &= -\frac{\Sigma_c'(\alpha_h)}{\mu_c\kappa^2} - \frac{(\lambda_c+\mu_c)(-\Sigma_c(\alpha_h)-\alpha_h\Sigma_c'(\alpha_h)+\lambda_c\lambda_2)}{\mu_c\kappa^2\hat{\mu}_c\alpha_h}\\
\gamma_3 &= -\frac{(-\Sigma_c(\alpha_h)-\alpha_h\Sigma_c'(\alpha_h)+\lambda_c\lambda_2)}{\hat{\mu}_c\alpha_h i\kappa}.
\end{aligned}$$

Notice that each one of the rescalings above has a coefficient of the type $e^{\gamma_0 t}$. Thus, it is natural to think that $\tilde{v}_w^1$ and $\tilde{v}_w^2$ may also have such a coefficient. This is indeed the case. Therefore, for the sake of simplifying our notation, we suppose now that

$$\begin{aligned}
\tilde{v}_w^1(\xi,t) &= e^{a_3 t}\overline{v}_w^1(\xi) = e^{(\gamma_0+b_1)t}\overline{v}_w^1(\xi)\\
\tilde{v}_w^2(\xi,t) &= e^{a_4 t}\overline{v}_w^2(\xi) = e^{(\gamma_0+b_2)t}\overline{v}_w^2(\xi).
\end{aligned}$$

First, we substitute these, along with the expressions already obtained for $\{\tilde{\alpha},\tilde{v}_c^1,\tilde{v}_c^2\}$, into the two equations of (79) that pertain to $\tilde{v}_w^1$ and $\tilde{v}_w^2$, i.e. into

$$\begin{cases}
0 &= \dfrac{\lambda_2}{1-\alpha_h}\Big(1+\xi\dfrac{\partial}{\partial\xi}\Big)\tilde{\alpha} + \dfrac{\alpha_h}{R_*}\dfrac{\partial\tilde{v}_c^1}{\partial\xi} + \dfrac{1-\alpha_h}{R_*}\dfrac{\partial\tilde{v}_w^1}{\partial\xi}\\
&\quad +\alpha_h i\kappa\tilde{v}_c^2 + (1-\alpha_h)i\kappa\tilde{v}_w^2\\
0 &= \dfrac{\alpha_h}{R_*^2}\dfrac{\partial}{\partial\xi}(\tilde{v}_w^2-\tilde{v}_c^2) - \dfrac{i\kappa\alpha_h}{R_*}(\tilde{v}_w^1-\tilde{v}_c^1) + \dfrac{i\kappa\lambda_2\xi}{1-\alpha_h}\tilde{\alpha}.
\end{cases}$$

Then, by using the same sort of case-by-case reasoning used to find $\{a_0,a_1,a_2\}$, we find a unique set of values for $\{b_1,b_2\}$ that allows for a non-trivial equation balance for each of these two equations and non-trivial $\{\overline{v}_w^1,\overline{v}_w^2\}$ for which we can solve.

Indeed, by substitution, we obtain that

$$\begin{cases} e^{b_1 t}\dfrac{d\overline{v}_w^1}{d\xi} + i\kappa R_0 e^{(b_2+\lambda_2)t}\overline{v}_w^2 = G_1(\xi,t) & (88) \\ i\kappa e^{b_1 t}\overline{v}_w^1 - \dfrac{1}{R_0}e^{(b_2-\lambda_2)t}\dfrac{d\overline{v}_w^2}{d\xi} = G_2(\xi,t), & (89) \end{cases}$$

where

$$\begin{aligned} G_1(\xi,t) &= -\frac{\lambda_2 R_0}{(1-\alpha_h)^2}\Big(1+\xi\frac{d}{d\xi}\Big)\overline{\alpha}(\xi) - \frac{\alpha_h i\kappa R_0\gamma_3}{1-\alpha_h}\overline{\alpha}(\xi) \\ &\quad - \frac{\alpha_h\gamma_1 R_0}{(1-\alpha_h)}\frac{1}{R_*(t)^2}\frac{d^2\overline{\alpha}}{d\xi^2}(\xi) \\ &\sim -\frac{\lambda_2 R_0}{(1-\alpha_h)^2}\Big(1+\xi\frac{d}{d\xi}\Big)\overline{\alpha}(\xi) - \frac{\alpha_h i\kappa R_0\gamma_3}{1-\alpha_h}\overline{\alpha}(\xi) =: \tilde{G}_1(\xi), \qquad t\to\infty \\ G_2(\xi,t) &= \frac{i\kappa\lambda_2 R_0\xi}{\alpha_h(1-\alpha_h)}\overline{\alpha}(\xi) + \frac{i\kappa\gamma_1 R_0}{R_*(t)^2}\frac{d\overline{\alpha}}{d\xi}(\xi) - \frac{R_0\gamma_3}{R_*(t)^2}\frac{d\overline{\alpha}}{d\xi}(\xi) \\ &\sim \frac{i\kappa\lambda_2 R_0\xi}{\alpha_h(1-\alpha_h)}\overline{\alpha}(\xi) =: \tilde{G}_2(\xi), \qquad t\to\infty. \end{aligned}$$

As before, for each of the two equations (88) and (89) above, there are four possibilities that may yield a non-trivial balance. Looking at the exponential prefactors in these equations, we see that such balances correspond to the following conditions:

Equation (88)**:**	**Equation** (89)**:**
Case I: $b_2+\lambda_2 = b_1 = 0$	**Case A:** $b_2-\lambda_2 = b_1 = 0$
Case II: $b_2+\lambda_2 = 0$ and $b_1 < 0$	**Case B:** $b_2-\lambda_2 = 0$ and $b_1 < 0$
Case III: $b_2+\lambda_2 = b_1 > 0$	**Case C:** $b_2-\lambda_2 = b_1 > 0$
Case IV: $b_2+\lambda_2 < 0$ and $b_1 = 0$	**Case D:** $b_2-\lambda_2 < 0$ and $b_1 = 0$

To have a non-trivial asymptotic balance for both of these equations, we must have a combination of one case from each of the two columns above. However, since we have restricted our analysis to consider only cases in which the travelling solution is one of a growing tumour, i.e. $\lambda_2 > 0$, then we have (trivially) that $b_2-\lambda_2 < b_2+\lambda_2$. Therefore, the only combinations

of two of these cases that are not contradictory, either in the value of b_1 or in the relationship between $b_2 - \lambda_2$ and $b_2 + \lambda_2$, are IV&D and I&D. For clarity, notice that these correspond to the following conditions:

Equations (88) **and** (89)**:**

Case IV&D: $b_2 - \lambda_2 < b_2 + \lambda_2 < 0$ and $b_1 = 0$

Case I&D: $b_2 + \lambda_2 = 0$ and $b_1 = 0$.

We shall consider these two possibilities separately.

First, suppose that $b_1 = 0$ and $b_2 - \lambda_2 < b_2 + \lambda_2 < 0$, i.e. Case IV&D. Then, for large t, at first order, equations (88) and (89) reduce to

$$\begin{cases} \tilde{G}_1(\xi) &= \dfrac{d\overline{v}_w^1}{d\xi} \\ \tilde{G}_2(\xi) &= i\kappa\overline{v}_w^1, \end{cases}$$

which is under-determined, as this asymptotic balance does not preserve any of the $\overline{v}_w^2$ terms. Therefore, this is not the balance for which we search.

Now, suppose that $b_1 = 0$ and $b_2 + \lambda_2 = 0$, i.e. Case I&D. Then, at order one, we have

$$\begin{cases} \tilde{G}_1(\xi) &= \dfrac{d\overline{v}_w^1}{d\xi} + i\kappa R_0 \overline{v}_w^2 \\ \tilde{G}_2(\xi) &= i\kappa\overline{v}_w^1. \end{cases}$$

This system can be solved for $\overline{v}_w^1$ and $\overline{v}_w^2$, which in turn yield the following expressions for $\tilde{v}_w^1$ and $\tilde{v}_w^2$:

$$\tilde{v}_w^1(\xi, t) = \frac{\lambda_2 R_0}{\alpha_h(1-\alpha_h)} e^{\gamma_0 t} \xi \overline{\alpha}(\xi)$$

$$\tilde{v}_w^2(\xi, t) = -e^{(\gamma_0 - \lambda_2)t} \left[\frac{\lambda_2}{i\kappa\alpha_h(1-\alpha_h)^2} \left(1 + \xi \frac{d}{d\xi}\right) \overline{\alpha}(\xi) + \frac{\alpha_h \gamma_3}{1-\alpha_h} \overline{\alpha}(\xi) \right].$$

Conclusion - Analytical Characterisation of Outer Solution

The non-trivial outer solution for ξ away from any possible boundary layers is, at first order,

$$\tilde{\alpha}(\xi,t) = e^{(\gamma_0-\lambda_2)t}\overline{\alpha}(\xi), \tag{90}$$

$$\tilde{v}_c^1(\xi,t) = \frac{\gamma_1}{R_0}e^{(\gamma_0-2\lambda_2)t}\frac{d\overline{\alpha}}{d\xi}(\xi), \tag{91}$$

$$\tilde{v}_c^2(\xi,t) = \gamma_3 e^{(\gamma_0-\lambda_2)t}\overline{\alpha}(\xi), \tag{92}$$

$$\tilde{v}_w^1(\xi,t) = \frac{\lambda_2 R_0}{\alpha_h(1-\alpha_h)}e^{\gamma_0 t}\xi\overline{\alpha}(\xi), \tag{93}$$

$$\tilde{v}_w^2(\xi,t) = -e^{(\gamma_0-\lambda_2)t}\left[\frac{\lambda_2}{i\kappa\alpha_h(1-\alpha_h)^2}\left(1+\xi\frac{d}{d\xi}\right)\overline{\alpha}(\xi) + \frac{\alpha_h\gamma_3}{1-\alpha_h}\overline{\alpha}(\xi)\right] \tag{94}$$

and it satisfies

$$\begin{cases} \dfrac{\partial\tilde{\alpha}}{\partial t} &= \Big[\dfrac{\partial S_c}{\partial\alpha}(\alpha_h, C_\infty) - \lambda_2\Big]\tilde{\alpha} - \alpha_h i\kappa\tilde{v}_c^2 \\ 0 &= -\Sigma_c'(\alpha_h)\dfrac{\partial\tilde{\alpha}}{\partial\xi} + (\lambda_c+\mu_c)i\kappa\dfrac{\partial\tilde{v}_c^2}{\partial\xi} - \mu_c\kappa^2 R_*\tilde{v}_c^1 \\ 0 &= \Big(-\Sigma_c(\alpha_h) - \alpha_h\Sigma_c'(\alpha_h) + \lambda_c\lambda_2\Big)i\kappa\tilde{\alpha} - \alpha_h\kappa^2\hat{\mu}_c\tilde{v}_c^2. \\ 0 &= \dfrac{\lambda_2}{1-\alpha_h}\Big(1+\xi\dfrac{\partial}{\partial\xi}\Big)\tilde{\alpha} + \dfrac{1-\alpha_h}{R_*}\dfrac{\partial\tilde{v}_w^1}{\partial\xi} + \alpha_h i\kappa\tilde{v}_c^2 + (1-\alpha_h)i\kappa\tilde{v}_w^2 \\ 0 &= -\dfrac{i\kappa\alpha_h}{R_*}\tilde{v}_w^1 + \dfrac{i\kappa\lambda_2\xi}{1-\alpha_h}\tilde{\alpha}, \end{cases}$$

where

$$\lambda_2 = \frac{\Sigma_c(\alpha_h)}{\hat{\mu}_c},$$

$$\gamma_0 = \frac{\partial S_c}{\partial\alpha}(\alpha_h, C_\infty) - \frac{\alpha_h\Sigma_c'(\alpha_h)}{\hat{\mu}_c} + \lambda_2\Big(\frac{\lambda_c}{\hat{\mu}_c} - 1\Big),$$

$$\gamma_1 = -\frac{\Sigma_c'(\alpha_h)}{\mu_c\kappa^2} - \frac{(\lambda_c+\mu_c)(-\Sigma_c(\alpha_h) - \alpha_h\Sigma_c'(\alpha_h) + \lambda_c\lambda_2)}{\mu_c\kappa^2\hat{\mu}_c\alpha_h},$$

$$\gamma_3 = -\frac{(-\Sigma_c(\alpha_h) - \alpha_h\Sigma_c'(\alpha_h) + \lambda_c\lambda_2)}{\hat{\mu}_c\alpha_h i\kappa}.$$

Notice that γ_0, λ_2, and therefore all the exponential decay rates specified for the outer solution, interestingly enough, do not depend on the wavelength κ of the perturbation in question.

8.2.2 *Comparison of Analytical vs. Numerical Outer Solution*

Motivation

Our objective here is to check these rescalings against numerical simulations of (79). Indeed, by simulating the system satisfied by the perturbations for time large enough, we hope to visualise decay that corresponds to the rescalings found analytically in the previous section. In other words, for ξ fixed away from the boundary layers, we hope to see as $t \to \infty$ that

$$\tilde{\alpha}(\xi, t) = O(e^{(\gamma_0 - \lambda_2)t}), \qquad \tilde{v}_c^1(\xi, t) = O(e^{(\gamma_0 - 2\lambda_2)t})$$

$$\tilde{v}_c^2(\xi, t) = O(e^{(\gamma_0 - \lambda_2)t}), \qquad \tilde{v}_w^1(\xi, t) = O(e^{\gamma_0 t}), \qquad \tilde{v}_w^2(\xi, t) = O(e^{(\gamma_0 - \lambda_2)t}).$$

For simulations in this chapter, we used the set of parameters in Case 1 defined in Chapter 3 with $\kappa = 1$, and obtained thus the following values for α_h, λ_2 and γ_0:

α_h	λ_2	γ_0
0.6071	0.0180	-2.4743

However, notice that

$$-2.5103 = \gamma_0 - 2\lambda_2 < \gamma_0 - \lambda_2 < \gamma_0 = -2.4743,$$

and particularly that the corresponding exponentials

$$e^{(\gamma_0 - \lambda_2)t}, \qquad e^{(\gamma_0 - 2\lambda_2)t}, \qquad e^{\gamma_0 t}$$

decay very quickly. Therefore, any computation involving terms with decay similar to such exponentials is deeply affected by machine inaccuracies for sufficiently large t. The time window on which our simulations are accurate is therefore limited by the machine precision.

Numerical Simulations - Comparison to Decay Obtained Analytically

From the discussion above, we expect to see a very fast exponential decay in numerical simulations of the system (79). Thus, results will not be observable for a large time period before the numerical scheme loses validity. Therefore, in order to improve the visualisation of the asymptotic behaviour found in this section, we will consider an initial condition based on the outer solution found analytically.

Indeed, we consider initial conditions obtained by choosing

$$\overline{\alpha}(\xi) = 100\xi^2(\xi-1)^2, \qquad \tilde{R}(0) = 1e-4, \qquad t = 0, \qquad \kappa = 1$$

in the expressions of the outer solution seen in (90), (91), (92), (93), (94).

Then, if we perform numerical simulations of the system (79) by using "*ode23t*," we obtain the following results for an array of $\xi \in [0.3, 0.6]$:

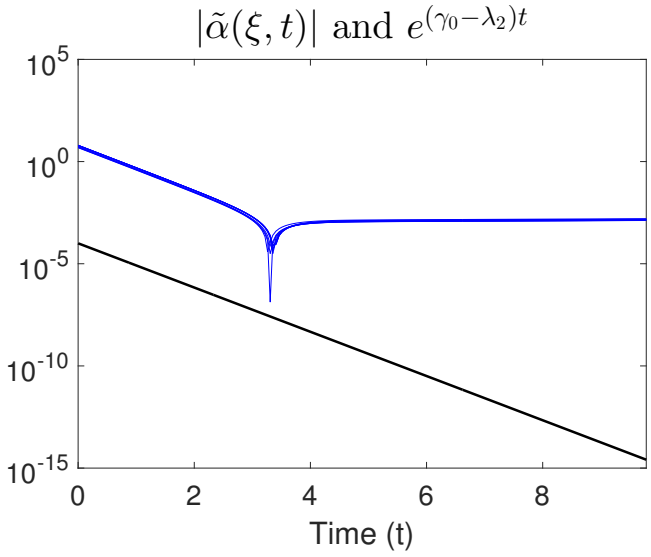


Figure 108.: Absolute value of the perturbation of the cell concentration $|\tilde{\alpha}(\xi,t)|$ for array of $\xi \in [0.3, 0.6]$ and a translation of an exponential that is indicative of the decay predicted by the analytical characterisation of the outer solution, namely $e^{(\gamma_0-\lambda_2)t}$.

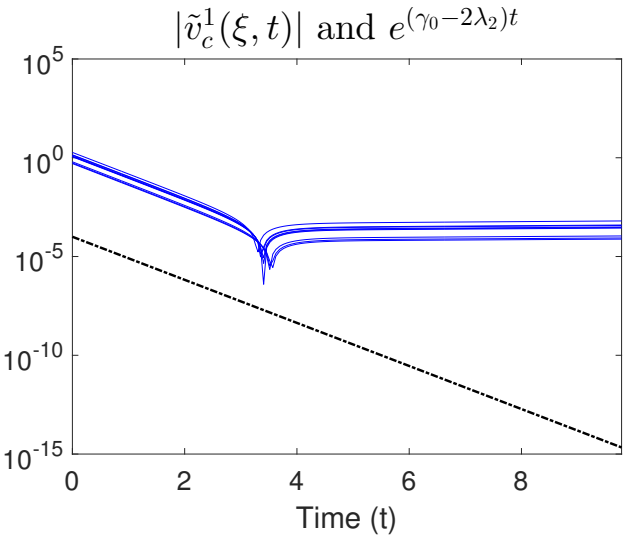


Figure 109.: Absolute value of the perturbation of the cell velocity in the x direction $|\tilde{v}_c^1(\xi,t)|$ for an array of $\xi \in [0.3, 0.6]$ and a translation of an exponential that is indicative of the decay predicted by the analytical characterisation of the outer solution, namely $e^{(\gamma_0-2\lambda_2)t}$.

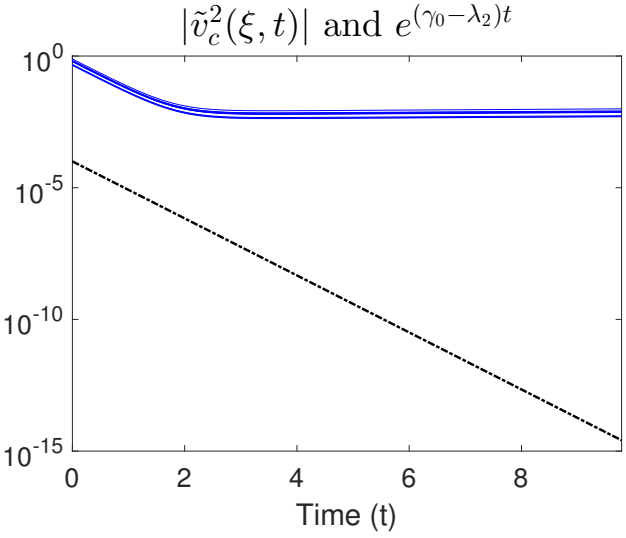


Figure 110.: Absolute value of the perturbation of the cell velocity in the y direction $|\tilde{v}_c^2(\xi,t)|$ for an array of $\xi \in [0.3, 0.6]$ and a translation of an exponential that is indicative of the decay predicted by the analytical characterisation of the outer solution, namely $e^{(\gamma_0-\lambda_2)t}$.

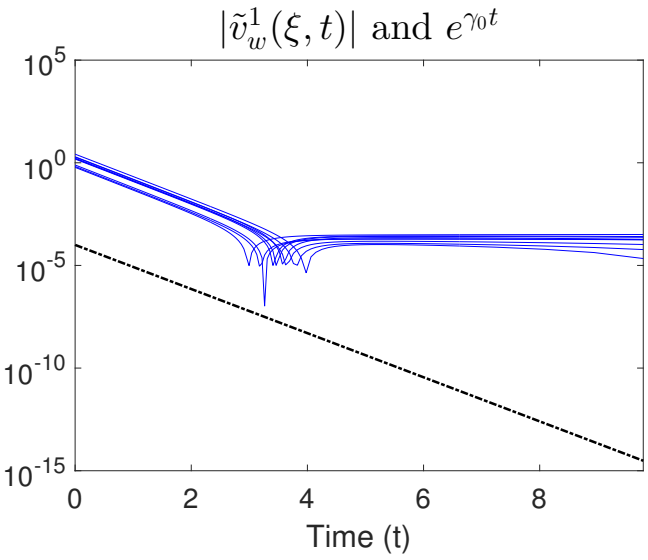


Figure 111.: Absolute value of the perturbation of the water velocity in the x direction $|\tilde{v}_w^1(\xi,t)|$ for an array of $\xi \in [0.3, 0.6]$ and a translation of an exponential that is indicative of the decay predicted by the analytical characterisation of the outer solution, namely $e^{\gamma_0 t}$.

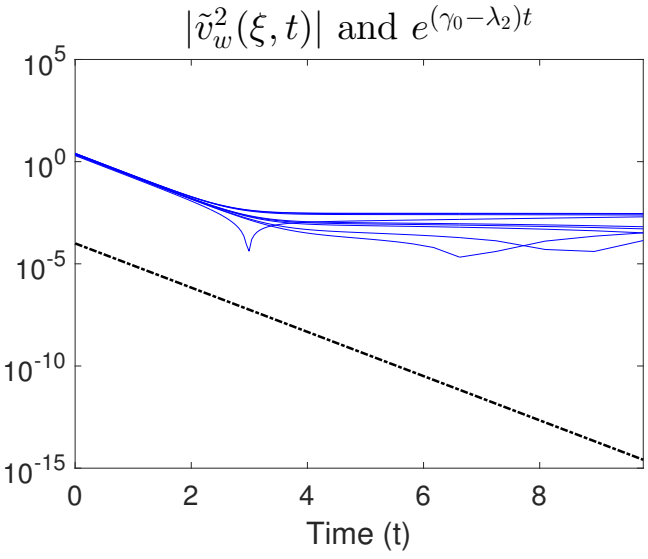


Figure 112.: Absolute value of the perturbation of the water velocity in the y direction $|\tilde{v}_w^2(\xi,t)|$ for an array of $\xi \in [0.3, 0.6]$ and a translation of an exponential that is indicative of the decay predicted by the analytical characterisation of the outer solution, namely $e^{(\gamma_0-\lambda_2)t}$.

In order to allow for comparison, in each graph above we have plotted a function that possesses the expected decay seen in our rescalings along with the numerical solution. Thus, we can see that there is reasonable agreement in the decays for a relatively small period of time.

Now, one might question if the agreements seen above are not driven by the initial condition chosen here. However, we can test that this is not the case by simulating the same problem with random initial conditions (of the same order of magnitude as above). In doing so, we obtained the following solutions:

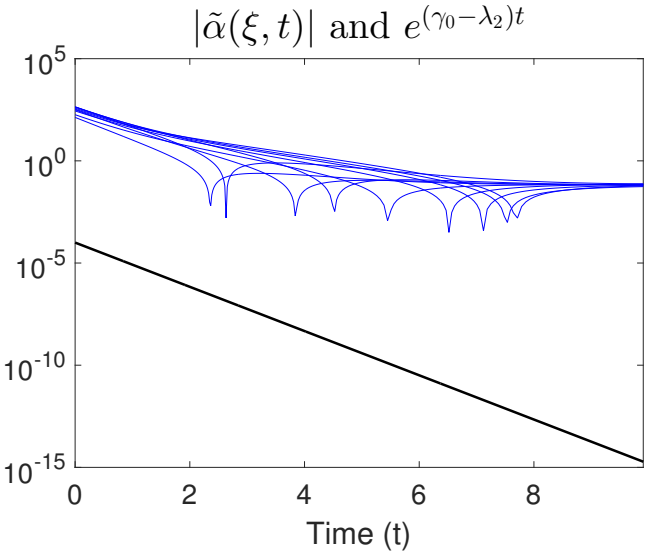


Figure 113.: Absolute value of the perturbation of the cell concentration $|\tilde{\alpha}(\xi,t)|$ calculated with random initial conditions and shown here for array of $\xi \in [0.3, 0.6]$ and a translation of an exponential that is indicative of the decay predicted by the analytical characterisation of the outer solution, namely $e^{(\gamma_0-\lambda_2)t}$.

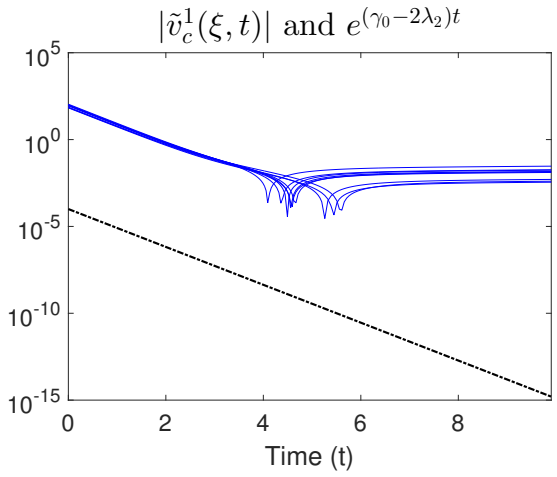


Figure 114.: Absolute value of the perturbation of the cell velocity in the x direction $|\tilde{v}_c^1(\xi,t)|$ calculated with random initial conditions and shown here for an array of $\xi \in [0.3, 0.6]$ and a translation of an exponential that is indicative of the decay predicted by the analytical characterisation of the outer solution, namely $e^{(\gamma_0-2\lambda_2)t}$.

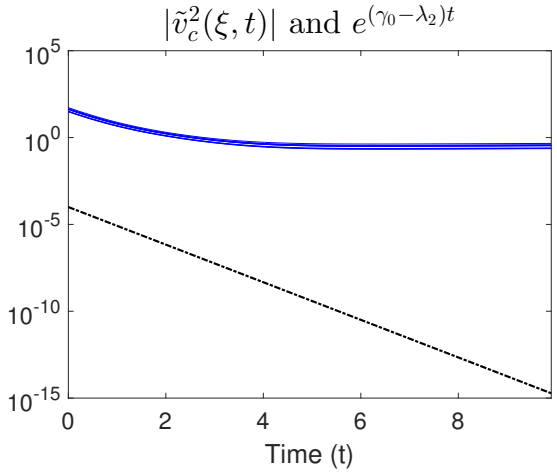


Figure 115.: Absolute value of the perturbation of the cell velocity in the y direction $|\tilde{v}_c^2(\xi,t)|$ calculated with random initial conditions and shown here for an array of $\xi \in [0.3, 0.6]$ and a translation of an exponential that is indicative of the decay predicted by the analytical characterisation of the outer solution, namely $e^{(\gamma_0-\lambda_2)t}$.

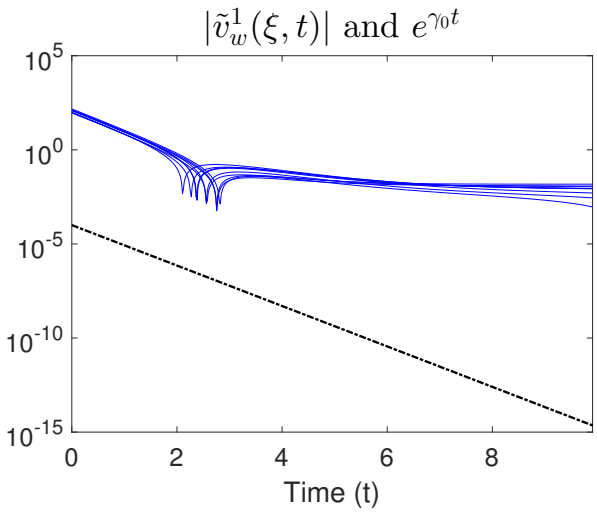


Figure 116.: Absolute value of the perturbation of the water velocity in the x direction $|\tilde{v}_w^1(\xi,t)|$ calculated with random initial conditions and shown here for an array of $\xi \in [0.3, 0.6]$ and a translation of an exponential that is indicative of the decay predicted by the analytical characterisation of the outer solution, namely $e^{\gamma_0 t}$.

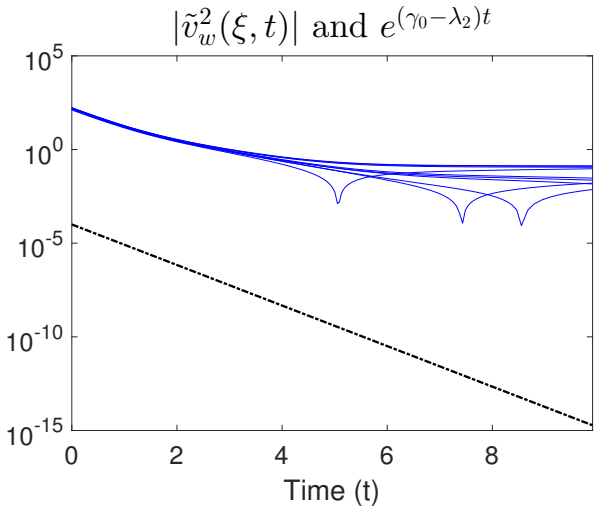


Figure 117.: Absolute value of the perturbation of the water velocity in the y direction $|\tilde{v}_w^2(\xi,t)|$ calculated with random initial conditions and shown here for an array of $\xi \in [0.3, 0.6]$ and a translation of an exponential that is indicative of the decay predicted by the analytical characterisation of the outer solution, namely $e^{(\gamma_0-\lambda_2)t}$.

Therefore, our numerics seems to confirm the analytical findings of the previous section, albeit for a relatively small period of time, which is restricted by the numerical computing capabilities of MATLAB®. The reason for this will be explored in more detail in Section 8.5.

Finding the Boundary Layers

Now, in order to find the location of possible boundary layers, we must be able to find if there are any regions where rapid change may be observed. For that, we tested different time frames of our solution and discovered the following behaviour in $\tilde{\alpha}$:

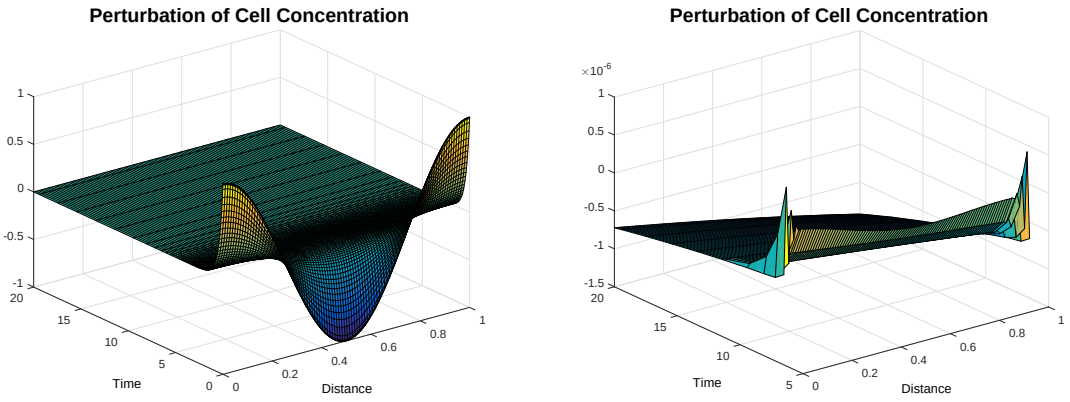


Figure 118.: Perturbation of the cell concentration $\tilde{\alpha}(\xi, t)$ for $t \in [0, 20]$ (on the left) and $t \in [5, 20]$ (on the right) showing rapid change near inner and outer boundaries $\xi = 0$ and $\xi = 1$, indicating the position of boundary layers.

The graph on the right represents the same data as the figure on the left, except that the figure on the right shows the behaviour for $\tilde{\alpha}$ for $t > 5$ rather than $t > 0$, as seen on the left. If we focus our attention on the graph on the right, we see that there are regions of rapid change near $\xi = 0$ and $\xi = 1$. This, in turn, suggests that there is a boundary layer near each of these boundaries.

8.3 INNER SOLUTION NEAR OUTER BOUNDARY

8.3.1 *Analytical Characterisation of Inner Solution near Outer Boundary $\xi = 1$*

Recall that, in the previous section, we have seen numerical results that suggest that there might be boundary layers near boundaries at $\xi = 0$ and $\xi = 1$, which we will call the inner and outer boundary, respectively. Having said that, in this section, we will analytically characterise an inner solution near the outer boundary. Indeed, by considering all possible asymptotic balances for our equations near $\xi = 1$, we obtain four possible non-trivial balances, which may be narrowed down to only one possibility that is non-trivial and allows for matching to be performed between the outer solution and the inner solution.

For this, consider the following change of variable

$$\xi = 1 - \frac{X}{R_*(t)^\beta}, \qquad \beta > 0, \qquad X = O(1) \quad \text{as} \quad t \to \infty.$$

This will allow us to focus within the boundary layer, a thin strip near the outer boundary $\xi = 1$. By the product rule, we then have

$$\begin{aligned}
\frac{\partial}{\partial t} &\longrightarrow \frac{\partial}{\partial t} + \beta\lambda_2 X \frac{\partial}{\partial X} \\
\frac{\partial}{\partial \xi} &\longrightarrow -R_*(t)^\beta \frac{\partial}{\partial X} \\
\frac{\partial^2}{\partial \xi^2} &\longrightarrow R_*(t)^{2\beta} \frac{\partial^2}{\partial X^2}.
\end{aligned}$$

Recall also that the outer solutions all had a common coefficient: $e^{\gamma_0 t}$. Thus, to facilitate matching between the outer and inner solutions, we will choose to assume that our inner solution is of the form

$$\tilde{\alpha}(X,t) = e^{\gamma_0 t}\overline{\alpha}(X,t), \quad \tilde{v}_c^1(X,t) = e^{\gamma_0 t}\overline{v}_c^1(X,t), \quad \tilde{v}_c^2(X,t) = e^{\gamma_0 t}\overline{v}_c^2(X,t),$$

$$\tilde{v}_w^1(X,t) = e^{\gamma_0 t}\overline{v}_w^1(X,t), \quad \tilde{v}_w^2(X,t) = e^{\gamma_0 t}\overline{v}_w^2(X,t).$$

Therefore, applying this rescaling and the variable change $(\xi, t) \to (X, t)$, we obtain the system with which we will work in this section:

$$\begin{cases} \dfrac{\partial \overline{\alpha}}{\partial t} = \Big[\dfrac{\partial S_c}{\partial \alpha}(\alpha_h, C_\infty) - \gamma_0 - \lambda_2\Big(1 + \beta X \dfrac{\partial}{\partial X}\Big)\Big]\overline{\alpha} + \alpha_h R_*^{\beta-1}\dfrac{\partial \overline{v}_c^1}{\partial X} - \alpha_h i\kappa \overline{v}_c^2 & (95) \\ 0 = \Sigma_c'(\alpha_h)\dfrac{\partial \overline{\alpha}}{\partial X} + \hat{\mu}_c R_*^{\beta-1}\dfrac{\partial^2 \overline{v}_c^1}{\partial X^2} - (\lambda_c + \mu_c) i\kappa \dfrac{\partial \overline{v}_c^2}{\partial X} - \dfrac{1}{R_*^{\beta-1}}\mu_c \kappa^2 \overline{v}_c^1 & (96) \\ 0 = \Big(-\Sigma_c(\alpha_h) - \alpha_h \Sigma_c'(\alpha_h) + \lambda_c \lambda_2\Big) i\kappa \overline{\alpha} \\ \quad + \mu_c \alpha_h R_*^{2\beta-2}\dfrac{\partial^2 \overline{v}_c^2}{\partial X^2} - (\mu_c + \lambda_c)\alpha_h i\kappa R_*^{\beta-1}\dfrac{\partial \overline{v}_c^1}{\partial X} - \alpha_h \kappa^2 \hat{\mu}_c \overline{v}_c^2 & (97) \\ 0 = \dfrac{\lambda_2}{1-\alpha_h}\Big[1 - (R_*^\beta - X)\dfrac{\partial}{\partial X}\Big]\overline{\alpha} - R_*^{\beta-1}\Big[\alpha_h \dfrac{\partial \overline{v}_c^1}{\partial X} + (1-\alpha_h)\dfrac{\partial \overline{v}_w^1}{\partial X}\Big] \\ \quad + \alpha_h i\kappa \overline{v}_c^2 + (1-\alpha_h) i\kappa \overline{v}_w^2 & (98) \\ 0 = \dfrac{i\kappa\lambda_2}{1-\alpha_h}(R_*^\beta - X)\overline{\alpha} - \alpha_h R_*^{2\beta-2}\dfrac{\partial}{\partial X}(\overline{v}_w^2 - \overline{v}_c^2) \\ \quad - i\kappa\alpha_h R_*^{\beta-1}(\overline{v}_w^1 - \overline{v}_c^1), & (99) \end{cases}$$

with boundary conditions at $X = 0$:

$$\begin{cases} 0 = -\Sigma_c'(\alpha_h)\overline{\alpha} - \hat{\mu}_c R_*^{\beta-1}\dfrac{\partial \overline{v}_c^1}{\partial X} + \lambda_c i\kappa \overline{v}_c^2, \\ \dfrac{\partial \overline{v}_c^1}{\partial t} - \dfrac{R_*^{\beta-1}}{i\kappa}\dfrac{\partial^2 \overline{v}_c^2}{\partial t \partial X} = -\dfrac{(\lambda_2(2-\beta) - \gamma_0)}{i\kappa} R_*^{\beta-1}\dfrac{\partial \overline{v}_c^2}{\partial X} - (\lambda_2 + \gamma_0)\overline{v}_c^1, \\ \overline{v}_w^2 = \dfrac{R_*}{2(1-\alpha_h)}\Big(R_*^{\beta-1}\dfrac{\partial \overline{v}_c^2}{\partial X} - i\kappa \overline{v}_c^1\Big) + \overline{v}_c^2, \end{cases}$$

and

$$\frac{d\tilde{R}}{dt}(t) = \lambda_2 \tilde{R}(t) + e^{\gamma_0 t}\overline{v}_c^1(0, t).$$

In the same way as before, we assume now that

$$\overline{\alpha}(X,t) = e^{a_0 t}A(X), \quad \overline{v}_c^1(X,t) = e^{a_1 t}V_c^1(X), \quad \overline{v}_c^2(X,t) = e^{a_2 t}V_c^2(X),$$

$$\overline{v}_w^1(X,t) = e^{b_1 t}V_w^1(X), \quad \overline{v}_w^2(X,t) = e^{b_2 t}V_w^2(X).$$

By substituting these into the system above and exploring the exponential pre-factors of each of its terms and their behaviour when $t \to \infty$, it is possible to prove through a case-by-case logic (similar to the one used before) that the only possible non-trivial asymptotic balances happen when:

Possible Non-trivial Asymptotic Balances for Inner Solution on Outer Boundary:

Case 1: $\beta > 1$ and $a_1 - a_0 + \lambda_2(\beta - 1) = 0, \quad a_2 - a_0 + 2\lambda_2(\beta - 1) = 0,$ $b_1 - a_0 - \lambda_2 = 0, b_2 - a_0 + \lambda_2(\beta - 2) = 0.$

Case 2: $\beta < 1$ and $a_1 - a_0 - \lambda_2(\beta - 1) = 0, \quad a_2 - a_0 = 0,$ $b_1 - a_0 - \lambda_2 = 0, \quad b_2 - a_0 - \lambda_2\beta = 0.$

Case 3: $\beta = 1$ and $a_0 = a_1 = a_2, \quad b_1 - a_0 - \lambda_2 = b_2 - a_0 - \lambda_2 > 0.$

Case 4: $\beta = 1$ and $a_0 = a_1 = a_2, \quad b_1 - a_0 - \lambda_2 = b_2 - a_0 - \lambda_2 = 0.$

I will describe the overall reasoning used to obtain these four cases. As we did in the derivation of the outer solution, we will split our problem into two parts, one regarding $\{A, V_c^1, V_c^2\}$ and then one regarding $\{V_w^1, V_w^2\}$. The perturbation $\tilde{R}$ will be treated separately on page 195.

Consider, initially, equation (95). After applying all the substitutions described above, we obtain

$$0 = \Big[\frac{\partial S_c}{\partial \alpha}(\alpha_h, C_\infty) - \gamma_0 - a_0 - \lambda_2\Big(1 + \beta X \frac{\partial}{\partial X}\Big)\Big] A + \alpha_h R_0^{\beta-1} e^{(a_1 - a_0 + \lambda_2(\beta-1))t} \frac{dV_c^1}{dX} - \alpha_h i\kappa e^{(a_2 - a_0)t} V_c^2. \tag{100}$$

We can enumerate the four cases that cause this equation to have a non-trivial asymptotic balance when $t \to \infty$ just as we did in the previous section by investigating the possible signs of

$$a_1 - a_0 + \lambda_2(\beta - 1), \qquad a_2 - a_0, \qquad a_1 - a_2 + \lambda_2(\beta - 1).$$

Now, if we apply the same substitutions that we described above to equations (96) and (97), we see that each of these equations has two terms that refer to V_c^1 and V_c^2, respectively, namely

$$\Big\{\frac{d^2 V_c^1}{dX^2}, V_c^1\Big\} \qquad \text{in equation} \qquad (96)$$

and

$$\Big\{\frac{d^2 V_c^2}{dX^2}, V_c^2\Big\} \qquad \text{in equation} \qquad (97).$$

Furthermore, these terms will have the following pre-factors:

Equation (96)

Term	**Pre-factor**
$\frac{d^2V_c^1}{dX^2}$	$e^{[a_1-a_0+\lambda_2(\beta-1)]t}$
V_c^1	$e^{[a_1-a_0-\lambda_2(\beta-1)]t}$

Equation (97)

Term	**Pre-factor**
$\frac{d^2V_c^2}{dX^2}$	$e^{[a_2-a_0+2\lambda_2(\beta-1)]t}$
V_c^2	$e^{(a_2-a_0)t}$

Now, to be able to work on a case-by-case basis we must know the relationship between these exponential pre-factors, i.e which one grows (or decays) slower (or faster). In other words, we must know the sign of

$$[a_1 - a_0 + \lambda_2(\beta - 1)] - [a_1 - a_0 - \lambda_2(\beta - 1)] = 2\lambda_2(\beta - 1),$$

from Equation (96) and the table on the left and

$$[a_2 - a_0 + 2\lambda_2(\beta - 1)] - (a_2 - a_0) = 2\lambda_2(\beta - 1),$$

from Equation (97) and the table on the right. Since these depend directly on the sign of $\beta - 1$, we were forced to separate our analysis into three cases, namely $\beta > 1$, $\beta < 1$, and $\beta = 1$. Within each of these cases, we investigated the four possible non-trivial balances of Equation (100) and proved that there is only one non-trivial possibility for $\{A, V_c^1, V_c^2\}$ in each of these cases, and they correspond to:

(This will yield Case 1:) $\beta > 1$ and $a_1 - a_0 + \lambda_2(\beta - 1) = 0$, $a_2 - a_0 + 2\lambda_2(\beta - 1) = 0$

(This will yield Case 2:) $\beta < 1$ and $a_1 - a_0 - \lambda_2(\beta - 1) = 0$, $a_2 - a_0 = 0$

(This will yield Cases 3 and 4:) $\beta = 1$ and $a_0 = a_1 = a_2$.

Once these were obtained, $\{b_1, b_2\}$ were found by substituting the ansatz on page 176 into Equations (98) and (99) and using the same reasoning employed above to find the possible non-trivial asymptotic balances for these two equations. This provides one possibility for each of the cases

$\beta > 1$ and $\beta < 1$ and two possibilities for the case $\beta = 1$. This is how we characterised Cases 1 through 4.

Having motivated the origin of these cases, we will now consider each one of them separately. For each case, we will state the associated asymptotic balances and attempt to perform matching between inner and outer solutions by matching a rescaling of the inner solution

$$\overline{\alpha}(X,t) = e^{a_0 t}A(X), \quad \overline{v}_c^1(X,t) = e^{a_1 t}V_c^1(X), \quad \overline{v}_c^2(X,t) = e^{a_2 t}V_c^2(X),$$

$$\overline{v}_w^1(X,t) = e^{b_1 t}V_w^1(X), \quad \overline{v}_w^2(X,t) = e^{b_2 t}V_w^2(X)$$

when $X \to \infty$ to the appropriate rescaling of the outer solution

$$e^{-\gamma_0 t}\tilde{\alpha}(\xi,t) = e^{-\lambda_2 t}\overline{\alpha}(\xi), \qquad e^{-\gamma_0 t}\tilde{v}_c^1(\xi,t) = \frac{\gamma_1}{R_0}e^{-2\lambda_2 t}\frac{d\overline{\alpha}}{d\xi}(\xi),$$

$$e^{-\gamma_0 t}\tilde{v}_c^2(\xi,t) = \gamma_3 e^{-\lambda_2 t}\overline{\alpha}(\xi), \qquad e^{-\gamma_0 t}\tilde{v}_w^1(\xi,t) = \frac{\lambda_2 R_0}{\alpha_h(1-\alpha_h)}\xi\overline{\alpha}(\xi),$$

$$e^{-\gamma_0 t}\tilde{v}_w^2(\xi,t) = -e^{-\lambda_2 t}\left[\frac{\lambda_2}{i\kappa\alpha_h(1-\alpha_h)^2}\left(1+\xi\frac{d}{d\xi}\right)\overline{\alpha}(\xi) + \frac{\alpha_h\gamma_3}{1-\alpha_h}\overline{\alpha}(\xi)\right],$$

when $\xi \to 1$.

Case 1: $\beta > 1$

Consider initially Case 1. Here, $\beta > 1$ and

$$a_1 - a_0 + \lambda_2(\beta - 1) = 0, \qquad a_2 - a_0 + 2\lambda_2(\beta - 1) = 0,$$
$$b_1 - a_0 - \lambda_2 = 0, \qquad b_2 - a_0 + \lambda_2(\beta - 2) = 0.$$

The asymptotic balance obtained in this case is given by:

$$\begin{cases} 0 &= \Big[\frac{\partial S_c}{\partial \alpha}(\alpha_h, C_\infty) - a_0 - \gamma_0 - \lambda_2\Big(1 + \beta X \frac{d}{dX}\Big)\Big] A + \alpha_h R_0^{\beta-1} \frac{dV_c^1}{dX} \\ 0 &= \Sigma_c'(\alpha_h)\frac{dA}{dX} + \hat{\mu}_c R_0^{\beta-1}\frac{d^2V_c^1}{dX^2} \\ 0 &= \Big(- \Sigma_c(\alpha_h) - \alpha_h\Sigma_c'(\alpha_h) + \lambda_c\lambda_2\Big) i\kappa A + \mu_c\alpha_h R_0^{2\beta-2}\frac{d^2V_c^2}{dX^2} \\ & \quad -(\mu_c + \lambda_c)\alpha_h i\kappa R_0^{\beta-1}\frac{dV_c^1}{dX} \\ 0 &= \frac{\lambda_2}{(1-\alpha_h)^2}\frac{dA}{dX} + \frac{1}{R_0}\frac{dV_w^1}{dX} \\ 0 &= -R_0^{\beta-1}\frac{dV_w^2}{\partial X} - i\kappa V_w^1 + \frac{i\kappa\lambda_2 R_0}{\alpha_h(1-\alpha_h)}A, \end{cases}$$

with conditions at $X = 0$:

$$\begin{cases} 0 &= \Sigma_c'(\alpha_h)A + \hat{\mu}_c R_0^{\beta-1}\frac{dV_c^1}{dX}, \\ 0 &= \frac{(\lambda_2(2-\beta) - \gamma_0 - a_2)}{i\kappa} R_0^{\beta-1}\frac{dV_c^2}{dX} + (\lambda_2 + \gamma_0 + a_1)V_c^1, \\ V_w^2 &= \frac{R_0}{2(1-\alpha_h)}\Big(R_0^{\beta-1}\frac{dV_c^2}{dX} - i\kappa V_c^1\Big). \end{cases}$$

By integration, using the first boundary condition and the first two equations above we may solve for $A(X)$ to obtain:

$$A(X) = C_1 X^{-\frac{(\frac{\lambda_2\lambda_c}{\hat{\mu}} + a_0)}{\lambda_2\beta}}.$$

Using this expression, we must match

$$e^{a_0 t}A(X) \text{ when } X \to \infty \qquad \text{to} \qquad e^{-\lambda_2 t}\overline{\alpha}(\xi) \text{ when } \xi \to 1.$$

However, using the relationship between X and ξ, i.e. $X = R_*(t)^\beta(1-\xi)$, we see that

$$e^{a_0 t}A(X) \sim C_1[R_0^\beta(1-\xi)]^{-\frac{(\frac{\lambda_2\lambda_c}{\hat{\mu}} + a_0)}{\lambda_2\beta}} e^{-\frac{\lambda_2\lambda_c}{\hat{\mu}_c}t}, \qquad X \to \infty, \quad \xi \to 1$$

which makes a non-trivial matching impossible since $\hat{\mu}_c = 2\mu_c + \lambda_c > \lambda_c$ and thus $-\dfrac{\lambda_2\lambda_c}{\hat{\mu}_c} > -\lambda_2$.

Case 2: $\beta < 1$

Here, $\beta < 1$ and

$$\begin{aligned} a_1 - a_0 - \lambda_2(\beta - 1) = 0, \qquad a_2 - a_0 = 0, \\ b_1 - a_0 - \lambda_2 = 0, \qquad b_2 - a_0 - \lambda_2\beta = 0. \end{aligned}$$

The asymptotic balance is given by:

$$\begin{cases} 0 &= \Big[\dfrac{\partial S_c}{\partial \alpha}(\alpha_h, C_\infty) - a_0 - \gamma_0 - \lambda_2\Big(1 + \beta X \dfrac{d}{dX}\Big)\Big] A - \alpha_h i\kappa V_c^2 \\ 0 &= \Sigma_c'(\alpha_h)\dfrac{dA}{dX} - (\lambda_c + \mu_c) i\kappa \dfrac{dV_c^2}{dX} - \dfrac{1}{R_0^{\beta-1}}\mu_c\kappa^2 V_c^1 \\ 0 &= \Big(- \Sigma_c(\alpha_h) - \alpha_h\Sigma_c'(\alpha_h) + \lambda_c\lambda_2\Big) i\kappa A - \alpha_h\kappa^2\hat{\mu}_c V_c^2 \\ 0 &= -\dfrac{\lambda_2}{(1-\alpha_h)^2} R_0^\beta \dfrac{dA}{dX} - R_0^{\beta-1}\dfrac{dV_w^1}{dX} + i\kappa V_w^2 \\ 0 &= -\dfrac{1}{R_0} V_w^1 + \dfrac{\lambda_2}{\alpha_h(1-\alpha_h)} A, \end{cases}$$

with conditions at $X = 0$:

$$\begin{cases} 0 &= -\Sigma_c'(\alpha_h) A + \lambda_c i\kappa V_c^2, \\ 0 &= \dfrac{(\lambda_2(2-\beta) - \gamma_0 - a_2)}{i\kappa} R_0^{\beta-1}\dfrac{dV_c^2}{dX} + (\lambda_2 + \gamma_0 + a_1) V_c^1 \\ V_w^2 &= \dfrac{R_0}{2(1-\alpha_h)}\Big(R_0^{\beta-1}\dfrac{dV_c^2}{dX} - i\kappa V_c^1\Big). \end{cases}$$

We can discard this case because it has already been studied as it corresponds to the outer solution asymptotic balance which has been characterised in the previous section.

Case 3: $\beta = 1$ and $b_1 - a_0 - \lambda_2 = b_2 - a_0 - \lambda_2 > 0$

Here, $\beta = 1$, and

$$a_0 = a_1 = a_2, \qquad b_1 - a_0 - \lambda_2 = b_2 - a_0 - \lambda_2 > 0.$$

The asymptotic balance is given by:

$$\begin{cases} 0 &= \Big[\frac{\partial S_c}{\partial \alpha}(\alpha_h, C_\infty) - \gamma_0 - a_0 - \lambda_2\Big(1 + X\frac{d}{dX}\Big)\Big]A + \alpha_h \frac{dV_c^1}{dX} - \alpha_h i\kappa V_c^2 \\ 0 &= \Sigma_c'(\alpha_h)\frac{dA}{dX} + \hat{\mu}_c \frac{d^2V_c^1}{dX^2} - (\lambda_c + \mu_c)i\kappa \frac{dV_c^2}{dX} - \mu_c \kappa^2 V_c^1 \\ 0 &= \Big(-\Sigma_c(\alpha_h) - \alpha_h \Sigma_c'(\alpha_h) + \lambda_c\lambda_2\Big)i\kappa A + \mu_c \alpha_h \frac{d^2V_c^2}{dX^2} \\ & \quad -(\mu_c + \lambda_c)\alpha_h i\kappa \frac{dV_c^1}{dX} - \alpha_h \kappa^2 \hat{\mu}_c V_c^2 \\ 0 &= -\frac{dV_w^1}{dX} + i\kappa V_w^2 \\ 0 &= -\frac{dV_w^2}{dX} - i\kappa V_w^1, \end{cases}$$

with conditions at $X = 0$:

$$\begin{cases} 0 &= -\Sigma_c'(\alpha_h)A - \hat{\mu}_c \frac{dV_c^1}{dX} + \lambda_c i\kappa V_c^2, \\ 0 &= \frac{(\lambda_2 - \gamma_0 - a_0)}{i\kappa}\frac{dV_c^2}{dX} + (\lambda_2 + \gamma_0 + a_0)V_c^1 \\ V_w^2 &= e^{(a_0 - b_2)t}V_c^2 + \frac{R_0 e^{(a_0 - b_2 + \lambda_2)t}}{2(1 - \alpha_h)}\Big[\frac{dV_c^2}{dX} - i\kappa V_c^1\Big]. \end{cases}$$

If we solve the last two equations of the system above for $V_w^1(X)$ and $V_w^2(X)$, we obtain

$$V_w^1(X) = C_1 e^{\kappa X} + C_2 e^{-\kappa X}, \qquad V_w^2(X) = i(C_2 e^{-\kappa X} - C_1 e^{\kappa X}).$$

However, for matching to be possible when $X \to \infty$, we must have $C_1 = 0$ and

$$e^{b_1 t}V_w^1(X) \to 0, \qquad e^{b_2 t}V_w^2(X) \to 0, \qquad \text{when} \qquad X \to +\infty.$$

From the corresponding outer solutions, we see that this implies that $b_1 = 0$ and $b_2 = -\lambda_2$, which contradicts $b_1 = a_0 + \lambda_2 = b_2$.

Case 4: $\beta = 1$ *and* $b_1 - a_0 - \lambda_2 = b_2 - a_0 - \lambda_2 = 0$

Therefore, the non-trivial case for which we search is Case 4, i.e. $\beta = 1$ and

$$a_0 = a_1 = a_2, \qquad b_1 - a_0 - \lambda_2 = b_2 - a_0 - \lambda_2 = 0,$$

where the asymptotic balance is given by

$$\begin{cases} 0 = \Big[\dfrac{\partial S_c}{\partial \alpha}(\alpha_h, C_\infty) - \gamma_0 - a_0 - \lambda_2\Big(1 + X\dfrac{d}{dX}\Big)\Big]A + \alpha_h \dfrac{dV_c^1}{dX} - \alpha_h i\kappa V_c^2 & (101) \\ 0 = \Sigma_c'(\alpha_h)\dfrac{dA}{dX} + \hat{\mu}_c \dfrac{d^2V_c^1}{dX^2} - (\lambda_c + \mu_c)i\kappa \dfrac{dV_c^2}{dX} - \mu_c \kappa^2 V_c^1 & (102) \\ 0 = \Big(- \Sigma_c(\alpha_h) - \alpha_h \Sigma_c'(\alpha_h) + \lambda_c\lambda_2\Big)i\kappa A + \mu_c \alpha_h \dfrac{d^2V_c^2}{dX^2} \\ \quad - (\mu_c + \lambda_c)\alpha_h i\kappa \dfrac{dV_c^1}{dX} - \alpha_h \kappa^2 \hat{\mu}_c V_c^2 & (103) \\ 0 = -\dfrac{\lambda_2 R_0}{(1-\alpha_h)^2}\dfrac{dA}{dX} - \dfrac{dV_w^1}{dX} + i\kappa V_w^2 & (104) \\ 0 = -\dfrac{dV_w^2}{dX} - i\kappa V_w^1 + \dfrac{i\kappa\lambda_2 R_0}{\alpha_h(1-\alpha_h)}A, & (105) \end{cases}$$

with conditions at $X = 0$:

$$\begin{cases} 0 &= -\Sigma_c'(\alpha_h)A - \hat{\mu}_c \dfrac{dV_c^1}{dX} + \lambda_c i\kappa V_c^2, \\ 0 &= \dfrac{(\lambda_2 - \gamma_0 - a_0)}{i\kappa}\dfrac{dV_c^2}{dX} + (\lambda_2 + \gamma_0 + a_0)V_c^1 \\ V_w^2 &= \dfrac{R_0}{2(1-\alpha_h)}\Big[\dfrac{dV_c^2}{dX} - i\kappa V_c^1\Big]. \end{cases}$$

Consider initially the first three equations (101)-(103) and the corresponding set $\{A, V_c^1, V_c^2\}$. Notice that the asymptotic balance of these equations preserves all the terms in the original system. Therefore, it is no surprise that we cannot solve this system by using basic ordinary differential equation methods as we have done in previous cases. However, we can begin to tackle equations (101)-(103) by defining $\{F_1, F_2\}$ as

$$F_1 = \frac{dV_c^1}{dX} - i\kappa V_c^2, \qquad F_2 = \frac{dV_c^2}{dX} + i\kappa V_c^1.$$

By substituting these into (101) and (102), we can find expressions for $\{F_1, F_2\}$ in terms of A which we can then substitute into (103) to obtain a third order ordinary differential equation for A:

$$0 = \lambda_2 X \frac{d^3A}{dX^3} + \Big[a_0 + \lambda_2\big(\frac{\lambda_c}{\hat{\mu}_c} + 2\big)\Big]\frac{d^2A}{dX^2} - \lambda_2\kappa^2 X\frac{dA}{dX} - \kappa^2(a_0 + \lambda_2)A. \quad (106)$$

Then, through some algebraic manipulations, the expressions for $\{F_1, F_2\}$ in terms of A allow us to recover $\{V_c^1, V_c^2\}$ by solving:

$$\begin{cases} \dfrac{d^2V_c^1}{dX^2} - \kappa^2 V_c^1 & = H_1 \\ V_c^2 - \dfrac{1}{i\kappa}\dfrac{dV_c^1}{dX} & = H_2, \end{cases} \quad (107)$$

where H_1 and H_2 depend only on A:

$$H_1 = \frac{\mu_c + \lambda_c}{\mu_c\alpha_h}\left[\Big(\frac{\partial S_c}{\partial\alpha}(\alpha_h, C_\infty) - \gamma_0 - a_0 - 2\lambda_2 - \frac{\alpha_h\Sigma_c'(\alpha_h)}{\mu_c + \lambda_c}\Big)\frac{dA}{dX} - \lambda_2 X\frac{d^2A}{dX^2}\right]$$

$$H_2 = \frac{1}{\alpha_h i\kappa}\Big(\frac{\partial S_c}{\partial\alpha}(\alpha_h, C_\infty) - \gamma_0 - a_0 - \lambda_2\Big)A - \frac{\lambda_2}{\alpha_h i\kappa}X\frac{dA}{dX}.$$

However, this whole simplification process relies on solving A from a third order ordinary differential equation, namely (106), which cannot be easily solved analytically. Therefore, we will approach the problem differently and find the asymptotic behaviour of $\{A, V_c^1, V_c^2\}$ when $X \to \infty$ in order to be able to perform matching between the outer and inner solutions to obtain a value for a_0 and consequently for $\{a_1, a_2, b_1, b_2\}$.

For this, consider $\hat{X} = \epsilon X$. Thus, equations (106) and (107) above may be found to be, at first order:

$$0 = \lambda_2\hat{X}\frac{dA}{d\hat{X}}(\hat{X}) + (a_0 + \lambda_2)A(\hat{X}), \quad V_c^1(\hat{X}) = 0,$$

$$V_c^2(\hat{X}) = \frac{1}{\alpha_h i\kappa}\Big[\frac{\partial S_c}{\partial\alpha}(\alpha_h, C_\infty) - \gamma_0 + \lambda_2\Big(1 - \hat{X}\frac{d}{d\hat{X}}\Big)\Big]A(\hat{X}).$$

Through traditional ordinary differential equation methods, these can be solved to find that

$$A(\hat{X}) = C_1\hat{X}^{-\frac{a_0+\lambda_2}{\lambda_2}}, \qquad V_c^1(\hat{X}) = 0, \qquad V_c^2(\hat{X}) = \gamma_3 C_1\hat{X}^{-\frac{a_0+\lambda_2}{\lambda_2}}.$$

Thus, as $X \to +\infty$,

$$A(X) \sim C_1 X^{-\frac{a_0+\lambda_2}{\lambda_2}}, \qquad V_c^1(X) \to 0, \qquad V_c^2(X) \sim \gamma_3 C_1 X^{-\frac{a_0+\lambda_2}{\lambda_2}}.$$

Now, by using this asymptotic behaviour and recasting it in terms of (ξ, t) using $X = (1-\xi)R_*(t)$, we see that as $X \to +\infty$,

$$\begin{aligned} e^{a_0 t} A(X) &\sim e^{a_0 t} C_1 X^{-\frac{a_0+\lambda_2}{\lambda_2}} = C_1 [R_0(1-\xi)]^{-\frac{a_0+\lambda_2}{\lambda_2}} e^{-\lambda_2 t}, \\ e^{a_0 t} V_c^1(X) &\to 0, \\ e^{a_0 t} V_c^2(X) &\sim e^{a_0 t} C_1 \gamma_3 X^{-\frac{a_0+\lambda_2}{\lambda_2}} = \gamma_3 C_1 [R_0(1-\xi)]^{-\frac{a_0+\lambda_2}{\lambda_2}} e^{-\lambda_2 t}. \end{aligned}$$

By matching these to the outer solutions, we see that $a_0 = -2\lambda_2$ and

$$\overline{\alpha}(\xi) \sim C_1 R_0 (1-\xi), \qquad \text{and} \qquad \frac{d\overline{\alpha}}{d\xi}(\xi) \to 0$$

when $\xi \to 1$. Furthermore, from the specifications of Case 4, we see that

$$a_0 = a_1 = a_2 = -2\lambda_2, \qquad b_1 = b_2 = a_0 + \lambda_2 = -\lambda_2,$$

and thus we have characterised the decay rates of the inner solution near the outer boundary.

If we apply the same process used above for $\{A, V_c^1, V_c^2\}$ now to $\{V_w^1, V_w^2\}$, we see that equations (104) and (105) imply that, at first order,

$$V_w^1(X) \sim \frac{\lambda_2 R_0}{\alpha_h(1-\alpha_h)} C_1 X \qquad \text{and} \qquad V_w^2(X) \to 0,$$

when $X \to \infty$ and matching can be performed due to values of b_1 and b_2 and the conditions previously imposed on $\overline{\alpha}(\xi)$, namely

$$\overline{\alpha}(\xi) \sim C_1 R_0 (1-\xi), \qquad \text{and} \qquad \frac{d\overline{\alpha}}{d\xi}(\xi) \to 0,$$

when $\xi \to 1$.

Now, notice that the two conditions above together imply that $C_1 = 0$ (via L'Hopital's Rule) and therefore that the asymptotic behaviour obtained here

when $X \to \infty$ is actually trivial. In order to remedy this, we must revisit equation (106), now with $a_0 = -2\lambda_2$, namely

$$0 = X\frac{d^3A}{dX^3} + \frac{\lambda_c}{\hat{\mu}_c}\frac{d^2A}{dX^2} - \kappa^2 X\frac{dA}{dX} + \kappa^2 A.$$

Notice that this is a third order ordinary differential equation, so we expect three linearly independent solutions and not just one, as we obtained previously with the first order approximation. Therefore, we will extract the other two solutions by applying a WKBJ expansion to $A(X)$.

Initially, consider $\hat{X} = \epsilon X$. Then, the equation above becomes:

$$0 = \epsilon^2\Big(\hat{X}\frac{d^3A}{d\hat{X}^3} + \frac{\lambda_c}{\hat{\mu}_c}\frac{d^2A}{d\hat{X}^2}\Big) - \kappa^2\Big(\hat{X}\frac{dA}{d\hat{X}} - A\Big).$$

Note that, at first order, we can retrieve the solution obtained in the previous section: $A(\hat{X}) = C_1\hat{X}$. Now, as usual in a WKBJ approximation, let

$$A(\hat{X},\epsilon) = \exp\Big\{\frac{G(\hat{X},\epsilon)}{\epsilon}\Big\}, \quad \text{where} \quad G(\hat{X},\epsilon) = G_0(\hat{X}) + \epsilon G_1(\hat{X}) + O(\epsilon^2).$$

Through substitution into the equation above, we obtain

$$0 = \hat{X}\left[\left(\frac{dG_0}{d\hat{X}}\right)^3 - \kappa^2\frac{dG_0}{d\hat{X}}\right] + \epsilon\left[\kappa^2 + \frac{\lambda_c}{\hat{\mu}_c}\left(\frac{dG_0}{d\hat{X}}\right)^2 + 3\hat{X}\frac{dG_0}{d\hat{X}}\frac{d^2G_0}{d\hat{X}^2}\right.$$
$$\left. + 3\hat{X}\left(\frac{dG_0}{d\hat{X}}\right)^2\frac{dG_1}{d\hat{X}} - \hat{X}\kappa^2\frac{dG_1}{d\hat{X}}\right] + O(\epsilon^2).$$

Equating terms in $O(1)$ and then $O(\epsilon)$, we see that either

$$\{G_0(\hat{X}) = \tilde{C}_0, \quad G_1(\hat{X}) = \ln(\hat{X}) + \tilde{C}_1\},$$

or

$$\{G_0(\hat{X}) = \pm\kappa\hat{X} + \tilde{C}_0, \quad G_1(\hat{X}) = \omega\ln(\hat{X}) + \tilde{C}_1\},$$

where $\omega = -\frac{1}{2}(1 + \frac{\lambda_c}{\hat{\mu}_c})$. Therefore, grouping the constants, we have

$$A(\hat{X},\epsilon) = \exp\Big\{\frac{G(\hat{X},\epsilon)}{\epsilon}\Big\} = \exp\Big\{\frac{G_0(\hat{X})}{\epsilon} + G_1(\hat{X})\Big\} = C_1\hat{X},$$

or

$$A(\hat{X},\epsilon) = \exp\Big\{\frac{G(\hat{X},\epsilon)}{\epsilon}\Big\} = \exp\Big\{\frac{G_0(\hat{X})}{\epsilon} + G_1(\hat{X})\Big\} = C_0\hat{X}^\omega\exp\Big\{\frac{\pm\kappa\hat{X}}{\epsilon}\Big\}.$$

Notice that the first solution is the same as found previously, by using a first order approximation. Thus, the latter equation corresponds to the other two solutions for which we searched. Therefore, since the equation for A is a third order ordinary differential equation, we thus conclude that $A(X)$ satisfies

$$A(X) \sim C_1 X + C_2 X^{\omega} e^{\kappa X} + C_3 X^{\omega} e^{-\kappa X}, \qquad \omega = -\frac{1}{2}\left(1 + \frac{\lambda_c}{\hat{\mu}_c}\right) \tag{108}$$

when $X \to \infty$ for some constants C_1, C_2, C_3. However, for matching to be possible, we must have $C_2 = 0$.

Recall now the equations in (107) for $\{V_c^1, V_c^2\}$ were obtained via algebraic manipulation and the definition of two auxiliary functions $\{F_1, F_2\}$ that depended on $\{V_c^1, V_c^2\}$. Similarly, we take an analogous approach to recast equations (104) and (105) to find $\{V_w^1, V_w^2\}$. To be more specific, we define

$$F_3 = \frac{dV_w^1}{dX} - i\kappa V_w^2, \qquad F_4 = \frac{dV_w^2}{dX} + i\kappa V_w^1,$$

and, through some algebraic manipulation, recast equations (104) and (105) as

$$\begin{cases} \dfrac{d^2 V_w^2}{dX^2} - \kappa^2 V_w^2 &= \dfrac{i\kappa R_0 \lambda_2}{\alpha_h (1-\alpha_h)^2} \dfrac{dA}{dX} \\ V_w^1 + \dfrac{1}{i\kappa} \dfrac{dV_w^2}{dX} &= \dfrac{\lambda_2 R_0}{\alpha_h (1-\alpha_h)} A. \end{cases} \tag{109}$$

Therefore, using the expression for A in (108), we can find the asymptotic behaviour of $\{V_c^1, V_c^2, V_w^1, V_w^2\}$ via equations (107) and (109). For this, we must solve two second order ordinary differential equations for $\{V_c^1, V_w^2\}$ and obtain $\{V_c^2, V_w^1\}$ by substitution of $\{A, V_c^1, V_w^2\}$ into the remaining equations.

Note also that the solution to the homogeneous version of the ordinary differential equations for $\{V_c^1, V_w^2\}$ will have both decaying and growing exponential terms of the type $e^{-\kappa X}$ and $e^{\kappa X}$, respectively. However, for matching to be possible, we cannot allow the existence of the growing exponential term of the type $e^{\kappa X}$. If this is taken into consideration, we can simplify our calculations by assuming any pre-factor of $e^{\kappa X}$ is null. Thus,

by inserting the expression for $A(X)$ into the equations above, we obtained that

$$\begin{aligned}
A(X) &\sim C_1 X + C_2 X^{\omega} e^{\kappa X} + C_3 X^{\omega} e^{-\kappa X} \\
&\implies C_2 = 0 \\
V_c^1(X) &\sim -C_1\gamma_1 + C_4 e^{\kappa X} + C_5 e^{-\kappa X} + C_3 X^{\omega} e^{-\kappa X} p_1^2(X) \\
&\implies C_4 = 0 \\
V_c^2(X) &\sim \gamma_3 C_1 X + C_5 i e^{-\kappa X} + C_3 X^{\omega-1} e^{-\kappa X} p_2^3(X) \\
V_w^1(X) &\sim \frac{\lambda_2 R_0}{\alpha_h(1-\alpha_h)} C_1 X + C_6 e^{-\kappa X} + C_3 X^{\omega-1} e^{-\kappa X} p_3^2(X) \\
V_w^2(X) &\sim \frac{\lambda_2 R_0 C_1}{i\kappa\alpha_h(1-\alpha_h)^2} + C_6 i e^{-\kappa X} + C_7 e^{\kappa X} + C_3 X^{\omega} e^{-\kappa X} p_4^1(X) \\
&\implies C_7 = 0,
\end{aligned}$$

when $X \to \infty$. Here we used the following notation:

$$p_i^n(X) = A_{i,0} + A_{i,1}X + A_{i,2}X^2 ... + A_{i,n}X^n, \qquad i = 1,2,3,4, \qquad n \in \mathbf{N},$$

where every $A_{i,j}$ is a constant that may be found explicitly in terms of the parameters of our system. Because these polynomials appear in terms that decay exponentially when $X \to \infty$, there is no need to make the expressions for $A_{i,j}$ explicit here as these are negligible terms for the purpose of matching.

In the process used to derive the expressions above, we also used the first order term of the following asymptotic expansion:

$$\begin{aligned}
\int^X e^{-2\kappa s} s^{\eta} ds \sim -\frac{X^{\eta} e^{-2\kappa X}}{2\kappa}\Big(1 + \frac{\eta}{2\kappa}\frac{1}{X} + \frac{\eta(\eta-1)}{(2\kappa)^2}\frac{1}{X^2} \\
+ \frac{\eta(\eta-1)(\eta-2)}{(2\kappa)^3}\frac{1}{X^3} + O\Big(\Big(\frac{1}{X}\Big)^4\Big)\Big),
\end{aligned}$$

when $X \to \infty$, which can be proven by integrating by parts repeatedly (See [68]).

The terms that grow exponentially must be discarded in order to allow us to perform matching when $X \to \infty$, and therefore $C_2 = C_4 = C_7 = 0$. This way, no exponentially growing term is carried along in the derivation

of V_c^1, V_c^2, V_w^1, and V_w^2 and we may obtain 3 boundary conditions for the inner solution when $X \to \infty$. Since there are 3 boundary conditions already at $X = 0$, this implies that we have a total of 6 boundary conditions that may be applied to the inner solution at $X = 0$ and when $X \to \infty$ in order to perform numerical simulations.

Notice that thus we have 4 degrees of freedom, corresponding to the constants $\{C_1, C_3, C_5, C_6\}$. However, $\{C_3, C_5, C_6\}$ do not play a role in matching, since these are the coefficients of terms that decay exponentially when $X \to \infty$.

That being said, we will now find a condition for C_1 by matching the inner solution to the outer solution when $X \to \infty$. Indeed, from the expressions above, we see that when $X \to \infty$, at first order

$$\begin{aligned} A(X) &\sim C_1 X \\ V_c^1(X) &\sim -C_1\gamma_1 \\ V_c^2(X) &\sim C_1\gamma_3 X \\ V_w^1(X) &\sim \frac{\lambda_2 R_0}{\alpha_h(1-\alpha_h)} C_1 X \\ V_w^2(X) &\sim \frac{\lambda_2 R_0 C_1}{i\kappa\alpha_h(1-\alpha_h)^2}. \end{aligned}$$

Notice that the asymptotic far-field behaviour found for A, V_c^2, and V_w^1 is the same as found previously, by using a first order approximation. However, instead of having

$$V_c^1(X) \to 0, \qquad \text{and} \qquad V_w^2(X) \to 0$$

when $X \to \infty$, we now have

$$V_c^1(X) \sim -C_1\gamma_1, \qquad \text{and} \qquad V_w^2(X) \sim \frac{\lambda_2 R_0 C_1}{i\kappa\alpha_h(1-\alpha_h)^2}$$

when $X \to \infty$. If we match these to the outer solution when $\xi \to 1$, we obtain that for matching to be possible we must have

$$C_1 = -\frac{1}{R_0}\lim_{\xi\to 1}\frac{d\overline{\alpha}}{d\xi}(\xi), \qquad \text{and} \qquad \overline{\alpha}(\xi) \sim C_1 R_0(1-\xi),$$

when $\xi \to 1$, where $\overline{\alpha}(\xi)$ is part of the outer solution.

Conclusion - Analytical Characterisation of Inner Solution near Outer Boundary $\xi = 1$

The inner solution near the outer boundary $\xi = 1$ satisfies at order one:

$$\begin{aligned}
\tilde{\alpha}(X,t) &= e^{(\gamma_0 - 2\lambda_2)t} A(X) \\
\tilde{v}_c^1(X,t) &= e^{(\gamma_0 - 2\lambda_2)t} V_c^1(X) \\
\tilde{v}_c^2(X,t) &= e^{(\gamma_0 - 2\lambda_2)t} V_c^2(X) \\
\tilde{v}_w^1(X,t) &= e^{(\gamma_0 - \lambda_2)t} V_w^1(X) \\
\tilde{v}_w^2(X,t) &= e^{(\gamma_0 - \lambda_2)t} V_w^2(X)
\end{aligned}$$

where

$$\xi = 1 - \frac{X}{R_*(t)}$$

and $A(X)$, $V_c^1(X)$, $V_c^2(X)$, $V_w^1(X)$, and $V_w^2(X)$ satisfy

$$\begin{cases}
0 &= \Big[\frac{\partial S_c}{\partial \alpha}(\alpha_h, C_\infty) - \gamma_0 + \lambda_2\Big(1 - X\frac{d}{dX}\Big)\Big] A + \alpha_h \frac{dV_c^1}{dX} - \alpha_h i\kappa V_c^2 \\
0 &= \Sigma_c'(\alpha_h)\frac{dA}{dX} + \hat{\mu}_c \frac{d^2 V_c^1}{dX^2} - (\lambda_c + \mu_c) i\kappa \frac{dV_c^2}{dX} - \mu_c \kappa^2 V_c^1 \\
0 &= \Big(- \Sigma_c(\alpha_h) - \alpha_h \Sigma_c'(\alpha_h) + \lambda_c \lambda_2 \Big) i\kappa A + \mu_c \alpha_h \frac{d^2 V_c^2}{dX^2} \\
&\quad - (\mu_c + \lambda_c)\alpha_h i\kappa \frac{dV_c^1}{dX} - \alpha_h \kappa^2 \hat{\mu}_c V_c^2 \\
0 &= -\frac{\lambda_2 R_0}{(1-\alpha_h)^2}\frac{dA}{dX} - \frac{dV_w^1}{dX} + i\kappa V_w^2 \\
0 &= -\frac{dV_w^2}{dX} - i\kappa V_w^1 + \frac{i\kappa \lambda_2 R_0}{\alpha_h(1-\alpha_h)} A,
\end{cases}$$

in $X > 0$ and at $X = 0$:

$$\begin{cases}
0 &= -\Sigma_c'(\alpha_h) A - \hat{\mu}_c \frac{dV_c^1}{dX} + \lambda_c i\kappa V_c^2, \\
0 &= \frac{(3\lambda_2 - \gamma_0)}{i\kappa}\frac{dV_c^2}{dX} + (\gamma_0 - \lambda_2) V_c^1 \\
V_w^2 &= \frac{R_0}{2(1-\alpha_h)}\Big[\frac{dV_c^2}{dX} - i\kappa V_c^1\Big].
\end{cases}$$

Also, the moving boundary condition yields for large t, that

$$\frac{d\tilde{R}}{dt}(t) = \lambda_2 \tilde{R}(t) + e^{(\gamma_0 - 2\lambda_2)t} V_c^1(0)$$

and therefore,

$$\tilde{R}(t) \sim C_0 e^{\lambda_2 t} + \frac{V_c^1(0)}{\gamma_0 - 3\lambda_2} e^{(\gamma_0 - 2\lambda_2)t}.$$

Far field behaviour when $X \to \infty$ is, at first order,

$$\begin{aligned} A(X) &\sim C_1 X \\ V_c^1(X) &\sim -C_1 \gamma_1 \\ V_c^2(X) &\sim C_1 \gamma_3 X \\ V_w^1(X) &\sim \frac{\lambda_2 R_0}{\alpha_h(1-\alpha_h)} C_1 X \\ V_w^2(X) &\sim \frac{\lambda_2 R_0}{i\kappa\alpha_h(1-\alpha_h)^2} C_1, \end{aligned}$$

where matching yields

$$C_1 = -\frac{1}{R_0} \lim_{\xi \to 1} \frac{d\overline{\alpha}}{d\xi}(\xi), \qquad \text{and} \qquad \overline{\alpha}(\xi) \sim C_1 R_0 (1-\xi),$$

when $\xi \to 1$.

As in the previous section, notice again that all the exponential decay rates specified for the inner solution near the outer boundary, interestingly enough, do not depend on the wavelength κ of the perturbation in question.

8.3.2 *Comparison of Analytical vs. Numerical Outer Boundary Inner Solution*

Motivation & Set-up

As done in the previous section, with the outer solution, consider the inner solution obtained above in comparison with the numerical simulations of the solutions to our original system. However, now we rewrite in terms of $X(\xi, t) = (1-\xi)R_*(t)$ in order to compare these quantities in a more straightforward way. This way, we expect that for fixed X near the inner boundary $X = 0$,

$$\begin{aligned} \tilde{\alpha}(X,t) &= O(e^{(\gamma_0 - 2\lambda_2)t}), \\ \tilde{v}_c^1(X,t) = O(e^{(\gamma_0 - 2\lambda_2)t}), &\qquad \tilde{v}_c^2(X,t) = O(e^{(\gamma_0 - 2\lambda_2)t}), \\ \tilde{v}_w^1(X,t) = O(e^{(\gamma_0 - \lambda_2)t}), &\qquad \tilde{v}_w^2(X,t) = O(e^{(\gamma_0 - \lambda_2)t}). \end{aligned}$$

Numerical Simulations - Comparison to Decay Obtained Analytically

Indeed, if we plot the numerical solutions for different values of X that correspond to ξ near the outer boundary $\xi = 1$, we obtain the following graphs. As before, we have graphed the expected decay against the numerical results for easy comparison.

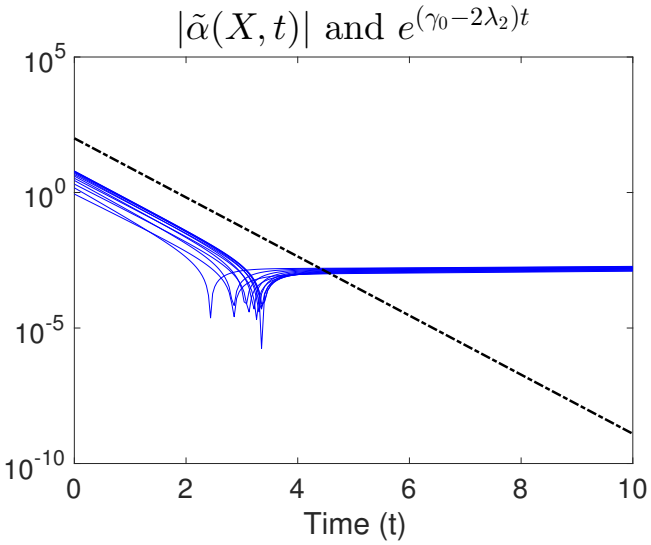


Figure 119.: Absolute value of the perturbation of the cell concentration $|\tilde{\alpha}(X,t)|$ for array of $X \in (0,\infty)$ and a translation of an exponential that is indicative of the decay predicted by the analytical characterisation of the outer boundary inner solution, namely $e^{(\gamma_0-2\lambda_2)t}$.

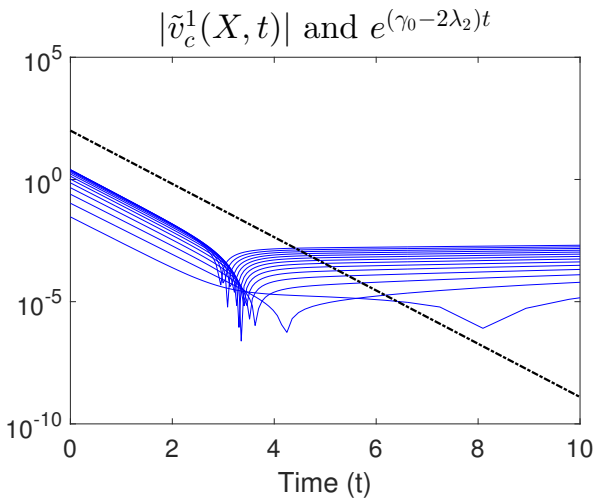


Figure 120.: Absolute value of the perturbation of the cell velocity in the x direction $|\tilde{v}_c^1(X,t)|$ for an array of $X \in (0,\infty)$ and a translation of an exponential that is indicative of the decay predicted by the analytical characterisation of the outer boundary inner solution, namely $e^{(\gamma_0-2\lambda_2)t}$.

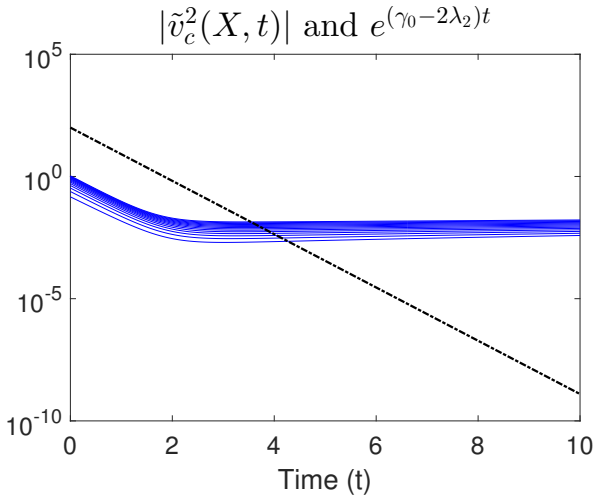


Figure 121.: Absolute value of the perturbation of the cell velocity in the y direction $|\tilde{v}_c^2(X,t)|$ for an array of $X \in (0,\infty)$ and a translation of an exponential that is indicative of the decay predicted by the analytical characterisation of the outer boundary inner solution, namely $e^{(\gamma_0-2\lambda_2)t}$.

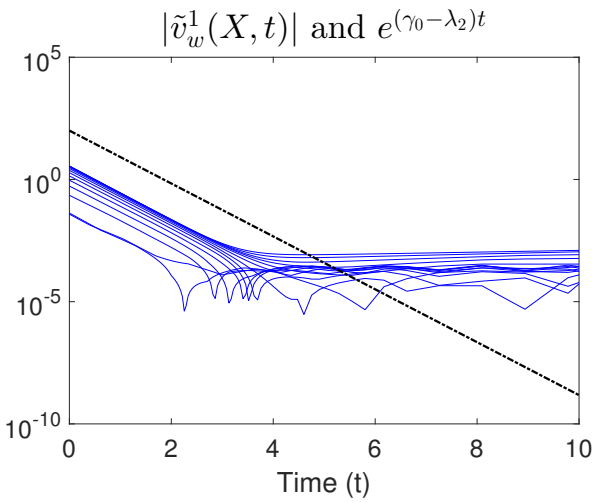


Figure 122.: Absolute value of the perturbation of the water velocity in the x direction $|\tilde{v}_w^1(X,t)|$ for an array of $X \in (0,\infty)$ and a translation of an exponential that is indicative of the decay predicted by the analytical characterisation of the outer boundary inner solution, namely $e^{(\gamma_0-\lambda_2)t}$.

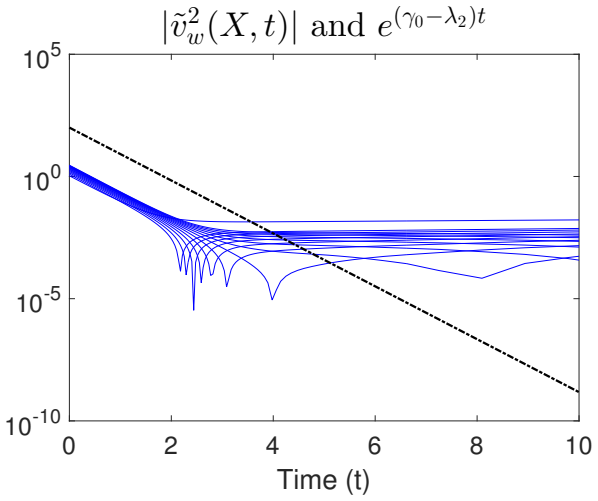


Figure 123.: Absolute value of the perturbation of the water velocity in the y direction $|\tilde{v}_w^2(X,t)|$ for an array of $X \in (0,\infty)$ and a translation of an exponential that is indicative of the decay predicted by the analytical characterisation of the outer boundary inner solution, namely $e^{(\gamma_0-\lambda_2)t}$.

A Word About $\tilde{R}(t)$

Notice that, in the previous section, regarding the outer solution, we omitted the graph of $\tilde{R}(t)$, since it is defined based on the equation

$$\frac{d\tilde{R}}{dt}(t) = \lambda_2 \tilde{R}(t) + \tilde{v}_c^1(1,t),$$

which depends on the value of $\tilde{v}_c^1$ at the outer boundary $\xi = 1$ (in the outer boundary layer). Thus, $\tilde{R}(t)$ is unrelated to the outer solution, since the outer solution is relevant only outside of all possible boundary layers.

Now, however, since we have characterized the decay of the inner solution near the outer $\xi = 1$ boundary, we can conclude that, when $t \to \infty$,

$$\frac{d\tilde{R}}{dt}(t) = \lambda_2 \tilde{R}(t) + e^{(\gamma_0 - 2\lambda_2)t} V_c^1(0)$$

and therefore,

$$\tilde{R}(t) \sim C_0 e^{\lambda_2 t} + \frac{V_c^1(0)}{\gamma_0 - 3\lambda_2} e^{(\gamma_0 - 2\lambda_2)t}. \tag{110}$$

In our simulations, since $\gamma_0 - 2\lambda_2 < 0$ and $\lambda_2 > 0$, we expect that $\tilde{R}(t) \sim C_0 e^{\lambda_2 t}$ when $t \to \infty$ for some C_0. Indeed, plotting a translation of the function $e^{\lambda_2 t}$ and the $\tilde{R}(t)$ obtained numerically, we see the following:

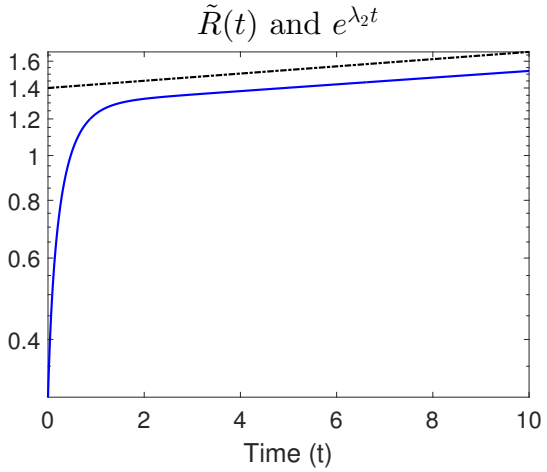


Figure 124.: Graph of the perturbation on the outer boundary $\tilde{R}(t)$ and a translation of an exponential that is indicative of the decay predicted by the analytical characterisation of the outer boundary inner solution $\tilde{v}_c^1(X,t)$ and its effect on the moving boundary equation.

8.4 INNER SOLUTION NEAR INNER BOUNDARY

8.4.1 *Analytical Characterisation of Inner Solution near Inner Boundary $\xi = 0$*

Finally, we will characterise the inner solution in the boundary layer near the inner boundary $\xi = 0$. For that, we have performed a process very similar to the one applied to the characterisation of the inner solution near the outer boundary. Most changes stem from different rescaling on ξ, namely

$$\xi = \frac{x}{R_*(t)^\beta}, \quad x = O(1) \text{ as } t \to \infty, \quad \beta > 0$$

instead of

$$\xi = 1 - \frac{X}{R_*(t)^\beta}, \quad X = O(1) \text{ as } t \to \infty, \quad \beta > 0.$$

Indeed, we now want to consider a thin strip near $\xi = 0$, rather than $\xi = 1$, which justifies the rescaling above. With it, we have, via the product rule, that

$$\begin{aligned}
\frac{\partial}{\partial t} &\longrightarrow \frac{\partial}{\partial t} + \beta\lambda_2 x \frac{\partial}{\partial x} \\
\frac{\partial}{\partial \xi} &\longrightarrow R_*(t)^\beta \frac{\partial}{\partial x} \\
\frac{\partial^2}{\partial \xi^2} &\longrightarrow R_*(t)^{2\beta} \frac{\partial^2}{\partial x^2}.
\end{aligned}$$

If we again factor out the $e^{\gamma_0 t}$ pre-factor from the perturbations, we obtain the system with which we will work in this section:

$$\begin{cases} \dfrac{\partial \overline{\alpha}}{\partial t} & = \Big[\dfrac{\partial S_c}{\partial \alpha}(\alpha_h, C_\infty) - \gamma_0 - \lambda_2\Big(1 + \beta x \dfrac{\partial}{\partial x}\Big)\Big]\overline{\alpha} - \alpha_h R_*^{\beta-1}\dfrac{\partial \overline{v}_c^1}{\partial x} - \alpha_h i\kappa \overline{v}_c^2 \\ 0 & = -\Sigma_c'(\alpha_h)\dfrac{\partial \overline{\alpha}}{\partial x} + \hat{\mu}_c R_*^{\beta-1}\dfrac{\partial^2 \overline{v}_c^1}{\partial x^2} + (\lambda_c + \mu_c) i\kappa \dfrac{\partial \overline{v}_c^2}{\partial x} - \dfrac{1}{R_*^{\beta-1}}\mu_c \kappa^2 \overline{v}_c^1 \\ 0 & = \Big(-\Sigma_c(\alpha_h) - \alpha_h \Sigma_c'(\alpha_h) + \lambda_c\lambda_2\Big) i\kappa\overline{\alpha} + \mu_c \alpha_h R_*^{2\beta-2}\dfrac{\partial^2 \overline{v}_c^2}{\partial x^2} \\ & \quad + (\mu_c + \lambda_c)\alpha_h i\kappa R_*^{\beta-1}\dfrac{\partial \overline{v}_c^1}{\partial x} - \alpha_h \kappa^2 \hat{\mu}_c \overline{v}_c^2 \\ 0 & = \dfrac{\lambda_2}{1-\alpha_h}\Big(1 + x\dfrac{\partial}{\partial x}\Big)\overline{\alpha} + \alpha_h R_*^{\beta-1}\dfrac{\partial \overline{v}_c^1}{\partial x} + (1-\alpha_h)R_*^{\beta-1}\dfrac{\partial \overline{v}_w^1}{\partial x} \\ & \quad + \alpha_h i\kappa \overline{v}_c^2 + (1-\alpha_h) i\kappa \overline{v}_w^2 \\ 0 & = \alpha_h R_*^{2\beta-2}\dfrac{\partial}{\partial x}(\overline{v}_w^2 - \overline{v}_c^2) - i\kappa\alpha_h R_*^{\beta-1}(\overline{v}_w^1 - \overline{v}_c^1) + \dfrac{i\kappa\lambda_2}{1-\alpha_h} x\overline{\alpha}, \end{cases}$$

and $\overline{v}_c^1(0,t) = \overline{v}_c^2(0,t) = \overline{v}_w^1(0,t) = 0$.

In very much the same way as before, we assume that

$$\overline{\alpha}(x,t) = e^{a_0 t}A(x), \quad \overline{v}_c^1(x,t) = e^{a_1 t}V_c^1(x), \quad \overline{v}_c^2(x,t) = e^{a_2 t}V_c^2(x),$$

$$\overline{v}_w^1(x,t) = e^{b_1 t}V_w^1(x), \quad \overline{v}_w^2(x,t) = e^{b_2 t}V_w^2(x).$$

Using the same case-by-case reasoning explained in the previous section, we can prove that the only possible non-trivial asymptotic balances happen when:

Case 1: $\beta > 1$, $a_1 - a_0 + \lambda_2(\beta - 1) = 0$, $\quad a_2 - a_0 + 2\lambda_2(\beta - 1) = 0$, $b_1 - a_0 + \lambda_2(\beta - 1) = 0$, $b_2 - a_0 + 2\lambda_2(\beta - 1) = 0$,

Case 2: $\beta < 1$, $a_1 - a_0 - \lambda_2(\beta - 1) = 0$, $\quad a_2 - a_0 = 0$, $b_1 - a_0 + \lambda_2(\beta - 1) = 0$, $\quad b_2 - a_0 = 0$,

Case 3: $\beta = 1$, $a_0 = a_1 = a_2$ and $b_1 = b_2 > a_0$,

Case 4: $\beta = 1$ and $a_0 = a_1 = a_2 = b_1 = b_2$.

Cases 1, 2 and 3 may be discarded as being trivial in the same manner as in the previous section. (Details can be found in Appendix C.) Therefore, we are left with analysing Case 4:

Case 4: $\beta = 1$ *and* $a_0 = a_1 = a_2 = b_1 = b_2$.

Here, $\beta = 1$ and $a_0 = a_1 = a_2 = b_1 = b_2$, and the system above becomes, at first order,

$$\begin{cases} 0 &= \Big[\dfrac{\partial S_c}{\partial \alpha}(\alpha_h, C_\infty) - \gamma_0 - a_0 - \lambda_2\Big(1 + x\dfrac{d}{dx}\Big)\Big] A - \alpha_h \dfrac{dV_c^1}{dx} - \alpha_h i\kappa V_c^2 \\ 0 &= -\Sigma_c'(\alpha_h)\dfrac{dA}{dx} + \hat{\mu}_c \dfrac{d^2V_c^1}{dx^2} + (\lambda_c + \mu_c) i\kappa \dfrac{dV_c^2}{dx} - \mu_c \kappa^2 V_c^1 \\ 0 &= \Big(- \Sigma_c(\alpha_h) - \alpha_h \Sigma_c'(\alpha_h) + \lambda_c \lambda_2 \Big) i\kappa A \\ &\quad + \mu_c \alpha_h \dfrac{d^2V_c^2}{dx^2} + (\mu_c + \lambda_c)\alpha_h i\kappa \dfrac{dV_c^1}{dx} - \alpha_h \kappa^2 \hat{\mu}_c V_c^2 \\ 0 &= \dfrac{\lambda_2}{1-\alpha_h}\big(1 + x\dfrac{d}{dX}\big) A + \alpha_h \dfrac{dV_c^1}{dx} + \alpha_h i\kappa V_c^2 \\ &\quad + (1-\alpha_h)\dfrac{dV_w^1}{dx} + (1-\alpha_h) i\kappa V_w^2 \\ 0 &= \dfrac{\lambda_2 i\kappa}{1-\alpha_h} x A + \alpha_h i\kappa V_c^1 - \alpha_h \dfrac{dV_c^2}{dx} - \alpha_h i\kappa V_w^1 + \alpha_h \dfrac{dV_w^2}{dx}, \end{cases}$$

with $V_c^1(0) = V_c^2(0) = V_w^1(0) = 0$.

Once again, we tackle this system with a strategy similar to the one used to tackle Case 4 of the inner solution in the outer boundary layer. Let

$$F_1 = \frac{dV_c^1}{dx} + i\kappa V_c^2, \qquad F_2 = \frac{dV_c^2}{dx} - i\kappa V_c^1.$$

Notice initially that F_1 and F_2 differ slightly from the ones used in the outer boundary inner layer. Indeed, the system of equations obtained in the Case 4 of the two boundary layers (near $\xi = 1$ and near $\xi = 0$) differ particularly in the sign of some terms. This difference comes from the distinct variable changes made from ξ to X and ξ to x.

Therefore, a change in the definition of $\{F_1, F_2\}$ allows us to use the exact same process employed in the previous section to recast the equations on $\{A, V_c^1, V_c^2\}$ as

$$\begin{cases} 0 &= -\lambda_2 x \dfrac{d^3A}{dx^3} - \Big[a_0 + \lambda_2(\dfrac{\lambda_c}{\hat{\mu}_c} + 2)\Big]\dfrac{d^2A}{dx^2} + \lambda_2\kappa^2 x\dfrac{dA}{dx} + \kappa^2(a_0+\lambda_2)A \\ H_1 &= \dfrac{d^2V_c^1}{dx^2} - \kappa^2 V_c^1 \\ H_2 &= V_c^2 + \dfrac{1}{i\kappa}\dfrac{dV_c^1}{dx} \end{cases}$$

where H_1 and H_2 depend only on A:

$$H_1 = -\frac{\mu_c+\lambda_c}{\mu_c\alpha_h}\left[\Big(\frac{\partial S_c}{\partial\alpha}(\alpha_h, C_\infty) - \gamma_0 - a_0 - 2\lambda_2 - \frac{\alpha_h\Sigma_c'(\alpha_h)}{\mu_c+\lambda_c}\Big)\frac{dA}{dx} - \lambda_2 x\frac{d^2A}{dx^2}\right]$$

$$H_2 = \frac{1}{\alpha_h i\kappa}\Big(\frac{\partial S_c}{\partial\alpha}(\alpha_h, C_\infty) - \gamma_0 - a_0 - \lambda_2\Big)A - \frac{\lambda_2}{\alpha_h i\kappa}x\frac{dA}{dx}.$$

Consider $\hat{x} = \epsilon x$. By solving the three equations above at first order and performing a matching between the inner and outer solutions when $x \to \infty$ and $\xi \to 0$, respectively, we obtain that

$$a_0 = a_1 = a_2 = b_1 = b_2 = -2\lambda_2$$

and

$$A(x) \sim D_1 x, \qquad V_c^1(x) \sim 0, \qquad V_c^2(x) \sim \gamma_3 D_1 x, \qquad \text{when } x \to \infty.$$

Consequently, if we substitute these expressions into the last two equations of Case 4, we can solve for $\{V_w^1, V_w^2\}$ at first order and obtain, after matching, that

$$V_w^1(x) \sim \frac{D_1\lambda_2}{\alpha_h(1-\alpha_h)}x^2, \qquad V_w^2(x) \sim D_1 B_1 x,$$

when $x \to \infty$, where

$$B_1 = -\frac{2\lambda_2}{i\kappa\alpha_h(1-\alpha_h)^2} + \frac{(-\Sigma_c(\alpha_h) - \alpha_h\Sigma_c'(\alpha_h) + \lambda_c\lambda_2)}{i\kappa\hat{\mu}_c(1-\alpha_h)}.$$

From matching, we also obtain the following conditions on $\overline{\alpha}$:

$$\overline{\alpha}(\xi) \sim D_1\xi R_0, \qquad \frac{d\overline{\alpha}}{d\xi}(\xi) \to 0$$

when $\xi \to 0$. Together, these two conditions imply that $D_1 = 0$, which makes this a trivial solution. Therefore, we must consider a WKBJ expansion of $A(x)$ to obtain the other two linearly independent solutions of the third order equation for $A(x)$, as was done in the previous section.

Because the process is analogous to the one done to $A(X)$ in the outer boundary inner solution, we only state the results obtained. Indeed, when $x \to \infty$,

$$\begin{aligned}
A(x) &\sim D_1 x + D_2 x^{\omega} e^{\kappa x} + D_3 x^{\omega} e^{-\kappa x} \\
&\implies D_2 = 0 \\
V_c^1(x) &\sim D_1 \gamma_1 + D_4 e^{\kappa x} + D_5 e^{-\kappa x} + D_3 x^{\omega} e^{-\kappa x} q_1^2(x) \\
&\implies D_4 = 0 \\
V_c^2(x) &\sim D_1 \gamma_3 x - D_5 i e^{-\kappa x} + D_3 x^{\omega-1} e^{-\kappa x} q_2^3(x) \\
V_w^1(x) &\sim \frac{\lambda_2}{\alpha_h(1-\alpha_h)} D_1 x^2 + D_1 B_0 + D_6 e^{-\kappa x} + D_3 x^{\omega-3} e^{-\kappa x} q_3^6(x) \\
V_w^2(x) &\sim D_1 B_1 x + D_7 e^{\kappa x} - D_6 i e^{-\kappa x} + D_3 x^{\omega-2} e^{-\kappa x} q_2^5(x), \\
&\implies D_7 = 0,
\end{aligned}$$

where

$$\begin{aligned}
B_0 &= \frac{1}{\kappa^2}\Big[\frac{2\lambda_2}{\alpha_h(1-\alpha_h)^2} - \frac{(-\Sigma_c(\alpha_h) - \alpha_h \Sigma_c'(\alpha_h) + \lambda_c \lambda_2)}{\hat{\mu}_c \alpha_h (1-\alpha_h)} \\
&\quad + \frac{\lambda_c + \mu_c}{\mu_c \alpha_h}\Big(\frac{\partial S_c}{\partial \alpha}(\alpha_h, C_\infty) - \gamma_0 - \frac{\alpha_h \Sigma_c'(\alpha_h)}{\mu_c + \lambda_c}\Big)\Big] \\
B_1 &= \frac{1}{i\kappa}\Big(\frac{(-\Sigma_c(\alpha_h) - \alpha_h \Sigma_c'(\alpha_h) + \lambda_c \lambda_2)}{\hat{\mu}_c (1-\alpha_h)} - \frac{2\lambda_2}{\alpha_h(1-\alpha_h)^2}\Big).
\end{aligned}$$

Here we use the following notation:

$$q_i^n(x) = B_{i,0} + B_{i,1} x + B_{i,2} x^2 ... + B_{i,n} x^n, \qquad i = 1,2,3,4, \qquad n \in \mathbf{N},$$

where every $B_{i,j}$ is a constant that may be found explicitly in terms of the parameters of our system. The terms that grow exponentially must be discarded in order to allow us to perform matching when $x \to \infty$, and therefore $D_2 = D_4 = D_7 = 0$ from which we may obtain 3 boundary conditions for the inner solution when $x \to \infty$. Since there are 3 boundary

conditions already at $x = 0$, this implies that we have a total of 6 boundary conditions that may be applied to the inner solution at $x = 0$ and when $x \to \infty$ in order to perform numerical simulations.

Notice that thus we have 4 degrees of freedom, corresponding to the constants $\{D_1, D_3, D_5, D_6\}$. However, $\{D_3, D_5, D_6\}$ do not play a role in matching, since these are the coefficients of terms that decay exponentially when $x \to \infty$.

In particular, far field behaviour when $x \to \infty$ is, at first order

$$\begin{aligned} A(x) &\sim D_1 x \\ V_c^1(x) &\sim D_1 \gamma_1 \\ V_c^2(x) &\sim D_1 \gamma_3 x \\ V_w^1(x) &\sim \frac{\lambda_2}{\alpha_h(1-\alpha_h)} D_1 x^2 \\ V_w^2(x) &\sim D_1 B_1 x. \end{aligned}$$

Notice that the asymptotic far-field behaviour found for A, V_c^2, and V_w^1 and V_w^2 are the same as found previously, by using a first order approximation. However, we have

$$V_c^1(x) \sim D_1 \gamma_1 \qquad \text{instead of} \qquad V_c^1(x) \to 0$$

when $x \to \infty$. If we attempt to match this to the outer solution when $\xi \to 1$, we see that, for matching to be possible, we must have

$$D_1 = \frac{1}{R_0} \lim_{\xi \to 0} \frac{d\overline{\alpha}}{d\xi}(\xi), \qquad \text{and} \qquad \overline{\alpha}(\xi) \sim D_1 R_0 \xi$$

when $\xi \to 0$.

Conclusion - Analytical Characterisation of Inner Solution near Inner Boundary $\xi = 0$

The inner solution near the inner boundary $\xi = 0$ satisfies at order one:

$$\begin{aligned}
\tilde{\alpha}(x,t) &= e^{(\gamma_0 - 2\lambda_2)t} A(x) \\
\tilde{v}_c^1(x,t) &= e^{(\gamma_0 - 2\lambda_2)t} V_c^1(x) \\
\tilde{v}_c^2(x,t) &= e^{(\gamma_0 - 2\lambda_2)t} V_c^2(x) \\
\tilde{v}_w^1(x,t) &= e^{(\gamma_0 - 2\lambda_2)t} V_w^1(x) \\
\tilde{v}_w^2(x,t) &= e^{(\gamma_0 - 2\lambda_2)t} V_w^2(x)
\end{aligned}$$

where

$$\xi = \frac{x}{R_*(t)}$$

and $A(x)$, $V_c^1(x)$, $V_c^2(x)$, $V_w^1(x)$, and $V_w^2(x)$ satisfy

$$\begin{cases}
0 &= \Big[\frac{\partial S_c}{\partial \alpha}(\alpha_h, C_\infty) - \gamma_0 + \lambda_2\Big(1 - x\frac{d}{dx}\Big)\Big] A - \alpha_h \frac{dV_c^1}{dx} - \alpha_h i\kappa V_c^2 \\
0 &= -\Sigma_c'(\alpha_h)\frac{dA}{dx} + \hat{\mu}_c \frac{d^2 V_c^1}{dx^2} + (\lambda_c + \mu_c) i\kappa \frac{dV_c^2}{dx} - \mu_c \kappa^2 V_c^1 \\
0 &= \Big(- \Sigma_c(\alpha_h) - \alpha_h \Sigma_c'(\alpha_h) + \lambda_c \lambda_2 \Big) i\kappa A + \mu_c \alpha_h \frac{d^2 V_c^2}{dx^2} \\
&\quad + (\mu_c + \lambda_c)\alpha_h i\kappa \frac{dV_c^1}{dx} - \alpha_h \kappa^2 \hat{\mu}_c V_c^2 \\
0 &= \frac{\lambda_2}{1 - \alpha_h}\big(1 + x\frac{d}{dx}\big) A + \alpha_h \frac{dV_c^1}{dx} + \alpha_h i\kappa V_c^2 \\
&\quad + (1 - \alpha_h)\frac{dV_w^1}{dx} + (1 - \alpha_h) i\kappa V_w^2 \\
0 &= \frac{\lambda_2 i\kappa}{1 - \alpha_h} x A + \alpha_h i\kappa V_c^1 - \alpha_h \frac{dV_c^2}{dx} - \alpha_h i\kappa V_w^1 + \alpha_h \frac{dV_w^2}{dx},
\end{cases}$$

and $V_c^1(0) = V_c^2(0) = V_w^1(0) = 0$.

Far field behaviour when $x \to \infty$ is, at first order

$$\begin{aligned}
A(x) &\sim D_1 x \\
V_c^1(x) &\sim D_1 \gamma_1 \\
V_c^2(x) &\sim D_1 \gamma_3 x \\
V_w^1(x) &\sim \frac{\lambda_2}{\alpha_h(1 - \alpha_h)} D_1 x^2 \\
V_w^2(x) &\sim D_1 B_1 x,
\end{aligned}$$

where matching yields

$$D_1 = \frac{1}{R_0} \lim_{\xi \to 0} \frac{d\overline{\alpha}}{d\xi}(\xi), \qquad \text{and} \qquad \overline{\alpha}(\xi) \sim D_1 R_0 \xi,$$

when $\xi \to 0$.

As in the previous sections, notice again that all the exponential decay rates specified for the inner solution near the inner boundary, interestingly enough, do not depend on the wavelength κ of the perturbation in question.

At this point, notice that the asymptotic characterisation of the outer and inner solutions has been obtained. A summary of the governing equations in each region can be found in Appendix E.

8.4.2 *Comparison of Analytical vs. Numerical Inner Boundary Inner Solution*

Motivation & Set-up

As before, we will compare the decay rates obtained above with numerical results. For that, we rewrite in terms of $x(\xi, t) = \xi R_*(t)$ in order to compare these quantities in a more straightforward way. This way, we expect that for fixed x near the inner boundary $x = 0$,

$$\begin{aligned} \tilde{\alpha}(x,t) &= O(e^{(\gamma_0 - 2\lambda_2)t}), \\ \tilde{v}_c^1(x,t) = O(e^{(\gamma_0 - 2\lambda_2)t}), &\qquad \tilde{v}_c^2(x,t) = O(e^{(\gamma_0 - 2\lambda_2)t}), \\ \tilde{v}_w^1(x,t) = O(e^{(\gamma_0 - 2\lambda_2)t}), &\qquad \tilde{v}_w^2(x,t) = O(e^{(\gamma_0 - 2\lambda_2)t}). \end{aligned}$$

Numerical Simulations - Comparison to Decay Obtained Analytically

Indeed, if we plot the numerical solutions for different values of x along with the exponentials above, we obtain the following graphs:

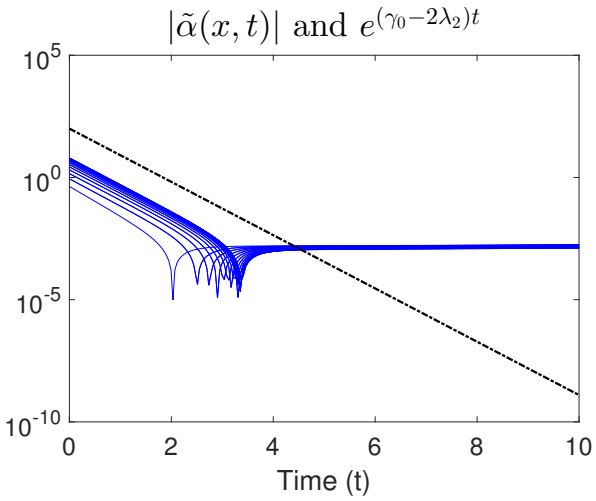


Figure 125.: Absolute value of the perturbation of the cell concentration $|\tilde{\alpha}(x,t)|$ for array of $x \in (0,\infty)$ and a translation of an exponential that is indicative of the decay predicted by the analytical characterisation of the inner boundary inner solution, namely $e^{(\gamma_0-2\lambda_2)t}$.

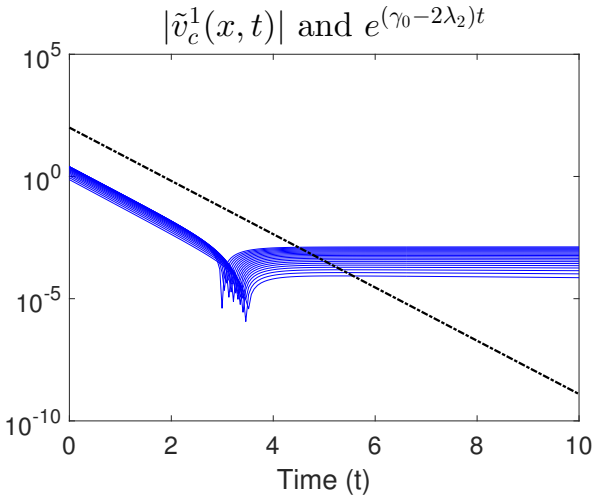


Figure 126.: Absolute value of the perturbation of the cell velocity in the x direction $|\tilde{v}_c^1(x,t)|$ for an array of $x \in (0,\infty)$ and a translation of an exponential that is indicative of the decay predicted by the analytical characterisation of the inner boundary inner solution, namely $e^{(\gamma_0-2\lambda_2)t}$.

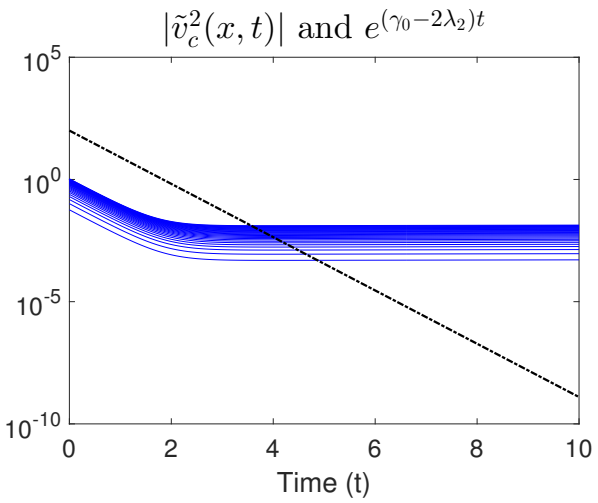


Figure 127.: Absolute value of the perturbation of the cell velocity in the y direction $|\tilde{v}_c^2(x,t)|$ for an array of $x \in (0,\infty)$ and a translation of an exponential that is indicative of the decay predicted by the analytical characterisation of the inner boundary inner solution, namely $e^{(\gamma_0-2\lambda_2)t}$.

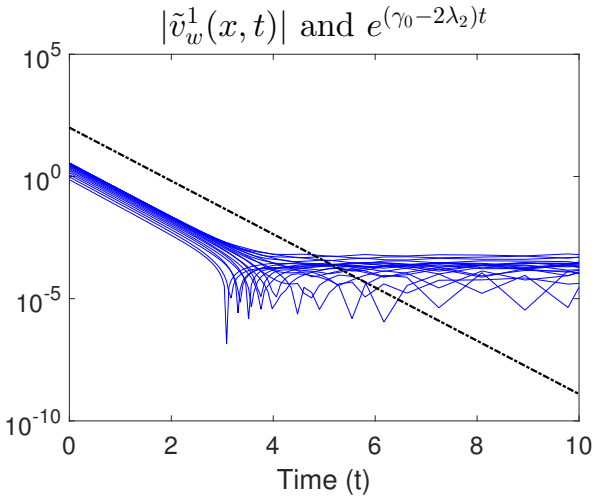


Figure 128.: Absolute value of the perturbation of the water velocity in the x direction $|\tilde{v}_w^1(x,t)|$ for an array of $x \in (0,\infty)$ and a translation of an exponential that is indicative of the decay predicted by the analytical characterisation of the inner boundary inner solution, namely $e^{(\gamma_0-2\lambda_2)t}$.

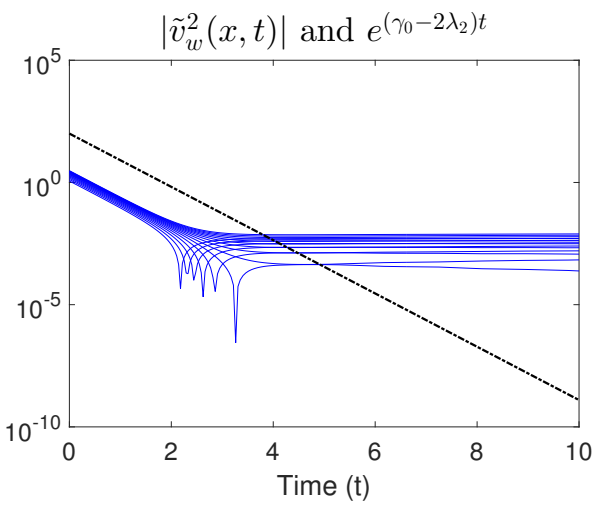


Figure 129.: Absolute value of the perturbation of the water velocity in the y direction $|\tilde{v}_w^2(x,t)|$ for an array of $x \in (0,\infty)$ and a translation of an exponential that is indicative of the decay predicted by the analytical characterisation of the inner boundary inner solution, namely $e^{(\gamma_0-2\lambda_2)t}$.

Of course, with all numerical results in this chapter, we see that there is a contradiction in seeing long time behaviour for $t < 10$, and we will explore this in the next section through the definition of a mock model that will exemplify the numerical limitations of the simulations performed above.

8.5 NUMERICAL LIMITATIONS

8.5.1 *Discussion and Definition of Mock Model*

One might find it strange that our long time behaviour deviates from the predictions relatively rapidly. To illustrate the reason for this, we would

like to propose a mock model made of the following system of independent equations:

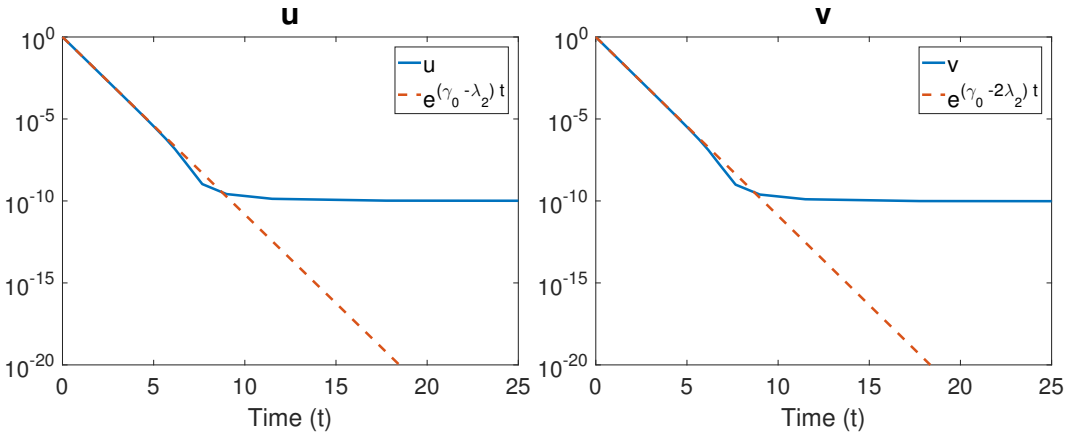
$$\begin{cases} \dfrac{\partial u}{\partial t} &= (\gamma_0 - \lambda_2)u \\ \dfrac{\partial v}{\partial t} &= (\gamma_0 - 2\lambda_2)v \\ \dfrac{\partial w}{\partial t} &= \gamma_0 w \end{cases}$$

with initial conditions $u(\xi, 0) = v(\xi, 0) = w(\xi, 0) = 1, \forall\, \xi \in (0, 1)$.

This example is the simplest two dimensional system we could construct where solutions have decay rates that are comparable to those expected to be found in our full model's solutions, i.e. are of the sort $e^{(\gamma_0 - \lambda_2)t}$, $e^{(\gamma_0 - 2\lambda_2)t}$ and $e^{\gamma_0 t}$. Indeed, if we solve the system above analytically we obtain the solution:

$$\begin{cases} u(\xi, t) &= e^{(\gamma_0 - \lambda_2)t} \\ v(\xi, t) &= e^{(\gamma_0 - 2\lambda_2)t} \\ w(\xi, t) &= e^{\gamma_0 t}, \qquad \forall\, \xi \in (0, 1). \end{cases}$$

However, if we simulate the solution to this system, using "*ode23t*" as we've done in our original system, we see that the analytical and numerical solutions are comparable only for relatively short times (see below). Therefore, it is no surprise that our full model's simulations is reacting similarly, since the same values of γ_0 and λ_2 were used here as in the previous section. See the graphs 108, 109, 110, 111, 112, 113, 114, 115, 116, 117, 119, 120, 121, 122, 123, 125, 126, 127, 128, 129 for comparison.



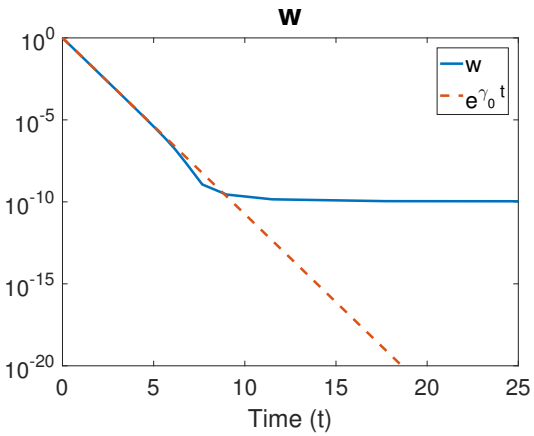


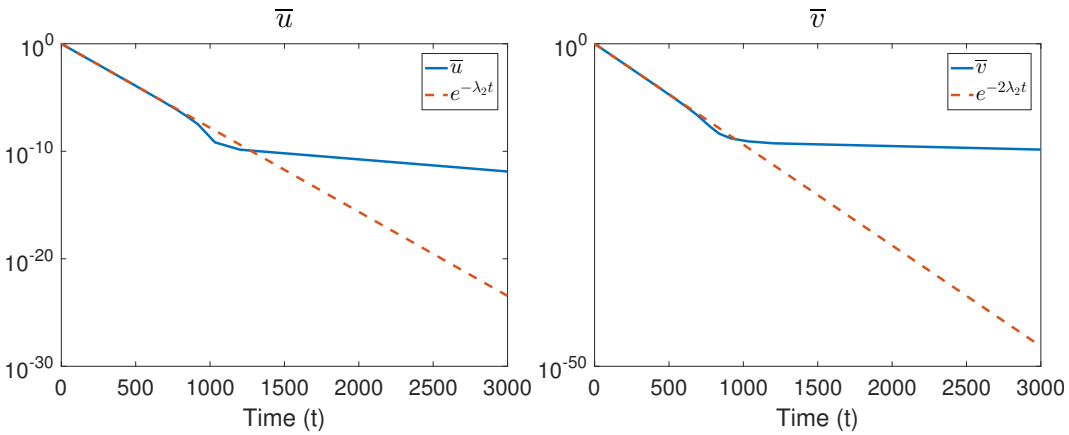
Figure 130.: Numerical simulations of the mock model as compared to the solution obtained analytically.

Therefore, much like in our model, the fast decay of these solution is creating numerical rounding errors that make the numerical approximation of solutions differ from the solutions obtained analytically.

In this case, since all of u, v, and w are decaying and the equations are independent, we can perform the following change of variable

$$\begin{cases} u(\xi,t) &= e^{\gamma_0 t}\overline{u}(\xi,t) \\ v(\xi,t) &= e^{\gamma_0 t}\overline{v}(\xi,t) \\ w(\xi,t) &= e^{\gamma_0 t}\overline{w}(\xi,t), \end{cases}$$

to obtain numerical simulations that run for longer periods of time and model $\overline{u}$, $\overline{v}$, and $\overline{w}$, which will have slower decay rates, since $|\lambda_2| < |\gamma_0|$. Indeed, when we do this, we obtain:



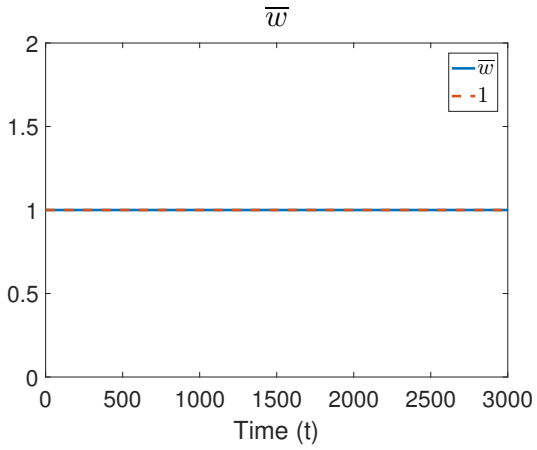


Figure 131.: Numerical simulations of a rescaling of the mock model as compared to the solution obtained analytically.

Thus, in this simple model, we have gone from numerically validating our analytical solution in (roughly) $[0,5]$ to $[0,600]$. Obviously, because of the simplicity of this mock model, this rescaling can be done optimally, as was done for w above, but this would not illustrate the point we attempt to make.

8.5.2 *Attempting to Apply Lessons from Mock Model onto Original Model*

Now, it is natural to think that one could do a similar rescaling with our original system, i.e:

$$\tilde{\alpha}(\xi,t) = e^{\gamma_0 t}\overline{\alpha}(\xi,t)$$
$$\tilde{v}_c^1(\xi,t) = e^{\gamma_0 t}\overline{v}_c^1(\xi,t) \qquad \tilde{v}_c^2(\xi,t) = e^{\gamma_0 t}\overline{v}_c^2(\xi,t)$$
$$\tilde{v}_w^1(\xi,t) = e^{\gamma_0 t}\overline{v}_w^1(\xi,t) \qquad \tilde{v}_w^2(\xi,t) = e^{\gamma_0 t}\overline{v}_w^2(\xi,t).$$

Indeed, in the equations of our model, using this rescaling, we would be able to cancel the $e^{\gamma_0 t}$ coefficient from each term and would be left with equations that model the decay of $\overline{\alpha}$, $\overline{v}_c^i$, and $\overline{v}_w^i$, $i = 1,2$, without needing ever to calculate $e^{\gamma_0 t}$. These rescaled unknowns, in turn, should be displaying smaller decay defined by a multiple of λ_2, which is small in

absolute value, and therefore should pose no numerical issues for larger times.

However, simulations were deemed sufficient in order to confirm decay rates of outer and inner solutions, and thus this was not investigated.

Several other validity tests were performed to guarantee that simulations analogous to those in this chapter are correct and these can be found in Appendix D.

8.6 CONCLUSION - LINEAR STABILITY

Recall that, in Chapter 4, we defined the travelling solutions to be unstable when

$$\lim_{t\to\infty}\left|\frac{\text{Perturbation}}{\text{Solution}}\right| = \infty$$

In the two dimensional case, we consider the travelling solutions to be unstable to two dimensional perturbations if one of the following has an infinite limit for some $(x, y) \in (0, R_*(t)) \times \mathbb{R}$ when $t \to \infty$:

$$\left|\frac{\hat{\alpha}(x,y,t)}{\alpha_h}\right|, \qquad \frac{||\hat{\mathbf{v}}_c(x,y,t)||}{||\mathbf{v}_{cs}(x)||}, \qquad \frac{||\hat{\mathbf{v}}_w(x,y,t)||}{||\mathbf{v}_{ws}(x)||}, \qquad \left|\frac{\hat{R}(y,t)}{R_*(t)}\right|,$$

where $||\cdot||$ is the euclidean norm. Equivalently, since the travelling solution is one dimensional, it is linearly unstable if one of the following is infinite for some $(x, y) \in (0, R_*(t)) \times \mathbb{R}$ when $t \to \infty$:

$$\left|\frac{\hat{\alpha}(x,y,t)}{\alpha_h}\right|, \qquad \left|\frac{\hat{v}_c^j(x,y,t)}{v_{cs}(x)}\right|, \qquad \left|\frac{\hat{v}_w^j(x,y,t)}{v_{ws}(x)}\right|, \qquad \left|\frac{\hat{R}(y,t)}{R_*(t)}\right|, \qquad j = 1, 2.$$

By inserting the definition of the travelling solutions into the ratios above and using the (ξ, t), (X, t) and (x, t) formulations defined in Sections 7.2, 8.3, and 8.4, through some algebraic manipulation, it is thus possible to prove that the travelling solution is linearly unstable to two dimensional perturbations if one of the following is infinite for some $\xi \in (0, 1)$, $X, x \in [0, \infty)$ when $t \to \infty$:

$$\begin{array}{lll} |\tilde{\alpha}(\xi,t)| & |\tilde{v}_c^j(\xi,t)|e^{-\lambda_2 t} & |\tilde{v}_w^j(\xi,t)|e^{-\lambda_2 t} \\ |\tilde{\alpha}(X,t)| & |\tilde{v}_c^j(X,t)|e^{-\lambda_2 t} & |\tilde{v}_w^j(X,t)|e^{-\lambda_2 t} \\ |\tilde{\alpha}(x,t)| & |\tilde{v}_c^j(x,t)| & |\tilde{v}_w^j(x,t)| \end{array}$$

for $j = 1, 2$ or

$$\lim_{t\to\infty} |\tilde{R}(t)|e^{-\lambda_2 t} = \infty.$$

By inserting the asymptotic characterisation of the perturbations obtained earlier in this chapter into the expressions above, we can find a condition for instability of the growing travelling solutions in terms of γ_0 and λ_2. Indeed, consider the values of η_0 where $e^{\eta_0 t}$ is the exponential pre-factor found in the previous sections for each one of the outer and inner solutions. These values of η_0 can be found in summarised form in the following table:

Table 11.: Rate of exponential decay of first order asymptotic expansions of outer and inner solutions

η_0 **Perturbation**	$\lvert\tilde{\alpha}\rvert$	$\lvert\tilde{v}_c^1\rvert$	$\lvert\tilde{v}_c^2\rvert$	$\lvert\tilde{v}_w^1\rvert$	$\lvert\tilde{v}_w^2\rvert$
Outer Solution	$\gamma_0 - \lambda_2$	$\gamma_0 - 2\lambda_2$	$\gamma_0 - \lambda_2$	γ_0	$\gamma_0 - \lambda_2$
Inner Solution Outer Boundary	$\gamma_0 - 2\lambda_2$	$\gamma_0 - 2\lambda_2$	$\gamma_0 - 2\lambda_2$	$\gamma_0 - \lambda_2$	$\gamma_0 - \lambda_2$
Inner Solution Inner Boundary	$\gamma_0 - 2\lambda_2$	$\gamma_0 - 2\lambda_2$	$\gamma_0 - 2\lambda_2$	$\gamma_0 - 2\lambda_2$	$\gamma_0 - 2\lambda_2$

Thus, the value η_1 of the prefactor $e^{\eta_1 t}$ of

$$\begin{array}{lll} |\tilde{\alpha}(\xi,t)| & |\tilde{v}_c^j(\xi,t)|e^{-\lambda_2 t} & |\tilde{v}_w^j(\xi,t)|e^{-\lambda_2 t} \\ |\tilde{\alpha}(X,t)| & |\tilde{v}_c^j(X,t)|e^{-\lambda_2 t} & |\tilde{v}_w^j(X,t)|e^{-\lambda_2 t} \\ |\tilde{\alpha}(x,t)| & |\tilde{v}_c^j(x,t)| & |\tilde{v}_w^j(x,t)| \end{array}$$

can be found by subtracting λ_2 from all the cells in the table above, except those in the first column and those in the last row, to obtain:

Table 12.: Rate of exponential decay of the ratio of perturbations to solution as per the asymptotic approximations.

η_1 **Ratio**	$\lvert\tilde{\alpha}\rvert$	$\lvert\tilde{v}_c^1\rvert$	$\lvert\tilde{v}_c^2\rvert$	$\lvert\tilde{v}_w^1\rvert$	$\lvert\tilde{v}_w^2\rvert$
Outer Solution	$\gamma_0 - \lambda_2$	$\gamma_0 - 3\lambda_2$	$\gamma_0 - 2\lambda_2$	$\gamma_0 - \lambda_2$	$\gamma_0 - 2\lambda_2$
Inner Solution Outer Boundary	$\gamma_0 - 2\lambda_2$	$\gamma_0 - 3\lambda_2$	$\gamma_0 - 3\lambda_2$	$\gamma_0 - 2\lambda_2$	$\gamma_0 - 2\lambda_2$
Inner Solution Inner Boundary	$\gamma_0 - 2\lambda_2$	$\gamma_0 - 2\lambda_2$	$\gamma_0 - 2\lambda_2$	$\gamma_0 - 2\lambda_2$	$\gamma_0 - 2\lambda_2$.

Additionally, with equation (110), we see that

$$|\tilde{R}(t)|e^{-\lambda_2 t} = |\tilde{R}(t)e^{-\lambda_2 t}| \sim \left|C_0 + \frac{V_c^1(0)}{\gamma_0 - 3\lambda_2} e^{(\gamma_0 - 3\lambda_2)t}\right|.$$

Therefore, from the table and equation above, we may conclude that for the growing travelling solution to be unstable, one of the following exponentials must tend to ∞ when $t \to \infty$:

$$e^{(\gamma_0 - \lambda_2)t}, \qquad e^{(\gamma_0 - 2\lambda_2)t}, \qquad e^{(\gamma_0 - 3\lambda_2)t}.$$

Thus, since $\lambda_2 > 0$, for instability we must have $\gamma_0 - \lambda_2 > 0$.

Conclusion

The growing travelling solutions $(\alpha_h, \mathbf{v}_{cs}, \mathbf{v}_{ws}, \mathbf{R}_*)$ of the two dimensional limit case system with negligible nutrient uptake and cell drag (78) are unstable to two dimensional perturbations when

$$\gamma_0 - \lambda_2 = \frac{\partial S_c}{\partial \alpha}(\alpha_h, C_\infty) - \frac{\alpha_h \Sigma_c'(\alpha_h)}{\hat{\mu}_c} + \lambda_2\Big(\frac{\lambda_c}{\hat{\mu}_c} - 2\Big) > 0,$$

where α_h and λ_2 are defined by

$$\hat{\mu}_c S_c(\alpha_h, C_\infty) = \alpha_h \Sigma_c(\alpha_h), \qquad \lambda_2 = \frac{\Sigma_c(\alpha_h)}{\hat{\mu}_c}.$$

9

CONCLUSION

9.1 SUMMARY

In this thesis, we have studied a two phase model of tumour growth in both one and two dimensions.

First, we performed numerical simulations in the one dimensional case and observed that this model predicts nutrient depletion, cell death, cell movement, the diffusion limited steady state, and the formation of a necrotic core and a thin proliferating rim.

We also explored a limit case with negligible viscosity by studying its well-posedness and performing numerical simulations. Particularly, we obtained the condition

$$\alpha > \alpha_d = 1 - \sqrt{1 - \alpha^*}$$

for the well-posedness of this model and confirmed this with simulations which broke down when the system became ill-posed, i.e. when $\alpha < \alpha_d$. Thus, we suggested and tested a parameter choice, namely $\alpha_{min} = \alpha_d$, that eliminated this problem.

However, due to modelling limitations of the non-viscous limit, we decided to revisit the study of the full one dimensional two phase model of tumour growth in order to characterise its steady state solutions and perform a stability analysis. In doing this, we discovered that the

homogeneous steady state solutions were all trivial and thus attempted to find a non-trivial non-homogeneous steady state.

During this search, we discovered a more tractable limit case (with negligible nutrient uptake and cell drag) with interesting non-homogeneous time dependent solutions, which we called travelling solutions, namely,

$$(\alpha_h, v_s(x), R_*(t)) = (\alpha_h, \lambda_2 x, R_0 e^{\lambda_2 t}),$$

where α_h and λ_2 are defined by

$$\hat{\mu}_c S_c(\alpha_h, C_\infty) = \alpha_h \Sigma_c(\alpha_h), \qquad \lambda_2 = \frac{\Sigma_c(\alpha_h)}{\hat{\mu}_c}.$$

Based on the biological implications of the definition

$$\Sigma_c(\alpha) = p_c - p_w,$$

we assumed a sign profile for $\Sigma_c(\alpha)$ in (55) with which it was possible to categorise the travelling solutions into two cases, depending on the sign of $\alpha_h - \alpha^*$. Indeed, these solutions represent a tumour growing exponentially with positive linear velocity in the x direction, or vice versa if

$$\alpha_h > \alpha^*, \quad \lambda_2 > 0 \qquad \text{or} \qquad \alpha_h < \alpha^*, \quad \lambda_2 < 0,$$

respectively. We defined a type of relative stability for these time dependent solutions and thus obtained a condition for instability, namely

$$\lambda_1 = \frac{\partial S_c}{\partial \alpha}(\alpha_h, C_\infty) - \frac{\alpha_h \Sigma_c'(\alpha_h)}{\hat{\mu}_c} - \lambda_2 > 0.$$

By staying in parameter regions were $\lambda_1 < 0$, i.e. where these solutions are stable, we were able to use the stability of the travelling solutions to analytically calculate a critical nutrient concentration that defines whether the tumour will grow or decay. By choosing the nutrient levels outside of the tumour to be $C_\infty = C_{crit} \pm \epsilon$, numerical simulations were performed to check that the tumour will grow if $C_\infty = C_{crit} + \epsilon$ and decay if $C_\infty = C_{crit} - \epsilon$, when all other conditions are kept the same. This was indeed true both in the limit case with negligible nutrient uptake and cell drag and in

the full one dimensional formulation with small nutrient uptake and cell drag. Additionally, we saw that stable travelling solutions were reasonable approximations for solutions of both formulations at least for intermediate times.

Driven by the possibility of gaining information of the full one dimensional formulation via the travelling solutions and the simpler limit case, we continued to work with the limit case in search for unstable solutions. For this, we characterised the relationship between the $\Sigma_c(\alpha)$ function and the instability parameter λ_1 and thus discovered that, with the $\Sigma_c(\alpha)$ function found in the literature, all growing travelling solutions were stable. Thus we performed numerical simulations on a decaying unstable solution with this $\Sigma_c(\alpha)$ and on a growing unstable solution with a newly defined $\Sigma_c(\alpha)$. Simulations of the limit case with negligible nutrient uptake and cell drag confirmed the linear stability analysis. The stable travelling solutions also helped predict the dynamics of the full one dimensional system with small nutrient uptake and cell drag, especially in cases where the tumour is decaying.

However, in comparing the stable travelling solutions with numerical results of the full one dimensional formulation with small nutrient uptake and cell drag in growing cases, we observed that the former approximate the latter only for the initial exponential growth phase and then differ as the tumour growth becomes linear and eventually plateaus (See Figure 102). This limitation accounts for the nutrient uptake becoming more significant as the tumour grows and cells are thus deprived of nutrients in the innermost part of the tumour.

Due to this restriction of the limit case, we attempted to perform a linear stability analysis on the one and two dimensional systems analytically without the assumption of negligible nutrient uptake and cell drag. For this, we formulated the two dimensional system by defining boundary conditions and linearised about a one dimensional solution. However, we concluded that, in both the one and two dimensional cases, this problem

was not tractable analytically. Thus, we decided to return to the two dimensional limit case and its travelling solutions.

Finally, we performed linear stability analysis of the one dimensional travelling solutions on the two dimensional limit case with negligible nutrient uptake and cell drag. For this, we restricted our analysis to travelling solutions where the tumour grows, i.e. $\lambda_2 > 0$, and used the method of matched asymptotic approximations to characterise an outer solution and two inner solutions in boundary layers near the outer and inner boundaries. Having obtained the growth/decay rates of these perturbations when $t \to \infty$, we compared these to the travelling solutions in order to obtain a condition for instability, namely,

$$\gamma_0 - \lambda_2 = \frac{\partial S_c}{\partial \alpha}(\alpha_h, C_\infty) - \frac{\alpha_h \Sigma_c'(\alpha_h)}{\hat{\mu}_c} + \lambda_2\Big(\frac{\lambda_c}{\hat{\mu}_c} - 2\Big) > 0.$$

9.2 CONCLUSION

Therefore, we were able to study the full two phase model in both one and two dimensions through the one dimensional travelling solutions of the limit case with negligible nutrient uptake and cell drag. By performing stability and asymptotic analysis on this limit case, we found conditions for instability of the travelling solutions in relation to both one and two dimensional perturbations. Through simulations, we were able to visualise the effect of instability on the full one dimensional model and also check the asymptotic approximations made for the perturbations in the two dimensional formulation.

9.3 LITERATURE CONTEXT

The two phase model used in this thesis, which was extracted from [19], has been highly cited in recent tumour growth modelling research. However, it has mostly been used as a stepping stone for the definition of more complex models, which are then often explored numerically in two and three dimensions. For example, it has been used as a basis for three, four and $N+1$ phase models of tumour growth in [10], [43] and [63], respectively. Some extensions also explore very complex geometries and intricate numerical schemes, such as [76], [33], and [21].

To my knowledge, the only paper that studies the two phase model found in [19] in detail via asymptotic limits is [9]. Although it deals with several limit cases in one dimension, it does not study the limit case we have chosen to explore in this thesis, with negligible nutrient uptake and cell drag. Therefore, this two phase model has not been studied previously in the context of the particular limit case and its travelling solutions that were defined in Chapter 4.

Additionally, the two dimensional definition of this two phase model has not been described completely (with boundary conditions and a moving boundary formulation) as it was in Chapter 7. Therefore, the asymptotic approximations and the stability result obtained in Chapter 8 are certainly a novelty in the literature.

9.4 BIOLOGICAL RELEVANCE

Through simulations, this work has provided a confirmation of the relevance of this two phase model in portraying expected tumour dynamics. Indeed, we observed nutrient depletion, cell death, cell movement, the diffusion limited steady state, and the formation of a necrotic core and a thin proliferating rim in the graphs of numerical solutions in Chapter 3.

Thus, with only two phases, the model is complex enough to portray the expected tumour dynamics.

Additionally, through linear stability analysis of the travelling solutions of the limit case, we were able to justify important predictions regarding the evolution of the tumour within the initial exponential grow or decay phase that also determine whether the tumour will grow and eventually reach a diffusion limited steady state or shrink and ultimately disappear. These were:

1. By exploring stable solutions, we were able to analytically define an approximation for a critical external nutrient concentration that dictates whether the tumour will grow or decay (Section 4.4).

2. Stable travelling solutions of the limit case predict behaviour of the solution of the original two phase model for intermediate times (Chapter 5).

3. Through the definition of a new $\Sigma_c(\alpha)$ function, we were able to see bistability and a critical natural cell packing density generated by the unstable solution (Section 5.3). This behaviour can eventually be used to test the plausibility of this new definition of $\Sigma_c(\alpha)$ (or any other that demonstrates bistability) through comparison with *in vitro* experiment results, but this was not within the scope of this thesis.

9.5 FUTURE WORK

Future work may include:

- Perform numerical simulations suggested in Section 8.5.
- Performing numerical simulations of the system of equations satisfied by the inner solutions in order to characterise the two dimensional perturbations further. For this, being that these systems are defined on semi-infinite domains, we must use the first order approximations of the far field behaviour (X, $x \to \infty$) obtained in the previous chapter in order to set appropriate boundary conditions.
- Performing numerical simulations of the two dimensional negligible nutrient uptake and cell drag limit model defined in Subsection 7.2. With this, we hope to observe the effects of the condition of instability obtained in the previous chapter.
- Finally, I hope to relate results obtained in the previous step to the full two phase model with small nutrient uptake and cell drag defined in Section 7.

A

SIMULATIONS OF 1-D MODEL: TESTING C_{crit}

We include in this appendix the results obtained by doing the process described in Section 4.4.

When $C_\infty = C_{crit} + \epsilon$, we may observe that

Table 13.: Important values for cases with $C_\infty = C_{crit} + \epsilon$

Case	C_{crit}	C_∞	α_h	α^*	λ_1	λ_2
Case 2^+	2.0000	2.1000	0.5538	0.55	-2.0017	0.0084
Case 4^+	1.2071	1.3071	0.3036	0.30	-0.6103	0.0052
Case 5^+	0.6598	0.7598	0.1389	0.10	-0.2885	0.0452
Case 6^+	0.5000	0.6000	0.1129	0.10	-0.1714	0.0145

Similarly, choosing $C_\infty = C_{crit} - \epsilon$, we have that

Table 14.: Important values for cases with $C_\infty = C_{crit} - \epsilon$

Case	C_{crit}	C_∞	α_h	α^*	λ_1	λ_2
Case 2^-	2.0000	1.9000	0.5459	0.55	-1.9063	-0.0091
Case 4^-	1.2071	1.1071	0.2960	0.30	-0.5736	-0.0057
Case 5^-	0.6598	0.5598	0.0492	0.10	-0.0843	-0.0534
Case 6^-	0.5000	0.4000	0.0850	0.10	-0.1157	-0.0164

Graphs included below.

$$C_\infty = C_{crit} + \epsilon, \quad \alpha_h > \alpha^*, \quad \lambda_2 > 0, \quad k_0 = Q_0 = 0$$

Case 2^+: $\alpha_h = 0.5538$ and $\lambda_2 = 0.0084$

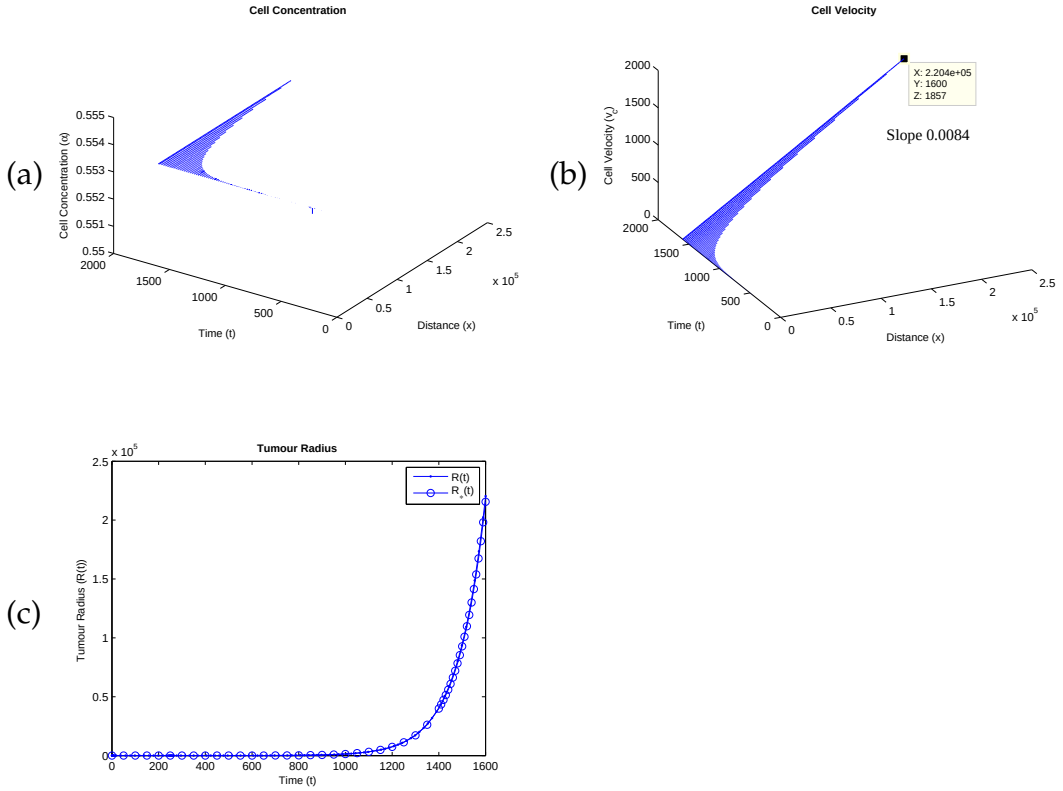
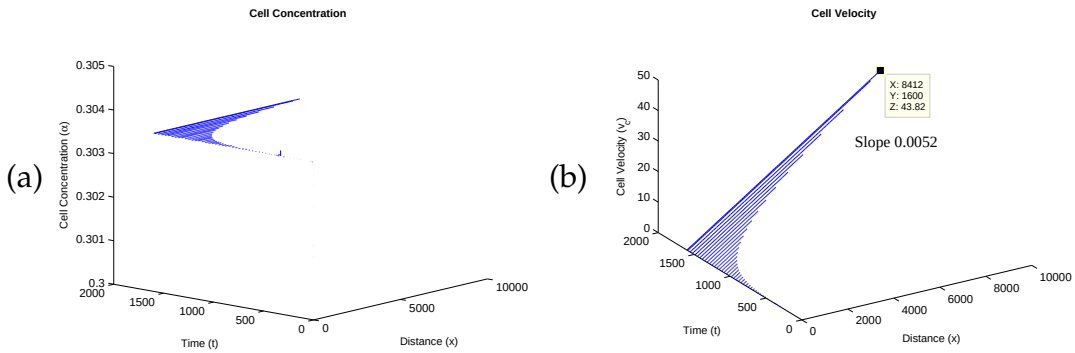


Figure 132.: Evolution of cell concentration (a), cell velocity (b), and tumour radius (c) in Case 2^+ in limit with negligible nutrient uptake and cell drag (i.e. $k_0 = Q_0 = 0$) and $C_\infty = C_{crit} + \epsilon$, $\alpha_h = 0.5538$, and $\lambda_2 = 0.0084$.

Case 4^+: $\alpha_h = 0.3036$ and $\lambda_2 = 0.0052$



(c)

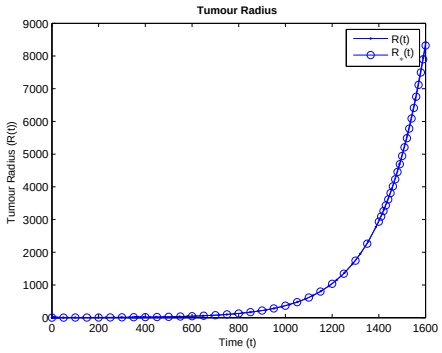
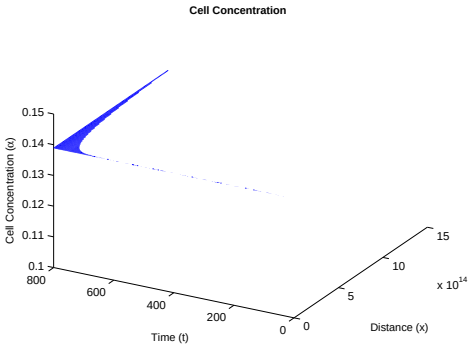


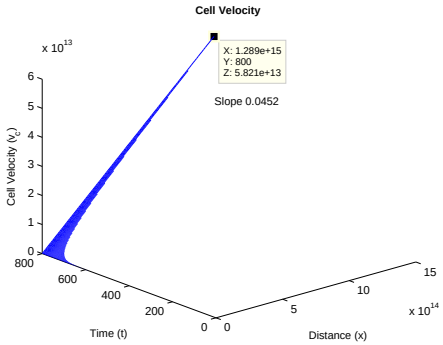
Figure 133.: Evolution of cell concentration (a), cell velocity (b), and tumour radius (c) in Case 4^+ in limit with negligible nutrient uptake and cell drag (i.e. $k_0 = Q_0 = 0$) and $C_\infty = C_{crit} + \epsilon$, $\alpha_h = 0.3036$, and $\lambda_2 = 0.0052$.

Case 5^+: $\alpha_h = 0.1389$ and $\lambda_2 = 0.0452$

(a)



(b)



(c)

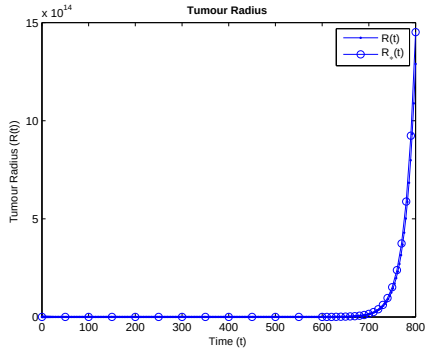


Figure 134.: Evolution of cell concentration (a), cell velocity (b), and tumour radius (c) in Case 5^+ in limit with negligible nutrient uptake and cell drag (i.e. $k_0 = Q_0 = 0$) and $C_\infty = C_{crit} + \epsilon$, $\alpha_h = 0.1389$, and $\lambda_2 = 0.0452$.

Case 6^+: $\alpha_h = 0.1129$ and $\lambda_2 = 0.0145$

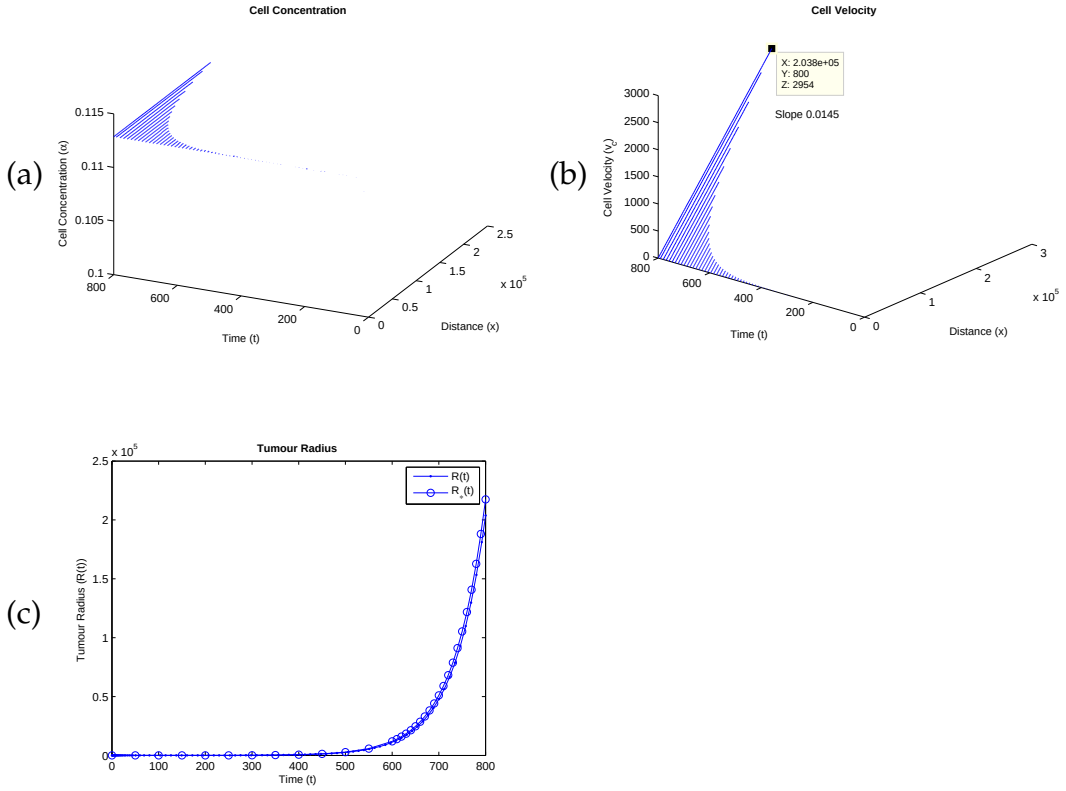
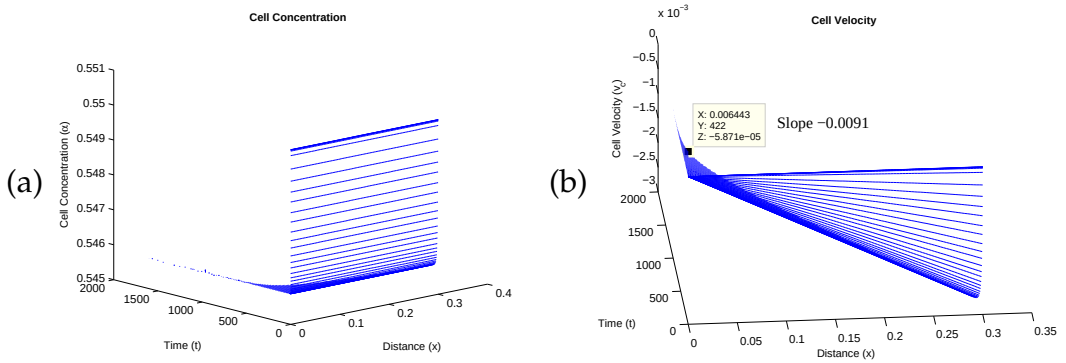


Figure 135.: Evolution of cell concentration (a), cell velocity (b), and tumour radius (c) in Case 6^+ in limit with negligible nutrient uptake and cell drag (i.e. $k_0 = Q_0 = 0$) and $C_\infty = C_{crit} + \epsilon$, $\alpha_h = 0.1129$ and $\lambda_2 = 0.0145$.

$$C_\infty = C_{crit} - \epsilon, \quad \alpha_h < \alpha^*, \quad \lambda_2 < 0, \quad k_0 = Q_0 = 0$$

Case 2^-: $\alpha_h = 0.5459$ and $\lambda_2 = -0.0091$



(c)

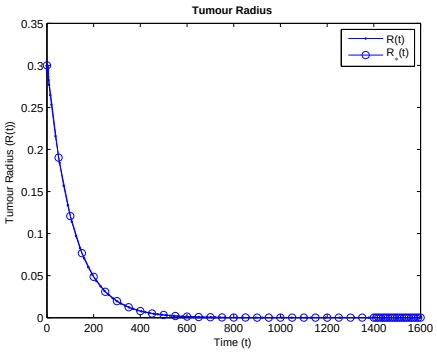
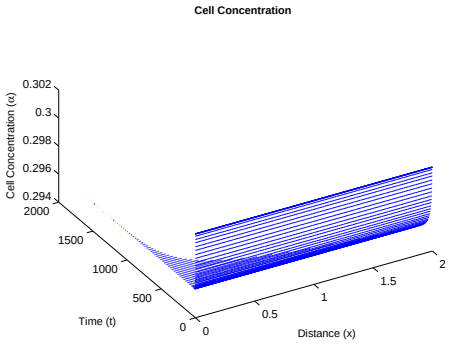


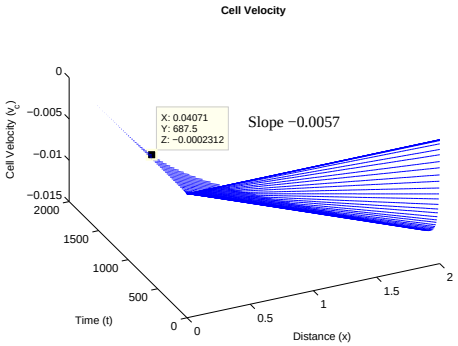
Figure 136.: Evolution of cell concentration (a), cell velocity (b), and tumour radius (c) in Case 2^- in limit with negligible nutrient uptake and cell drag (i.e. $k_0 = Q_0 = 0$) and $C_\infty = C_{crit} - \epsilon$, $\alpha_h = 0.5459$ and $\lambda_2 = -0.0091$.

Case 4^-: $\alpha_h = 0.2960$ and $\lambda_2 = -0.0057$

(a)



(b)



(c)

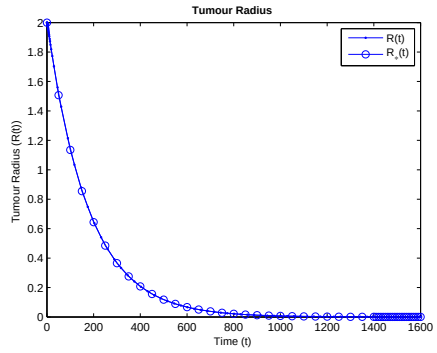


Figure 137.: Evolution of cell concentration (a), cell velocity (b), and tumour radius (c) in Case 4^- in limit with negligible nutrient uptake and cell drag (i.e. $k_0 = Q_0 = 0$) and $C_\infty = C_{crit} - \epsilon$, $\alpha_h = 0.2960$ and $\lambda_2 = -0.0057$.

Case 5$^-$: $\alpha_h = 0.0492$ and $\lambda_2 = -0.0534$

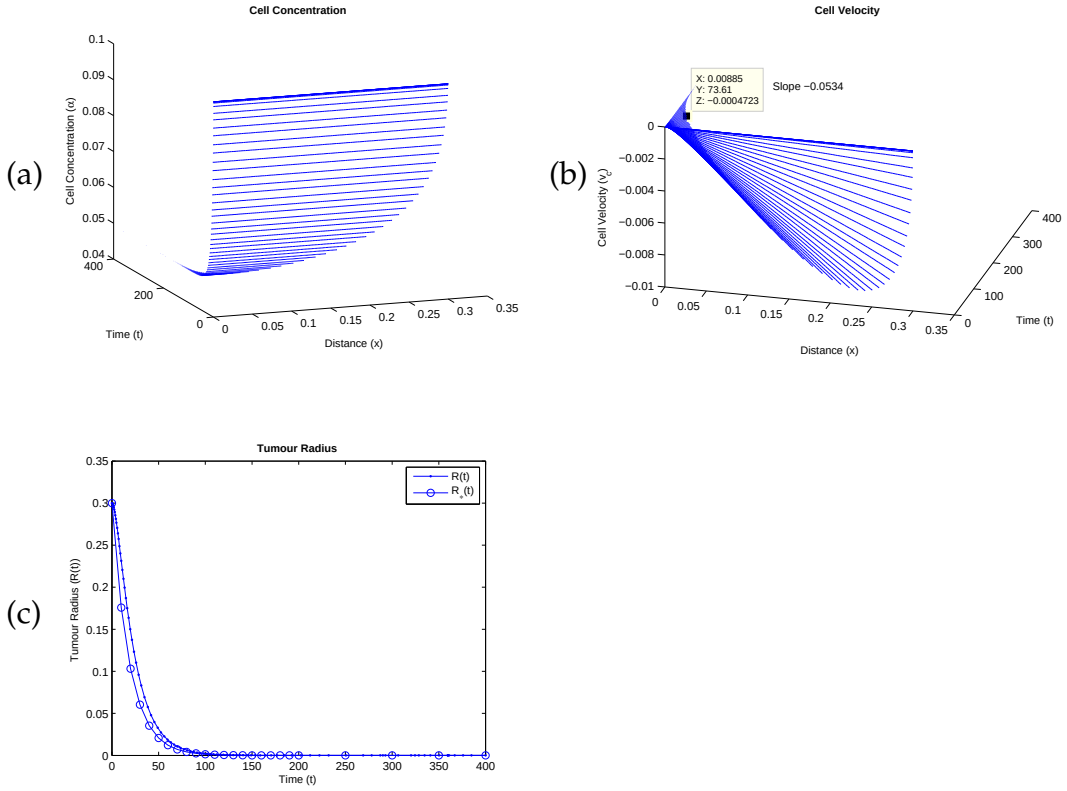
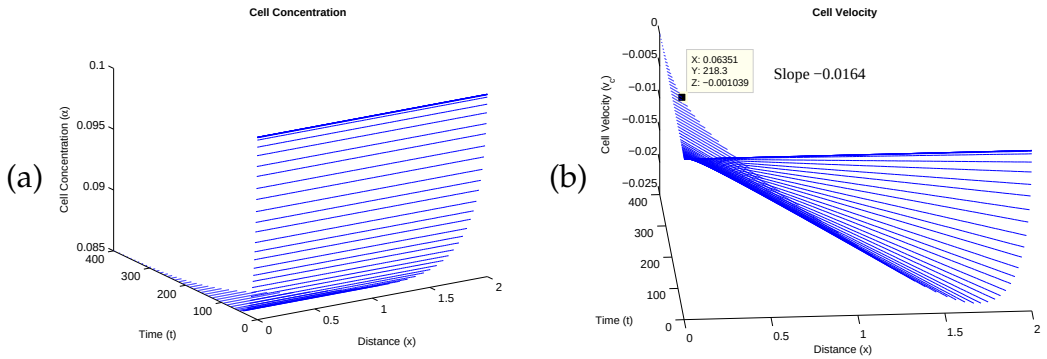


Figure 138.: Evolution of cell concentration (a), cell velocity (b), and tumour radius (c) in Case 5$^-$ in limit with negligible nutrient uptake and cell drag (i.e. $k_0 = Q_0 = 0$) and $C_\infty = C_{crit} - \epsilon$, $\alpha_h = 0.0492$ and $\lambda_2 = -0.0534$.

Case 6$^-$: $\alpha_h = 0.0850$ and $\lambda_2 = -0.0164$



(c)

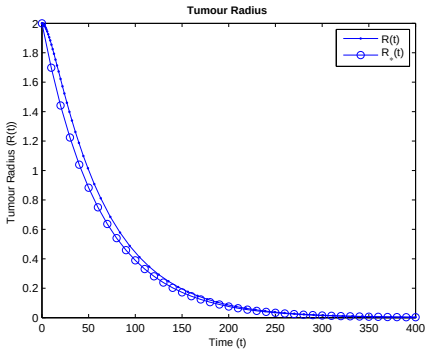


Figure 139.: Evolution of cell concentration (a), cell velocity (b), and tumour radius (c) in Case 6^- in limit with negligible nutrient uptake and cell drag (i.e. $k_0 = Q_0 = 0$) and $C_\infty = C_{crit} - \epsilon$, $\alpha_h = 0.0850$ and $\lambda_2 = -0.0164$.

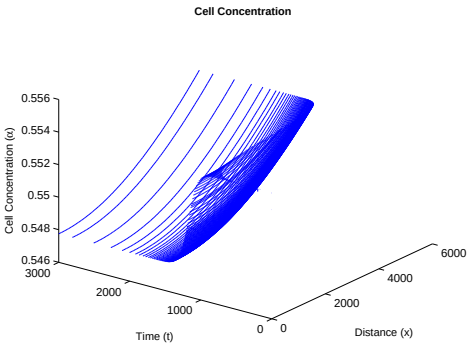
Since $\alpha(x,0)$ is taken to be α^*, rather than a value closer to α_h, the fit will not be perfect, especially when α^* is very small, as in Cases 5 & 6. However, since the purpose of Section 4.4 is to view the dependence of the solution on C_∞ we chose to keep all other parameters fixed and vary only C_∞.

Now consider the same graphs as above, but obtained from the full one dimensional system with small nutrient uptake and cell drag.

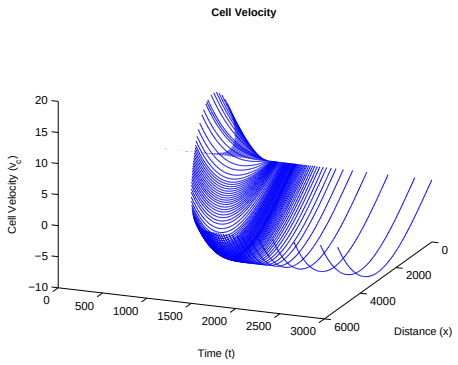
$C_\infty = C_{crit} + \epsilon, \quad \alpha_h > \alpha^*, \quad \lambda_2 > 0, \quad k_0, Q_0$ small

Case 2^+: $\alpha_h = 0.5538$ and $\lambda_2 = 0.0084$

(a)



(b)



(c)

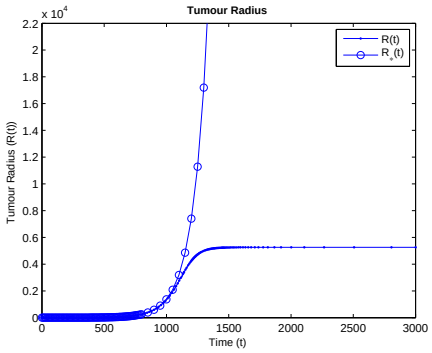
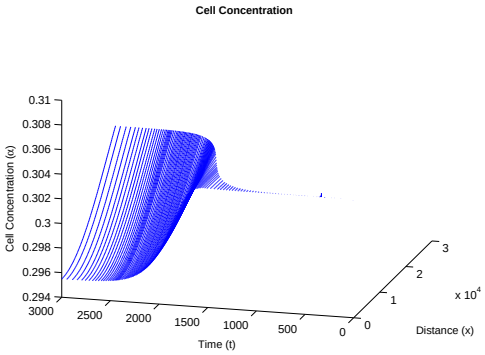


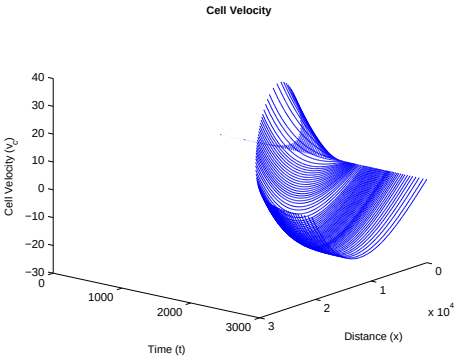
Figure 140.: Evolution of cell concentration (a), cell velocity (b), and tumour radius (c) in Case 2^+ with small nutrient uptake and cell drag (i.e. k_0, Q_0 small) and $C_\infty = C_{crit} + \epsilon$, $\alpha_h = 0.5538$, and $\lambda_2 = 0.0084$.

Case 4^+: $\alpha_h = 0.3036$ and $\lambda_2 = 0.0052$

(a)



(b)



(c)

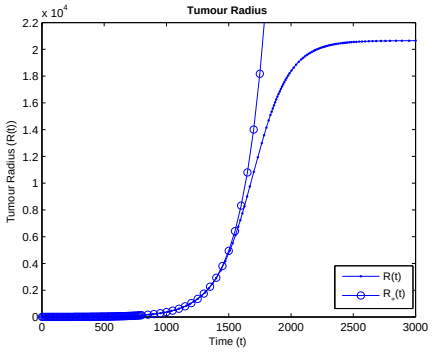
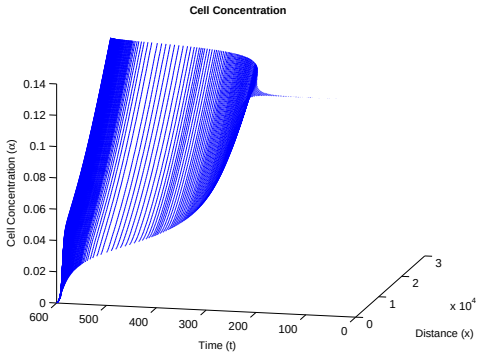


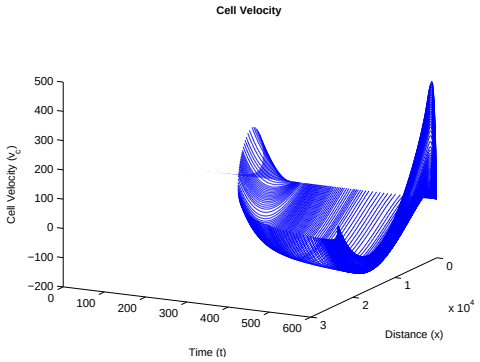
Figure 141.: Evolution of cell concentration (a), cell velocity (b), and tumour radius (c) in Case 4^+ with small nutrient uptake and cell drag (i.e. k_0, Q_0 small) and $C_\infty = C_{crit} + \epsilon$, $\alpha_h = 0.3036$, and $\lambda_2 = 0.0052$.

Case 5^+: $\alpha_h = 0.1389$ and $\lambda_2 = 0.0452$

(a)



(b)



(c)

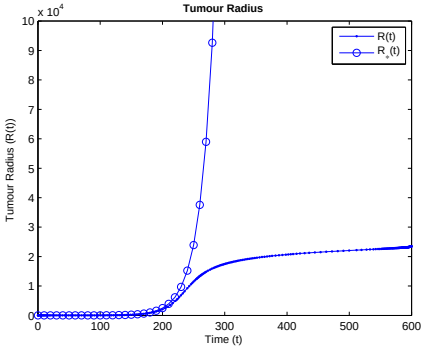
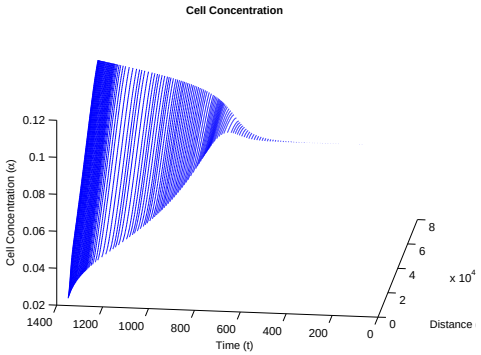


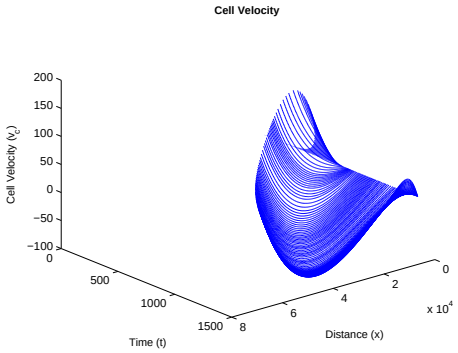
Figure 142.: Evolution of cell concentration (a), cell velocity (b), and tumour radius (c) in Case 5^+ with small nutrient uptake and cell drag (i.e. k_0, Q_0 small) and $C_\infty = C_{crit} + \epsilon$, $\alpha_h = 0.1389$, and $\lambda_2 = 0.0452$.

Case 6^+: $\alpha_h = 0.1129$ and $\lambda_2 = 0.0145$

(a)



(b)



(c)

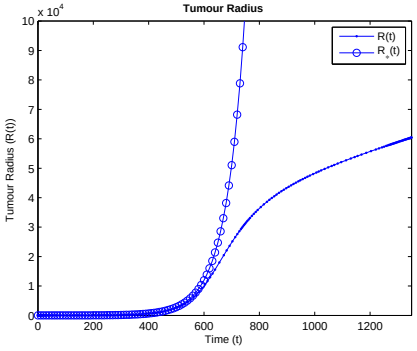
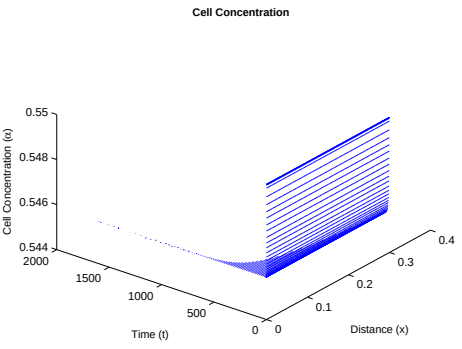


Figure 143.: Evolution of cell concentration (a), cell velocity (b), and tumour radius (c) in Case 6^+ with small nutrient uptake and cell drag (i.e. k_0, Q_0 small) and $C_\infty = C_{crit} + \epsilon$, $\alpha_h = 0.1129$, and $\lambda_2 = 0.0145$.

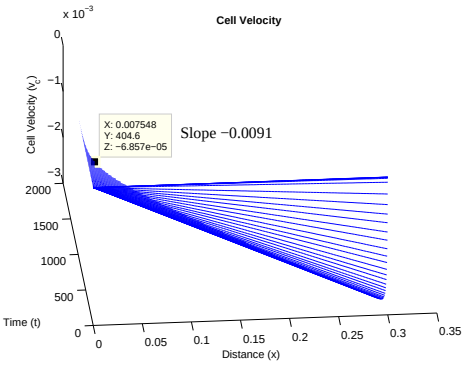
$$C_\infty = C_{crit} - \epsilon, \quad \alpha_h < \alpha^*, \quad \lambda_2 < 0, \quad k_0, Q_0 \text{ small}$$

Case 2^-: $\alpha_h = 0.5459$ and $\lambda_2 = -0.0091$

(a)



(b)



(c)

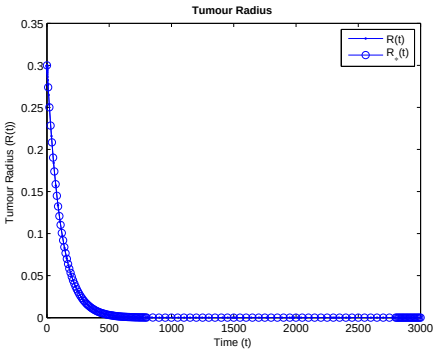
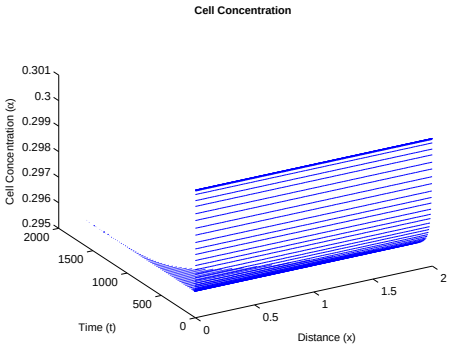


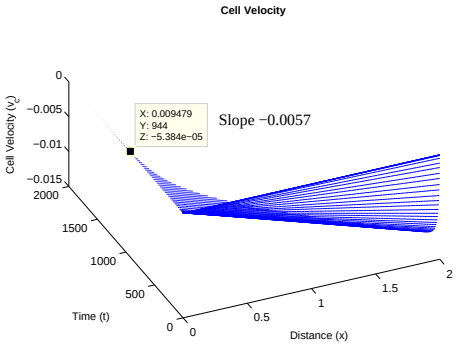
Figure 144.: Evolution of cell concentration (a), cell velocity (b), and tumour radius (c) in Case 2^- with small nutrient uptake and cell drag (i.e. k_0, Q_0 small) and $C_\infty = C_{crit} - \epsilon$, $\alpha_h = 0.5459$, and $\lambda_2 = -0.0091$.

Case 4^-: $\alpha_h = 0.2960$ and $\lambda_2 = -0.0057$

(a)



(b)



(c)

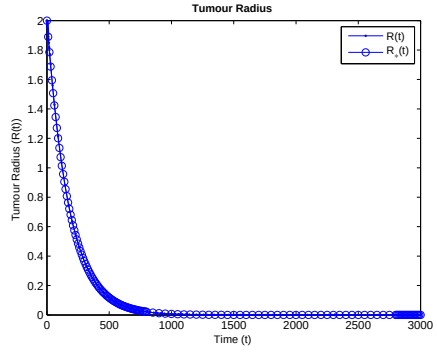


Figure 145.: Evolution of cell concentration (a), cell velocity (b), and tumour radius (c) in Case 4^- with small nutrient uptake and cell drag (i.e. k_0, Q_0 small) and $C_\infty = C_{crit} - \epsilon$, $\alpha_h = 0.2960$, and $\lambda_2 = -0.0056$.

Case 5$^-$: $\alpha_h = 0.0492$ and $\lambda_2 = -0.0534$

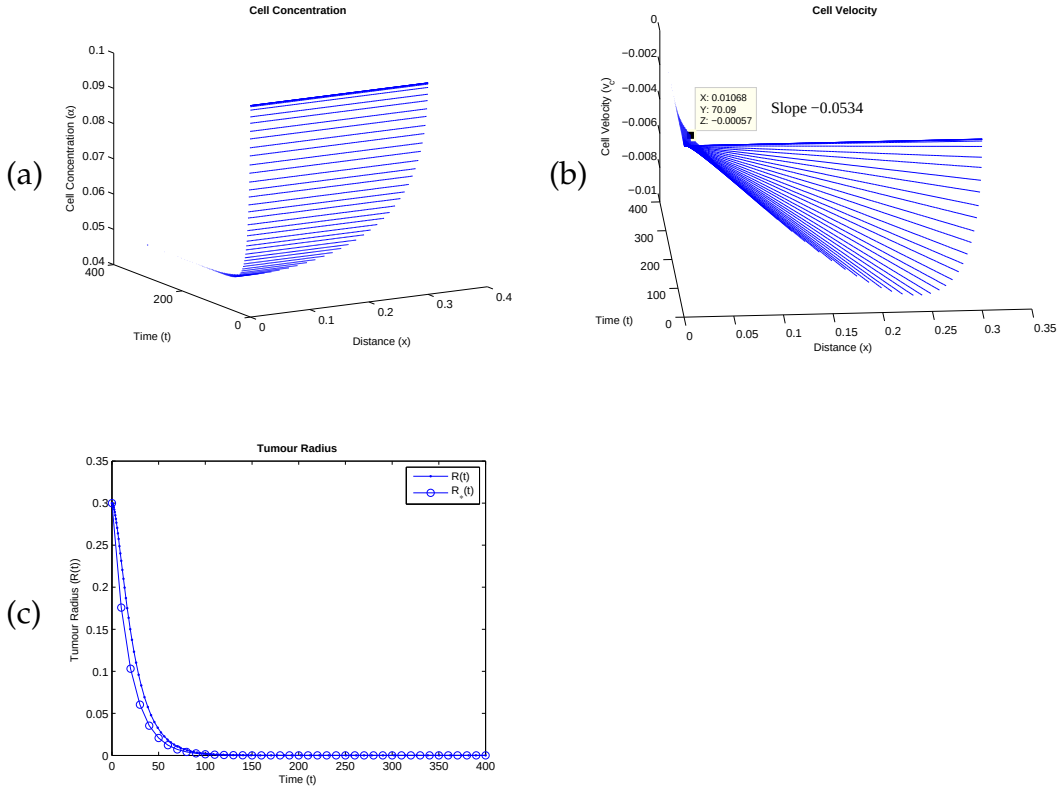


Figure 146.: Evolution of cell concentration (a), cell velocity (b), and tumour radius (c) in Case 4$^-$ with small nutrient uptake and cell drag (i.e. k_0, Q_0 small) and $C_\infty = C_{crit} - \epsilon$, $\alpha_h = 0.0492$, and $\lambda_2 = -0.0534$.

Case 6$^-$: $\alpha_h = 0.0850$ and $\lambda_2 = -0.0164$

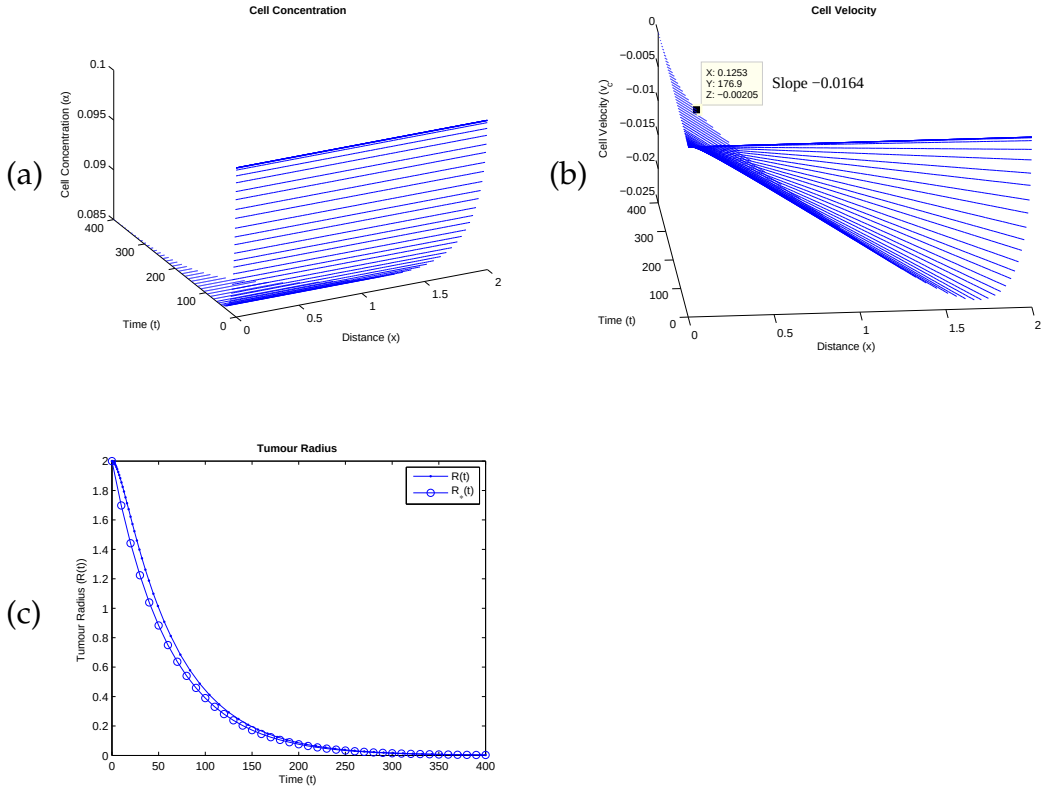


Figure 147.: Evolution of cell concentration (a), cell velocity (b), and tumour radius (c) in Case 4$^-$ with small nutrient uptake and cell drag (i.e. k_0, Q_0 small) and $C_\infty = C_{crit} - \epsilon$, $\alpha_h = 0.0850$, and $\lambda_2 = -0.0164$.

B

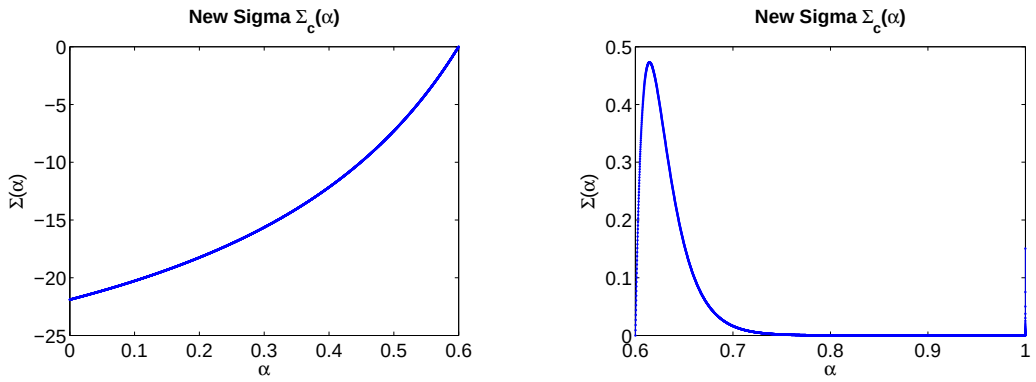
SIMULATIONS OF ONE DIMENSIONAL MODEL WITH DIFFERENT $\Sigma_c(\alpha)$

Consider a new definition for Σ_c:

$$\Sigma_c(\alpha) = \frac{\hat{\Sigma}_c}{b-a} \cdot \frac{e^{-a(\alpha-\alpha^*)} - e^{-b(\alpha-\alpha^*)}}{1-\alpha} H(\alpha-\alpha^*) + \frac{\hat{\Sigma}_c(\alpha-\alpha^*)}{1-\alpha} H(\alpha^*-\alpha), \tag{111}$$

where $a = 50$, $b = 100$ again, and $\hat{\Sigma}_c = 36.5$. We have chosen coefficient $\frac{\hat{\Sigma}_c}{b-a}$ to guarantee continuity of $\Sigma_c'(\cdot)$ at $\alpha = \alpha^*$ and the value of $\hat{\Sigma}_c$ in order to obtain very similar solutions obtained in section 5.3, for the sake of comparison.

Then, $\Sigma_c(\alpha)$ looks like this:



The greatest difference between this Σ_c and the previous one takes place when $\alpha < \alpha^*$, i.e. the graph on the left. Therefore, since the three solutions obtained in the previous section were growing (i.e. $\alpha_h > \alpha^*$), we do not expect much of a difference in the behaviour of these solutions, and

indeed simulations show that this is also a bistable case and solutions are comparable to those obtained in Section the Section 5.3

Indeed, in this case we also obtain bi-stability and, with the notation used in the chapter 4, the solutions are defined by the values

i	α_{h_i}	λ_1	λ_2
1	0.6044	-26.5396	0.2913
2	0.6425	4.2117	0.2151
3	0.7492	-1.4418	0.0017

We will call these solutions 1, 2, and 3, respectively. Since $\lambda_2 > 0$, these are all cases where $R_*(t)$ grows exponentially, and $\lambda_1 > 0$ in the second solution implies that solution 2 is unstable.

Indeed, if we simulate solutions with initial conditions near each one of these solutions, we see the following results, which mirror those seen in Section 5.3.

Perturbation off of Solution 1, with $k_0 = 0 = Q_0$, $\lambda_2 > 0$, $\lambda_1 < 0$, $\alpha_h > 0$,

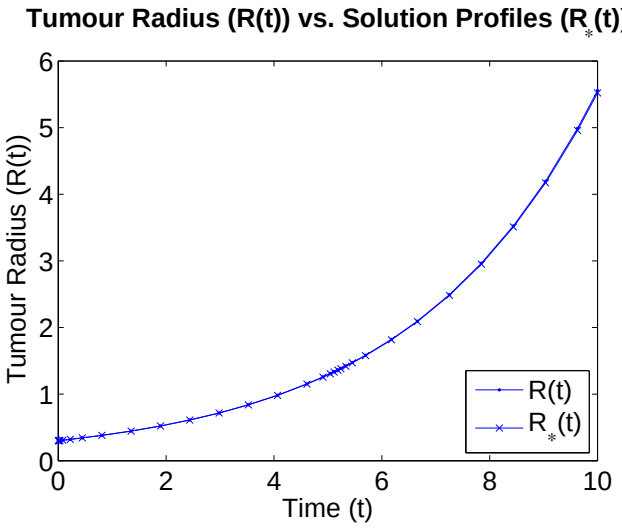


Figure 148.: Evolution of tumour radius, with $k_0 = 0 = Q_0$

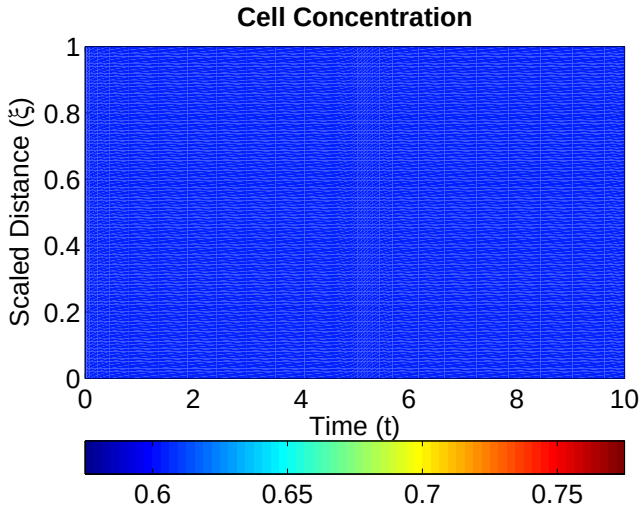


Figure 149.: Evolution of the cell concentration, with $k_0 = 0 = Q_0$

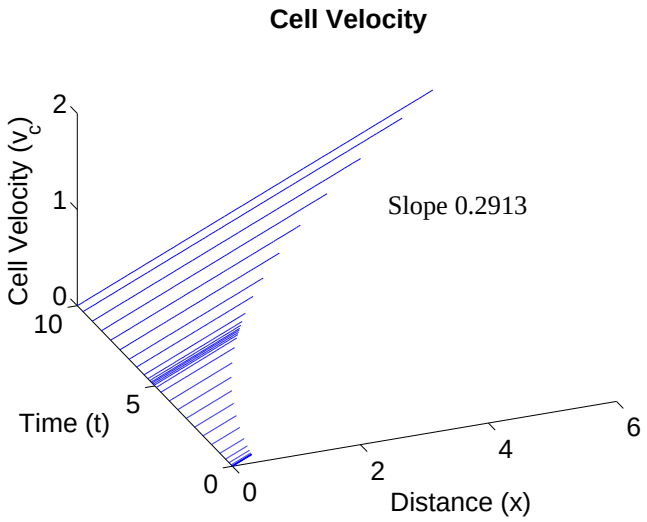


Figure 150.: Evolution of the cell velocity, with $k_0 = 0 = Q_0$

Perturbation above Solution 2, with $k_0 = 0 = Q_0$

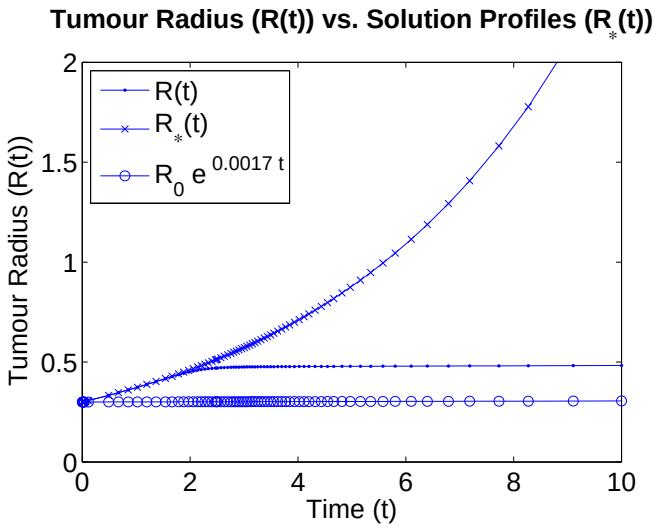


Figure 151.: Evolution of tumour radius, with $k_0 = 0 = Q_0$

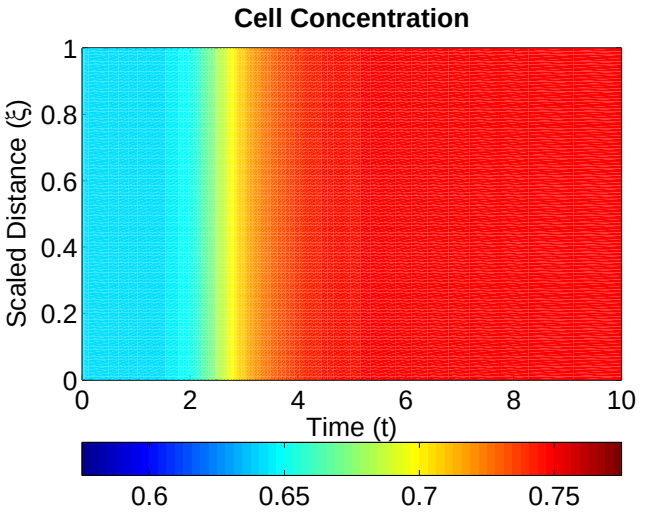


Figure 152.: Evolution of the cell concentration, with $k_0 = 0 = Q_0$

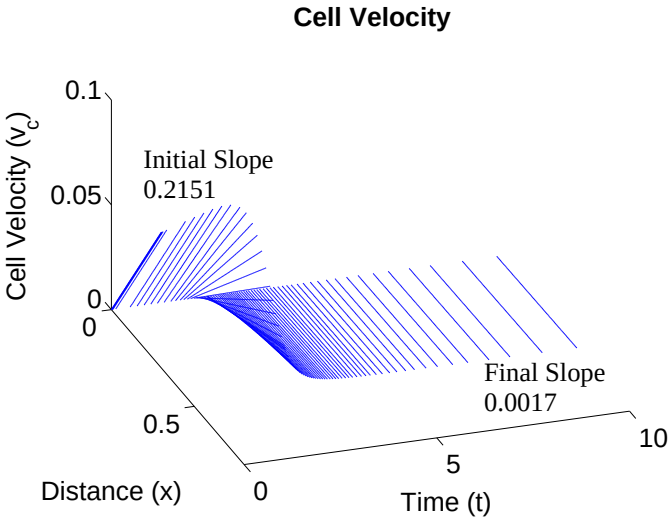


Figure 153.: Evolution of the cell velocity, with $k_0 = 0 = Q_0$

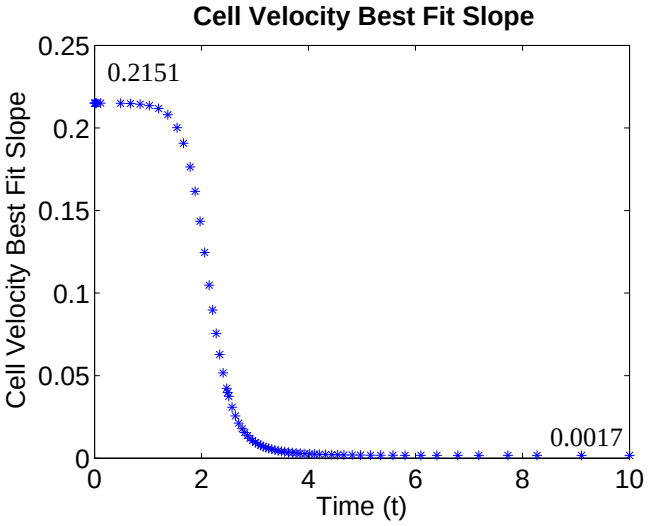


Figure 154.: Evolution of the slope of cell velocity, with $k_0 = 0 = Q_0$

Perturbation below Solution 2, with $k_0 = 0 = Q_0$

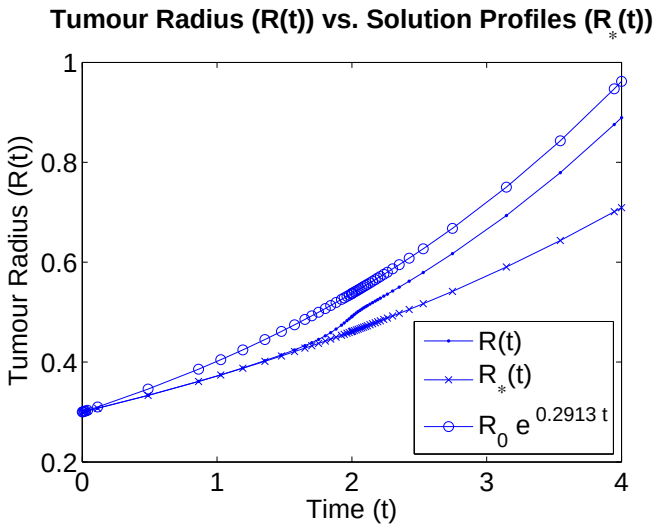


Figure 155.: Evolution of tumour radius, with $k_0 = 0 = Q_0$

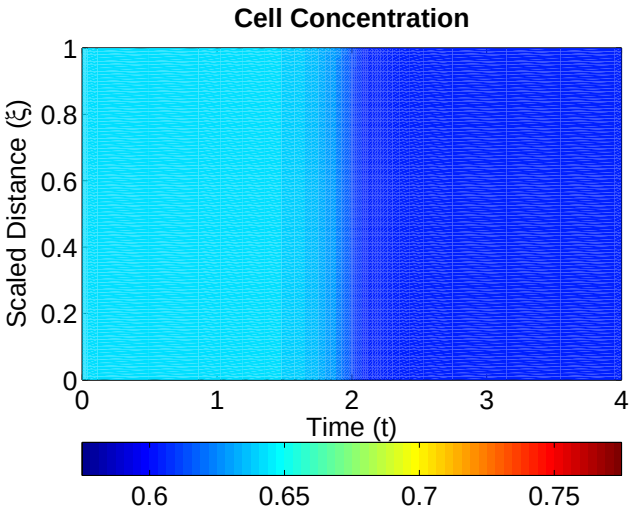


Figure 156.: Evolution of the cell concentration, with $k_0 = 0 = Q_0$

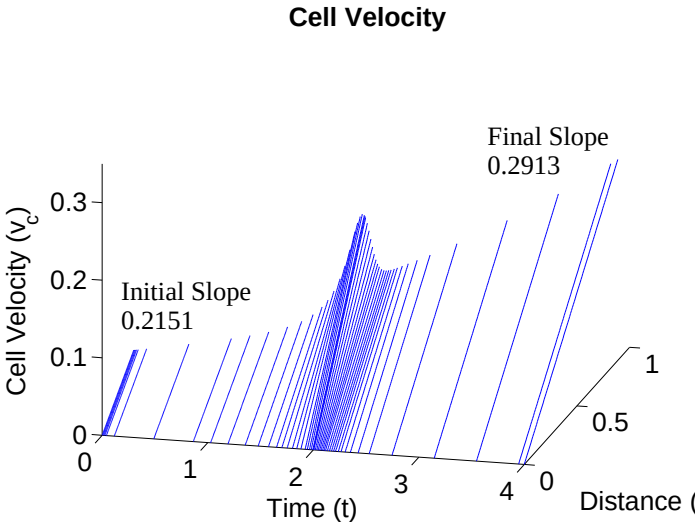


Figure 157.: Evolution of the cell velocity, with $k_0 = 0 = Q_0$

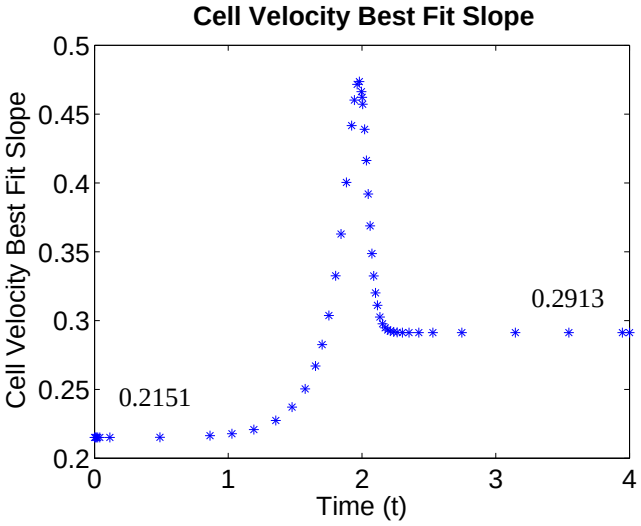


Figure 158.: Evolution of the slope of cell velocity, with $k_0 = 0 = Q_0$

Perturbation off of Solution 3, with $k_0 = 0 = Q_0$

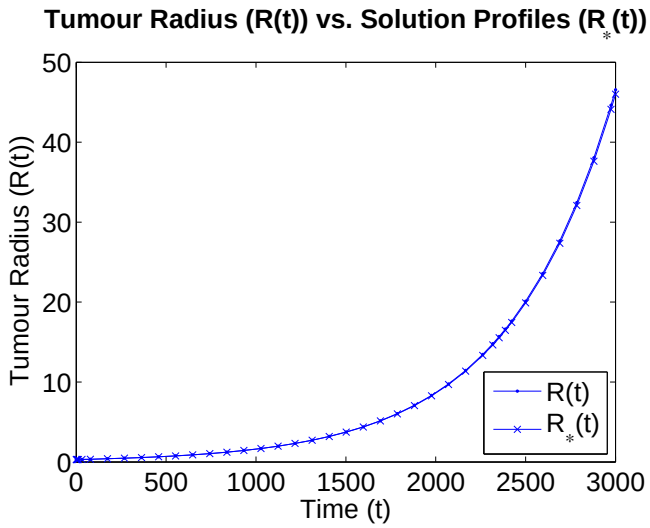


Figure 159.: Evolution of tumour radius, with $k_0 = 0 = Q_0$

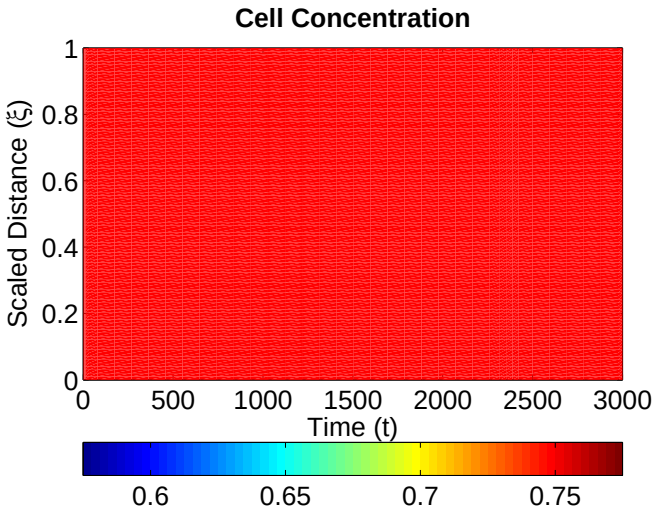


Figure 160.: Evolution of the cell concentration, with $k_0 = 0 = Q_0$

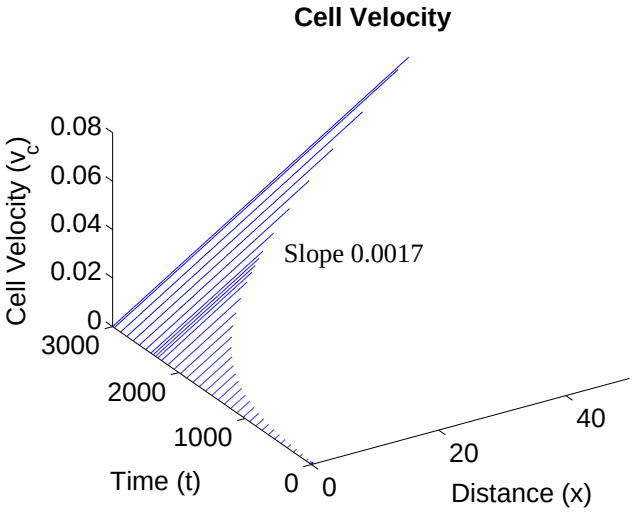


Figure 161.: Evolution of the cell velocity, with $k_0 = 0 = Q_0$

Perturbation off of Solution 1, with k_0, Q_0 small

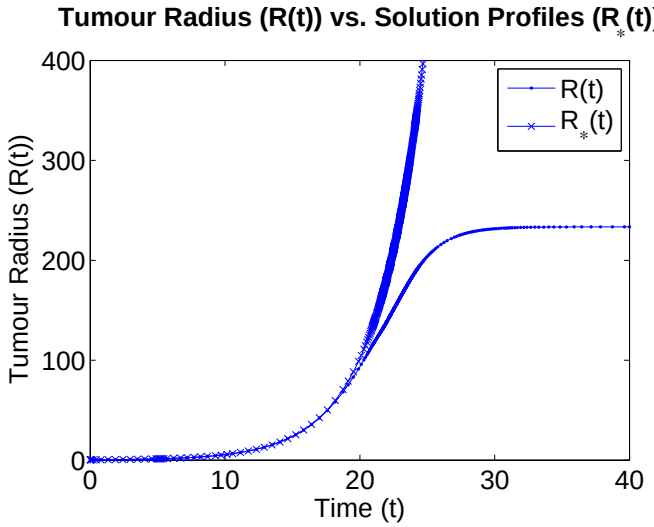


Figure 162.: Evolution of tumour radius, with k_0, Q_0 small

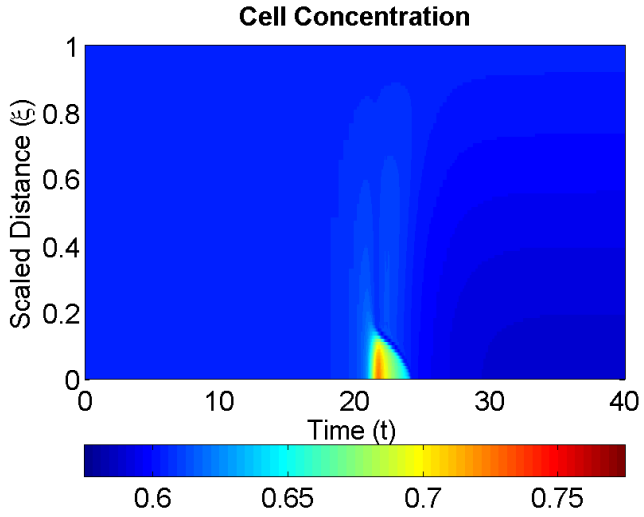


Figure 163.: Evolution of the cell concentration, with k_0, Q_0 small

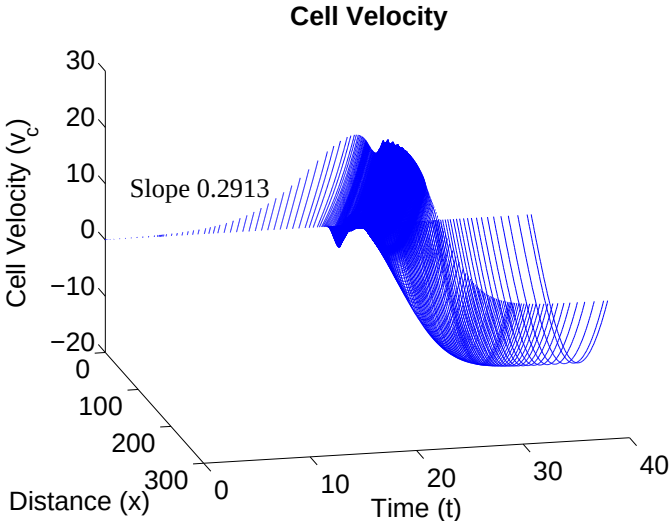


Figure 164.: Evolution of the cell velocity, with k_0, Q_0 small

Perturbation above Solution 2, with k_0, Q_0 small

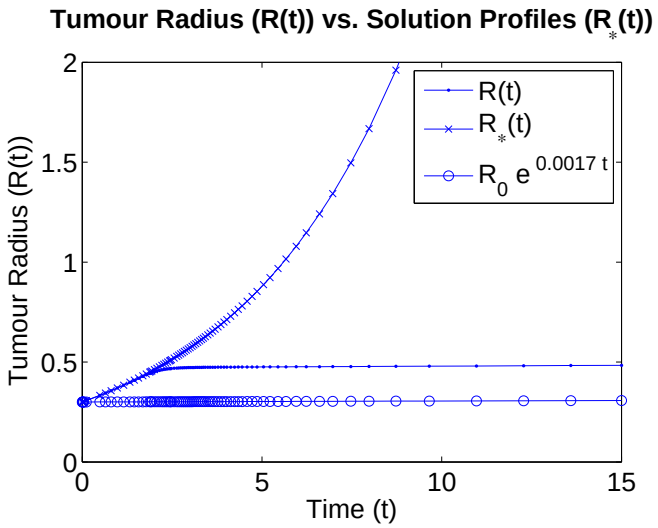


Figure 165.: Evolution of tumour radius, with k_0, Q_0 small

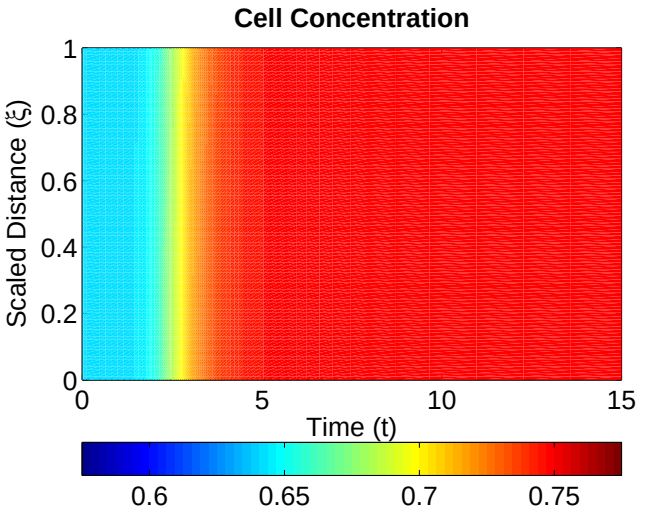


Figure 166.: Evolution of the cell concentration, with k_0, Q_0 small

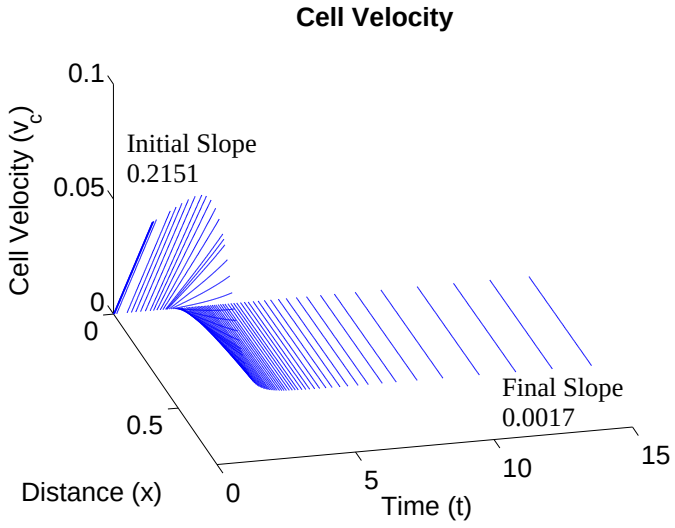


Figure 167.: Evolution of the cell velocity, with k_0, Q_0 small

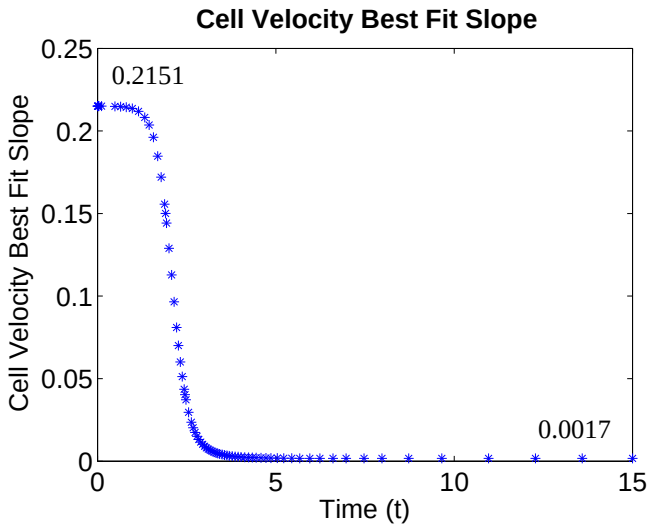


Figure 168.: Evolution of the slope of cell velocity, with k_0, Q_0 small

Perturbation below Solution 2, with k_0, Q_0 small

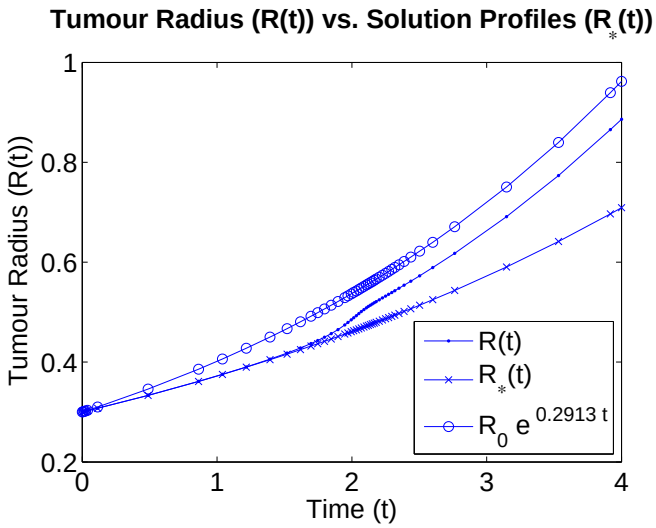


Figure 169.: Evolution of tumour radius, with k_0, Q_0 small

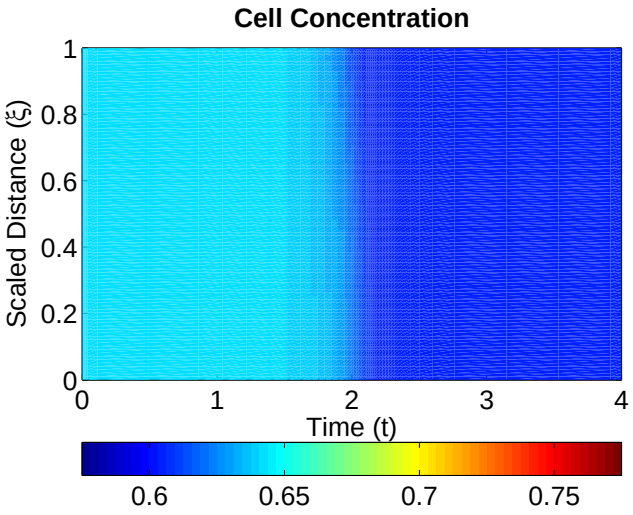


Figure 170.: Evolution of the cell concentration, with k_0, Q_0 small

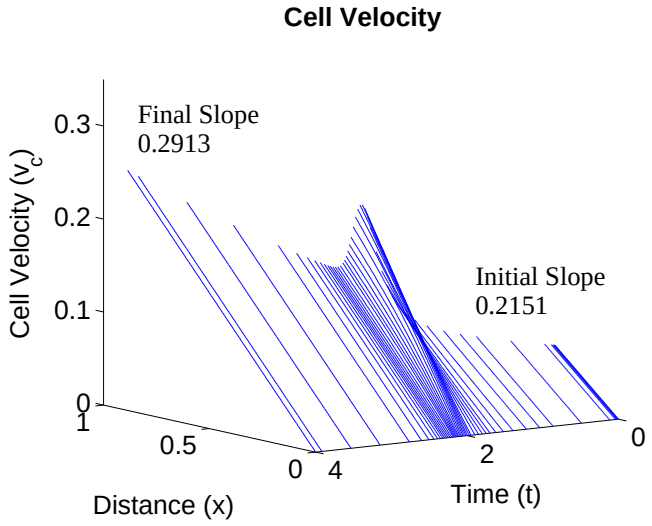


Figure 171.: Evolution of the cell velocity, with k_0, Q_0 small

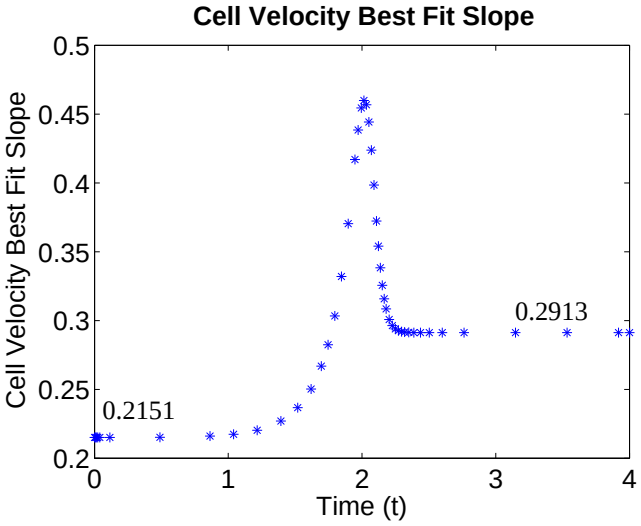


Figure 172.: Evolution of the slope of cell velocity, with k_0, Q_0 small

Perturbation off of Solution 3, with k_0, Q_0 small

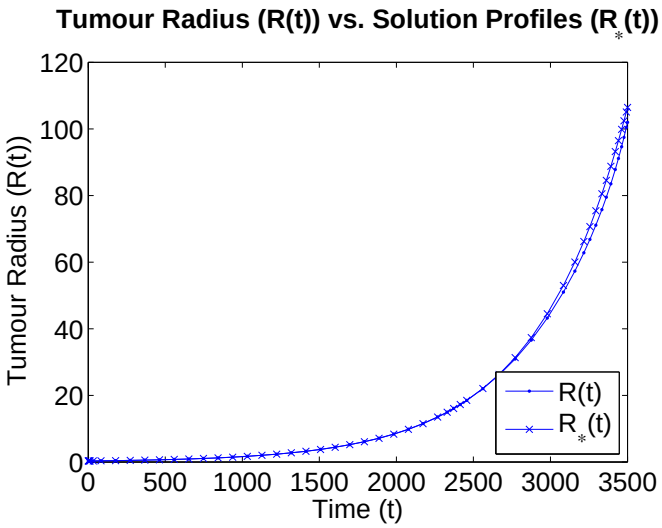


Figure 173.: Evolution of tumour radius, with k_0, Q_0 small

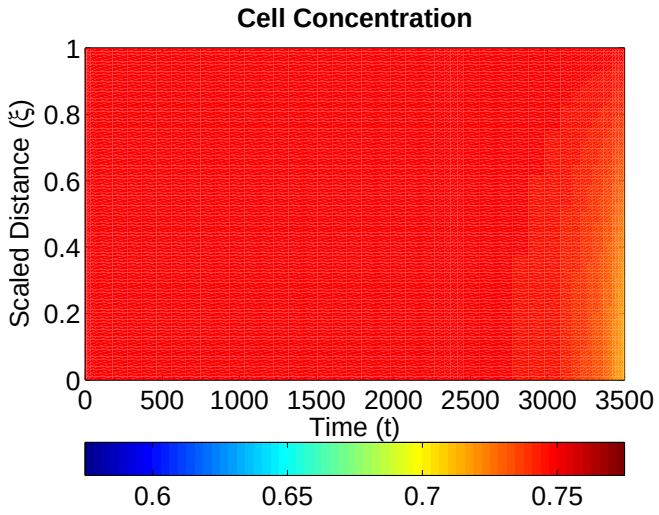


Figure 174.: Evolution of the cell concentration, with k_0, Q_0 small

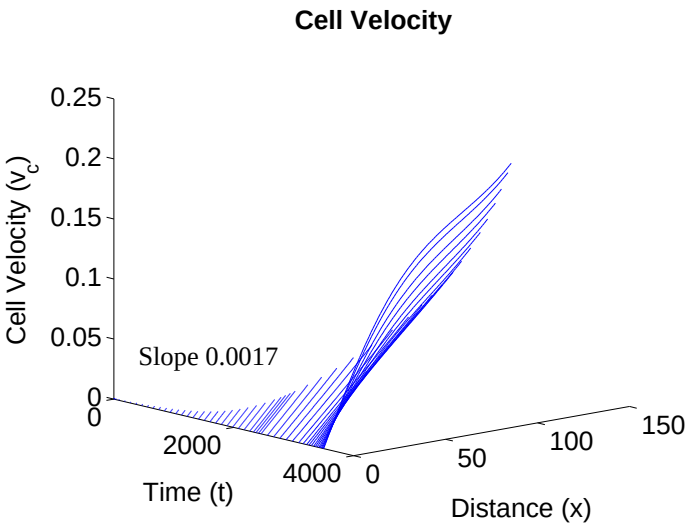


Figure 175.: Evolution of the cell velocity, with k_0, Q_0 small

C

DETAILS OF CHAPTER 8

C.1 DISCARDING TRIVIAL ASYMPTOTIC BALANCES

In Chapter 8, we stated that the possible asymptotic balances for the inner solution near the inner boundary $\xi = 0$ are

Case 1: $\beta > 1$, $a_1 - a_0 + \lambda_2(\beta - 1) = 0, \quad a_2 - a_0 + 2\lambda_2(\beta - 1) = 0,$
$b_1 - a_0 + \lambda_2(\beta - 1) = 0$, $b_2 - a_0 + 2\lambda_2(\beta - 1) = 0,$

Case 2: $\beta < 1$, $a_1 - a_0 - \lambda_2(\beta - 1) = 0, \quad a_2 - a_0 = 0,$
$b_1 - a_0 + \lambda_2(\beta - 1) = 0, \quad b_2 - a_0 = 0,$

Case 3: $\beta = 1$, $a_0 = a_1 = a_2$ and $b_1 = b_2 > a_0$,

Case 4: $\beta = 1$ and $a_0 = a_1 = a_2 = b_1 = b_2$.

Indeed, these cases can be characterized in the same way as in Section 8.3.

In this section, we will consider Cases 1, 2, and 3 separately in order to explain why these cases may be discarded as being trivial.

Case 1: $\beta > 1$

Here, $\beta > 1$ and

$$\begin{aligned} a_1 - a_0 + \lambda_2(\beta - 1) &= 0, \qquad a_2 - a_0 + 2\lambda_2(\beta - 1) = 0, \\ b_1 - a_0 + \lambda_2(\beta - 1) &= 0, \qquad b_2 - a_0 + 2\lambda_2(\beta - 1) = 0, \end{aligned}$$

and the asymptotic balance obtained in this case is given by the following ordinary differential system:

$$\begin{cases} 0 &= \Big[\frac{\partial S_c}{\partial \alpha}(\alpha_h, C_\infty) - a_0 - \gamma_0 - \lambda_2\Big(1+\beta x\frac{d}{dx}\Big)\Big]A - \alpha_h R_0^{\beta-1}\frac{dV_c^1}{dx} \\ 0 &= -\Sigma_c'(\alpha_h)\frac{dA}{dx} + \hat{\mu}_c R_0^{\beta-1}\frac{d^2V_c^1}{dx^2} \\ 0 &= \Big(-\Sigma_c(\alpha_h) - \alpha_h\Sigma_c'(\alpha_h) + \lambda_c\lambda_2\Big)i\kappa A + \mu_c\alpha_h R_0^{2\beta-2}\frac{d^2V_c^2}{dx^2} \\ &\quad +(\mu_c+\lambda_c)\alpha_h i\kappa R_0^{\beta-1}\frac{dV_c^1}{dx} \\ 0 &= \frac{\lambda_2}{1-\alpha_h}\Big(1+x\frac{d}{dx}\Big)A + \alpha_h R_0^{\beta-1}\frac{dV_c^1}{dx} + (1-\alpha_h)R_0^{\beta-1}\frac{dV_w^1}{dx} \\ 0 &= \frac{i\kappa\lambda_2}{1-\alpha_h}xA + i\kappa\alpha_h R_0^{\beta-1}(V_c^1 - V_w^1) + \alpha_h R_0^{2(\beta-1)}\frac{d}{\partial x}(V_w^2 - V_c^2), \end{cases}$$

with $V_c^1(0) = V_c^2(0) = V_w^1(0) = 0$.

We can solve the system of ordinary differential equations in Case 1 to obtain possible non-trivial solutions. Suppose initially that $a_0 \neq -\frac{\lambda_2\lambda_c}{\hat{\mu}_c}$ and $a_0 \neq \lambda_2(\beta - \frac{\lambda_c}{\hat{\mu}_c})$. Therefore, by solving the first two ordinary differential equations in Case 1, we obtain

$$A(x) = D_1 x^{-\frac{a_0+\frac{\lambda_2\lambda_c}{\hat{\mu}_c}}{\lambda_2\beta}} - \frac{\alpha_h D_0}{\hat{\mu}_c(a_0+\frac{\lambda_2\lambda_c}{\hat{\mu}_c})},$$

$$V_c^1(x) = D_0B_0x - \frac{D_1B_1\lambda_2\beta}{(a_0+\lambda_2(\frac{\lambda_c}{\hat{\mu}_c}-\beta))}x^{-\frac{a_0+\lambda_2(\frac{\lambda_c}{\hat{\mu}_c}-\beta)}{\lambda_2\beta}},$$

where

$$B_0 = \frac{1}{\hat{\mu}_c R_0^{\beta-1}}\Big(1 - \frac{\alpha_h\Sigma_c'(\alpha_h)}{\hat{\mu}_c(a_0+\frac{\lambda_2\lambda_c}{\hat{\mu}_c})}\Big), \qquad B_1 = \frac{\Sigma_c'(\alpha_h)}{\hat{\mu}_c R_0^{\beta-1}}.$$

As before, the terms $e^{a_0t}A(x)$ and $e^{a_1t}V_c^1(x)$ must be matched with the corresponding outer solutions

$$e^{-\gamma_0 t}\tilde{\alpha}(\xi,t) = e^{-\lambda_2 t}\overline{\alpha}(\xi), \qquad e^{-\gamma_0 t}\tilde{v}_c^1(\xi,t) = \frac{\gamma_1}{R_0}e^{-2\lambda_2 t}\frac{d\overline{\alpha}}{d\xi}(\xi),$$

when $x \to \infty$. Indeed, by recasting $A(x)$ in terms of ξ and t using $x = \xi R_*(t)^\beta$, we see that as $x \to +\infty$

$$e^{a_0t}A(x) \sim D_1(R_0^\beta\xi)^{-\frac{a_0+\frac{\lambda_2\lambda_c}{\hat{\mu}_c}}{\lambda_2\beta}}e^{-\frac{\lambda_2\lambda_c}{\hat{\mu}_c}t} - \frac{\alpha_h D_0}{\hat{\mu}_c(a_0+\frac{\lambda_2\lambda_c}{\hat{\mu}_c})}e^{a_0t}.$$

Thus, for matching to be possible, we must have $a_0 = -\lambda_2$ and $D_1 = 0$ because $\hat{\mu}_c = 2\mu_c + \lambda_c > \lambda_c$ and thus $-\frac{\lambda_2\lambda_c}{\hat{\mu}_c} > -\lambda_2$. Similarly, by recasting $V_c^1(x)$ in terms of ξ and t, we see that as $x \to +\infty$

$$e^{a_1 t} V_c^1(x) \sim C_0 B_0(R_0^\beta \xi).$$

Therefore, matching is impossible unless $D_0 = 0$, which would imply that $V_c^1(x) = A(x) = 0$. Thus, this is a trivial case.

If $a_0 = -\dfrac{\lambda_2\lambda_c}{\hat{\mu}_c}$ or $a_0 = \lambda_2(\beta - \dfrac{\lambda_c}{\hat{\mu}_c})$, the expressions for $A(x)$ and $V_c^1(x)$ will be different, but the same reasoning can prove that these are also trivial cases.

Case 2: $\beta < 1$

Here, $\beta < 1$ and

$$\begin{aligned} a_1 - a_0 - \lambda_2(\beta - 1) &= 0, \qquad & a_2 - a_0 &= 0, \\ b_1 - a_0 + \lambda_2(\beta - 1) &= 0, \qquad & b_2 - a_0 &= 0, \end{aligned}$$

and the equations become, in first order,

$$\begin{cases} 0 &= \Big[\dfrac{\partial S_c}{\partial \alpha}(\alpha_h, C_\infty) - a_0 - \gamma_0 - \lambda_2\Big(1 + \beta x \dfrac{d}{dx}\Big)\Big] A - \alpha_h i\kappa V_c^2 \\ 0 &= -\Sigma_c'(\alpha_h)\dfrac{dA}{dx} + (\lambda_c + \mu_c) i\kappa \dfrac{dV_c^2}{dx} - \dfrac{1}{R_0^{\beta-1}} \mu_c \kappa^2 V_c^1 \\ 0 &= \Big(- \Sigma_c(\alpha_h) - \alpha_h \Sigma_c'(\alpha_h) + \lambda_c\lambda_2 \Big) i\kappa A - \alpha_h \kappa^2 \hat{\mu}_c V_c^2 \\ 0 &= \dfrac{\lambda_2}{1 - \alpha_h}\Big(1 + x\dfrac{d}{dx}\Big) A + \alpha_h i\kappa V_c^2 + R_0^{\beta-1}(1 - \alpha_h)\dfrac{dV_w^1}{dx} + i\kappa(1 - \alpha_h) V_w^2 \\ 0 &= \dfrac{\lambda_2}{1 - \alpha_h} x A - \alpha_h R_0^{\beta-1} V_w^1, \end{cases}$$

with $V_c^1(0) = V_c^2(0) = V_w^1(0) = 0$.

We can discard this case because it has already been studied as it corresponds to the outer solution asymptotic balance which has been characterised in section 8.2. Therefore, we may discard Case 2.

in the section where we characterised the outer solution, namely 8.2.

Case 3: $\beta = 1$, $a_0 = a_1 = a_2$ and $b_1 = b_2 > a_0$

Here, $\beta = 1$ and $a_0 = a_1 = a_2$ and $b_1 = b_2 > a_0$ and

$$\begin{cases} 0 &= \Big[\frac{\partial S_c}{\partial \alpha}(\alpha_h, C_\infty) - \gamma_0 - a_0 - \lambda_2\Big(1 + x\frac{d}{dx}\Big)\Big]A - \alpha_h \frac{dV_c^1}{dx} - \alpha_h i\kappa V_c^2 \\ 0 &= -\Sigma_c'(\alpha_h)\frac{dA}{dx} + \hat{\mu}_c \frac{d^2V_c^1}{dx^2} + (\lambda_c + \mu_c)i\kappa \frac{dV_c^2}{dx} - \mu_c \kappa^2 V_c^1 \\ 0 &= \Big(- \Sigma_c(\alpha_h) - \alpha_h \Sigma_c'(\alpha_h) + \lambda_c\lambda_2\Big) i\kappa A + \mu_c \alpha_h \frac{d^2V_c^2}{dx^2} \\ & \quad + (\mu_c + \lambda_c)\alpha_h i\kappa \frac{dV_c^1}{dx} - \alpha_h \kappa^2 \hat{\mu}_c V_c^2 \\ 0 &= \frac{dV_w^1}{dx} + i\kappa V_w^2 \\ 0 &= \frac{dV_w^2}{dx} - i\kappa V_w^1, \end{cases}$$

with $V_c^1(0) = V_c^2(0) = V_w^1(0) = 0$.

Case 3 can be quickly discarded also. Notice that the last two equations in Case 3 (regarding V_w^1 and V_w^2), along with the boundary condition $V_w^1(0) = 0$, imply that $V_w^1(x) = C\sinh(x)$. Consequently, for matching to be possible, we must have $C = 0$ and thus $V_w^1 \equiv 0$. Therefore, although the balance is not trivial, the solution to this case is trivial.

D

VALIDATION OF NUMERICAL RESULTS OF CHAPTER 8

All the numerical checks below were done with the solution of (79) with the boundary condition

$$\tilde{v}_w^2(0,t) = 0$$

instead of the one applied in Chapter 8, namely,

$$\tilde{v}_w^2(1,t) = \frac{i\kappa\lambda_2 R_*(t)}{1-\alpha_h}\tilde{R}(t) + \tilde{v}_c^2(1,t).$$

However, since the checks were performed mainly to confirm the correctness of the code and the asymptotic balance of the outer solution for ξ sufficiently far from $\xi = 0$ and $\xi = 1$ boundaries, we expect that the same can be done for the case with the new boundary condition to obtain similar results.

D.1 CHECKING NUMERICAL DEFINITION OF EQUATION'S RHS

Consider

$$\tilde{\alpha} = -\frac{\lambda_c k}{\Sigma_c'(\alpha_h)}\xi^2, \qquad \tilde{v}_c^1 = \sin\left(\frac{\pi}{2}\xi\right), \qquad \tilde{v}_c^2 = i\sin\left(\frac{\pi}{2}\xi\right),$$
$$\tilde{v}_w^1 = \sin\left(\frac{\pi}{2}\xi\right), \qquad \tilde{v}_w^2 = i\sin\left(\frac{\pi}{2}\xi\right), \qquad \tilde{R} = -\frac{1}{2\lambda_2},$$

which we will call "test functions." Notice initially that these test functions satisfy the boundary conditions. Other than this property, they have been

randomly selected. Now, if we take these and substitute into the right hand side of our equations in (79), we should have

$$\begin{cases} \text{Eq 1} & = -\dfrac{\lambda_c k}{\Sigma_c'(\alpha_h)}\Big[\dfrac{\partial S_c}{\partial \alpha}(\alpha_h, C_\infty) - \lambda_2\Big]\xi^2 - \dfrac{\alpha_h \pi}{2R_*}\cos\left(\dfrac{\pi\xi}{2}\right) + \alpha_h \kappa \sin\left(\dfrac{\pi\xi}{2}\right) \\ \text{Eq 2} & = \dfrac{2\lambda_c \kappa \xi}{R_*} - \Big[\dfrac{\hat{\mu}_c \pi^2}{4R_*^2} + \mu_c \kappa^2\Big]\sin\left(\dfrac{\pi\xi}{2}\right) - \dfrac{(\lambda_c + \mu_c)\pi k}{2R_*}\cos\left(\dfrac{\pi\xi}{2}\right) \\ \text{Eq 3} & = -\dfrac{\Big(-\Sigma_c(\alpha_h) - \alpha_h \Sigma_c'(\alpha_h) + \lambda_c\lambda_2\Big)\lambda_c i\kappa^2}{\Sigma_c'(\alpha_h)}\xi^2 \\ & \quad -\Big[\dfrac{\mu_c \alpha_h i \pi^2}{4R_*^2} + \alpha_h \hat{\mu}_c \kappa^2 i\Big]\sin\left(\dfrac{\pi\xi}{2}\right) + \dfrac{(\lambda_c + \mu_c)\alpha_h \pi i\kappa}{2R_*}\cos\left(\dfrac{\pi\xi}{2}\right) \\ \text{Eq 4} & = -\dfrac{3\lambda_2\lambda_c\kappa}{\Sigma_c'(\alpha_h)(1-\alpha_h)}\xi^2 + \dfrac{\pi}{2R_*}\cos\left(\dfrac{\pi\xi}{2}\right) - k\sin\left(\dfrac{\pi\xi}{2}\right) \\ \text{Eq 5} & = -\dfrac{i\kappa^2\lambda_c\lambda_2}{\Sigma_c'(\alpha_h)(1-\alpha_h)}\xi^3 \\ \text{Eq 6} & = \dfrac{1}{2}. \end{cases}$$

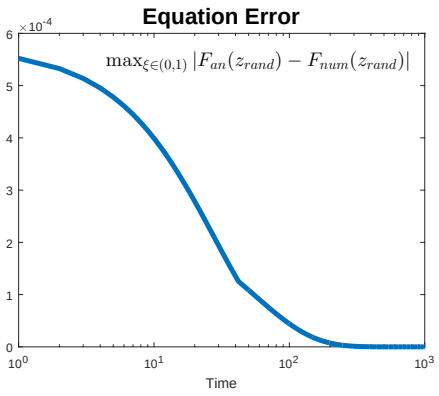
Notice that this was obtained analytically, and thus involves no numerical error.

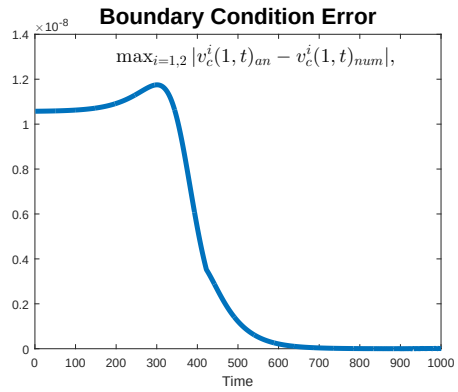
Now, recall that in numerical simulations, we defined a function $F(z,t)$ that represents an approximation of the right hand side of our equations. Applying the function F to the test functions defined above for every $t \in \{1, 2 \dots 1000\}$, we may obtain the numerical approximation of the right hand side of our equations. This, in turn, should be comparable to the equations calculated analytically, represented above. Notice that the only error incurred by using the function F is the one due to the difference approximations of the derivatives in space. Therefore, if the code that defines F is correct, we must expect these to have an error of order $(\Delta\xi)^2$, which in this case is 10^{-4}.

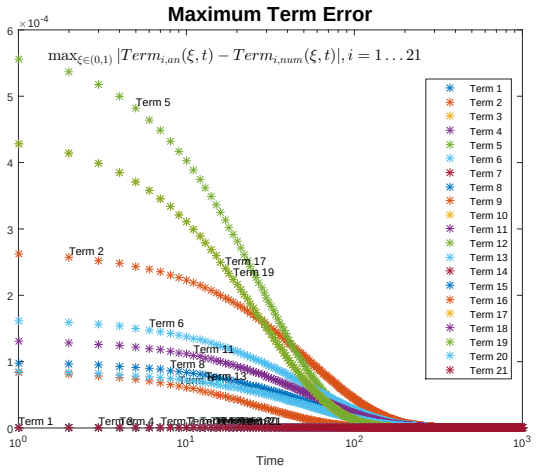
Indeed, we obtain the following maximum error over time and space for each equation:

Equation	Error
1	$2.6196e-04$
2	$5.5216e-04$
3	$9.6894e-05$
4	$2.1575e-04$
5	$1.0164e-05$
6	$1.0573e-08.$

Similarly, we can also track the maximum error of all these equations and boundary values through time and term-by-term to obtain the following results:







In the graph above, terms are counted according to the order corresponding to the terms

$$(\tilde{\alpha}, \tilde{v}_c^1, \tilde{v}_c^2, \tilde{v}_w^1, \tilde{v}_w^2, \tilde{R})$$

in equations 1-6, sequentially. This way, as expected, the last graph shows that terms that do not include a derivative in ξ actually present no error, and are thus represented by the horizontal line at 0×10^{-4}.

Therefore, we conclude that the function F provided to the "ode23t" solver is indeed a faithful approximation of the right hand side of our equations. Furthermore, from the second graph above, we also deduce that the calculation of the values of both $\tilde{v}_c^1(1,t)$ and $\tilde{v}_c^2(1,t)$ (at the boundary) is also adequate.

D.2 CHECKING OUTER SOLUTION

Since all simulations of both outer and inner solutions show a discrepancy with asymptotic approximations for larger times, the checks performed on the outer solutions are enough to prove that these simulations are indeed all correct.

D.2.1 *Checking Outer Solution Asymptotic Balance*

The non-trivial asymptotic balance found analytically for the outer solution in Section 8.2 considers the equations below with the boxed terms being of order smaller than 1:

$$
\begin{cases}
\dfrac{\partial\tilde{\alpha}}{\partial t} &= \Big[\dfrac{\partial S_c}{\partial\alpha}(\alpha_h, C_\infty) - \lambda_2\Big]\tilde{\alpha} - \boxed{\dfrac{\alpha_h}{R_*(t)}\dfrac{\partial\tilde{v}_c^1}{\partial\xi}} - \alpha_h i\kappa\tilde{v}_c^2 \\
0 &= -\dfrac{\Sigma_c'(\alpha_h)}{R_*(t)}\dfrac{\partial\tilde{\alpha}}{\partial\xi} + \boxed{\dfrac{\hat{\mu}_c}{R_*(t)^2}\dfrac{\partial^2\tilde{v}_c^1}{\partial\xi^2}} + \dfrac{(\lambda_c+\mu_c)i\kappa}{R_*(t)}\dfrac{\partial\tilde{v}_c^2}{\partial\xi} - \mu_c\kappa^2\tilde{v}_c^1 \\
0 &= \Big(-\Sigma_c(\alpha_h) - \alpha_h\Sigma_c'(\alpha_h) + \lambda_c\lambda_2\Big)i\kappa\tilde{\alpha} + \boxed{\dfrac{\mu_c\alpha_h}{R_*(t)^2}\dfrac{\partial^2\tilde{v}_c^2}{\partial\xi^2}} \\
&\quad + \boxed{(\mu_c+\lambda_c)\dfrac{\alpha_h i\kappa}{R_*(t)}\dfrac{\partial\tilde{v}_c^1}{\partial\xi}} - \alpha_h\kappa^2\hat{\mu}_c\tilde{v}_c^2 \\
0 &= \dfrac{\lambda_2}{1-\alpha_h}\Big(1+\xi\dfrac{\partial}{\partial\xi}\Big)\tilde{\alpha} + \boxed{\dfrac{\alpha_h}{R_*(t)}\dfrac{\partial\tilde{v}_c^1}{\partial\xi}} + \dfrac{1-\alpha_h}{R_*(t)}\dfrac{\partial\tilde{v}_w^1}{\partial\xi} \\
&\quad + \alpha_h i\kappa\tilde{v}_c^2 + (1-\alpha_h)i\kappa\tilde{v}_w^2 \\
0 &= \boxed{\dfrac{\alpha_h}{R_*(t)^2}\dfrac{\partial}{\partial\xi}(\tilde{v}_w^2 - \tilde{v}_c^2)} - \dfrac{i\kappa\alpha_h}{R_*(t)}\tilde{v}_w^1 + \boxed{\dfrac{i\kappa\alpha_h}{R_*(t)}\tilde{v}_c^1} + \dfrac{i\kappa\lambda_2\xi}{1-\alpha_h}\tilde{\alpha}.
\end{cases}
\tag{112}
$$

Thus, we employ the following test. Choose $\overline{\alpha}(\xi) = 100\xi^2(x-1)^2$ and calculate

$$\begin{aligned}
\tilde{\alpha}(\xi,t) &= R_0\frac{e^{\gamma_0 t}}{R_*(t)}\overline{\alpha}(\xi),\\
\tilde{v}_c^1(\xi,t) &= R_0\gamma_1\frac{e^{\gamma_0 t}}{R_*(t)^2}\frac{d\overline{\alpha}}{d\xi}(\xi),\\
\tilde{v}_c^2(\xi,t) &= R_0\gamma_3\frac{e^{\gamma_0 t}}{R_*(t)}\overline{\alpha}(\xi),\\
\tilde{v}_w^1(\xi,t) &= \frac{\lambda_2 R_0}{\alpha_h(1-\alpha_h)}e^{\gamma_0 t}\xi\overline{\alpha}(\xi),\\
\tilde{v}_w^2(\xi,t) &= -R_0\frac{e^{\gamma_0 t}}{R_*(t)}\left[\frac{\lambda_2}{i\kappa\alpha_h(1-\alpha_h)^2}\left(1+\xi\frac{d}{d\xi}\right)\overline{\alpha}(\xi)+\frac{\alpha_h\gamma_3}{1-\alpha_h}\overline{\alpha}(\xi)\right],
\end{aligned}$$

as defined for the outer solution by analytical calculations in Section 8.2. On the other hand, simulate the system above without the highlighted terms. Then, for t large and ξ sufficiently far from $\xi = 0$ and $\xi = 1$, we expect these two solutions (one found analytically and one numerically) to have a fairly good agreement. Indeed, for $\xi \in (0.05, 0.95)$ and $t > 5$, we obtain the following errors:

Unknown	Error
$\tilde{\alpha}$	$2.4815e-06$
$\tilde{v}_c^1$	$5.9490e-05$
$\tilde{v}_c^2$	$6.4655e-06$
$\tilde{v}_w^1$	$7.8167e-06$
$\tilde{v}_w^2$	$1.0506e-05$

D.2.2 *Considering a Different Asymptotic Balance*

The non-trivial asymptotic balance found analytically for the outer solution in Section 8.2 considers the equations below with the boxed terms being of order smaller than 1:

$$\begin{cases} \dfrac{\partial \tilde{\alpha}}{\partial t} &= \Big[\dfrac{\partial S_c}{\partial \alpha}(\alpha_h, C_\infty) - \lambda_2\Big]\tilde{\alpha} - \boxed{\dfrac{\alpha_h}{R_*(t)}\dfrac{\partial \tilde{v}_c^1}{\partial \xi}} - \alpha_h i\kappa \tilde{v}_c^2 \\ 0 &= -\dfrac{\Sigma_c'(\alpha_h)}{R_*(t)}\dfrac{\partial \tilde{\alpha}}{\partial \xi} + \boxed{\dfrac{\hat{\mu}_c}{R_*(t)^2}\dfrac{\partial^2 \tilde{v}_c^1}{\partial \xi^2}} + \dfrac{(\lambda_c+\mu_c)i\kappa}{R_*(t)}\dfrac{\partial \tilde{v}_c^2}{\partial \xi} - \mu_c \kappa^2 \tilde{v}_c^1 \\ 0 &= \Big(-\Sigma_c(\alpha_h) - \alpha_h \Sigma_c'(\alpha_h) + \lambda_c\lambda_2\Big) i\kappa\tilde{\alpha} + \boxed{\dfrac{\mu_c \alpha_h}{R_*(t)^2}\dfrac{\partial^2 \tilde{v}_c^2}{\partial \xi^2}} \\ &\quad + (\mu_c + \lambda_c)\boxed{\dfrac{\alpha_h i\kappa}{R_*(t)}\dfrac{\partial \tilde{v}_c^1}{\partial \xi}} - \alpha_h \kappa^2 \hat{\mu}_c \tilde{v}_c^2. \end{cases} \tag{113}$$

OBJECTIVE:

I aim to show that adding any of the boxed terms in the approximation would generate a contradiction if no variable change is applied on ξ.

REASONING:

If any of the $\tilde{v}_c^1$ terms were added, the the last term in the second equation would imply that

$$\tilde{v}_c^1 \text{ would scale like } \frac{1}{R_*(t)^2}\frac{\partial^2 \tilde{v}_c^1}{\partial \xi^2}.$$

Similarly, if we attempt to revive any of the $\tilde{v}_c^2$ terms, the last term in the third equation would imply that

$$\tilde{v}_c^2 \text{ would scale like } \frac{1}{R_*(t)^2}\frac{\partial^2 \tilde{v}_c^2}{\partial \xi^2}.$$

Neither of these would be possible unless we impose a change in variable of the sort:

$$x = R_*(t)\xi,$$

and a return to the moving boundary scenario or the inner boundary layer formulation in Section 8.4.

D.2.3 *Numerical Checks with Larger Times*

In order to check that the asymptotic balance of the outer solution is reasonable, we will once again compare it against the numerical simulations of this system. For this, we need large time behaviour, which is not initially given by the code, as it breaks near $t = 160.7954$. However, if we require that "NormControl" be "on" in the options given to "ode23t," this nuisance is avoided and we may obtain solutions up to $t = 1000$, which is enough for our purposes. Turning on "NormControl" requires the solver to limit local error e to be smaller than $max(RelTol * norm(y), AbsTol)$, where "RelTol" and "Abstol" are the default relative and absolute tolerances (i.e. $1e-3$ and $1e-6$), respectively. Because some of the values are quite small, this solves our problem and we can thus use our numerical results to check our asymptotic approximations.

With this, we can graph ratios of the solutions for $t \in (550, 700)$ and $\xi = 0.2424$ and compare them to the respective ratios of the rescaled $\tilde{\cdot}$ variables. For example, applying the the outer solution characterisation found in Section 8.2, we expect that, roughly:

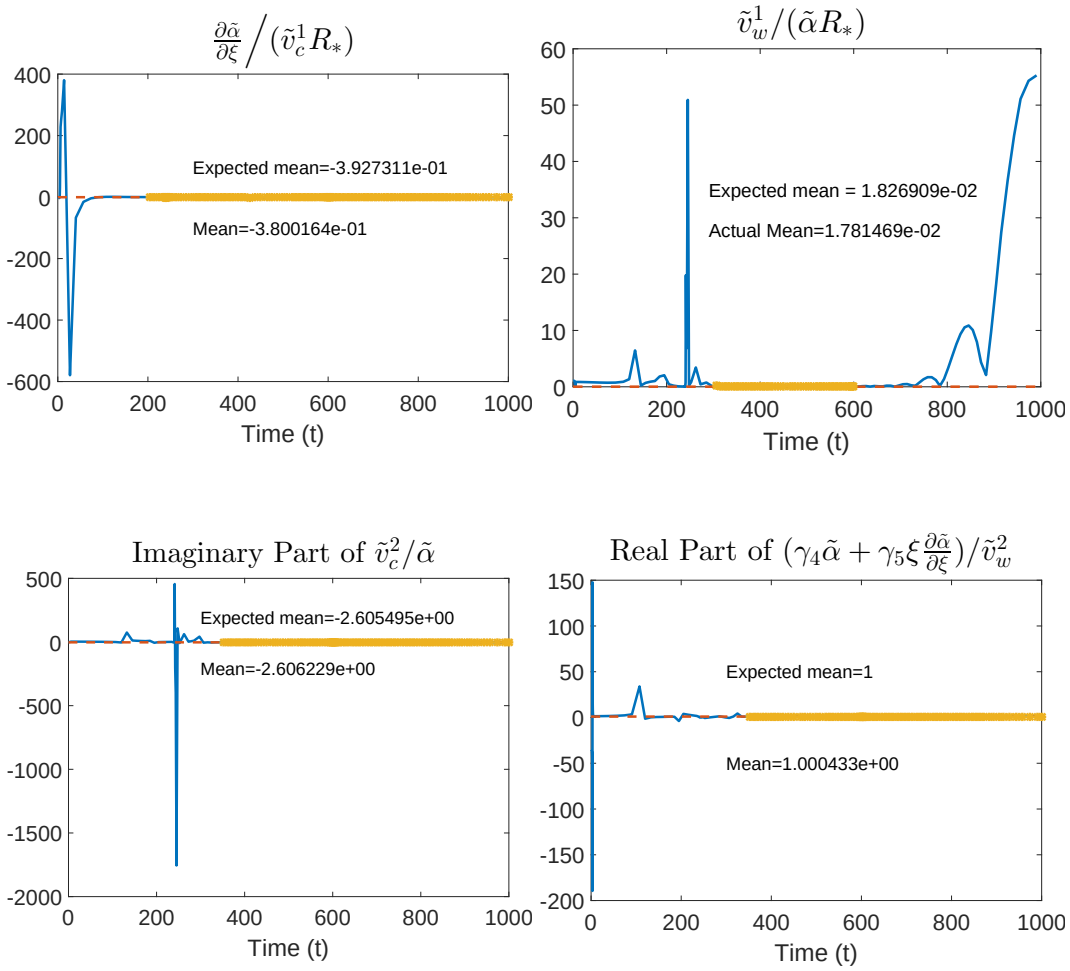
$$\frac{1}{\gamma_1} = \frac{\frac{\partial \overline{\alpha}}{\partial \overline{\xi}}}{\overline{v}_c^1} = \frac{\frac{\partial \tilde{\alpha}}{\partial \tilde{\xi}}}{\tilde{v}_c^1 R_*} \tag{114}$$

$$\gamma_2 \xi = \frac{\overline{v}_w^1}{\overline{\alpha}} = \frac{\tilde{v}_w^1}{\tilde{\alpha} R_*} \tag{115}$$

$$\gamma_3 = \frac{\overline{v}_c^2}{\overline{\alpha}} = \frac{\tilde{v}_c^2}{\tilde{\alpha}} \tag{116}$$

$$1 = \frac{\gamma_4 \overline{\alpha} + \gamma_5 \xi \frac{\partial \overline{\alpha}}{\partial \xi}}{\overline{v}_w^2} = \frac{\gamma_4 \tilde{\alpha} + \gamma_5 \xi \frac{\partial \tilde{\alpha}}{\partial \xi}}{\tilde{v}_w^2}. \tag{117}$$

If we graph the far right hand side terms of the equations above and compare the mean of these graphs to the respective left hand side, which we call "Expected mean", we see that:



Conclusion

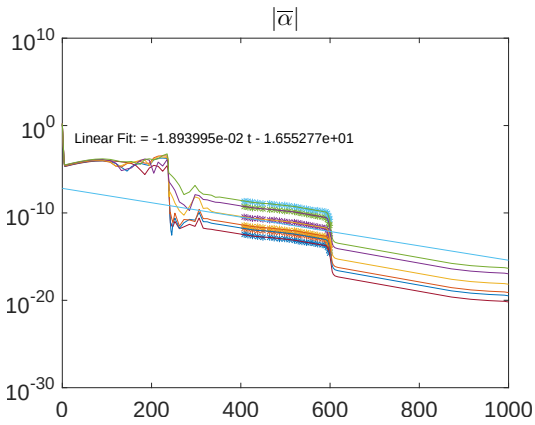
All graphs above denote a strong compatibility between the expected and actual means, which signifies that the relationship between $\overline{\alpha}$ and all the other unknowns $\bar{\cdot}$ is correct. In other words, this confirms the outer solution found in Section 8.2.

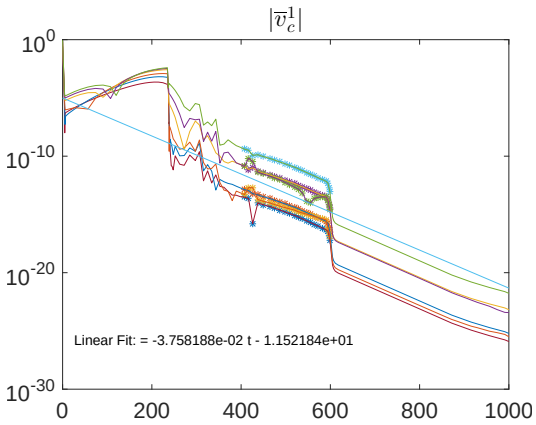
D.2.4 *Taking a Hint from Numerics*

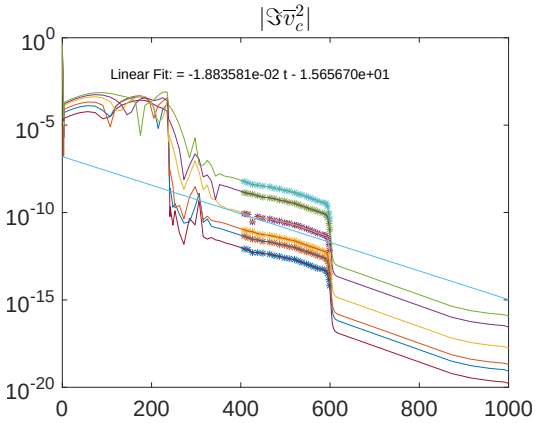
Consider the following graphs of the numerical solutions of this system. Since

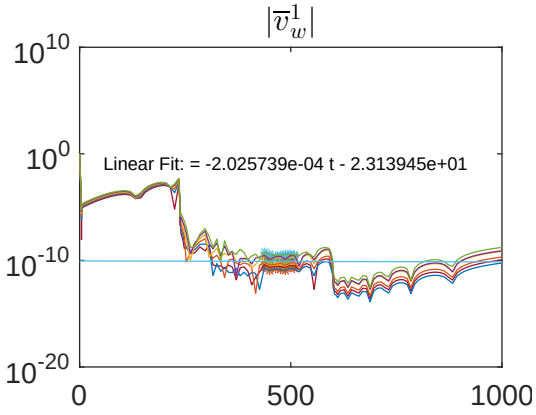
$$\lambda_2 = 1.7976 \times 10^{-2}, \qquad 2\lambda_2 = 3.5952 \times 10^{-2},$$

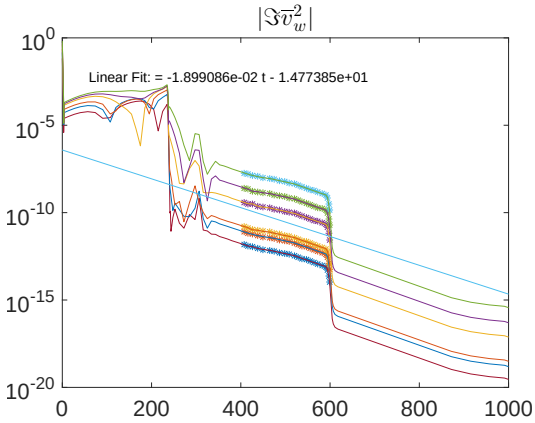
the slope of the linear fit of these following graphs suggest that we can rescale each component of the solution by a suitable power of $R_*(t) = R_0 e^{\lambda_2 t}$.

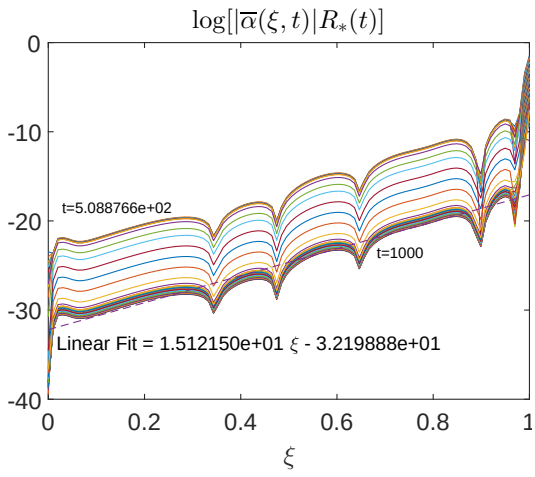


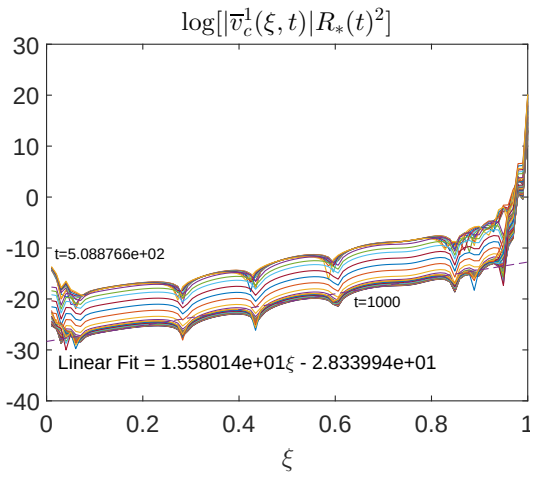


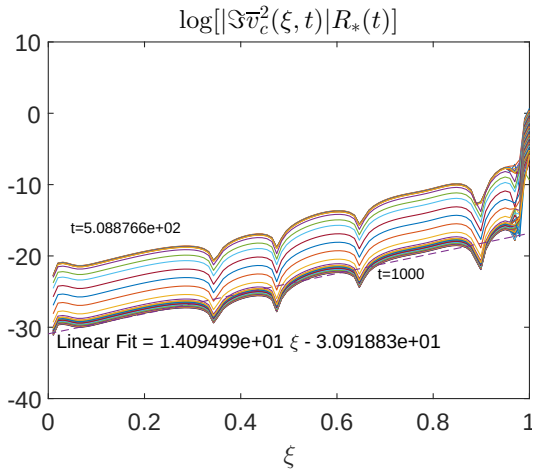


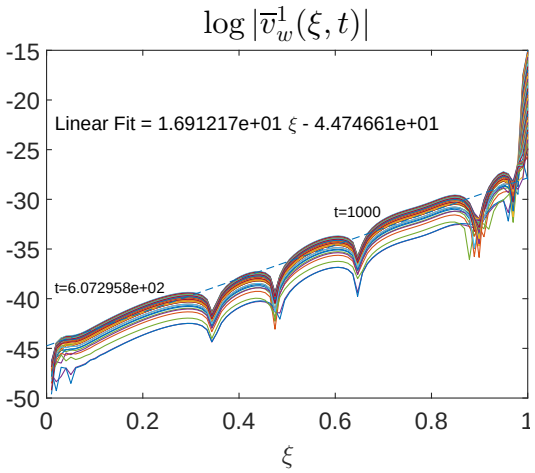


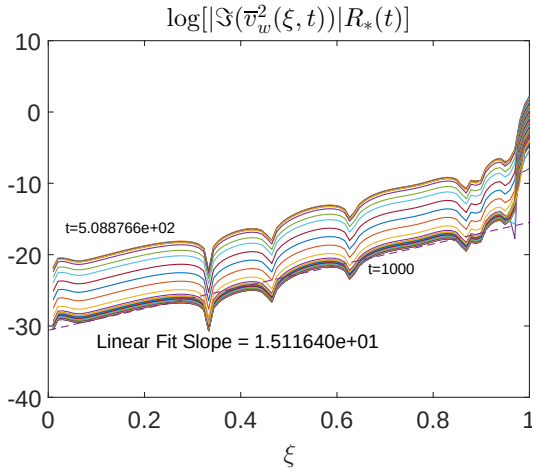



$\log[|\overline{\alpha}(\xi,t)|R_*(t)]$
t=5.088766e+02
t=1000
Linear Fit = 1.512150e+01 ξ - 3.219888e+01
ξ


$\log[|\overline{v}_c^1(\xi,t)|R_*(t)^2]$
t=5.088766e+02
t=1000
Linear Fit = 1.558014e+01ξ - 2.833994e+01
ξ


$\log[|\Im\overline{v}_c^2(\xi,t)|R_*(t)]$
t=5.088766e+02
t=1000
Linear Fit = 1.409499e+01 ξ - 3.091883e+01
ξ


$\log|\overline{v}_w^1(\xi,t)|$
Linear Fit = 1.691217e+01 ξ - 4.474661e+01
t=1000
t=6.072958e+02
ξ

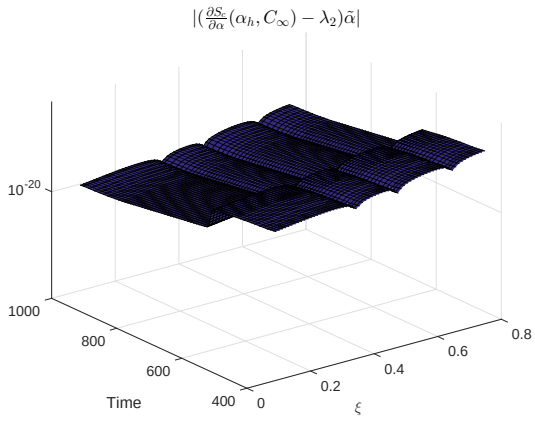

$\log[|\Im(\overline{v}_w^2(\xi,t))|R_*(t)]$
t=5.088766e+02
t=1000
Linear Fit Slope = 1.511640e+01
ξ

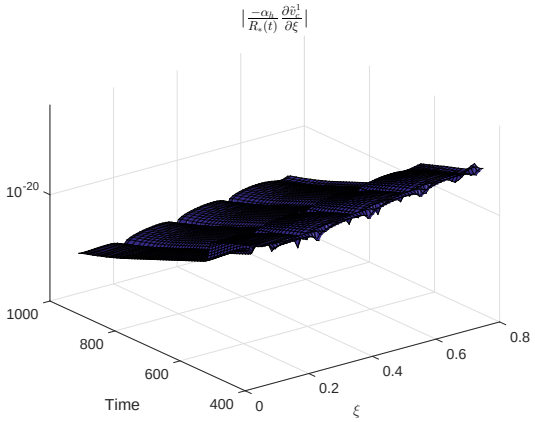
D.2.5 *Comparing Magnitudes*

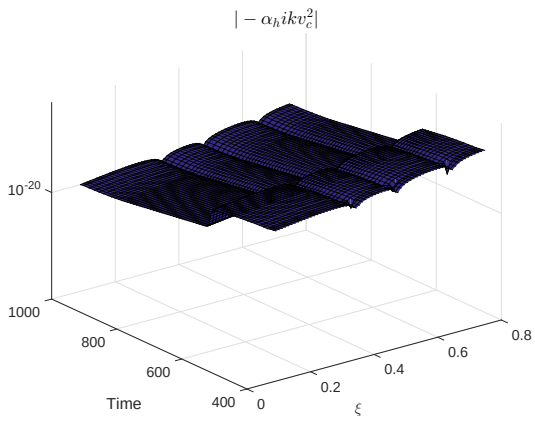
The last check performed on the outer solution asymptotic balance was to graph the first three equations of the system 79, term by term. This way, we can compare magnitudes in order to see which terms are dominant when $t \to \infty$. Doing this to the first three equations allows us to confirm that the balance is one in which the boxed terms below are deemed to be of smaller order than the other terms and, particularly, that $\beta = 1$ as all the other values of β proved to have different asymptotic balances (see Chapter 8).

First Equation

$$\frac{\partial \tilde{\alpha}}{\partial t} = \left[\frac{\partial S_c}{\partial \alpha}(\alpha_h, C_\infty) - \lambda_2\right]\tilde{\alpha} - \boxed{\frac{\alpha_h}{R_*(t)}\frac{\partial \tilde{v}_c^1}{\partial \xi}} - \alpha_h i\kappa \tilde{v}_c^2$$

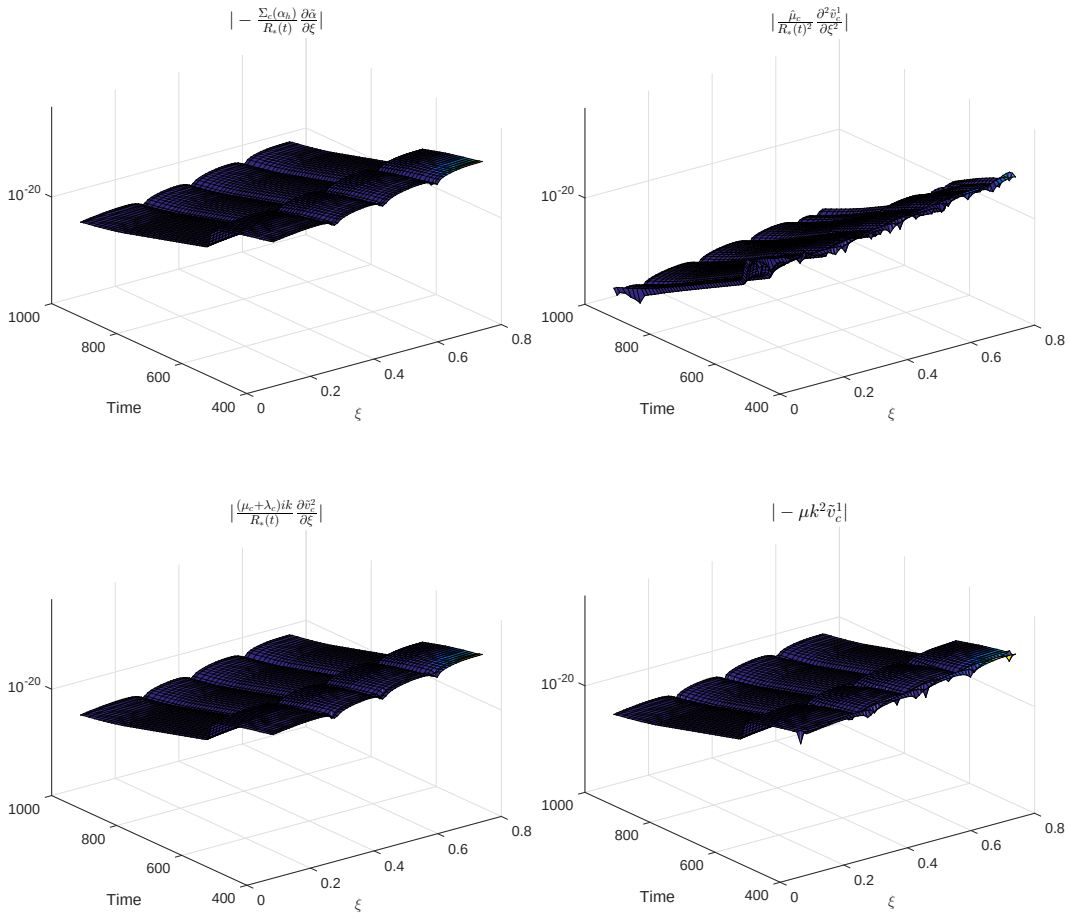






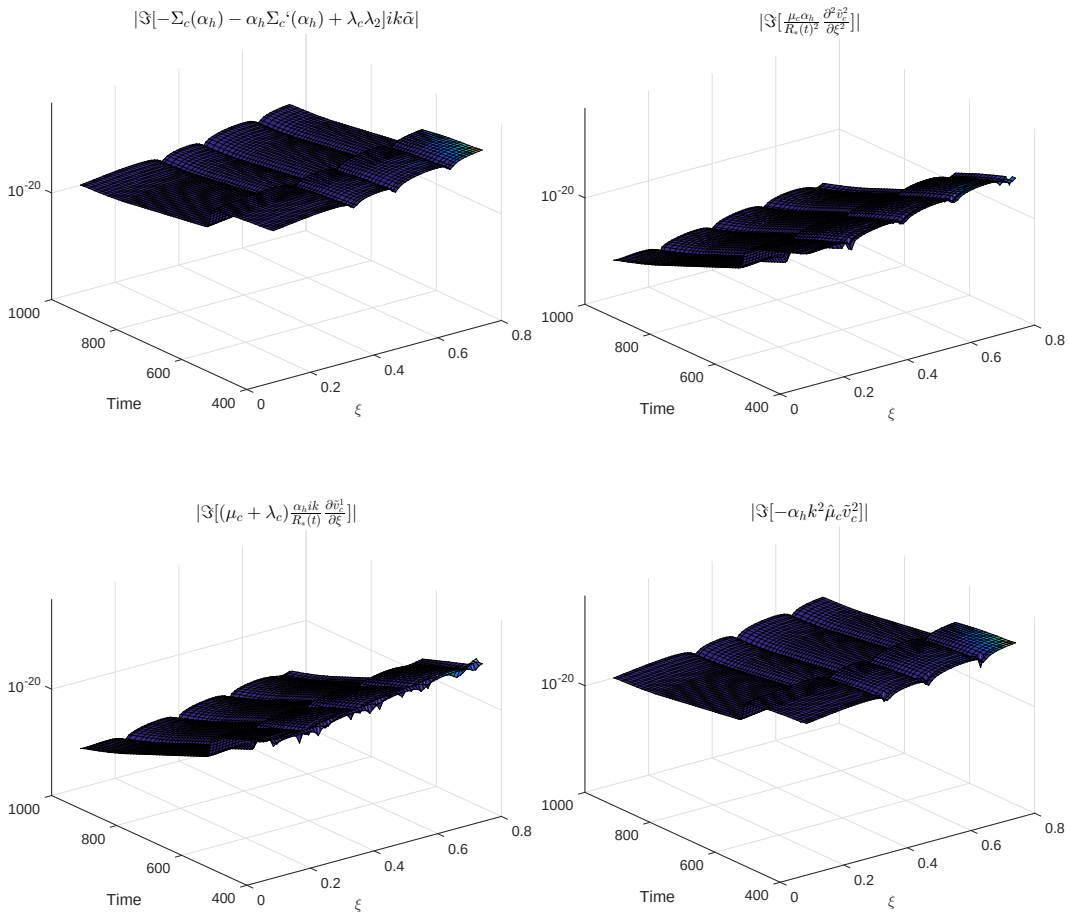
Second Equation

$$0 = -\frac{\Sigma_c'(\alpha_h)}{R_*(t)}\frac{\partial \tilde{\alpha}}{\partial \xi} + \frac{\hat{\mu}_c}{R_*(t)^2}\frac{\partial^2 \tilde{v}_c^1}{\partial \xi^2} + \frac{(\lambda_c+\mu_c)i\kappa}{R_*(t)}\frac{\partial \tilde{v}_c^2}{\partial \xi} - \mu_c \kappa^2 \tilde{v}_c^1$$



Third Equation

$$0 = \Big(-\Sigma_c(\alpha_h) - \alpha_h \Sigma_c'(\alpha_h) + \lambda_c \lambda_2\Big) i\kappa\tilde{\alpha} + \frac{\mu_c \alpha_h}{R_*(t)^2}\frac{\partial^2 \tilde{v}_c^2}{\partial \xi^2}$$
$$+ (\mu_c + \lambda_c)\frac{\alpha_h i\kappa}{R_*(t)}\frac{\partial \tilde{v}_c^1}{\partial \xi} - \alpha_h \kappa^2 \hat{\mu}_c \tilde{v}_c^2$$


$|\Im[-\Sigma_c(\alpha_h) - \alpha_h\Sigma_c`(\alpha_h) + \lambda_c\lambda_2]ik\tilde{\alpha}|$
$|\Im[\frac{\mu_c\alpha_h}{R_*(t)^2}\frac{\partial^2\tilde{v}_c^2}{\partial\xi^2}]|$
$|\Im[(\mu_c + \lambda_c)\frac{\alpha_h ik}{R_*(t)}\frac{\partial\tilde{v}_c^1}{\partial\xi}]|$
$|\Im[-\alpha_h k^2\hat{\mu}_c\tilde{v}_c^2]|$
10^{-20}
1000
800
600
400
Time
0
0.2
0.4
0.6
0.8
ξ

E

ASYMPTOTIC ANALYSIS SUMMARY

Outer Solution

Outer solution is governed by equations

$$\begin{cases} \dfrac{\partial \tilde{\alpha}}{\partial t} &= \Big[\dfrac{\partial S_c}{\partial \alpha}(\alpha_h, C_\infty) - \lambda_2\Big]\tilde{\alpha} - \alpha_h ik\tilde{v}_c^2 \\ 0 &= -\Sigma_c'(\alpha_h)\dfrac{\partial \tilde{\alpha}}{\partial \xi} + (\lambda_c + \mu_c)ik\dfrac{\partial \tilde{v}_c^2}{\partial \xi} - \mu_c k^2 R_*(t)\tilde{v}_c^1 \\ 0 &= \Big(- \Sigma_c(\alpha_h) - \alpha_h\Sigma_c'(\alpha_h) + \lambda_c\lambda_2\Big)ik\tilde{\alpha} - \alpha_h k^2\hat{\mu}_c\tilde{v}_c^2. \\ 0 &= \dfrac{\lambda_2}{1-\alpha_h}\Big(1 + \xi\dfrac{\partial}{\partial \xi}\Big)\tilde{\alpha} + \dfrac{1-\alpha_h}{R_*(t)}\dfrac{\partial \tilde{v}_w^1}{\partial \xi} + \alpha_h ik\tilde{v}_c^2 + (1-\alpha_h)ik\tilde{v}_w^2 \\ 0 &= -\dfrac{ik\alpha_h}{R_*(t)}\tilde{v}_w^1 + \dfrac{ik\lambda_2\xi}{1-\alpha_h}\tilde{\alpha}. \end{cases} \tag{118}$$

Outer Boundary Inner Solution

Outer boundary inner solution is governed by equations

$$\begin{cases} 0 &= \Big[\frac{\partial S_c}{\partial \alpha}(\alpha_h, C_\infty) - \gamma_0 + \lambda_2\Big(1 - X\frac{d}{dX}\Big)\Big]A + \alpha_h\frac{dV_c^1}{dX} - \alpha_h ikV_c^2 \\ 0 &= \Sigma_c'(\alpha_h)\frac{dA}{dX} + \hat{\mu}_c\frac{d^2V_c^1}{dX^2} - (\lambda_c+\mu_c)ik\frac{dV_c^2}{dX} - \mu_c k^2 V_c^1 \\ 0 &= \Big(-\Sigma_c(\alpha_h) - \alpha_h\Sigma_c'(\alpha_h) + \lambda_c\lambda_2\Big)ikA + \mu_c\alpha_h\frac{d^2V_c^2}{dX^2} \\ & \quad -(\mu_c+\lambda_c)\alpha_h ik\frac{dV_c^1}{dX} - \alpha_h k^2\hat{\mu}_c V_c^2 \\ 0 &= -\frac{\lambda_2 R_0}{(1-\alpha_h)^2}\frac{dA}{dX} - \frac{dV_w^1}{dX} + ikV_w^2 \\ 0 &= -\frac{dV_w^2}{dX} - ikV_w^1 + \frac{ik\lambda_2 R_0}{\alpha_h(1-\alpha_h)}A, \end{cases}$$

in $X > 0$ and at $X = 0$:

$$\begin{cases} 0 &= -\Sigma_c'(\alpha_h)A - \hat{\mu}_c\frac{dV_c^1}{dX} + \lambda_c ikV_c^2, \\ 0 &= \frac{(3\lambda_2-\gamma_0)}{ik}\frac{dV_c^2}{dX} + (\gamma_0-\lambda_2)V_c^1 \\ V_w^2 &= \frac{R_0}{2(1-\alpha_h)}\Big[\frac{dV_c^2}{dX} - ikV_c^1\Big], \end{cases}$$

where

$$\xi = 1 - \frac{X}{R_*(t)}.$$

Also, the moving boundary condition yields, in first order,

$$\frac{d\tilde{R}}{dt}(t) = \lambda_2\tilde{R}(t) + e^{(\gamma_0-2\lambda_2)t}V_c^1(0)$$

and therefore,

$$\tilde{R}(t) \sim C_0 e^{\lambda_2 t} + \frac{V_c^1(0)}{\gamma_0 - 3\lambda_2}e^{(\gamma_0-2\lambda_2)t}.$$

Inner Boundary Inner Solution

Similarly, the inner solution near $\xi = 0$ is governed by

$$\begin{cases} 0 &= \Big[\frac{\partial S_c}{\partial \alpha}(\alpha_h, C_\infty) - \gamma_0 + \lambda_2\Big(1 - x\frac{d}{dx}\Big)\Big]A - \alpha_h\frac{dV_c^1}{dx} - \alpha_h ikV_c^2 \\ 0 &= -\Sigma_c'(\alpha_h)\frac{dA}{dx} + \hat{\mu}_c\frac{d^2V_c^1}{dx^2} + (\lambda_c + \mu_c)ik\frac{dV_c^2}{dx} - \mu_c k^2 V_c^1 \\ 0 &= \Big(-\Sigma_c(\alpha_h) - \alpha_h\Sigma_c'(\alpha_h) + \lambda_c\lambda_2\Big)ikA + \mu_c\alpha_h\frac{d^2V_c^2}{dx^2} \\ &\quad +(\mu_c + \lambda_c)\alpha_h ik\frac{dV_c^1}{dx} - \alpha_h k^2\hat{\mu}_c V_c^2 \\ 0 &= \frac{\lambda_2}{1-\alpha_h}\big(1 + x\frac{d}{dx}\big)A + \alpha_h\frac{dV_c^1}{dx} + \alpha_h ikV_c^2 \\ &\quad +(1-\alpha_h)\frac{dV_w^1}{dx} + (1-\alpha_h)ikV_w^2 \\ 0 &= \frac{\lambda_2 ik}{1-\alpha_h}xA + \alpha_h ikV_c^1 - \alpha_h\frac{dV_c^2}{dx} - \alpha_h ikV_w^1 + \alpha_h\frac{dV_w^2}{dx}, \end{cases}$$

and $V_c^1(0) = V_c^2(0) = V_w^1(0) = 0$, where

$$\xi = \frac{x}{R_*(t)}.$$

BIBLIOGRAPHY

[1] JA Adam. A simplified mathematical model of tumor growth. *Mathematical biosciences*, 81(2):229–244, 1986.

[2] B Alberts, D Bray, J Lewis, M Raff, K Roberts, JD Watson, and AV Grimstone. Molecular biology of the cell (3rd edn). *Trends in Biochemical Sciences*, 20(5):210–210, 1995.

[3] RP Araujo and DLS McElwain. A history of the study of solid tumour growth: the contribution of mathematical modelling. *Bulletin of mathematical biology*, 66(5):1039–1091, 2004.

[4] RM Bowen. Theory of mixtures. *Continuum physics*, 3(Pt I), 1976.

[5] RM Bowen. Incompressible porous media models by use of the theory of mixtures. *International Journal of Engineering Science*, 18(9):1129–1148, 1980.

[6] RM Bowen. Compressible porous media models by use of the theory of mixtures. *International Journal of Engineering Science*, 20(6):697–735, 1982.

[7] RM Bowen and JC Wiese. Diffusion in mixtures of elastic materials. *International Journal of Engineering Science*, 7(7):689–722, 1969.

[8] CJW Breward, HM Byrne, and CE Lewis. Modelling the interactions between tumour cells and a blood vessel in a microenvironment within a vascular tumour. *European Journal of Applied Mathematics*, 12(05):529–556, 2001.

[9] CJW Breward, HM Byrne, and CE Lewis. The role of cell-cell interactions in a two-phase model for avascular tumour growth. *Journal of Mathematical Biology*, 45(2):125–152, 2002.

[10] CJW Breward, HM Byrne, and CE Lewis. A multiphase model describing vascular tumour growth. *Bulletin of mathematical biology*, 65(4):609–640, 2003.

[11] N Britton. *Essential mathematical biology*. Springer Science & Business Media, 2012.

[12] AC Burton. Rate of growth of solid tumours as a problem of diffusion. *Growth*, 30(2):157–176, 1966.

[13] H Byrne and L Preziosi. Modelling solid tumour growth using the theory of mixtures. *Mathematical Medicine and Biology*, 20(4):341–366, 2003.

[14] Helen M Byrne. Dissecting cancer through mathematics: from the cell to the animal model. *Nature Reviews Cancer*, 10(3):221–230, 2010.

[15] HM Byrne, T Alarcon, MR Owen, SD Webb, and PK Maini. Modelling aspects of cancer dynamics: a review. *Philosophical Transactions of the Royal Society of London A: Mathematical, Physical and Engineering Sciences*, 364(1843):1563–1578, 2006.

[16] HM Byrne and MAJ Chaplain. Growth of nonnecrotic tumors in the presence and absence of inhibitors. *Mathematical biosciences*, 130(2):151–181, 1995.

[17] HM Byrne and MAJ Chaplain. Necrosis and apoptosis: distinct cell loss mechanisms in a mathematical model of avascular tumour growth. *Computational and Mathematical Methods in Medicine*, 1(3):223–235, 1998.

[18] HM Byrne and Mark AJ Chaplain. Free boundary value problems associated with the growth and development of multicellular spheroids. *European Journal of Applied Mathematics*, 8(06):639–658, 1997.

[19] HM Byrne, JR King, DLS McElwain, and L Preziosi. A two-phase model of solid tumour growth. *Applied Mathematics Letters*, 16(4):567–573, 2003.

[20] MAJ Chaplain. Avascular growth, angiogenesis and vascular growth in solid tumours: The mathematical modelling of the stages of tumour development. *Mathematical and computer modelling*, 23(6):47–87, 1996.

[21] Ying Chen and John S Lowengrub. Tumor growth in complex, evolving microenvironmental geometries: a diffuse domain approach. *Journal of theoretical biology*, 361:14–30, 2014.

[22] W Cramer. The prevention of cancer. *The Lancet*, 223(5758):1–5, 1934.

[23] J Cruveilhier. *Anatomie pathologique du corps humain*. Bailliere, 1829.

[24] I Churchill Davidson, C Sanger, and RH Thomlinson. High-pressure oxygen and radiotherapy. *The Lancet*, 265(6874):1091–1095, 1955.

[25] DA Drew. Averaged field equations for two-phase media. *Studies in Applied Mathematics*, 50(2):133–166, 1971.

[26] DA Drew and SL Passman. *Theory of multicomponent fluids*, volume 135. Springer Science & Business Media, 2006.

[27] DA Drew and LA Segel. Averaged equations for two-phase flows. *Studies in Applied Mathematics*, 50(3):205–231, 1971.

[28] J Folkman. Tumor angiogenesis. *Advances in cancer research*, 19:331–358, 1974.

[29] J Folkman, P Cole, and S Zimmerman. Tumor behavior in isolated perfused organs: in vitro growth and metastases of biopsy material in rabbit thyroid and canine intestinal segment. *Annals of surgery*, 164(3):491, 1966.

[30] J Folkman and M Hochberg. Self-regulation of growth in three dimensions. *The Journal of experimental medicine*, 138(4):745–753, 1973.

[31] M Fowler. *Analysis patterns: reusable object models*. Addison-Wesley Professional, 1997.

[32] JE Frampton and GM Keating. Bevacizumab. *BioDrugs*, 22(2):113–120, 2008.

[33] Hermann B Frieboes, Fang Jin, Yao-Li Chuang, Steven M Wise, John S Lowengrub, and Vittorio Cristini. Three-dimensional multispecies nonlinear tumor growth—ii: tumor invasion and angiogenesis. *Journal of theoretical biology*, 264(4):1254–1278, 2010.

[34] RA Gatenby and PK Maini. Mathematical oncology: cancer summed up. *Nature*, 421(6921):321–321, 2003.

[35] Robert A Gatenby and Edward T Gawlinski. A reaction-diffusion model of cancer invasion. *Cancer research*, 56(24):5745–5753, 1996.

[36] B Gompertz. On the nature of the function expressive of the law of human mortality, and on a new mode of determining the value of life contingencies. *Philosophical transactions of the Royal Society of London*, 115:513–583, 1825.

[37] LH Gray, AD Conger, M Ebert, S Hornsey, and OCA Scott. The concentration of oxygen dissolved in tissues at the time of irradiation as a factor in radiotherapy. *The British journal of radiology*, 26(312):638–648, 1953.

[38] HSN Greene. Heterologous transplantation of mammalian tumors i. the transfer of rabbit tumors to alien species. *The Journal of experimental medicine*, 73(4):461–474, 1941.

[39] HP Greenspan. Models for the growth of a solid tumor by diffusion. *Studies in Applied Mathematics*, 51(4):317–340, 1972.

[40] HP Greenspan. On the growth and stability of cell cultures and solid tumors. *Journal of theoretical biology*, 56(1):229–242, 1976.

[41] M Hejmadi. *Introduction to cancer biology*. Bookboon, 2009.

[42] R Hesketh. *Introduction to cancer biology*. Cambridge University Press, 2013.

[43] ME Hubbard and HM Byrne. Multiphase modelling of vascular tumour growth in two spatial dimensions. *Journal of theoretical biology*, 316:70–89, 2013.

[44] MA Knowles and P Selby. Introduction to the cellular and molecular biology of cancer, 2005.

[45] AK Laird. Dynamics of tumour growth. *British journal of cancer*, 18(3):490, 1964.

[46] KA Landman and CP Please. Tumour dynamics and necrosis: surface tension and stability. *Mathematical Medicine and Biology*, 18(2):131–158, 2001.

[47] G Lemon and JR King. Multiphase modelling of cell behaviour on artificial scaffolds: effects of nutrient depletion and spatially nonuniform porosity. *Mathematical Medicine and Biology*, 24(1):57–83, 2007.

[48] G Lemon, JR King, HM Byrne, OE Jensen, and KM Shakesheff. Mathematical modelling of engineered tissue growth using a multiphase porous flow mixture theory. *Journal of mathematical biology*, 52(5):571–594, 2006.

[49] LA Liotta, J Kleinerman, and GM Saidel. Quantitative relationships of intravascular tumor cells, tumor vessels, and pulmonary metastases following tumor implantation. *Cancer research*, 34(5):997–1004, 1974.

[50] LA Liotta, J Kleinerman, and GM Saldel. The significance of hematogenous tumor cell clumps in the metastatic process. *Cancer research*, 36(3):889–894, 1976.

[51] R Lomer. *Zur frage der heilbarkeit des carcinoms*. publisher not identified, 1920.

[52] WV Mayneord. On a law of growth of jensen's rat sarcoma. *The American Journal of Cancer*, 16(4):841–846, 1932.

[53] DLS McElwain and LE Morris. Apoptosis as a volume loss mechanism in mathematical models of solid tumor growth. *Mathematical Biosciences*, 39(1):147–157, 1978.

[54] Ingrid Moen and Linda EB Stuhr. Hyperbaric oxygen therapy and cancer—a review. *Targeted oncology*, 7(4):233–242, 2012.

[55] JC Mottram. On the alteration in the sensitivity of cells towards radiation produced by cold and by anaerobiosis. *The British Journal of Radiology*, 8(85):32–39, 1935.

[56] JC Mottram. A factor of importance in the radio sensitivity of tumours. *The British Journal of Radiology*, 9(105):606–614, 1936.

[57] W Mueller-Klieser. Tumor biology and experimental therapeutics. *Critical reviews in oncology/hematology*, 36(2):123–139, 2000.

[58] RD O'dea, SL Waters, and HM Byrne. A two-fluid model for tissue growth within a dynamic flow environment. *European Journal of Applied Mathematics*, 19(06):607–634, 2008.

[59] RD O'Dea, SL Waters, and HM Byrne. A multiphase model for tissue construct growth in a perfusion bioreactor. *Mathematical Medicine and Biology*, page dqp003, 2009.

[60] SL Passman, JW Nunziato, and EK Walsh. A theory of multiphase mixtures. In *Rational thermodynamics*, pages 286–325. Springer, 1984.

[61] CP Please, G Pettet, and DLS McElwain. A new approach to modelling the formation of necrotic regions in tumours. *Applied mathematics letters*, 11(3):89–94, 1998.

[62] CP Please, GJ Pettet, and DLS McElwain. Avascular tumour dynamics and necrosis. *Mathematical Models and Methods in Applied Sciences*, 9(04):569–579, 1999.

[63] Luigi Preziosi and Luigi Graziano. Multiphase models of tumour growth: general framework and particular cases. In *Mathematical Modeling and Computer in Biology and Medicine Proceedings of the 5th Conference on the ESMTB (Springer, Berlin)*, pages 622–628, 2003.

[64] KR Rajagopal and L Tao. *Mechanics of mixtures*, volume 35. World scientific, 1995.

[65] T Roose, SJ Chapman, and PK Maini. Mathematical models of avascular tumor growth. *Siam Review*, 49(2):179–208, 2007.

[66] JA Sherratt and MA Nowak. Oncogenes, anti-oncogenes and the immune response to cancer: a mathematical model. *Proceedings of the Royal Society of London B: Biological Sciences*, 248(1323):261–271, 1992.

[67] Robert M Sutherland, John A McCredie, and W Rodger Inch. Growth of multicell spheroids in tissue culture as a model of nodular carcinomas. *Journal of the National Cancer Institute*, 46(1):113–120, 1971.

[68] NM Temme. *Asymptotic methods for integrals*, volume 11. World Scientific, 2014.

[69] RH Thomlinson and LH Gray. The histological structure of some human lung cancers and the possible implications for radiotherapy. *British journal of cancer*, 9(4):539, 1955.

[70] C Truesdell. W. noll the non-linear field theories of mechanics. *Handbuch der Physik, III/3. Berlin-Heidelberg-New York: Springer*, 1965.

[71] C Truesdell and R Toupin. The classical field theories. In *Principles of Classical Mechanics and Field Theory/Prinzipien der Klassischen Mechanik und Feldtheorie*, pages 226–858. Springer, 1960.

[72] JP Ward and JR King. Mathematical modelling of avascular-tumour growth. *Mathematical Medicine and Biology*, 14(1):39–69, 1997.

[73] JP Ward and JR King. Mathematical modelling of avascular-tumour growth ii: modelling growth saturation. *Mathematical Medicine and Biology*, 16(2):171–211, 1999.

[74] JP Ward and JR King. Mathematical modelling of the effects of mitotic inhibitors on avascular tumour growth. *Computational and Mathematical Methods in Medicine*, 1(4):287–311, 1999.

[75] L Weiss. The morphologic documentation of clinical progression, invasion metastasis-staging. *Cancer and Metastasis Reviews*, 19(3):303–313, 2000.

[76] Steven M Wise, John S Lowengrub, Hermann B Frieboes, and Vittorio Cristini. Three-dimensional multispecies nonlinear tumor growth—i: model and numerical method. *Journal of theoretical biology*, 253(3):524–543, 2008.